CRANFIELD UNIVERSITY

MARCO CUMMAUDO

IDENTIFICATION OF HUMAN VS NON-HUMAN BONE (*SUS SCROFA*) IN FORENSIC ANTHROPOLOGY: HISTOLOGICAL PERSPECTIVES

CRANFIELD FORENSIC INSTITUTE

PhD Thesis

2018

Supervisor: Dr. Nicholas Márquez-Grant
Secondary supervisor: Professor Cristina Cattaneo

September 2018

CRANFIELD UNIVERSITY

CRANFIELD FORENSIC INSTITUTE

PhD Thesis

2018

MARCO CUMMAUDO

IDENTIFICATION OF HUMAN VS NON-HUMAN BONE (*SUS SCROFA*) IN FORENSIC ANTHROPOLOGY: HISTOLOGICAL PERSPECTIVES

Supervisor: Dr. Nicholas Márquez-Grant
Secondary supervisor: Professor Cristina Cattaneo

September 2018

This thesis is submitted in partial fulfillment of the requirements for the degree of PhD

ABSTRACT

In the event of natural disasters, residential and commercial fires, aircraft accidents as well as in clandestine burials, fragmented remains of pets, wildlife animals or other animals used for meat consumption (e.g. pig, cattle), can frequently become commingled with human remains. In such cases, forensic anthropologists are often asked to assist law enforcement in identifying the human or nonhuman origin of the remains.

When the skeletal material is highly fragmented lacking any diagnostic feature, species discrimination by the assessment of gross morpohological characteristics may not be exploitable. Thus, forensic anthropologists must turn to other methods, such as the histological analysis. Though bone histology of mammals has been deeply explored since at least the seventeenth century, quantitative data available to perform species discrimination by histological analysis is still scarce and, above all, there is a lack of knowledge on the extent of variability in different bones of the skeleton, considering that most of the previous investigations focused exclusively on some specific bones (e.g. femur, rib), rather than having a wider overview of the entire skeleton.

In this regard, this thesis aimed to investigate the intra- and inter-species variability of bone microscopic structure in human and pig (*Sus scrofa*) at different stages of skeletal maturity from both a qualitative (type of tissues) and quantitative perspectives (measurements of diameter, area and perimeter of secondary osteons and osteocyte lacunae). More than 3000 osteons and Haversian canals were measured during the analyses, as well as over 1200 osteocyte lacunae.

This research demonstrated a significant intra-individual, intra-species and inter-species variability of bone microarchitecture which can have implications not only when

assessing the origin of an unknown bone fragment, but also when performing histological age-at-death estimation. Overall, it makes a significant contribution to knowledge of bone histomorphology and histomorphometry in human and pig since it represents the first attempt in investigating bone microarchitecture along the entire human and pig skeleton and provides new insight for species discrimination from a histological perspective.

ACKNOWLEDGEMENTS

Firstly, I would like to express my sincere gratitude to my supervisors, Dr Nicholas Márquez-Grant and Prof Cristina Cattaneo for the patient guidance, encouragement and advice they have provided throughout the research process.

I would also like to thank the rest of my thesis committee: Prof Keith Rogers, Prof Peter Zioupos and Dr Sophie Beckett for their invaluable advice and feedback on my research.

I thank my fellow labmates for their continued support and for helping me keep things in perspective, especially during hard times.

I am grateful to all of those with whom I have had the pleasure to work during this and other related projects.

Last but not the least, I would like to thank my family: my parents, my brother and sister for supporting me spiritually throughout writing this thesis and my life in general.

TABLE OF CONTENTS

LIST OF TABLES

LIST OF FIGURES

GLOSSARY

Nomenclature

On.Dm	osteon diameter
On.Ar	osteon area
On.Pm	osteon perimeter
On.Cr	osteon circularity
HC.Dm	Haversian canal diameter
HC.Ar	Haversian canal area
HC.Pm	Haversian canal perimeter
Lc.Dm	osteocyte lacuna diameter
Lc.Pm	osteocyte lacuna perimeter
Lc.Ar	osteocyte lacuna area
Lc.N	number of osteocyte lacunae

Abbreviations

ANOVA	one-way analysis of variance
p	p-value
max	maximum value
min	minimum value
St. Dev.	standard deviation of the mean

Units

μm	micrometre (1 μm = 1 x 10^{-6} m)

CHAPTER 1

INTRODUCTION

Forensic anthropology is a discipline that deals with the analysis and identification of human remains. The American Board of Forensic Anthropology (ABFA) defines forensic anthropology as "*the application of the science of physical or biological anthropology to the legal process Physical or biological anthropologists who specialize in forensics primarily focus their studies on the human skeleton*" (http://www.theabfa.org/). Experts in this discipline, in fact, apply their knowledge of skeletal variation to aid law enforcement achieving a correct identification of unknown decedents and, when possible, provide information about the cause of death (Tersigni-Tarrant and Shirley 2013). Generally, the forensic anthropologist steps in when the decomposition of human remains is so advanced that other medical forensic specialists are not able to determine demographic characteristics (e.g. age, ancestry) and time since death (Byers 2017). The process of identification starts with building a detailed biological profile by estimating ancestry, sex, age and height of the individual. When evidence of traumatic injury to bone (e.g. stab wounds, bullet holes) are present, forensic anthropologists seek to obtain information regarding the cause and manner of death (Byers 2017; Christensen *et al.* 2014; Franklin and Marks 2017). Moreover, these experts have often a role in the localization and recovery of surface or buried remains, ensuring that all relevant evidence is gathered (Byers 2017; Cattaneo 2007). These tasks regard single cases of unidentified human remains, as well other scenarios such as mass graves and mass disasters.

Generally, when skeletal material is found, both in forensic and archaeological contexts, one of the first question these experts have to answer is whether this material is human or

non-human (Cattaneo 1999; Mulhern and Ubelaker 2012). In medico-legal investigations, quickly identifying a bone as non-human and therefore not forensically significant is vital, since it allows to save time and resources, avoiding further investigations (Mulhern and Ubelaker 2012; Mundorff 2012).

There is a variety of circumstances which can bring nonhuman skeletal remains to the attention of forensic anthropologists, including residential and commercial fires, aircraft accidents and natural disasters (Stout 2009; Marks *et al.* 2009). In such cases, in fact, fragmented and/or charred remains of pets, wildlife animals or other animals used for meat consumption, can frequently become commingled with human remains.

The commingling of human and nonhuman remains can also frequently occur in case of clandestine burials, in which nonhuman bones are intentionally placed over the victim in order to conceal the remains (Reinecke and Hochrein 2008).

In addition, the recovery of a single bone or bone fragment is not uncommon during the search operations for missing persons and frequently turns out to be the remains of a hunted animal which have been butchered outdoor (Franklin and Marks 2017).

Commingled assemblages of human and animal bones are frequently recovered also during archaeological excavations, especially in prehistoric contexts (Bond 1996; Outram *et al.* 2005). Species discrimination can be, at times, a difficult task to be accomplished, especially in case of cremated remains (Cuijpers 2006; Cattaneo *et al.* 1999). However, discriminating between human and nonhuman bone in an archaeological context can be a precious source of information regarding paleoecology and animal biogeography (Baker and Shaffer 1999; Gilmore 1949), as well as funerary archaeology (Thompson 2015). Faunal identifications, in fact, can allow archaeologists to investigate the development of prehistoric pastoral economies, herding strategies as well as funerary rituals.

In the last decades, several authors have reported statistics regarding the presence of nonhuman bones in forensic cases.

According to Bass and Driscoll (1983), in Tennessee, from 1971 to 1981, for a sample of 111 forensic cases involving unknown skeletal material, 20% turned out to be nonhuman. In the mid-nineties, Marks (1995) reported a raise in this percentage to approximately 30%. Ubelaker (2000) compiled a sample of 254 cases examined by T. Dale Stewart at the Smithsonian Institution in Washington, D.C., and noted the presence of nonhuman remains in 10% of the cases. Similarly, Falsetti (1999) noted that, among a sample of 999 forensic cases investigated by William R. Maples at the University of Florida, 11% turned out to be nonhuman. According to Grisbaum and Ubelaker (2001), 28% of cases out of 474 cases examined from 1962 to 1994 at the Smithsonian Institution, were characterized by the presence of nonhuman remains. Finally, a work by Pokines (2015) provided also statistics on the occurrence of the different taxa in 355 forensic cases involving nonhuman remains turned over to the OCME (Office of the Chief Medical Examiner) in Boston from 2011 to 2014 (Table 1.1). Cattle, white-tailed deer and pig were the most common taxa, representing almost ninety percent of the total. The majority of cases (84.8%) regarded a single taxon, represented by postcranial elements (94.1%). With regard to the developmental age, fifty-one percent of cases consisted of adult individuals only, followed by juvenile individuals (23.4%), and bones in both adult and juvenile stages of development (9.3%). For the remaining 16.3% of cases the developmental age was not determined.

Common Name	Taxon	Number of Cases	% of (n=355) Cases
Cattle	*Bos taurus*	105	29.6
White-tailed deer	*Odocoileus virginianus*	104	29.3
Pig	*Sus scrofa*	93	26.2
True seals	Phocidae	24	6.8
Unknown large bird	Aves	22	6.2
Chicken	*Gallus gallus*	19	5.4
Sheep/goat	*Ovis aries/Capra hircus*	15	4.2
Dog	*Canis familiaris*	14	3.9
Unknown mammal	Mammalia	12	3.4
Geese and swans	Anserinae	7	2.0
Cat	*Felis catus*	6	1.7
Bony fish	Osteichthyes	5	1.4
Turkey	*Meleagris gallopavo*	4	1.1
Black bear	*Ursus americanus*	3	0.8
Sea turtle	Chelonioidea	2	0.6
Horse	*Equus caballus*	2	0.6
Mute swan	*Cygnus olor*	2	0.6
Rat	*Rattus* sp.	2	0.6
Woodland vole	*Microtus pinetorum*	1	0.3
Leatherback turtle	*Dermochelys coriacea*	1	0.3
Oceanic dolphin	Delphinidae	1	0.3
Snake	Colubridae	1	0.3
Gull	Laridae	1	0.3

Table 1.1 – Frequency of taxa identified among 355 forensic cases turned over to the Office of the Chief Medical Examiner in Boston from 2011 to 2014 (from Pokines 2015)

Although the amount of cases involving nonhuman remains is influenced by several extrinsic factors, such as the local geography and fauna, and the public sensitivity of the forensic significance of skeletal material (Franklin and Marks 2017), this data highlights the importance of forensic practitioners with an adequate training in nonhuman bone identification in order to achieve a faster case resolution (Pokines 2015).

In fact, although one may think that any competent physician can easily determine whether or not skeletal remains are of human origin, very few medical examiners have a training in distinguishing human from nonhuman bones (Cattaneo 2007; Ubelaker and

Scammell 1992). In this regard, analysts with a training in human osteology and comparative anatomy, such as forensic anthropologists can provide a precious contribution in assessing the origin of unknown skeletal remains (Cattaneo 2007).

If bones are preserved in their integrity, a well-trained forensic anthropologist/bioarchaeologist can usually discriminate between species by the assessment of gross morphology, given the inter-species variation of skeletal characteristics (Saulsman *et al.* 2010; Hillier and Bell 2007). On the contrary, when severe fragmentation, burning and/or commingling occur, such as in the event of mass disasters, in which a wide range of extreme forces can be involved such as heat, crushing (e.g. structure collapse), impact, explosion and environmental influences (e.g. animal scavenging, temperature, humidity), determining the human or nonhuman origin of the skeletal remains may not be straightforward (Blau and Briggs 2011).

In this regard, the Bretón case provides a good example which highlights the importance of species discrimination in forensic context (Albert, 2012$_{a,b}$; Albert 2013). On October 8$_{th}$, 2011 José Bretón, an unemployed former army driver, claimed to the police that his two children José (six years old) and Ruth (two years old), had been kidnapped at a park in Córdoba. During the interrogation, the investigators noted several inconsistencies in his story and arrested him as a suspect. A police investigation on a property belonging to Bretón's parents, led to the discovery of severely fragmented and burnt bones which were identified as non-human by a physician of the scientific police. For months, Bretón's ex-wife insisted that the man had kidnapped or killed the children to take revenge of her leaving him. Almost a year later, further examinations of the remains by two forensic anthropologists refuted the first diagnosis and determined that the bones and teeth were of human origin and belonged to a child aged between two and three, and a child aged

about six. In the light of this new evidence, José Bretón was condemned to twenty years in jail for each child. In this case, the determination of human origin of bone fragments was essential for the conviction of the murderer.

Another good example which underlines the importance of species discrimination of bone fragments regards the World Trade Center disaster, in which the collapse of the towers and the fire that burned at the site, caused an extremely poor condition of the remains and the commingling of thousands of human and nonhuman bone fragments, given that numerous restaurants were located in the area of the destruction (Mundorff 2014).

The first assessment of the remains after being recovered from the site of a mass disaster is generally called "triage" (Mittleman *et al.* 2000). An anthropologist or pathologist usually directs a triage team, but the composition of the team may varies depending on the type of disaster and the condition of the remains. The main role of the triage team is to sort out the material before processing it through the disaster morgue. This includes several tasks, such as reassociate separate pieces within a body or identify and discard nonhuman remains (Mundorff 2014; Sledzik *et al.* 2009). Since these tasks require a thorough knowledge of human and nonhuman osteology, the triage team is more effective when directed by an anthropologist (MacKinnon and Mundorff 2006; Byrd and Adams 2003).

When extreme fragmentation occurs, species discrimination of skeletal remains by macroscopic analysis may not be exploitable, thus bioarchaeologists and forensic anthropologists must turn to other methods, such as biomolecular analysis, chemical analysis and histological analysis (see paragraph 1.2).

The research presented in this thesis focuses on the microscopical architecture of bone tissue in human and pig (*Sus scrofa*) from both a qualitative (histomorphological) and quantitative (histomorphometric) perspective. Despite the plethora of studies on bone histology in different mammals (see Chapter 3), quantitative data available to perform species discrimination by histological analysis is still scarce. Moreover, those investigations generally focused on some specific bones (e.g. femur, rib) without considering the possible intra- and interspecies variability of bone microarchitecture between different bones of the skeleton.

This research make a significant contribution to knowledge of bone histomorphology and histomorphometry in human and pig since it represents the first attempt in investigating the variability of bone microarchitecture along the entire human and pig skeleton and provides new insight for species discrimination from a histological perspective.

1.1 THESIS OUTLINE

This thesis presents the results of a histomorphological and histomorphometric analysis of bone tissue in human and pig (*Sus scrofa*) at different stages of skeletal maturity, within the context of species discrimination of skeletal remains.

An overview of bone from a histological perspective is introduced in chapter 2. The current knowledge of bone histomorphology and histomorphometry in the context of species discrimination and the rationale of the present research are presented and discussed in chapter 3.

The research hypotheses and aims are presented in chapter 4, whereas the materials and methods are introduced in chapter 5. Results are presented in chapter 6 and discussed in chapter 7 within the context of: describing general characteristics of human and pig bone from both a qualitative and quantitative perspective, the extent of intra-individual, intra- and inter-species variation, the interpretation of the observed variation from both a biological and biomechanical basis, the limitations of the histomorphometric analysis and, the implications of the results obtained during the research.

Chapter 8 presents the conclusions of the investigation, the contribution to knowledge deriving from the work and several suggestions for further research.

1.2 CURRENT METHODS FOR SPECIES DISCRIMINATION OF SKELETAL REMAINS

This section provides an overview of the methods currently used for species discrimination of skeletal material and highlights benefits and limitation of each method.

When compared to other species, humans are characterized by different growth patterns, nutritional requirements and mechanical strain and such differences are reflected in the skeleton at different scales, ranging from gross morphological and microstructural characteristics to chemical and molecular composition (Mulhern and Ubelaker 2012).

Currently, there are several approaches to address the issue of species discrimination: macroscopic, histological, biomolecular and chemical analysis.

1.2.1 MACROSCOPIC ANALYSIS

When skeletal remains are well-preserved, and their integrity has not been compromised, a well-trained anthropologist with a background in physical/biological/forensic anthropology can usually easily perform species discrimination based on macroscopic analysis (Hillier and Bell 2007). Comparative anatomy, in fact, allows discriminating between human and non-human bone by the examination of gross morphological characteristics (France 2009, 2011, 2017; Adams and Crabtree 2008).

The shape of animal bones is mainly influenced by the type of locomotion and the bone specific function. For example, bovines such as cow and buffalo do not need to move quickly, and their skeleton must support a massive body mass. Therefore, their bones are

considerably larger and more robust when compared with small mammals such as dogs and cats which are fast runners (France 2011).

As regard the vertebral column, humans and nonhumans have generally the same number of vertebrae but the shape of their vertebral bodies as well as that of the column clearly differ between the two. The human vertebral column has an S-shape whereas quadrupeds has a single curve from the neck to the pelvic girdle. Human vertebrae resemble a wedge and their bodies become larger from the neck towards the pelvis due to the progressive increase in weight which they must support; on the contrary quadrupeds have more elongated and cylindrical vertebral bodies which are similar in length in the different regions of their body (France 2009). Moreover, since quadrupeds need to bear the weight of their head, the nuchal musculature is well-developed and therefore, the area of muscle insertion along the spine (spinous process) are very large compared to the overall size of the vertebral body (Fig. 1.1). The same applies to the occipital region of the cranium in which large neck muscles are attached holding the head up against gravity. On the contrary, in humans, the bipedal locomotion implies that the cranium needs to be balanced atop vertebral column. For this reason, in humans the foramen magnum is located under the cranium whereas in quadrupeds is located more posteriorly (Russo and Kirk 2013; France 2011).

Figure 1.1 – Spinous process of thoracic vertebra in bison (left) and human (right) (from France 2009)

The locomotion affects also the morphology of the pelvis which is long and narrow in quadrupeds whereas in bipeds it is shorter and wider.

Concerning long bones, differences between human and nonhuman bones are particularly evident in the areas of muscular and tendon attachment given the different locomotion patterns and different center of gravity (France 2011; Komar and Buikstra 2008). In quadrupeds, in fact, the center of gravity tends to be closer to the forelimbs. As a consequence, their forelimbs and hindlimbs are almost of equal length while in humans the forelimbs are significantly shorter than the hindlimbs.

Generally, the articular surfaces of long bones (epiphyses) are particularly useful to distinguish between human and nonhuman. The epiphyses are usually more sculpted in quadrupeds than in humans (Fig. 1.2), as the former need more power to their legs in order to support their weight (Komar and Buikstra 2008).

Figure 1.2 – Femoral distal epiphysis in human (left) and moose (right) (from France 2009)

Unlike humans, large quadrupeds have no rotary motion of their feet since their radius and ulna fuse during growth and their fibula is considerably small (France 2008).

A recent study by Johnson and colleagues (Johnson *et al.* 2017) investigated the location and orientation of nutrient foramina in humeri and femora of human, pig and sheep by CT analysis. The authors pointed out that in human femora, nutrient foramina are located on the posterior bone surface whereas in pig and sheep they are found on the anterior bone surface. Similarly, human humeral nutrient foramina are found on the medial surface while in pig and sheep the nutrient foramina are located on the posterior bone surface. With regard to the orientation, pig and sheep femoral nutrient foramina have a distal directionality whereas human nutrient foramina have a proximal directionality. Both human and sheep humeral foramina have a distal directionality while in pig they are transversally oriented.

Macroscopic analysis guarantees a good ability to discriminate between species and a considerable advantage, in terms of cost, over other methods. Nonetheless, in case of fragmentary and/or severely degraded bones due to taphonomic alterations or in the event of mass disasters (e.g. structure collapse, plane crash, explosions), macroscopic analysis is not helpful (Cattaneo *et al.* 1999; Hillier and Bell 2007; Martiniaková *et al.* 2006a).
It is necessary to keep in mind that not all the surface of a bone is significant for species discrimination. Usually, a possible confusion in species discrimination may arise with fragments of the diaphysis of long bones or carpal and tarsal bones which are very similar between several mammals (e.g. human vs bear or human vs pig), especially in the case of juvenile individuals in which the epiphyses are still not fused (Byard *et al.* 2001).

Even species discrimination of fragments of the cranium may be problematic: fragments of dog nasal bone are quite similar to the corresponding human bone. Similarly, bone fragments of juvenile mammals or large birds might be confused with human infants, as well as bone fragments of small birds may resemble bones of a newborn (Cattaneo and Grandi 2004). As a general rule, in case of small fragments, the thickness of cortical bone might help, since in human bone, it generally not exceeds 25% of the entire cross-sectional (Croker *et al.* 2009). However, a recent study by Rerolle and colleagues (2013), which investigated the possibility to use the corticomedullary index (CMI) of long bones to distinguish between human and nonhuman bones, reached a correct evaluation for only 22.6% of the study sample.

Finally, even species discrimination of teeth can be particularly challenging. Bovine and ovicaprid incisors, especially when worn or damaged, have a morphology which is very similar to that of human incisors. Likewise, pig lower fourth premolar can be easily confused for a human upper third molar (Hillson 2003; Cattaneo and Grandi 2004).
Thus, the discrimination of human from nonhuman teeth requires the expertise of a physical anthropologist or anatomist. When skeletal remains are highly fragmented lacking any diagnostic feature, one may turn to other methods such as biomolecular or histological analysis.

1.2.2 BIOMOLECULAR ANALYSIS

When macroscopic analysis is not exploitable due to a high fragmentation of skeletal remains, DNA analysis represents the most powerful tool for species identification. It consists in the extraction and identification of species-specific molecules with the aid of biomolecular techniques in order to match an unknown evidence sample to a known reference sample (Dawnay *et al.* 2007).

Despite recent advance in in the branch of molecular biology (e.g. DNA sequencer, the use of PCR), there are three technical problems that often afflict genetic investigations on skeletal material: degradation, contamination and the extraction problem (Siriboonpiputtana *et al.* 2018).

As the decomposition processes progress, or after exposure to atmospheric agents (e.g. water, fire), the deoxyribonucleic acid chain may undergo degradation undermining the analysis of the genetic region useful for species diagnosis (Cattaneo *et al.* 1999; Hansen *et al.* 2017). There are, in fact, few studies reporting successful extraction of amplifiable DNA and species-specific proteins from burned or ancient cremated bones (Cattaneo *et al.* 1992a; Cattaneo *et al.* 1994; Brown *et al.* 1995; Sajantila *et al.* 1991).

The issue of degradation can be partially solved by using mitochondrial DNA (mtDNA) instead of nuclear DNA, as the former is present in a higher number of copies per cell. Moreover, mitochondrial molecules are characterized by a circular shape which hinder its degradation and therefore increases the possibility of acquiring results from degraded DNA samples (Pereira *et al.* 2010).

As regards contamination, it is essential to put in place preventive measures to avoid it, given the extreme sensibility of genetic techniques, even if reliable results can be achieved even in the presence of low levels of contamination (Carracedo *et al.* 2000).

The last problem concerns the affinity that DNA has for the inorganic component of calcified tissues, in particular for hydroxyapatite (Pagan *et al.*, 2013; Marshall *et al.* 2014). The physical and chemical properties of bone constitute a barrier that make it resistant to degradation but, at the same time, obstruct the access of reagents in the extraction process (Davoren *et al.* 2007; Pagan *et al.*, 2013). Several extraction methods have been developed, whose purpose is to promote the splitting of the bond between DNA and hydroxyapatite (Köchl *et al.* 2005; Walsh *et al.* 1991; Marshall *et al.* 2014). One of the most used extraction methods involves the use of phenol-chloroform (Köchl *et al.* 2005) but it consists of several steps which make it time consuming, increasing the chances of contamination and, especially in case of degraded samples, it can provide inconsistent results (Pagan *et al.*, 2013; Pereira *et al.* 2010).

Other commonly utilized methods are the silica-based extraction protocol (Höss and Pääbo 1993) and the total demineralization method (Loreille et at. 2007) which both proved to be successful at extracting DNA from degraded bone samples.

In addition, immunological methods which allow to identify particular epitopes of species-specific proteins have proved to be successful in exploiting the antigen-antibody reaction in order to highlight the presence of human material. Lowenstein, during his studies on ancient bone (Lowenstein 1980; Lowenstein *et al.* 1981), pointed out that proteins such as collagen and albumin are species-specific, and they can be detected by using a protein radioimmunoassay (pRIA) technique which allows a high degree of reliability in discriminating between human and animal bone. Nonetheless, the number

of species for comparison is limited and diagenetic alteration of proteins in severely degraded skeletal remains might cause misidentification and cross-reactions (Potter *et al.* 2010).

Similarly, during a series of investigations by Cattaneo and colleagues (Cattaneo *et al.* 1990, 1992a, 1992b) human albumin was successfully identified in buried bone up to 4000 years old by enzyme-linked immunosorbent assay (ELISA) using monoclonal antibodies.

As regard collagen, Buckley and colleagues (2009) developed a new method to correctly identify bone fragments from several mammals by mass spectrometric analysis of genus-specific collagen peptides. The authors identified 92 peptide markers useful for species identification and asserted that, unlike DNA analysis, this method is not affected by contamination and guarantee good results also with archaeological bones. Notwithstanding, there is the need to test this technique also on bones coming from different burial environments and different taphonomic context since factors such as extreme pH are known to affect collagen survival (Collins *et al.* 2002).

In conclusion, although more research is needed, protein analysis seems to have a great potential for species discrimination, also considering that proteins resist better than DNA to many environmental factors (Cattaneo 2007). Nonetheless, the exposure of bone to high temperature may hinder the survival of the material useful for species identification. Indeed, an experimental study by Cattaneo and colleagues (1999) demonstrated that mitochondrial DNA and albumin did not survive in bone heated to temperature ranging between 800 °C and 1200 °C. In such case, histological analysis may be a better solution since bone microscopic structure proved to survive even after the exposure to high temperature (Cattaneo *et al.* 1999).

1.2.3 HISTOLOGICAL ANALYSIS

Histological analysis consists in the examination of bone thin sections, approximately 40-100 μm thick, in order to evaluate the microscopic structural architecture of bone tissue (histomorhology) as well as quantify the histological structures within the tissue (histomorphometry) (Hillier and Bell 2007). This approach is particularly useful for discriminating between human and nonhuman especially in case of bone fragments which have been affected by taphonomic alterations making macroscopic and biomolecular analyses not exploitable.

The first studies which compared bones of different species from a histological perspective, focused mainly on the histomorphological appearance of bone tissue. These investigations (Quekett 1849, Foote 1916, Enlow and Brown 1956, 1957, 1958) offered accurate descriptions of cortical bone tissue of various mammals but they lacked sufficient quantitative data.

At histological level, bone classification is based on the organization of the bone matrix (woven or lamellar bone), the type of vascularization (e.g. longitudinal vascular canals) and the type of bone deposition (primary or secondary; Fig. 1.3) (Cuijpers 2006; Francillon-Viellot *et al.* 1990).

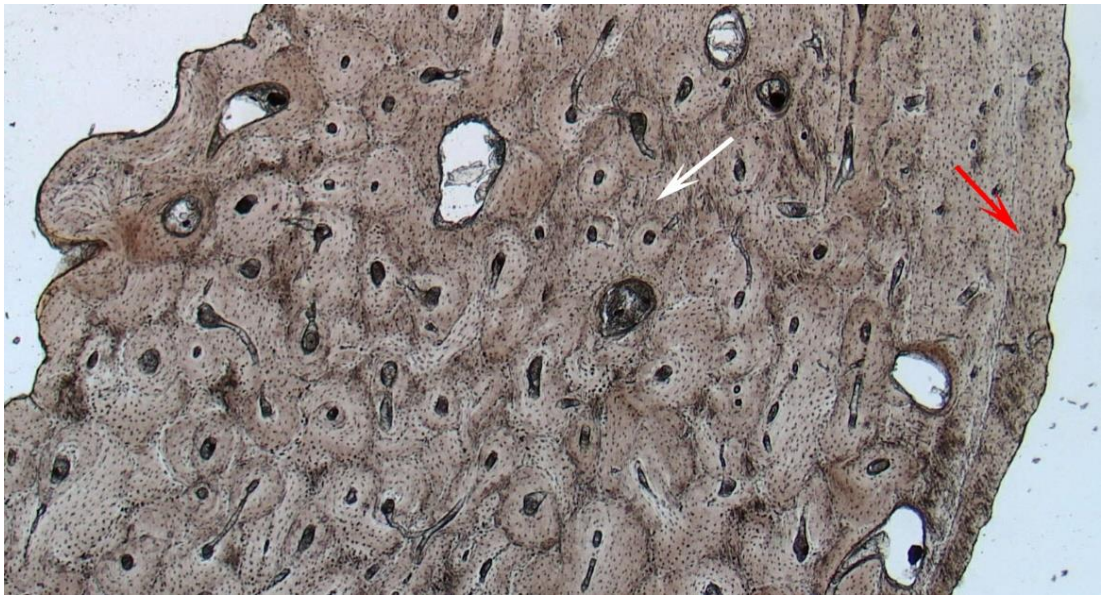

Figure 1.3 – Types of bone deposition in the tibia of a juvenile human individual: primary circumferential lamellar bone at the periosteal surface (red arrow) and Haversian bone in the middle cortex (white arrow)

According to literature, the orders Insectivora, Chiroptera, Monotremata, Rodentia and Edentata, and the Infraclass Metatheria are the ones that look less like human given the general absence of Haversian bone (Foote 1916, Enlow and Brown 1956, 1957, 1958). Only Rodentia show occasional presence of secondary osteons (Singh *et al.* 1974).

As regards the mammalian orders Lagomorpha, Perissiodactyla, Artiodactyla, Carnivora, Primates, Cetacea, Sirenia, Proboscidae and Xenarthra, they all show Haversian bone, although a great variability exists between the various taxa in the amount of the Haversian tissue and the size of structures (Foote 1916; Enlow and Brown 1958; Martiniaková *et al.* 2006; Stover *et al.* 1992; Mori *et al.* 2003, 2005; Cuijpers 2006; Mulhern and Ubelaker 2001; Rajtová *et al.* 1995; Morris 2007; Skedros *et al.* 2003; Diaz and Rajtová 1975; Georgia and Albu 1988; Hidaka *et al.* 1998; Przybeck 1985; Shaffer and Burr 1984; Singh *et al.* 1974; Pfeiffer 1996).

Large sized mammals generally exhibit plexiform bone (Fig. 1.4), a primary bone tissue characterized by alternating sheets of woven and lamellar bone. This type of tissue is

generally considered a nonhuman characteristic although it can be present also in human fetal bones (Enlow 1963; Caccia *et al.* 2016; Cuijpers 2006).

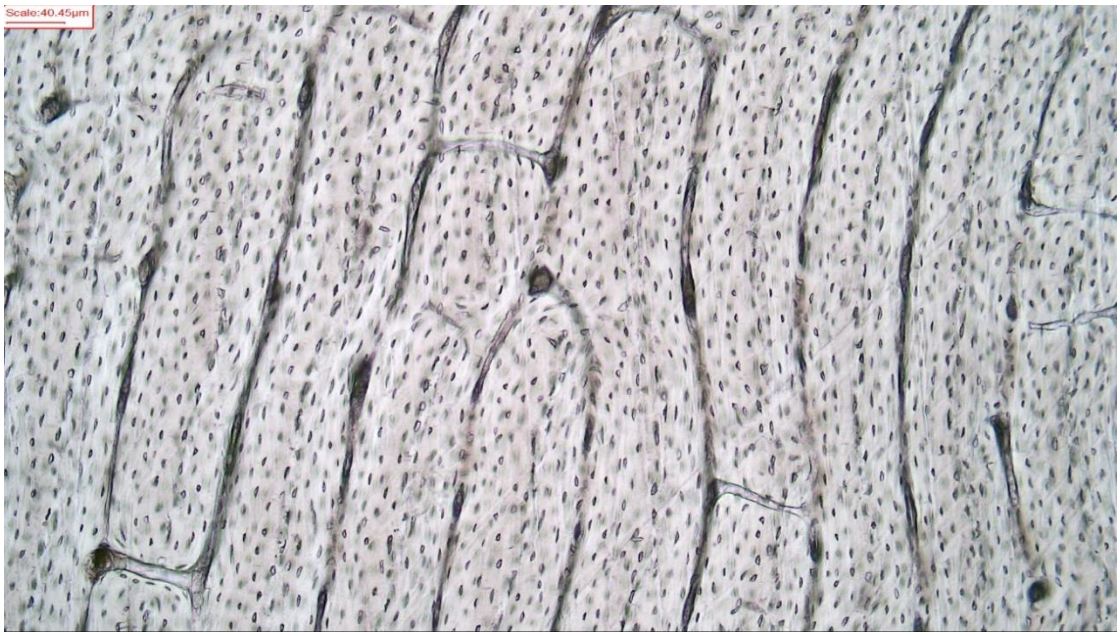

Figure 1.4 – Plexiform tissue in the humeral diaphysis of a calf, x100

Another common feature to distinguish between human and nonhuman bone regards the pattern of osteon organization, with a particular focus on the so called "osteon banding", a linear arrangement of primary or secondary osteons surrounded by lamellar or plexiform bone (Fig. 1.5). Mulhern and Ubelaker (2001) observed that osteon banding occurs more frequently in nonhuman bone tissue. In addition, the authors pointed out that osteon banding clearly differs between human and nonhuman bone since the former is characterized by short isolated rows of osteon whereas the latter consists in multiple consecutive bands. Nonetheless, there is the need for further research on the frequency of banding in younger human bone as well as in mature nonhuman bone.

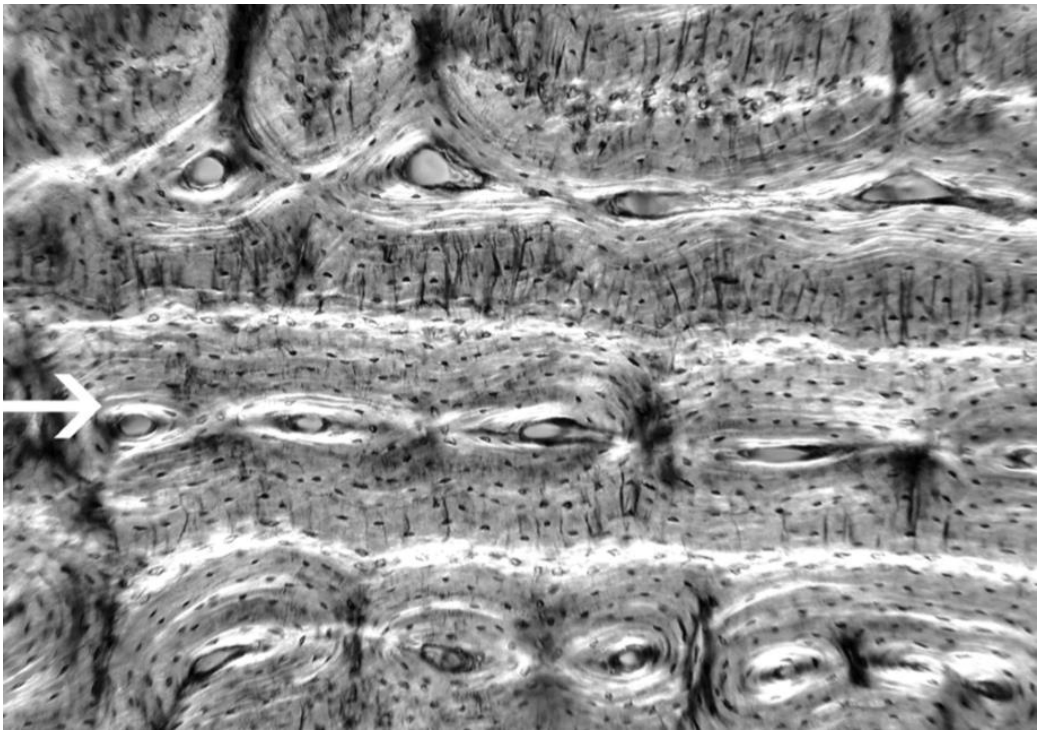

Figure 1.5 – Osteon banding in horse bone (adapted from Cuijpers 2008)

More recently, the advances in technology and the use of image software have allowed to undertake more extensive investigations on bone microscopic architecture also from a metric point of view. Quantitative studies generally included the size (diameter, perimeter and area) of secondary osteons and Haversian canals as well as osteon density (osteon/mm^2). The latter is not considered useful for species discrimination since it is known to be influenced by chronological age and the location within the bone (Mulhern and Ubelaker 2012).

According to literature, the most consistent distinguishing feature is the dimension of the Haversian canal, which is usually smaller in nonhuman taxa (Cattaneo *et al.* 2009; Martiniaková *et al.* 2006a; Urbanová and Novotný 2005). Cattaneo and colleagues (2009) were able to successfully discriminate between human and nonhuman bone developing an algorithm which however seem limited to adult long bones. Similarly, Martiniaková and colleagues (2006a) utilized a discriminant function analysis based on osteon

parameters in different species achieving a correct assessment for 76.2% of the study sample.

Another new line of research focused on osteon circularity to discriminate between human and nonhuman secondary osteons (Tersigni 2008; Crescimanno and Stout 2012; Dominguez and Crowder 2012; Keenan *et al.* 2017). Secondary osteons seem to be less circular in human bone compared to nonhuman bone, although the regression equations formulated by the authors appeared to be suitable only for adult long bones.

At present, despite bone histology has been explored since at least the seventeenth century (Havers 1691), no consensus has been reached among researchers on how to tackle the issue of species discrimination from a histological point of view. A combination of qualitative and quantitative analysis should be performed when trying to determine the origin of an unknown bone fragment (Hillier and Bell 2007).

However, it is fundamental to take into account the limitations of such approaches.

Many studies on bone histomorphometry are based on small sample sizes, with little or no information on the ages of the specimens, making it difficult to compare between the quantitative data available (Mulhern and Ubelaker 2012).

Moreover, the majority of investigations have been carried out on some specific elements (femur, tibia and rib) without considering the histomorphological and histomorphometric variability that may exist between different bones of the same skeleton and even different portions of the same bone (Enlow 1966). Frequently, in forensic and archaeological casework, the analyst has to deal with extremely fragmented skeletal remains without any clue about the bone to which they belong. Therefore, an in-depth knowledge on the morphological and metric intra-species variability of bone tissue is paramount in order to

ensure more reliable interpretations of the origin of unknown bone fragments by histological analysis.

Lastly, diagenetic alterations may affect the microstructural arrangement of bone and it is fundamental to be able to identify these alterations when performing any histological analysis (Hedges *et al.* 1995). The most common alterations to which bone is subjected are due to microbial attack and fire. Various environmental factors, such as temperature and soil pH, can cause the dissolution of bone's mineral phase, exposing collagen to microbial enzymes (e.g. collagenase) which digest bone collagen and open a passage for microbial attack. The peculiar bone destruction caused by these bacteria is known as "tunnels" or "boring" and can hinder any histological analysis (Jans *et al.* 2004)

With regard to fire, several studies have investigated its effect on bone microstructure (Bradtmiller and Buikstra 1984; Shipman *et al.* 1984; Nelson 1992; Cattaneo *et al.* 1999) Heat can cause the mineral component to melt and recrystallize with significant modifications of the microstructure architecture of bone, including blurring of the individual lamellae and osteon shrinkage (Nelson 1992). However, there is a general agreement among researchers that shrinkage is insignificant up to 800 °C and the histomorphological appearance of bone tissue can still be used for species discrimination (Cattaneo *et al.* 1999).

1.2.4 OTHER ANALYSIS

In the last decades, several researchers have investigated the possibility to use the elemental composition of bone to discriminate between species (McLaughlin and Lednev 2012; Bratter *et al.* 1977; Biltz and Pellegrino 1969; Aerssens *et al.* 1998).

At present, among chemical analyses, Raman spectroscopy seems to have the better potential (Zimmerman *et al.* 2014). Raman spectroscopy is a non-destructive analytical technique which uses a monochromatic laser beam with a wavelength in the visible, near infrared, or ultraviolet to irradiate a sample. The laser interacts with the molecules of the sample, producing a scattered light whose photons have a higher or lower energy than those of the incident photons. This shift in energy is used to generate a Raman spectrum which provides quantifiable information on the composition and molecular structure of the sample (Larkin 2011). In forensic context, this technique is commonly utilized for the identification of biomaterials such as bodily fluids and soft tissues (Virkler and Lednev 2009a,b; Edwards 2004).

In a recent investigation by McLaughlin and Lednev (2012), Raman spectroscopy was used in order to discriminate between bones of different species (chicken, turkey, cow and pig). Results of this research seem promising since the authors were able to successfully discriminate between the spectra of the four species. Nonetheless, there are several limitations regarding the study sample. The number of species is limited and consists of fresh bones from a grocery meat market. Taphonomic insults which may alter the composition of bone after death need to be investigated in order to standardize this method. In addition, there is the need to test this technique also on human bone, as well as adding more variables such as bone type and specimen age as they may give rise to changes in the bone composition.

Another analytical technique for the characterization of materials is the laser-induced breakdown spectroscopy (LIBS) which was recently used both in forensic and archaeological context for paint and glass analysis (Sigman 2010; Bridge *et al.* 2007), trace element analysis of human teeth (Alvira *et al.* 2010), the analysis of cremated remains (Martin *et al.* 2007) and differentiating between human and nonhuman bone (Collins and Vaas 2003; Vass *et al.* 2005). Like Raman spectroscopy, LIBS involve the use of a short laser which forms, on the surface of the sample material, a highly energetic plasma which contains excited atoms and ions. Once the laser pulse ends, the plasma on the surface starts to cool, returning to the ground state and emits a radiation with a specific wavelength. The emitted radiation from the plasma is collected analysed by a spectrograph detector module which identifies the elemental composition of the sample material (Singh and Rai 2011).

This technique has several advantages such as minimal destruction, it allows a rapid data collection and it requires no sample preparation. Unfortunately, detection limits and precision are lower as compared to other conventional techniques (Singh and Rai 2011)

More recently, Becket and colleagues (Beckett *et al.* 2011) investigated the variation of bone mineral (b-HAP) behaviour upon heating by X-ray diffraction analysis (XRD). This technique employs x-ray diffraction patterns to obtain the three-dimensional structure of crystalline solids (Waseda *et al.* 2011). The authors exploited the changes to bone mineral on heating given their dependence on the composition and the structure of bone. Twelve species, including human, were analysed in this study, demonstrating a significant inter-species variation in terms of at least one bone mineral characteristic. Nonetheless, there is the need for further research on pathological bone (e.g. osteoporotic bone) and on the effect of taphonomic alterations which may affect bone mineral crystallinity (Beckett *et al.* 2011).

CONCLUDING REMARKS

At present, despite a plethora of studies on species discrimination in the field of forensic anthropology and archaeology, there are no guidelines on which technique the analyst should use when trying to identify skeletal remains of unknown origin.

Some techniques such as the histological and DNA analysis have been deeply explored in the last decades; others, such as chemical analysis have been employed for species discrimination only recently and need further research. Each technique has its own benefits and limitations (Table 1.2).

Ideally, non-destructive analysis such as macroscopic analysis should be preferred but in case of highly fragmented or severely degraded remains, it is necessary to turn to other methods. On one hand, DNA analysis proved to be the most powerful tool but has limitations especially regarding degradation and contamination; on the other end, proteins demonstrated a better resistance to degradation compared to DNA, but immunological techniques still need to be tested on a wider range of species as well as in different taphonomic conditions.

Despite the great potential for species discrimination, the histological analysis has some limitations. Most of the studies on bone microscopic structure in different mammals focused only on some specific bones (femur, tibia, rib) without taking into consideration the intra-species variability which may exist in different bones of the same individual and even in different portion of the same bone. Moreover, there is still a paucity of data regarding juvenile individuals.

Finally, the potential of chemical methods to discriminate between human and nonhuman bone has been tested only recently. Although the results obtained with these techniques seem promising, there is the need to test different variables such as bone type, gender, age, pathology and different taphonomic conditions since they may alter the reliability of these techniques.

Macroscopic analyses	Benefits	Limitations
Gross morphological characteristics	• Non-destructive • Fast technique • Does not require sample preparation • Several atlases that aid species identification • Sometimes can be done remotely via photographs	• Difficult with highly fragmented and/or severely degraded bones
Corticomedullary index (CMI)	• Non-destructive • Does not require sample preparation	• Poor results in discriminating between species given the high intra- and interspecies variation • High variability of CMI within the length of the bone • No reference database available
Nutrient foramina location and orientation	• Non-destructive • Does not require sample preparation	• Limited sample size • Few species investigated • Does not consider juvenile individuals and variation in the position of nutrient foramina
Biomolecular analyses	**Benefits**	**Limitations**
DNA analysis	• Extremely sensitive • Wide reference sample of species-specific molecules • Minimally destructive	• Degradation of DNA due to taphonomic alterations (e.g. fire) • Possible contamination • Difficult extraction procedures • Cost
Protein radioimmunoassay (pRIA)	• High degree of reliability in species discrimination	• Limited number of species for comparison • Diagenetic alterations of proteins might cause misidentification • Requires specialized equipment and substances
Enzyme-linked immunosorbent assay (ELISA)	• High level of specificity and sensitivity • Albumin was detected in buried bone up to 4000 years old • Not affected by the physical integrity of the skeletal material • Can detect extremely small amounts of protein (10ng) • Not affected by contamination	• Mainly tested on human material. Monoclonal antibodies against the albumin of other species need to be tested • The success of antigen detection depends on the amount of material available • Need for further research on the effect of different taphonomic conditions on the survival of specific antigens
Mass spectrometric analysis	• Good survival of collagen peptides in archaeological samples • Not affected by contamination • Tested on fifty-one species	• Need for further research on the temperature at which the collagen starts to break down • Need to be tested on bones coming from different taphonomic context (e.g. extremes of pH) and different burial environments

	• Allow to discriminate to the level of family	
Histological analyses	**Benefits**	**Limitations**
Histomorphology	• Cheap and easy technique • Good preservation of bone structure in archaeological bones • Exploitable also in burned bone	• Some species share common microscopic architecture of bone tissue • More research is needed on the intra-species variability and on juvenile individuals • Microbiological attack may hinder the analysis
Histomorphometry	• Cheap and easy technique • Good preservation of bone structure in archaeological bones • Haversian canal dimension has a great potential in discriminating between human and non-human bone	• Overlap between osteon dimensions in different species • Most of the studies focused on some specific bone (femur, tibia, rib) with limited sample sizes • More research is needed on the intra-species variability and on juvenile individuals • Heat can cause the shrinkage of bone structures
Chemical analyses	**Benefits**	**Limitations**
Raman spectroscopy	• Non-destructive • Does not require sample preparation	• Tested on a limited number of species • Need to test different variables (bone type, gender, age) • Taphononic alterations may affect bone composition
Laser-induced breakdown spectroscopy (LIBS)	• Minimal destructivity • Does not require sample preparation • Rapid data collection	• Lower detection limits and precision compared to other conventional methods
X-ray diffraction analysis (XRD)	• Excellent potential in species discrimination of heated bone	• More species need to be added to database • Need to be tested on pathological bone (e.g. osteoporotic bone) • Taphonomic alterations may affect bone mineral crystallinity

Table 1.2 - Benefits and limitations of the current methods of species discrimination of skeletal material

1.3 FORENSIC CASEWORK INVOLVING HUMANS VS NONHUMAN BONE DISCRIMINATION

In this section, a number of examples have been selected from the literature which highlights the importance of discriminating human from non-human bone. Although these examples emphasize the excellent potential of the histological analysis as a tool for species discrimination, there are still many aspects of human and non-human bone histology which need further research.

1.3.1 BONE FRAGMENT FROM ALASKA

In the early 1990's, the FBI received a fragment of bone from Alaska (Fig. 1.6) with a deeply imbedded metal plate, which had been screwed into the midshaft to correct a pseudoarthrosis long before death given the extensive bone remodeling (Ubelaker and Scammell 1992). The evidence for surgery led local authorities to advance the hypothesis of human origin. The fragment was then analyzed by almost every orthopedic surgeon in Alaska but none of them recognized it as his work. Afterwards the bone was sent to the Smithsonian Institution where a sample of bone was taken in order to prepare a thin section to be analyzed at the microscope. The section revealed a pattern of osteon organization, consisting in linear rows of osteons (osteon banding) surrounded by lamellar bone which was compared with a known dog bone exhibiting a similar pattern. It was concluded that the bone belonged to a large dog and that a veterinary mended the pseudoarthrosis with the metal prosthesis (Ubelaker and Scammell 1992; Mulhern and Ubelaker 2001). This case showed the usefulness of the histological analysis in

discriminating between species when a macroscopic assessment based on gross morphological characteristics is not exploitable.

Figure 1.6 – Dog bone with a metal prosthesis which has led to initial misinterpretation during an FBI case (Christensen *et al.* 2014)

1.3.2 BONE FRAGMENTS IN A CAR: DISCRIMINATING BETWEEN HUMAN AND DEER

A summary of a case taken from Owsley and colleagues (1985) dating back to the mid-eighties is provided below.

The decomposed body of a middle-aged female was found on the Mississippi River bank in Louisiana. The autopsy revealed two wounds by shotgun blasts, one on the right side of the chest and the other on the left side of the head. Both blasts provoked extensive fractures of the cranial bones and the humerus. Part of the humeral diaphysis was missing. A suspect was charged with the crime by the investigators, who believed that the man shot the victim on the passenger seat of his car, and then washed the latter at a local gas station. Inside the car of the suspect, blood, tissue and a total of four tiny bone fragments

were found. A subsequent search at the gas station led to the discovery of other two bone fragments. Among all the fragments, no one were identified as belonging to the skull. Three fragments were from a long bone as they showed a clear periosteal and endosteal surface. Unfortunately, none of these fragments could be joined to the fractured humerus of the victim, although the cortical thickness was compatible.

During the interrogation, the suspect justified the presence of blood and bone fragments in his car, asserting to have hit a deer and put it in the car to avoid detection.

Therefore, a comparative histological analysis was performed in order to assess whether the microscopic appearance of the unknown bone fragments corresponded that of a deer bone or if it matched with the victim's bone sample taken during the autopsy.

Thin-sections of a deer humerus, the unknown bone fragments and the bone sample from the autopsy were analyzed at the Department of Anthropology of the University of Massachusetts. Osteon density and Haversian canal diameter were measured in order to make a morphometric comparison between the specimens. Ventral and medial aspects of deer humerus consisted in plexiform bone without any secondary osteons and were consequently excluded from the analysis. The rest of the cortical bone showed the presence of solely tightly packed primary osteons, uniform in size and shape. On the contrary, both the bones from the vehicle and the gas station, as well as that from the autopsy showed no plexiform bone and the presence of secondary osteons and osteon fragments. Osteon density in deer bone was higher than all the other bones and Haversian canal diameters were significantly smaller in deer when compared to those of the victim and the unknown bones. Few days before the trial the suspect confessed the murder.

In this case, the histological analysis proved to be particularly useful in discriminating between species as the unknown bone fragments, unlike those of deer, showed a

microscopic architecture which was consistent with that of the victim from both a qualitative and quantitative perspective.

1.3.3 BURIED BODY IN THE NORTH OF ITALY

The following example was taken from a report on a casework addressed by the forensic team of LABANOF laboratory in Milan.

In 2011, in a wooded area in the North of Italy, the confession of a murderer led to the discovery of a clandestine burial. The perpetrator confessed to the police to having beheaded the victim after having shot him. After the excavation, the skeletal material was transported to LABANOF (Laboratory of Forensic Anthropology and Odontology) for the anthropological analysis.

Several nonhuman bones were successfully identified and discarded with the exception of a rib fragment (Fig. 1.7) for which it was not possible to make a diagnosis of species by the assessment of gross morphology. Therefore, an undecalcified thin section of the rib fragment was prepared in order to perform a histological analysis.

The histomorphological analysis revealed a bone tissue composed of Haversian bone which could not completely exclude a nonhuman origin of the fragment. Results of a subsequent histomorphometric analysis has made the anthropologists to lean for a human origin of the fragment since the values of Haversian canal area were compatible with those reported in literature on the size of human secondary osteons.

In that case, the identification of that fragment as human had a particular value as it showed signs of sharp wounds which indicate that the murderer had also stabbed the

victim. This, obviously, represents an information which can have important repercussions during the trial.

Figure 1.7 – Rib fragment with signs of sharp wounds

CONCLUDING REMARKS

This section presented three forensic scenarios which involved the use of histological analysis to discriminate between human and nonhuman fragmented skeletal remains.

In the first case the histological analysis allowed to avoid further investigations, contradicting the first hypothesis on the human origin of the bone fragment.

In the second case, the results of the analysis helped to refute the testimony of the suspect, proving that the microscopic structure of the bone fragments was not compatible with that of a deer. In the latter, determining the human origin of the rib fragment had a significant repercussion during the trial given the presence of sharp wound which added more information on the dynamics of the murder.

CHAPTER 2
BONE

In order to have an easier comprehension of the issues addressed in the following chapters, it is worth introducing bone from a histological perspective. This chapter provides an overview of the different types of tissues and structures of which bone is composed, how they form and the relationship between bone microscopic structure and its physical properties.

2.1 BONE MODELING AND REMODELING

From a histological perspective, bone is governed by the collaborative activity of cells. There are four kinds of cells involved in the formation and development of bone tissue: osteoprogenitor cells, osteoblasts, osteocytes and osteoclasts (Majeska 2001).

Osteoprogenitor cells originates from primitive mesenchymal stem cells in the bone marrow and are able to differentiate into chondroblasts (cartilage cells) or osteoblasts (bone cells) depending on the signaling molecules they are exposed to (Zoetis *et al.* 2003).

Osteoblasts are mononucleated cells which originate from local mesenchymal stem cells and are responsible for bone formation. Their main function is to synthesize type I collagen, proteoglycans and glycoproteins which serve as a template for the following deposition of crystals of hydroxyapatite (Reid *et al.* 2011).

In skeletally mature adult bone tissue, osteocytes are the most abundant cell type of bone. They arise from osteoblasts that become encased in bone matrix during bone formation (Zerwekh 1992; Freemont 1993).

Osteoclasts are large multinucleated cells which originate from hematopoietic mononuclear cells in the bone marrow. They closely adhere to the bone surface and are primarily responsible for bone resorption by secreting acid and proteases which dissolve bone mineral and destroy the organic matrix (Lowe and Anderson 2015).

Given the mineralized nature of bone, the result of the activity of these cells is encrypted in bone histomorphology and regards two distinct processes, namely "modeling" and "remodeling" (Enlow 1963; Stout and Crowder 2012).

Bone modeling is related to the changes in the biomechanical environment which occur during skeletal growth and consist in the adjustment of the amount and spatial distribution of bone tissue by adding or removing bone from periosteal and endosteal surfaces (Gosman 2012)

On the contrary bone remodeling is a continuous process throughout the life of an individual which modifies material organization of the bone and is responsible for its distinctive histomorphological features as well as its mechanical properties (e.g. resistance to fatigue failure) (Martin *et al.* 2015). Older bone is replaced by the combined activity of osteoclasts (bone-resorption) and osteoblasts (bone formation) which together constitute the basic multicellular unit (BMU), the activity of which leads to the formation of the basic structural unit (BSU), namely Haversian system or secondary osteon (Frost 1973). Remodeling exists in two basic forms: stochastic and targeted (Burr 2002; Parfitt 1983). Stochastic remodeling serves metabolic function and retain bone integrity and

homeostasis within the matrix; targeted remodeling serves a repairing function in the occurrence of microdamage in bone (Burr *et al.* 1985).

The entire process can be divided into three distinct phases: activation, resorption and formation (ARF) (Stout and Crowder 2012). Osteocyte is responsible for the activation phase by responding to systemic and biomechanical factors (Schaffler and Kennedy 2012). Osteocytes, in fact, constantly send signals that hinder the activation of the basic multicellular unit (BMU) of remodeling (Stout and Crowder 2012). The disruption of the canalicular connections between osteocytes due to microfractures or osteocytes apoptosis, provides the stimulus to trigger the remodeling process (Parfitt 2005; Martin 2000; Frost 1985).

Osteoclasts remove existing bone to create a resorption space or cutting cone with an approximate diameter of 150-350 μm (van Oers 2008). A group of mononuclear cells lining the edges of the resorptive bay smooth off the rough edges of its periphery and deposit a thin layer of matrix called reversal line or cement line which represent the cross-sectional size of the secondary osteon and separates it from the surrounding interstitial lamellae (Robling *et al.* 2006; Everts *et al.* 2002). After the resorption phase, osteoblasts begin to deposit the organic matrix called osteoid, which consists of type I collagen, proteins and water (Martin *et al.* 2015). Starting from the edges of the resorptive bay and moving to the center of the tunnel, the new matrix is laid down in concentric lamellae leaving a central canal, which house nerves and blood vessels called Haversian canal (Stout and Crowder 2012). When this process is over osteoclasts and some osteoblasts undergo apoptosis while the remaining osteoblasts have two possible fates: they can become trapped in the bone matrix becoming osteocytes or they become flattened bone lining cells (BLC) which line bone surfaces (Stout and Crowder 2012). They both play a fundamental role in bone metabolism (Nijweide *et al.* 2002).

2.2 BONE MICROARCHITECTURE

Although bone histology has been deeply explored since the first research of Clopton Havers (1961) at the end of seventeenth century, there is still a lack of consensus regarding the classification and the terminology to be used when describing the histomorphology of bone tissues.

Some tissue types are often described incorrectly or wrongly identified (Locke and Dean 2003; Locke 2004), such as plexiform bone vs laminar bone.

Recently Cuijpers (2006) has developed a classification system that takes its cue from a previous work by Francillon-Viellot and colleagues (1990). This classification is based on three different criteria: a) the organization of the bone matrix; b) the type of vascularization; c) the type of bone deposition.

From this classification bone tissue is divided into primary and secondary bone.

Primary bone consists of new bone laid down in layers during the appositional growth and usually contains primary osteons which provide nutrients and aid the removal of toxins from the bone tissue (Francillon-Viellot *et al.* 1990; Malluche and Faugere 1990). Primary bone is then divided according to the composition of the bone matrix: non-lamellar and lamellar tissue (Fig. 2.1).

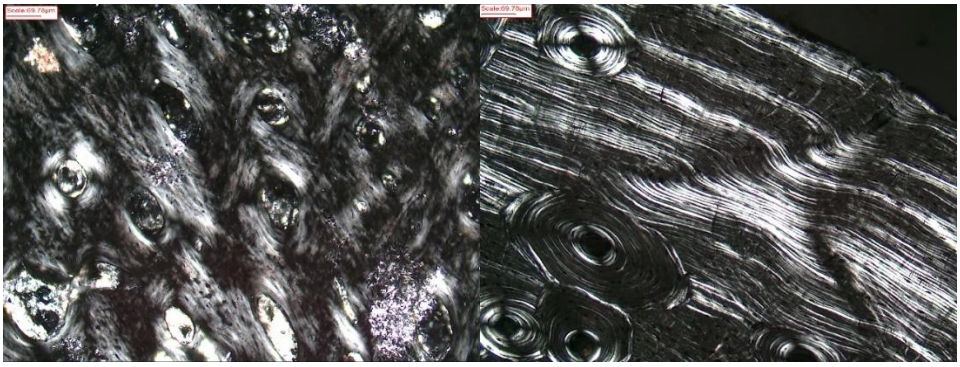

Figure 2.1 – Types of bone matrix: woven bone (left) and lamellar bone (right), x100. Polarized light

Non-lamellar tissue can be woven or parallel-fibered in composition. The former is characterized by randomly oriented collagen bundles (under polarized light it does not show birefringence as lamellar tissue). Generally, in this type of matrix, osteocyte lacunae are distributed more irregularly than those of lamellar bone (Enlow 1966; Francillon-Viellot *et al.* 1990). It is laid down at a rate of at least 4μm per day and it's associated with rapid osteogenesis, produced in periods of immediate need, such as embryonic growth, during repair processes and in response to pathological conditions (Martin and Burr 1989; Hillier and Bell 2007).

On the contrary, parallel-fibered bone consists of collagen fibers which are all oriented in the same plane, running parallel to each other (Enlow 1966; Francillon-Viellot *et al.* 1990).

Lamellar tissue is characterized by a bone matrix which consists of thin layers of lamellae successively laid down. Each lamella is composed of collagen fibers which have a different orientation compared to that of the fibers of the previous lamella (Enlow 1966; Currey 2012). This type of tissue has a high spatial organization due to the slower time of deposition (1μm per day) compared with non-lamellar bone tissue (Hillier and Bell 2007). When observed by normal light microscopy, lamellar and parallel-fibered tissue are difficult to distinguish. However, under polarized light, the former shows an alternation of bright and dark lamellae, whereas the latter looks homogenously bright or dark (Enlow 1966; Francillon-Viellot *et al.* 1990).

Lamellar bone comprises secondary bone, which substitutes existing bone, as well as primary bone, which is laid down ex novo on an existing bone surface.

The former is laid down in concentric layers by osteoblasts in order to form secondary osteons, whereas the latter is generally deposited in the endosteal and periosteal layers,

respectively in the form of inner and outer circumferential lamellae, and gradually replaces the natal woven bone (Mulhern and Ubelaker 2012). During the life of an individual, the outer circumferential lamellae undergoes remodeling more rapidly than the inner circumferential lamellae due to a higher stress along the outer surface of the bones compared to the inner cortex (Kerley 1965; Heller *et al.* 2001). As a consequence, inner circumferential lamellae can be found even in individuals approaching the fifth decade of life. Afterwards, this primary endosteal tissue is gradually removed by either remodeling or endocortical resorption (Maggiano *et al.* 2011)

Both the lamellar bone and the woven bone may lack vascularization (avascular tissue) or present various types of vascularization (Francillon-Viellot *et al.* 1990).

The vascular bone tissue is then divided into sub-categories based on the orientation and the nature (simple primary canals or primary osteons) of its vascular canals.

Primary osteons can be randomly scattered, organized in linear rows crossing the cortex (radial), or arranged in circumferential rows around the medullary cavity. In long bones, simple vascular canals can be either oriented parallel or perpendicular to the long axis of the bone (respectively longitudinal and radial vascular canals) or irregularly oriented (reticular).

The orientation of the vascular canals can be used also to describe another kind of primary bone called fibro-lamellar bone, which is a combination of woven and lamellar bone (Mulhern and Ubelaker 2012). It consists in alternating sheets of woven and lamellar bone and a large network of vascular canals. Fibro-lamellar bone is commonly found in large mammals, whose bones have to grow rapidly in diameter (Currey 2002; Hillier and Bell 2007; Cuijpers 2006). Indeed, the extensive vascularization allow a higher rate of deposition compared to lamellar bone. Fibro-lamellar bone is then divided into plexiform

and laminar bone (Fig. 2.2), according to the spatial arrangement of the vascular canals (Cuijpers 2006).

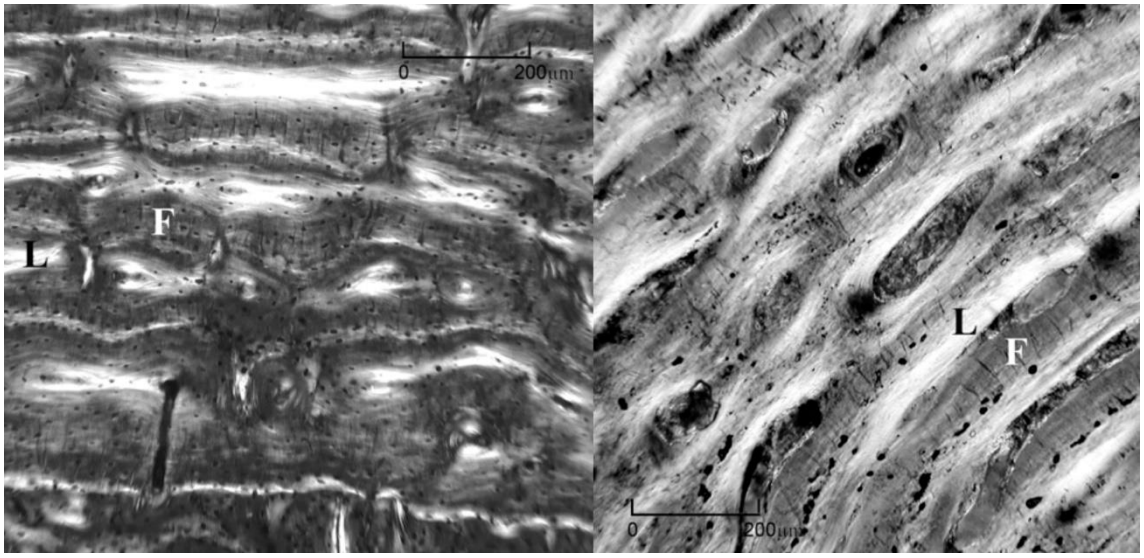

Figure 2.2 – Two types of fibrolamellar bone: plexiform bone (left) and laminar bone (right). F=fibrous component, L=lamellar component (adapted from Cuijpers 2009)

In the former, the vascularization consists of primary osteons interconnected by vascular canals oriented in three dimensions (longitudinal, circular and radial), resulting in a characteristic "brick-wall" appearance; the latter consists a two-dimensional network of vascular canals (longitudinal and circular), sandwiched between a series of bony laminae. Laminar bone is commonly found in ectotherms, due to their cyclical interruption of growth caused by metabolic changes (e.g. hibernation) (Currey 2002).

Unlike primary bone, secondary bone tissue is laid in areas where existing bone is reabsorbed by osteoclasts. It is characterized by the presence of secondary osteons which can be easily distinguished from primary osteons as they are bordered by a cement line (or reversal line), which is the outermost lamella (Francillon-Viellot *et al.* 1990; Currey 2002).

Secondary bone is then divided into subcategories according to the density of secondary osteons and their organization (Cuijpers 2006). In secondary bone tissue, Haversian systems can be scattered in a lamellar matrix (irregular Haversian bone; Fig 2.3b) or they can be tightly packed with few or no interstitial lamellae (dense Haversian bone; Fig. 2.3a). With increasing age, the entire cortex can become completely remodeled, reaching the so called "osteon asymptote" so that old osteons are gradually replaced by new osteons but the proportion of remodeled cortex does not increase (Robling and Stout 2008). Osteoclasts can either completely remove or partially remove old osteons leaving osteon fragments.

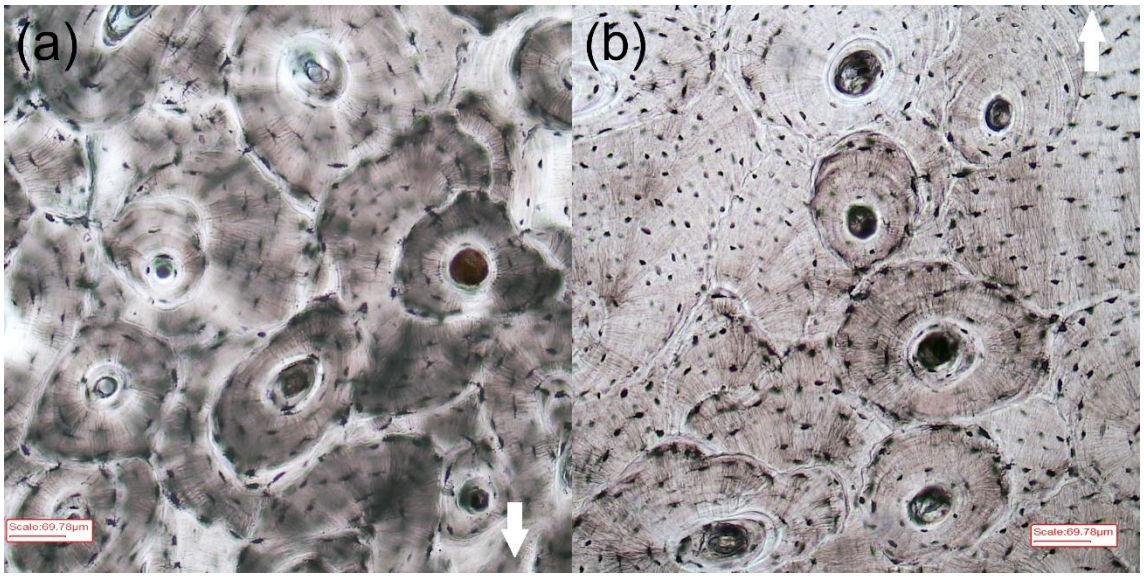

Figure 2.3 – (a) Dense Haversian bone and (b) irregular Haverisan bone. White arrows point towards the periosteum, x100 (from Cummaudo *et al.* 2018)

When the osteons are scattered, they can be arranged in linear rows (osteon banding) or without any spatial organization; similarly, when the osteons are tightly packed, these can have no spatial organization, or they can be arranged in rows roughly parallel to the medullary cavity.

In secondary bone, Haversian systems can have different morphologies. Among these there are the "double-zonal" osteon and the "embedded" osteon (Robling and Stout 1999; Crescimanno and Stout 2012). The former shows an interruption during its formation in the form of a hypercalcified ring; the latter consists in a smaller osteon which develop within a pre-existing secondary osteon without crossing its cement line (Fig. 2.4).

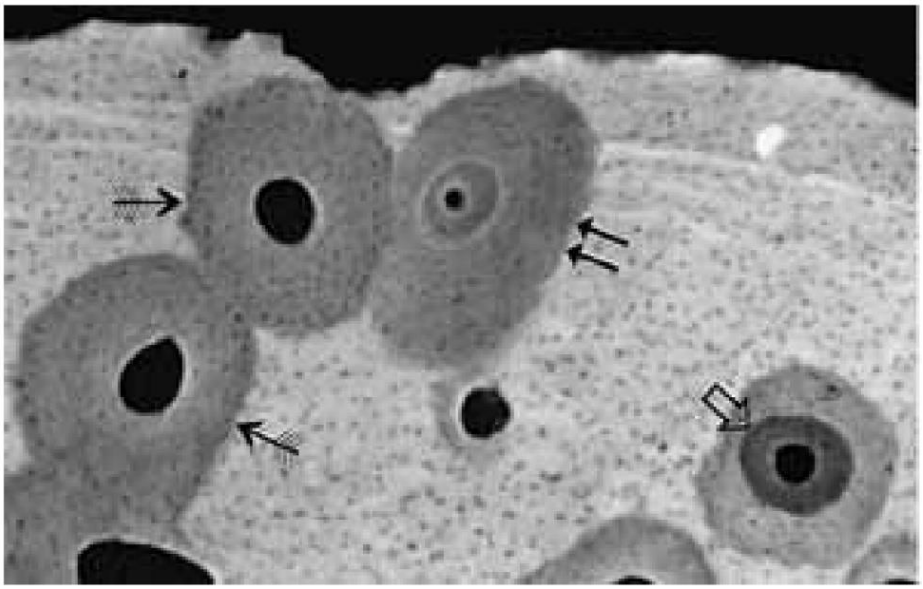

Figure 2.4 – Microradiograph from the cortex of a human long bone showing different types of osteons: classic secondary osteons (feathered arrows), double-zonal osteons (double arrows), embedded osteon (open arrow), (from Robling and Stout 1999)

Another type of secondary osteon is the so-called "drifting osteon" or "waltzing osteon" (Robling and Stout 1999; Frost 1964), which is characterized by continuous resorption on one side and continuous deposition on the other (Fig. 2.5). In cross section it appears as osteon with a tail of lamellae. This type of osteon is frequently found in juvenile bones but, at present, the stimulus which trigger its formation is still unknown (Robling and Stout 1999; Burton *et al*. 1989).

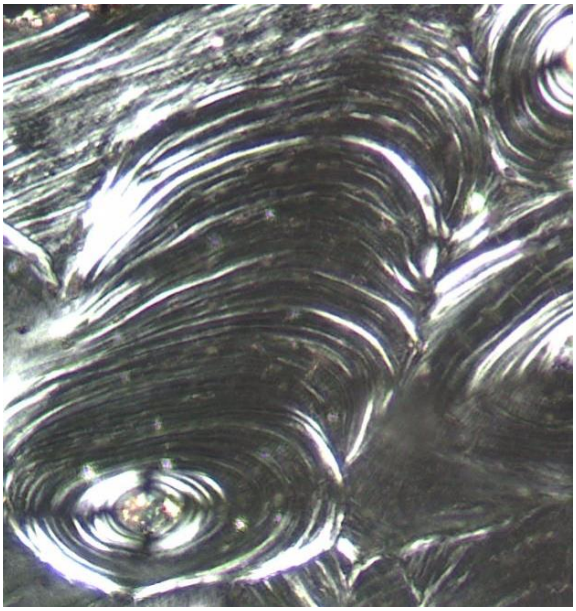

Figure 2.5 – Drifting osteon in the diaphysis of a human ulna, x100. Polarized light (adapted from Cummaudo *et al.* 2018)

2.3 CHANGES IN BONE MISCROSCOPIC STRUCTURE DURING ONTOGENY

2.3.1 HUMAN

During fetal development, bone can be characterized by either cartilaginous tissue, woven bone and/or Haversian bone (Baltadjiev 1995; Burton *et al.* 1989).

Up to 3 months *in utero* fetal long bones exhibit a central portion consisting of cartilaginous tissue surrounded by a layer of periosteal bone with primary vascular canals. Around 4 months *in utero* the cortex is composed of woven bone organized in concentric layers with the appearance of the medullary canal. Generally, secondary osteons start to appear by the fifth month *in utero* (Baltadjiev 1995). These secondary osteons show wide Haversian canals and few concentric lamellae. Between the seventh and the ninth month,

bone start to exhibit a more mature organization with secondary osteons characterized by a higher number of lamellae and narrower Haversian canals (Baltadjiev 1995).

With regards to juveniles, Goldman and colleagues (2009) analyzed the femoral diaphysis of 14 individuals ranging from 2 to 19 years. They observed transitional fibro-lamellar bone at the periosteal cortex in infants between 2 and 4 years, indicating a period of rapid growth. The author defined it "transitional" fibro-lamellar to differentiate this tissue from the classic fibro-lamellar which is characterized by a more rapid depositional rate (>5-10 µm/day), often exhibiting a bricklike plexiform structure, typical of nonhuman bone. The endosteal surface exhibited a thin layer of inner circumferential lamellae, whereas the middle cortex showed numerous Haversian systems, often in the form of "drifting osteons". Several longitudinal studies of human growth patterns (Ruff 2003; Gasser *et al.* 1991; Smith and Buschang 2004), indicated a growth spurt in the femur at 1-2 years of age, and a reduced growth velocity by the beginning of the third year. Therefore, this growth spurt may be a consequence of changes in biomechanical loading due to the transition from crawling to walking (Ruff 2003).

Between 5 and 8 years, the periosteal cortex consisted almost entirely of lamellar bone with longitudinal vascular canals and primary osteons although some remnants of transitional fibro-lamellar bone may be still present. The middle cortex was characterized by a high rate of remodeling.

In older children (9-11 years), a high variability in tissue type distribution was observed. Some individuals showed characteristics seen in the younger age groups (periosteal fibro-lamellar) while others resembled those of the early adolescents.

Between 14 and 19 years, the primary periosteal cortex was entirely lamellar with extensive remodeling at the middle cortex and at the endosteal surface. Few scattered secondary osteons started to appear at the periosteal surface.

With increasing age, adult cortical bone exhibits an increase in the number and a consequent decrease in size of secondary osteons (Kerley 1965; Currey 1964; Evans 1976; Jowsey 1966).

2.3.2 NON-HUMAN

The early stages of development of non-human bone are characterized by a deposition of a woven scaffolding which is rapidly filled by sheets of lamellar bone forming a fibrolamellar tissue (Hillier and Bell 2007; de Margerie *et al.* 2002; Currey 2003).

Generally, bones that need to grow fast for precocial ambulation (e.g. limb bones of artiodactyls) are characterized by fibrolamellar bone earlier in their growth. This type of tissue, in fact, is strong in longitudinal loading but weak across the grain (Reilly and Burstein 1975; Currey 2003).

Contrary to human bone and that of other primates and carnivores, many other mammalian groups, such as bovids and cervids, keep their primary fibrolamellar structure through life, experiencing remodeling only in small regions (e.g. site of muscle attachment). In other small mammals such as rats, remodeling may be totally absent (Currey 2002; Enlow and Brown 1958).

The mechanisms that determine how and when the remodeling occurs, which are a consequence of bone's function and physical properties are discussed in the following section.

2.4 RELATIONSHIP BETWEEN BONE MICROSCOPIC STRUCTURE AND ITS PHYSICAL PROPERTIES

As stated in paragraph 2.1, modeling and remodeling are two distinct processes which are responsible respectively for the adjustment of the structural characteristics of bone (e.g. cross-sectional shape), and the modification of the material organization of the bone by the formation of secondary osteons. These two processes determine the main mechanical properties of bone, which are stiffness, strength, toughness and fatigue resistance (Skedros 2012).

The former consists in the resistance to deformation under an applied load; strength measures the load necessary to cause bone failure; toughness is related to the amount of energy necessary to cause bone fracture (the higher amount of energy required, the tougher the bone), whereas fatigue resistance is the highest stress that bone can endure when loaded repeatedly without breaking (Currey 2002; Skedros 2012).

Structural adjustments in strength and stiffness can be achieved by modeling whereas local material adjustments in toughness and fatigue resistance can be achieved by remodeling.

Bones can be subjected to three strain modes, namely shear, tension and compression (Fig. 2.6). Shear is the most deleterious and refers to bones subjected to torsion whereas tension and compression to bones subjected to bending (Reilly and Currey 2000; Skedros and Baucom 2007; Taylor *et al.* 2003; Turner *et al.* 2001).

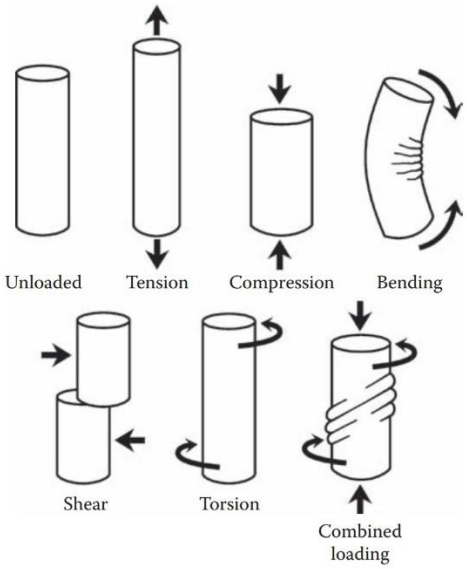

Figure 2.6 – Different load conditions to which a bone or bone region can be subjected (from Skedros 2012)

High stress and/or repeated stress cycles can cause an accumulation of microdamage which can led to stress fractures (O'Brien *et al.* 2005).

Generally, these fractures are a consequence of repetitive activities (e.g. running or marching) and occur when the accumulation of microdamage occur at a rate that outreach the capacity for bone repair (Taylor and Kuiper 2001). Similarly, fragility fractures often occur to elderly individuals due to a deficient bone repair mechanism which is unable to limit the propagation of microcracks, even when accumulating at a normal rate (Schaffler *et al.* 1995).

Bone may resist to fatigue failure by increasing the cortical thickness (modeling), but this would result in thick and heavy bone, representing a disadvantage in terms of metabolism and energetic requirements (Martin 2003). Hence, in order to avoid microdamage accumulation, the microstructural accommodation for regional strain-mode disparities can be achieved by a repair mechanism, the remodeling process (Skedros 2012). Several authors, in fact, pointed out that mechanical stress (e.g. muscle pull) influences the rate

of Haversian remodeling (Bradley 1959; Romanus 1974; Lanyon *et al.* 1979, 1982; Carter *et al.* 1980). These investigations on mammalian long bones demonstrated that regions with muscle, tendon or ligament attachments experience a higher rate of remodeling.

Thus, Haversian remodeling acts as a repairing process which help maintaining bone structural integrity by limiting the propagation of microcracks. Recent studies (Gibson *et al.* 2006; Liu *et al.* 2000; O'Brien *et al.* 2005) demonstrated that cement lines, and more in general secondary osteons, play an important role in limiting microcrack propagation. This might be the reason why, at least in human, with advancing age, the number of cement lines increases due to a reduction in osteons size and the increase in osteon density (Lipson and Katz 1984).

Another way for bone to accommodate regional strain disparities and avoid microdamage accumulation can be achieved by variating the predominant collagen fiber orientation (CFO) and with the formation of strain-mode-specific osteon morphotypes (Hiller *et al.* 2003; Skedros *et al.* 2009, 2011). These specific osteon morphotypes, along with the cement lines of secondary osteons enhance the toughening of bone.

Martin *et al.* (1996) described six osteon morphotypes in the diaphyseal cortex of adult equine third metacarpal. Under polarized light, as shown in Fig. 2.7, these morphotypes are distinguishable by variation in birefringent patterns which relate to their lamellar collagen organization and orientation.

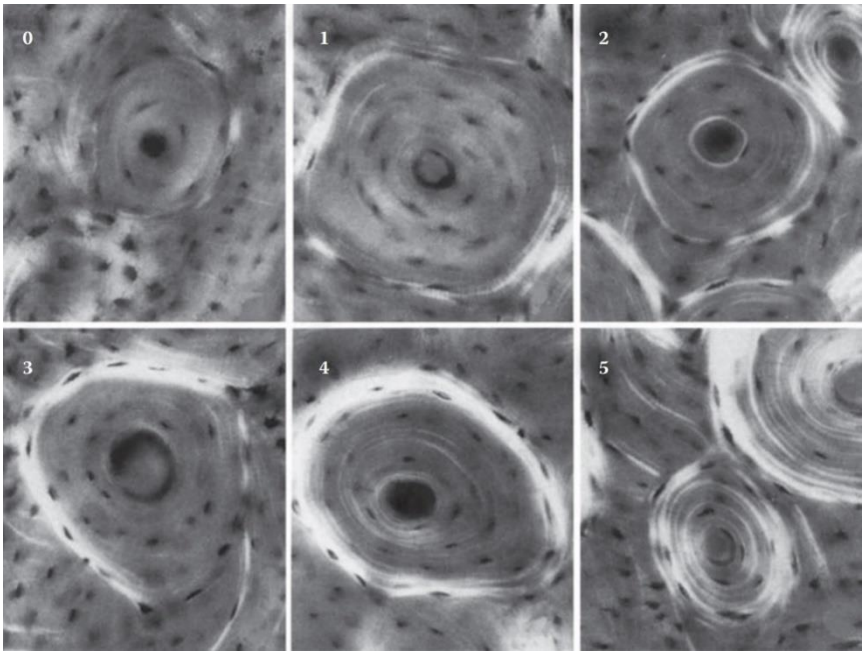

Figure 2.7 – Classification of the osteon morphotypes based on the completeness and birefringence strength of the peripheral ring: **0**=dark osteon with no birefringent lamellae; **1**= dark interior but the birefringent ring is weak and incomplete; **2**=dark interior but the birefringent ring is weak; **3**= dark interior but the birefringent ring is incomplete; **4**=dark interior and strongly birefringent peripheral lamellae; **5**=birefringent lamellae are distributed throughout the wall of the osteon (includes bright osteons and alternating osteons) (from Martin *et al.* 1996)

This scoring system is used to calculate the osteon morphotype score (MTS) of entire microscopic images in order to interpret relationships of morphotypes with specific load environments. Studies using polarized light images (Skedros *et al.* 2009; Bromage *et al.* 2003) pointed out the importance of osteon morphotypes in order to discriminate between the two types of strain produced by habitual bending: compression and tension. Bone portions subjected mainly to compression show osteon morphotypes which appears bright given the greater amounts of transverse collagen, while bones subjected to tension are characterized by darker osteon morphotypes with more longitudinal collagen. On the contrary, shear stresses, which are produced by torsion don't seem to cause regional

variation in osteon morphotypes which appear to be hybrids of those in tension and compression regions.

Although further research is needed, these studies highlight the utility of Haversian remodeling and osteon morphotypes to interpret load history of cortical bone and make functional inferences about the different bones of the skeleton.

CHAPTER 3
HISTOLOGICAL SPECIES DISCRIMINATION: STATE OF THE ART

This chapter focuses on the current knowledge on the microscopic differences between human bone and the bone of other mammals. The first part of the chapter describes the main qualitative characteristics of bone microarchitecture (histomorphology) in different taxa, followed by a summary of the studies on the quantitative differences between human and nonhuman bone microstructure (histomorphometry). The conclusion of the chapter discusses the main limitations of the current histological techniques for species discrimination.

3.1 QUALITATIVE STUDIES

3.1.1 ORDER PERISSODACTYLA

Horse long bones exhibit a reticular pattern characterized by randomly oriented vascular canals, sometimes resembling a plexiform pattern. Haversian bone is present, ranging from isolated to dense secondary osteons (Foote 1916; Enlow and Brown 1958). Thin layers of outer and inner circumferential lamellae are generally present at the periosteal and endosteal surfaces. Numerous resorption spaces can be found at the endosteal surface (Foote 1916).

Stover and colleagues (1992) investigated the microscopic appearance of the dorsal cortex of the third metacarpal of thoroughbred horses at different stages of skeletal maturity. In horses younger than six months, the authors observed no remodeling of primary bone and the presence of radially oriented vascular canals as well as rows of primary osteons. Between one and two years numerous resorption spaces and immature

secondary osteons were observed. In horses older than three years the number of resorption spaces decreased whereas there was an increase in the number of secondary osteons. Horses older than five years showed large and irregular resorption spaces.

3.1.2 ORDER LAGOMORPHA

Rabbit femora do not exhibit plexiform bone. Their tissue generally consists of primary vascular longitudinal bone with irregular or dense Haversian bone in the mesosteal layer (Martiniakova 2006a).

Hare long bones and ribs consist of a wide layer of outer circumferential lamellae and a thin layer of inner circumferential lamellae (Foote 1916). The mesosteal portion exhibits dense Haversian bone with small Haversian canal (Enlow and Brown 1958; Harsányi 1993; Foote 1916).

3.1.3 ORDER ARTIODACTYLA

Bones of artiodactyla are generally characterized by plexiform bone in the periosteal surface and dense Haversian bone in the mesosteal and endosteal layers (Martiniaková *et al.* 2006a; Enlow and Brown 1958).

Domestic pig and wild boar femora share a similar microarchitecture which consists mainly in plexiform tissue. The medioposterior and lateroposterior portion of the bone exhibit numerous secondary osteons across the whole cortex (Foote 1916; Harsányi 1993). Numerous resorption spaces are usually found between secondary osteons in the

anteromedial cortex (Martiniaková *et al.* 2006a). In pig femora and humeri, Morris (2007) observed plexiform bone, which was absent in ribs.

Immature pig femora consist of plexiform tissue. In the endosteal surface osteon banding can frequently found, consisting in linear rows of five to twenty primary osteons. Within these linear bands, immature pigs can exhibit few secondary osteons and resorption spaces, indicating that the secondary bone formation might follow the primary osteon bands (Mulhern ad Ubelaker 2001). Nonetheless, Foote (1916) and Benedix (2004) argued that in long bones of immature pig, Haversian tissue or osteon banding may be totally absent, exhibiting a cortex entirely composed of plexiform tissue. Similarly, Morris (2007) observed no osteon banding in pig humeri and ribs.

Deer long bone microarchitecture at different ages has been investigated by several authors (Owsley *et al.* 1985; Harsányi 1993; Foote 1916; Skedros *et al.* 2003; Skedros *et al.* 2004). Long bones of fetal and new-born deer are characterized by plexiform and reticular tissue with areas of acellular and avascular bone (Singh *et al.* 1974). Immature deer exhibit plexiform bone in the periosteal surface and Haversian bone in the endosteal surface. In mature deer, in particular in the posterior portion of the bone and close to the endosteal surface, plexiform bone is replaced by dense Haversian bone (Skedros *et al.* 2003). Morris (2007) observed the presence of osteon banding in deer femora and humerus.

Martiniaková and colleagues (2006b) studied 15 mature cow femora which were characterized by plexiform bone with some dense Haversian bone in the middle portion of the compacta. Some peculiarities have been observed along the lateral periosteal surface as well as in the anterior and posterior endosteal surfaces which exhibit avascular

bone tissue. In immature cow, Haversian bone is located in the endosteal surface, plexiform bone in the periosteal surface and osteon banding in frequently found in the middle portion of the compacta (Enlow and Brown 1958; Foote 1916; Whitman 2004).

Immature sheep femora are mainly characterized by plexiform tissue throughout the entire cortex with occasional scattered secondary osteons in the posterior aspect of the bone (Foote 1916; Mulhern and Ubelaker 2001). Linear rows of primary osteons can be present in the endosteal surface (Mulhern and Ubelaker 2001). As regards the tibia, Mori and colleagues (2005) observed occasional Haversian systems in the mesosteal layer of a 1-year-old sheep, whereas no Haversian bone were found in sheep younger than six months. Rajtová and colleagues (1995) observed dense secondary osteons in the humerus, the radius and the metatarsus of ten three-year-old sheep.

Foote (1916) and Martiniaková and colleagues (2007) investigated adult sheep femora and observed, particularly the anterolateral periosteal border, the presence of irregular Havesian bone with scattered and isolated secondary osteons.

Ribs of adult sheep exhibit plexiform tissue with limited replacement by Haversian bone (Enlow and Brown 1958).

Long bones of mature goat exhibit both plexiform and Haversian bone. Generally, the periosteal surface consists in plexiform bone with sporadic scattered secondary osteons, whereas the endosteal surface is characterized by dense Haversian bone. The middle portion of the compacta exhibits a mixture of primary tissue and occasional large secondary osteons (Enlow and Brown 1958; Foote 1916; Rajtová *et al.* 1995). Thin layers of outer and inner circumferential lamellae are commonly found in the periosteal and endosteal surface (Foote 1916). Dense Haversian bone was found in mature goat ribs (Enlow and Brown 1958) as well as in the metacarpus and metatarsus of 3- to 4-year old goats (Rajtová *et al.* 1995).

3.1.4 ORDER CARNIVORA

From the existing literature (Enlow and Brown 1958; Foote 1916; Diaz and Rajtová 1975; Georgia and Albu 1988; Whitman 2004; Morris 2007; Hidaka *et al.* 1998), they are more likely to be confused with human bone based on pattern. They are generally characterized by dense Haversian bone even if they can exhibit some primary bone (plexiform or primary osteons arranged in bands) towards the outer layers of the compacta.

Dog femora can exhibit plexiform bone in the outer layers whereas inner layers are characterized by dense Haversian bone (Enlow and Brown 1958; Morris 2007). Plexiform bone is absent in dog humeri and ribs which consists of Haversian bone without any linear bands of osteons (Morris 2007). According to Diaz and Rajtová (1975), dog tibia exhibits many tightly packed round shape secondary osteons throughout the cortex. Plexiform bone and remnants of osteon banding can be frequently found in the outer layers of immature dog bone (Enlow and Brown 1958; Whitman 2004).

Similarly, bear ribs are almost completely characterized by Haversian bone, whereas their long bones exhibit dense Haversian bone in the inner layers of the compacta and plexiform bone in the outer layers (Enlow and Brown 1958).

Cat long bones and ribs are characterized by a thin layer of outer circumferential lamellae (periosteal surface) and a thick layer of inner circumferential lamellae (endosteal surface). The middle portion of the compacta exhibit dense Haversian bone with numerous Volkmann's canals (Foote 1916; Enlow 1958). In addition, Diaz and Rajtová (1975) observed linear bands of primary osteons in the periosteal surface.

Raccoon dog long bones exhibit round-shaped secondary osteons. In immature raccoon dogs, primary bone with reticular and radial vascular canals can be present (Hidaka *et al.* 1998; Enlow and Brown 1958).

According to Diaz and Rajtová (1975), mink femora showed Haversian systems with irregular shapes in the inner layers, whereas the periosteal surfaces were characterized by scattered primary osteons. Enlow and Brown (1958) observed a reticular pattern in mink long bones, whereas ribs exhibited scattered secondary osteons and primary longitudinal vascular canals.

Skunk long bones exhibit reticular or radial vascular canals with occasional Haversian bone replacement in the epiphyses (Enlow and Brown 1958). Skunk shafts are characterized by primary canals near the periosteum and numerous Haversian systems in the mesosteal layers.

According to Hidaka and colleagues (1998), long bones of adult badger consists mainly in Haversian bone characterized by secondary osteons elliptic in shape. In immature badger, primary tissue characterized by reticular or radial vascular canals can be present (Hidaka *et al.* 1998; Enlow and Brown 1958).

Grey foxes exhibit a similar structure to that of the dog, exhibiting dense secondary osteons in the middle portion of the cortex and plexiform bone in the outer cortex (Foote 1916).

3.1.5 ORDER PRIMATES

Generally, primate bone is characterized by lamellar tissue with longitudinal vascular canals which is replaced during growth by Haversian bone, especially in the middle and inner cortex (Enlow and Brown 1958).

According to Foote (1916), orangutan, gorilla and chimpanzee femora exhibit a slightly different bone microstructure. The former showed Haversian bone throughout most of the cortex with thin layers of inner and outer circumferential lamellae. Gorilla exhibits thicker inner and outer circumferential lamellae with longitudinal vascular canals and a ring of Haversian bone in the mesosteal layer. The only exception regards the posterior aspect of the bone, where secondary bone is present throughout the entire cortex. Like gorilla, chimpanzee exhibits mainly lamellar bone with longitudinal vascular canals. Haversian bone is located in the inner layers of the anterolateral and posterior portion of the bone. Mulhern and Ubelaker (2003) compared the histological bone development of chimpanzee and human, observing that juvenile chimpanzee showed slightly more secondary osteons compared to juvenile human. Like human, juvenile chimpanzee femora showed an increase in the number of secondary osteons compared to the tibia and fibula.

With regard to Old World monkeys (baboons, macaques, mandrills and mangabeys) and New World monkeys (spider monkey, squirrel monkey and capuchin monkey), their bone microstructure consists in thin layers of inner and outer circumferential lamellae and dense Haversian bone in the middle portion of the cortex. In immature individuals the amount of primary longitudinal bone is higher and areas of replacing Haversian bone develop in the endosteal surface (Singh et al 1974; Foote 1916; Schaffler and Burr 1984).

Spot-nosed monkey and white-handed gibbon exhibited mainly primary bone with longitudinal vascular canals and occasional Haversian systems in the middle portion of the cortex (Singh *et al.* 1974; Foote 1916).

3.2 QUANTITATIVE STUDIES

Histomorphometric studies on human and nonhuman bone are based on the measurements of osteon parameters, namely: Haversian canal and osteon diameter, perimeter and area.

Since the second half of twentieth century, several authors have performed histomorphometric investigations of both human and nonhuman bone tissue (Jowsey 1966; Diaz and Ratjová 1975; Georgia *et al.* 1982; Albu *et al.* 1990; Owsley *et al.* 1992; Ratjová *et al.* 1995; Martin *et al.* 1996; Dittman 2003; Havill 2004; Urbanová and Novotny 2005; Martiniaková *et al.* 2006a; Morris 2007; Cattaneo *et al.* 2009).

The quantitative data of these studies are summarized in Table 3.

As previously stated in paragraph 1.2.3, there are several problems relating to the current quantitative data of human and nonhuman bone histology.

The first investigations were carried out without the current technological equipment (e.g. digital microscope cameras and image analysis software), and therefore, they were limited to measuring diameters. Since osteons do not have a perfectly circular section, estimating areas from the diameters would certainly introduce additional errors (Mulhern and Ubelaker 2012). Moreover, even the more recent studies were often based on small sample sizes and did not provide the age of the specimens, which is a paramount information since age is related to both the microarchitecture and the size of the histological structures of bone (Hillier and Bell 2007). Finally, as shown in Tables 3 and 4, almost all the analyses were performed on some specific bone, primarily femur, tibia, metacarpal and rib. Therefore, these data do not take into the account the possible morphometric variability of secondary osteons in different bone (Enlow 1966).

Given these premises, comparing between the quantitative data available can be problematic.

According to literature (Table 3.1), the average osteon area of the human femur ranges from 37762,06 μm^2 in modern adult individuals (Martiniaková *et al.* 2006a) to 44533 μm^2 in adult individuals from 18_{th} century London (Pfeiffer 1998). With regard to ribs, average osteon area ranges from 28442 μm^2 in modern adult South Africans (Pfeiffer 1998) to 44000 μm^2 in modern young individuals (Qiu *et al.* 2003).

The average Haversian canal area of the human femur ranges from 2100 μm^2 in ancient Nubian (Mulhern and Van Gerven 1997) to 3665 μm^2 in adult individuals from 18_{th} century London (Pfeiffer 1998). As regard ribs, the Haversian canal area ranges from 1100 μm^2 in ancient Nubian (Mulhern 2000) to 2000 μm^2 in modern young individuals (Qiu *et al.* 2003).

Sample	Bone	n°	On.Dm$_{max}$ (µm)	On.Dm$_{min}$ (µm)	On.Ar (µm^2)	On.Pm (µm)	HC.Dm$_{max}$ (µm)	HC.Dm$_{min}$ (µm)	HC.Ar (µm^2)	HC.Pm (µm)	Study
Human adult	Femur	19	199,9±27,5	/	/	/	77,4±20,6	/	/	/	Currey 1964
Human adult	Femur	26	223±50	/	/	/	/	/	/	173±45	Jowsey 1966
Human adult	Femur, tibia	?	263,91 ±3,89	206,44 ±3,04	44119,88 ±1301,64	837,59 ±13,92	68,73 ±1,10	47,15 ±0,77	2877,37 ±90,68	196,73 ±3,01	Urbanová and Novotny 2005
Human adult (male Native American)	Femur	28	/	/	34345 ±9765	668,10 ±91,62	/	/	2267 ±904	161,03 ±25,13	Burr *et al*. 1990
Human adult (female Native American)	Femur	23	/	/	40778 ±8918	733,26 ±82,99	/	/	2404 ±821	167,84 ±25,87	Burr *et al*. 1990
Human adult (18th century, London)	Femur	20	/	/	44533 ±22443	/	/	/	3667,4 ±3901	/	Pfeiffer *et al.* 2006
Human adult (ancient Nubian)	Femur	45	/	/	38000 ±6557	/	/	/	2100 ±656	/	Mulhern and Van Gerven 1997
Human	Femur	15	263,76 ±60,08	90,20 ±19,19	37762,06 ±12860,20	550,85 ±102,48	59,99 ±21,59	32,26 ±7,23	2164,15 ±1096,98	127,09 ±35,84	Martiniaková *et al*. 2006a
Human adult (male)	Femur, tibia, fibula	17	/	/	40000		/	/	/	/	Evans 1976
Human adult	Humerus	4	282±70	/	/	/	72±23	/	/	/	Pirok *et al.* 1996
Human adult	Clavicle	15	255±52	/	/	/	64±12	/	/	/	Pirok *et al.* 1996
Human adult	Rib	45	/	/	40000 ±6710	/	/	/	/	/	Stout and Lueck 1995
Human adult (18th century London)	Rib	19	/	/	31142 ±12622	/	/	/	1377 ±879	/	Pfeiffer *et al.* 2006
Human adult	Rib	80	/	/	36000 ±894	/	/	/	1100 ±170	/	Mulhern 2000
Human adult (Cape Town)	Rib	30			28442 ±16606				1886 ±3119		Pfeiffer 1998
Human	Rib	9	/	/	44000 ±18000	/	/	/	2000 ±1000	165±54	Qiu *et al.* 2003
Human adult (European-American)	Rib	34	/	/	39000 ±5830	/	/	/	/	/	Cho *et al.* 2002
Human adult (African-American)	Rib	69	/	/	36000 ±8310	/	/	/	/	/	Cho *et al.* 2002

Table 3.1 – Osteon and Haversian canal dimensions in human bone reported in literature

Comparing the available data, Haversian canal size seems the most consistent distinguishing feature in order to discriminate between human and nonhuman bone (Hillier and Bell 2007; Mulhern and Ubelaker 2012). Nonhuman taxa, in fact, are characterized by smaller Haversian canals (Table 3.2).

In some Order such as Lagomorpha (rabbit), the range of Haversian canal size is well under that of human and no overlap is present (Martiniaková *et al.* 2003, 2006). In other order such as Perissodactyla and Carnivores quantitative data are inconsistent (Mulhern and Ubelaker 2012).

Research quantifying the size of osteons and Haversian canals in horse bone is scarce and do not allow a proper comparison with human. However, Urbanová and Novotny (2005) provided values for horse secondary osteon and Haversian canal which overlap with the range reported for human, thus further research is needed.

Reported values for dog indicate that Haversian canals are generally significantly smaller than human, although osteons dimension can overlap between the two (Urbanová and Novotny 2005; Morris 2007). Unfortunately, quantitative data are scarce, and, above all, there is no information regarding the dog breeds of the specimens. This can represent a limitation since body size may influence secondary osteon dimension (Mulhern and Ubelaker 2012).

With regard to Artiodactyla, the histomorphometric investigations are somewhat more consistent, comprising slightly higher number of specimens even if they almost exclusively concern the femur.Besides the study by Dittman (2003), in which the author reported osteon and Haversian canal size well under the range of human, other investigations on cow bone

showed average values that are within the human range, especially with regard to the osteon size (Urbanová and Novotny 2005; Martiniaková *et al.* 2006a; Albu *et al.* 1990).

Investigations on sheep bone provided average values for the Haversian canal, ranging approximately from 300 to 500 μm^2, which are well below those reported for human bone. On the contrary, reported values for osteon size showed a great variability. On the one hand, Martiniaková and colleagues (2006a) provided an average area of 21034,67 ± 8425,89 μm^2 which overlap with the human range; on the other hand, Dittman(2003) reported an average area of 10568.11 ± 5436.51 μm^2 which are quite smaller but still within the lower end of the human range.

As regard goat bone, although the available data is limited, reported values of Haversian canals are well below the human range allowing the discrimination between the two species. On the contrary, pig secondary osteons may overlap in size with those found in humans, whereas Haversian canals are generally smaller (Morris 2007; Dittman 2003; Albu *et al.* 1990; Urbanová and Novotny 2005). Nonetheless, Martiniaková and colleagues (2006a) reported values for Haversian canals which are within the low end of the human range (1015,21 ± 539,63 μm^2). Femur and humerus showed larger dimensions of osteons and Haversian canals compared to ribs and metacarpals, indicating that there may be some variability throughout the skeleton.

Regarding deer, there is a general agreement between the values of the various studies, which indicate that osteon and Haversian canal sizes are considerably smaller compared to the values reported for human bone (Owsley *et al.* 1985; Urbanová and Novotny 2005; Morris 2007).

Recent investigations on primate bone indicated that, unlike other mammals, Haversian canal sizes are generally within the human range, whereas osteons are smaller than those

found in humans. Osteon size ranges from 23471 ± 4367,31 μm^2 in gibbon (Dittman 2003) to 38018 ± 1809,35 μm^2 in gorilla (Dittman 2003). Haversian canal size ranges from 1300 ± 300 μm^2 in juvenile chimpanzee (Mulhern and Ubelaker 2009) to 2356,2 ± 619,1 μm^2 in gorilla (Dittman 2003).

In parallel to the studies on the sizes of osteons and Haversian canals in mammals, other researchers started to investigate the possibility to use osteon circularity as a new parameter to discriminate between human and nonhuman bone (Crescimanno and Stout 2012; Dominguez and Crowder 2012; Keenan *et al.* 2017).

Crescimanno and Stout (2012) studied osteon circularity in femur, humerus and rib of human, dog, deer and pig. The authors found statistically significant difference in osteon circularity between human (0,850) and nonhuman (0,871) and developed a predictive model, based on a minimum of twelve osteon circularity measurements, which allowed to achieve a correct classification for 76,5% of the study sample. No statistically significant differences were found between males and females, as well as between dog, pig and deer. Since the reported difference in circularity between human and nonhuman osteons is just 2%, the authors stressed out the need for accurate measurements by trained researchers. However, more research is needed in order to validate this method since human samples consisted exclusively in mature individuals and age is known to influence osteon circularity (Currey 1964). Moreover, the variability of osteon circularity between different bones need to be investigated both in human and nonhuman species as it may be related to different locomotion patterns and/or metabolic rates.

Dominguez and Crowder (2012) carried out a similar study on femur, humus and rib of human, dog and deer. The authors obtained better results combining osteon area and

circularity achieving a correct classification in 92,1% of cases. However, they pointed out that the overlap between species is markedly higher for circularity than for area.

Keenan and colleagues (2017) investigated the utility of osteon circularity for species identification and the possible relationship between osteon shape and the load history in primates and nonprimates bone. The authors found limited value of osteon circularity in distinguishing between regional prevalent strain-mode distribution (e.g. tension vs compression regions), load-complexity categories (low, moderate, high), as well as in discriminating between different nonhuman species.

However, in this study osteon circularity allowed a high accuracy in discriminating between human and nonhuman bone achieving a correct classification in more than 95% of cases.

Recent studies successfully applied discriminant function analysis based on osteon and Haversian canal parameters in order to distinguish human and nonhuman bone (Cattaneo *et al.* 1999; Urbanová and Novotny 2005; Martiniaková *et al.* 2006a).

Cattaneo and colleagues (1999) formulated a canonical discriminant function based on the size of Haversian canal (area and maximum and minimum diameter) obtaining a predicted correct classification in 79,3% of cases. A test on 21 long bones allowed a correct classification as human or nonhuman in 100% of cases.

A subsequent test of the equation on juvenile long and flat bones achieved excellent results in discriminating nonhuman samples, whereas results for human samples were not as promising. The authors achieved a correct classification in 100% of quail, chicken, and cat samples, in 98,7% of pig samples, in 98,1% of wolf samples and 95,3% of cow samples. As regard human samples, adult long bones showed the best percentage of correct classification (70%), followed by juvenile long bones (43,9%). Human adult flat bones were correctly classified in just 28,2% of cases and juvenile flat bones in 40% of cases. Finally, with regard

to human newborn samples, long bones were wrongly identified in 93,3% of cases, whereas flat bones in 68% of cases.

These results stressed out the importance of conducting further research on the histomorphometry of bone tissue at different stages of skeletal maturity as well as in different bone types.

Urbanová and Novotny (2005) formulated two series of equations for discriminating between human and nonhuman species: the first is based on osteon density (On/mm^2), osteon maximum diameter and Haversian canal area; the second included also midshaft cortical thickness. The human sample comprised 45 femora and 8 tibiae, whereas nonhuman sample consisted in bones from 10 animal taxa (ox, horse, dog, sheep, pig, Euroasian wild boar, red deer, European roe deer, domestic turkey and domestic fowl). Unfortunately, number of specimens and bone types for the nonhuman samples were not provided. In order to avoid the effect of mistakes in measurements or exceptions in bone structure, the authors utilized statistical median instead of statistical mean. The first equation allowed a correct classification in 94% of cases and the second in 100% of cases.

Martiniaková and colleagues (2006a) formulated classification functions based on osteon and Haversian canal parameters (maximum and minimum diameter, area and perimeter) that allow discriminating between human, pig, cow, sheep, and rabbit femora. Unlike the two previous studies, the authors provided classification functions for the investigated species, obtaining a cross-validated correct classification in 76.1% of cases. Nonetheless, an important limitation of this investigation concerns the study sample as it consists exclusively in femora and does not consider the extent of variability which may exist in different bone types.

Sample	Bone	n°	On.Dm$_{max}$ (µm)	On.Dm$_{min}$ (µm)	On.Ar (µm^2)	On.Pm (µm)	HC.Dm$_{max}$ (µm)	HC.Dm$_{min}$ (µm)	HC.Ar (µm^2)	HC.Pm (µm)	Study
Horse	Femur, tibia	?	238,50 ±5,17	224,69 ±189,74	35506,87 ±1602,37	700,80 ±15,02	45,12 ±1,17	29,37 ±0,76	1213,83 ±69,53	128,93 ±3,10	Urbanová and Novotny 2005
Horse (juvenile)	Femur	5	/	/	/	/	58,78	36,21	/	/	Albu *et al.* 1990
Horse	Metacarpal	5	205,75 ±18,42	158,2 ±14,03	27294,34 ±4781,25	619,61 ±54,12	33,66 ±4,03	26,94 ±3,20	786,66 ±200,43	100,25 ±12,09	Dittman 2003
Horse	Metacarpal, radius	6	/	/	15900 ±2280	/	/	/	1300 ±200	/	Owsley *et al.* 1992
Horse	Metacarpal	24	172 ±19	/	/	/	31,3 ±4	/	/	/	Martin *et al.* 1996
Rabbit	Femur	6	98 ±22	/	/	/	/	/	/	54 ±24	Jowsey 1966
Rabbit	Femur	10	129,05 ±29,74	41,05 ±12,34	8339,98 ±3255,10	261,96 ±50,68	26,31 ±12,09	8,66 ±2,95	367,48 ±229,79	53,96 ±20,23	Martiniaková *et al.* 2003
Rabbit	Femur	15	130,81 ±29,28	41,81 ±12	8631,22 ±3455,78	265,96 ±51,58	26,85 ±11,97	8,96 ±2,99	384,01 ±227,45	55,23 ±19,74	Martiniaková *et al.* 2006a
Cow	Metacarpal, radius	4	157,51 ±10,32	121,72 ±6,72	474,25 ±27,96	474,25 ±27,96	23,55 ±2,79	18,41 ±1,85	368,11 ±87,67	69,45 ±8,02	Dittman 2003
Cow (adult)	Femur	15	269,63 ±69,15	76,22 ±14,63	32664,97 ±11110,13	533,61 ±107,31	48,76 ±15,59	15,58 ±4,32	1224,71 ±653,33	99,72 ±26,49	Martiniaková *et al.* 2006a
Cow	Femur, tibia	?	238,46 ±8,07	181,49 ±5,65	36067,23 ±2951,58	698,71 ±22,86	42,56 ±1,38	30,99 ±1,16	1176,37 ±79,35	123,41 ±4,01	Urbanová and Novotny 2005
Cow (adult)	Femur	4	250 ±40	/	/	/	/	/	/	213 ±47	Jowsey 1966
Sheep	Femur	15	206,27 ±66,87	65,11 ±17,31	21034,67 ±8425,89	419,82 ±94,62	33,63 ±8,65	11,46 ±3,07	609,23 ±234,15	69,60 ±14,12	Martiniaková *et al.* 2006a
Sheep	Femur, tibia	?	169,66 ±3,50	123,79 ±2,42	16457,60 ±599,95	486,09 ±9,28	31,76 ±1,14	18,36 ±0,60	574,13 ±38,44	88,55 ±2,97	Urbanová and Novotny 2005
Sheep	Metacarpal, radius	4	130,72 ±33,79	86,45 ±28,83	10568,11 ±5436,51	372,89 ±106,65	25,35 ±1,75	19,22 ±2,69	396,53 ±83,5	101,3 ±7,24	Dittman 2003
Sheep	Various	10-12	320	55	/	/	70	15	/	/	Ratjová *et al.* 1995
Goat	Metacarpal, radius	5	176,85 ±14,48	123,92 ±15,04	17880,68 ±3310,18	513,76 ±43,64	18,75 ±3,25	14,45 ±2,88	233,44 ±102,33	55,11 ±10,18	Dittman 2003
Goat	Various	10	360	78	/	/	120	18	/	/	Ratjová *et al.* 1995
Pig	Femur	15	211,07 ±55,42	83,15 ±17,24	28031,80± 10004,39	459,27 ±97,53	40,60 ±14,55	15,61 ±5,18	1015,21 ±539,63	87,40 ±25,04	Martiniaková *et al.* 2006a

Sample	Bone	n°	On.Dm$_{max}$ (µm)	On.Dm$_{min}$ (µm)	On.Ar (µm^2)	On.Pm (µm)	HC.Dm$_{max}$ (µm)	HC.Dm$_{min}$ (µm)	HC.Ar (µm^2)	HC.Pm (µm)	Study
Pig	Femur, tibia	?	232,26 ±11,95	180,72 ±9,88	33118,87 ±3239,81	681,48 ±34,49	36,18 ±1,37	26,23 ±1,39	826,45 ±66,88	106,03 ±4,28	Urbanová and Novotny 2005
Pig	Femur	5	/	/	/	/	39,85	28,73	/	/	Albu *et al.* 1990
Pig	Femur	6	/	/	13900 ±650	/	/	/	645 ±341	/	Morris 2007
Pig	Humerus	4	/	/	25100 ±166	/	/	/	775 ±560	/	Morris 2007
Pig	Metacarpal, radius	2	142,51 ±4,95	114,91 ±8,88	13701,48 ±593,29	436,90 ±19,66	21,54 ±3,09	17,54 ±2,29	325,53 ±96,56	65,01 ±8,75	Dittman 2003
Pig	Rib	5	/	/	11300 ±570	/	/	/	602 ±469	/	Morris 2007
Wild pig	Femur, tibia	?	207,78 ±8,23	162,56 ±5,92	27168,05 ±1907,80	610,24 ±22,76	32,36 ±1,24	23,36 ±0,92	672,01 ±47,99	95,02 ±3,35	Urbanová and Novotny 2005
Deer	Femur	6	/	/	13900 ±650	/	/	/	387 ±205	/	Morris 2007
Red deer	Femur, tibia	?	110,11 ±2,75	85,01 ±2,10	7410,84 ±357,90	321,99 ±7,72	24,97 ±0,74	17,80 ±0,58	409,35 ±22,26	73,75 ±2,08	Urbanová and Novotny 2005
European roe deer	Femur, tibia	?	127,72 ±3,37	100,96 ±2,51	9900,04 ±455,86	514,30 ±13,09	23,72 ±0,92	15,13 ±0.63	327,58 ±23,08	69,34 ±2,38	Urbanová and Novotny 2005
Deer	Humerus	5	/	/	14700 ±600	/	/	/	401 ±186	/	Morris 2007
Deer	Rib	6	/	/	11300 ±590	/	/	/	245 ±164	/	Morris 2007
Dog	Femur, tibia	?	151,59 ±2,35	117,15 ±1,74	14034,94 ±141,11	444,74 ±6,48	34,42 ±0,68	21,11 ±0,40	694,37 ±26,03	98,23 ±1,79	Urbanová and Novotny 2005
Dog	Femur	5	/	/	/	/	69,09	26,3	/	/	Georgia *et al.* 1982
Dog	Femur	4	154 ±38	/	/	/	/	/	/	85 ±37	Jowsey 1966
Dog	Femur	6	/	/	15600 ±670	/	/	/	432 ±314	/	Morris 2007
Dog	Humerus	6	/	/	14900 ±740	/	/	/	314 ±227	/	Morris 2007
Dog	Rib	6	/	/	10300 ±540	/	/	/	392 ±259	/	Morris 2007
Cat	Femur	6	163 ±60	/	/	/	/	/	/	102 ±36	Jowsey 1966
Cat	Tibia	1	155	110	/	/	/	/	/	/	Diaz and Ratjová 1975

Sample	Bone	n°	On.Dm$_{max}$ (µm)	On.Dm$_{min}$ (µm)	On.Ar (µm^2)	On.Pm (µm)	HC.Dm$_{max}$ (µm)	HC.Dm$_{min}$ (µm)	HC.Ar (µm^2)	HC.Pm (µm)	Study
Wild cat	Tibia	1	175	90	/	/	/	/	/	/	Diaz and Ratjová 1975
Mink	Tibia	1	90	65	/	/	/	/	/	/	Diaz and Ratjová 1975
Martin	Tibia	1	165	86	/	/	/	/	/	/	Diaz and Ratjová 1975
Macaque	Femur	75	/	/	23765,02 ±5479,19	/	/	/	1486,39 ±502,66	/	Havill 2004
Rhesus monkey	Femur	2	216 ±52	/	/	/	/	/	/	167 ±46	Jowsey 1966
Chimpanzee (juvenile)	Femur	12	/	/	33000 ±600	/	/	/	1600 ±500	/	Mulhern and Ubelaker 2009
Chimpanzee (juvenile)	Humerus	8	/	/	33000 ±5000	/	/	/	1300 ±300	/	Mulhern and Ubelaker 2009
Chimpanzee	Metacarpal, radius	5	215,6 ±27,24	150,8 ±9,89	27858 ±4855,76	633,3 ±70,35	49,8 ±4,6	36,1 ±2,9	1547,5 ±347,56	143,1 ±13,06	Dittman 2003
Gibbon	Metacarpal, radius	5	203,4 ±12,10	139,1 ±14,12	23471 ±4367,31	597,20 ±44,60	45,4 ±3,94	33,4 ±3,71	1256,1 ±254,97	132,7 ±12,67	Dittman 2003
Gorilla	Metacarpal, radius	3	251 ±17,5	186,2 ±4,50	38018 ±1809,35	746 ±29,50	59,9 ±6,24	47,4 ±9,08	2356,2 ±619,1	176,8 ±20,04	Dittman 2003
Orangutan	Metacarpal, radius	4	236,7 ±12,34	177,5 ±3,88	34640,5 ±3447,9	719,3 ±30,53	54,5 ±5,96	43 ±5,54	1992,5 ±490,01	164,2 ±16,41	Dittman 2003

Table 3.2 – Osteon and Haversian canal dimensions in the main mammals reported in literature.

3.3 LIMITATIONS AND FURTHER INVESTIGATIONS

The examination of the scientific literature on species discrimination of skeletal material by histological analysis shows a promising scenario, although with several limitations due to the insufficient knowledge on the variability of bone microstructure.

In most cases, the evaluation of bone histomorphology can allow to successfully rule out the human origin of a bone (e.g. presence of plexiform bone). However, several nonhuman Order (e.g. Carnivora, Artiodactyla) can exhibit a micro-structural pattern which resembles that of human (Haversian bone). The quantification of the size of osteons and Haversian canals can allow, in most cases, a correct classification of human and nonhuman bone. Nonetheless, in several nonhuman species the sizes of these structures overlap with that of human.

The main limitations of these studies on species discrimination concern the study sample which generally consisted in few bone types (e.g. femur, rib). The different bones of both human and nonhuman skeletons are subjected to different biomechanical environments and, even within the same bone, each region (anterior, posterior, medial and lateral) experience different mechanical strains which may result in regional differences in bone tissue organization (see paragraph 2.3). At present, no study has ever examined systematically bone histomorphology and histomorphometry of entire human and non-human skeletons. Therefore, a thorough understanding of the histomorphological and histomorphometric variability throughout the skeleton of human and nonhuman species is essential in order to develop reliable methodologies for species discrimination by histological analysis.

In addition, although the influence of age on bone microarchitecture is well-known, the ages of the specimens are rarely reported in these studies. This does not allow direct

comparisons between data from these investigations. There is the need for further research on bone histology of different mammals at different stages of skeletal maturity in order to have a wider overview on the species whose histological appearance may be confused with the human one.

Finally, all the previous investigations on the histomorphometry of mammalian bone were based on the measurement of the classic parameters of secondary osteons and Haversian canals (diameter, area and perimeter). At present, no attempt has been made in order to evaluate the potential of other features of bone tissue to discriminate between species. For example, osteocyte lacunae, which are known to play a major role in bone adaptation to stress and in the regulation of bone metabolism, have been studied in the last decades in terms of density, shape and size by several researchers both in human (Ardizzoni 2001; Qiu *et al.* 2006; Ascenzi *et al.* 2008; Dong *et al.* 2014) and nonhuman species (Skedros *et al.* 2005; Hobdell and Howe 1971; Remaggi *et al.* 1998; Ferretti *et al.* 1999). However, these investigations were undertaken mainly for clinical applications. A new line of research for species discrimination might aim at verifying whether there are significant quantitative differences in the size of osteocyte lacunae between human and other mammals.

CHAPTER 4

AIMS AND OBJECTIVES

As previously stated in chapter 1, the determination of the human origin of fragmented skeletal material is paramount in medico-legal investigations. The presence of nonhuman remains or the commingling of human and nonhuman remains is, in fact, a common event in forensic context, especially in case of mass disasters (Franklin and Marks 2017). In addition, the overall reportage of all kinds of skeletal material (often nonhuman) has risen in the last decades given the increasing awareness of the public about the forensic significance of skeletal remains (Pokines 2015). Hence, there is the need for reliable and cost-effective methods for discriminating between human and nonhuman remains.

In this regard, this thesis aims to investigate the intra- and inter-species variability of bone microscopic structure in human and pig (*Sus scrofa*) at different stages of skeletal maturity from both a qualitative (type of tissues) and quantitative perspectives (measurements of diameter, area and perimeter of secondary osteons).

According to literature (Pokines 2015; Bass 2005; Morris 2007), in fact, *Sus scrofa* represents one of the most frequent taxa recovered in forensic scenarios given its large use for meat consumption.

Although macroscopically human and pig bones are easily distinguishable, in case of severe fragmentation and/or degradation of the skeletal elements, species discrimination can be particularly challenging (Blau and Briggs 2011).

Previous studies on species discrimination by histological analysis have pointed out some extent of overlap between human and pig in the size of microstructural parameters, such as diameter, area and perimeter of secondary osteons and Haversian canals (Martiniaková 2006a; Urbanová and Novotny 2005; Morris 2007; Dittman 2003). However, these

investigations focused exclusively on some specific bones (generally the femur), without considering the differences that may exists between other skeletal elements. The studies presented in chapter 2 showed that bone modifies its microstructural architecture in order to accommodate regional strain-mode disparities which characterize the different bones of the skeleton. Therefore, an in-depth knowledge of the intra- and inter-species variability which may exist within the different bones of the skeleton is the most important prerequisite in order to develop a reliable histological method for species discrimination of fragmented bone.

Finally, as previously stated in paragraph 3.3, there is the need for new features/parameters which can aid species discrimination by histological analysis. An exploratory research was undertaken on human and pig secondary osteons with similar dimensions, so as to verify whether the size and number of osteocyte lacunae differ significantly between the two species.

4.1 INTRA-INDIVIDUAL VARIABILITY

Aim 1 - To investigate the extent of intra-individual variability in bone histomorphology and histomorphometry of both human and pig

Objectives:

- To prepare histological sections of different bones of the same individual (e.g. long, flat and irregular bones) and different portions of the same bone (e.g. proximal metaphysis, diaphysis and distal metaphysis)
- To perform a histomorphological analysis on the thin sections in order to assess the organization of the bone matrix, the type of vascularization and the type of bone deposition

- To perform a histomorphometric analysis on the thin sections in order to measure the size of secondary osteons and Haversian canals
- To perform a statistical analysis so as to verify whether the size of osteons and Haversian canals significantly differ between the different bones of the skeleton and in different portions of the same bone

4.2 INTRA-SPECIES VARIABILITY

Aim 2 - To investigate the extent of intra-species variability in bone histomorphology and histomorphometry of both human and pig

Objectives:

- To reduce the number of bone types to sample and increase the number of individuals
- To perform a histomorphological analysis on the thin sections in order to assess the organization of the bone matrix, the type of vascularization and the type of bone deposition
- To perform a histomorphometric analysis on the thin sections in order to measure the size of secondary osteons and Haversian canals
- To perform a statistical analysis so as to verify whether the size of osteons and Haversian canals significantly differ between different individuals of the same species

4.3 INTER-SPECIES VARIABILITY

Aim 3 – To demonstrate that it is possible to discriminate between human and pig bones by histological analysis.

Objectives:

- To compare the organization of the bone matrix, the type of vascularization and the type of bone deposition in human and pig bone
- To verify if there are some distinctive morphological features which can aid the discrimination between the two species
- To perform a statistical analysis on the data acquired during the histomorphometric analysis so as to verify the possibility to use osteon and Haversian canal parameters to discriminate between human and pig
- To select a number of secondary osteons with similar dimensions and verify whether there is a statistically significant difference in the number and size of their osteocyte lacunae between human and pig.

CHAPTER 5
MATERIALS AND METHODS

This chapter describes the materials and methods used. Paragraph 5.1 provides details on the number and types of bone used for each analysis, while paragraph 5.2 describes the procedures used to prepare bone samples for the histological analyses. A description of the techniques employed for the analysis is provided in paragraph 5.3, whereas paragraph 5.4 outline the statistical tests used to analyze data.

5.1 MATERIALS

5.1.1 HUMAN SPECIMENS

Human samples were obtained from eighteen adults, one juvenile and a foetus. Details regarding number of bones sampled, number of thin sections, source, sex and age of the individuals are shown in Table 5.1.

The age of the human individuals ranged from 30±2 weeks *in utero* (foetus) to 84 years, and were collected from several sources: archaeological, cemeterial and autopsy.

	individual	n° of bones sampled	n° of thin sections	Source	Sex	Age (years)
HUMAN SAMPLES	HA1	22	49	Archaeological	Male	26-45
	HA2	3	3	Cemeterial	Female	70
	HA3	4	4	Cemeterial	Male	73
	HA4	2	2	Cemeterial	Male	82
	HA5	2	2	Cemeterial	Male	84
	HA6	5	5	Cemeterial	Male	76
	HA7	4	4	Cemeterial	Female	73
	HA8	1	1	Autopsy	Female	48
	HA9	1	1	Autopsy	Male	30
	HA10	1	1	Autopsy	Male	47
	HA11	1	1	Autopsy	Male	33
	HA12	1	1	Autopsy	Male	26
	HA13	5	5	Autopsy	Male	38
	HA14	1	1	Cemeterial	Male	39-57
	HA15	1	1	Cemeterial	Female	35-53
	HA16	1	1	Cemeterial	Male	46-64
	HA17	1	1	Cemeterial	Female	49-67
	HA18	1	1	Cemeterial	Male	36-54
	HF	7	7	Cemeterial	Male	30±2 weeks *in utero*
	HJ	9	23	Archaeological	n.d.	7-8

Table 5.1 – Details of the human study sample (HA= human adult; HF= human foetus; HJ=human juvenile)

Individual HA1 (Fig. 5.1) was utilized to test the intra-individual, the intra-species and inter-species histomorphological and histomorphometric variability (see chapter 4) and consisted in a well-preserved archaeological skeleton.

It was recovered in 1983 during an archaeological excavation by Lombardia Archaeological Superintendency at San Martino di Serravalle's church, in the north of Italy (Brogiolo and Mariotti 2009).

Figure 5.1– Study sample: a human adult skeleton from the archaeological site of San Martino di Serravalle, Italy

A morphological analysis was performed to estimate sex and the age at death of the individual following a number of techniques (Beauthier *et al.* 2010; Brooks and Suchey 1990; Buikstra and Ubelaker 1994; İscan *et al.* 1984; Rougé-Maillart *et al.* 2009). It revealed that the skeleton belonged to a Caucasoid male individual aged between 26 and 45 years without any clear sign of pathological conditions, except an osteoma on the right zygomatic arch (Fig. 5.2). The skeleton was well preserved with minor signs of erosion on the epiphyses of long bones.

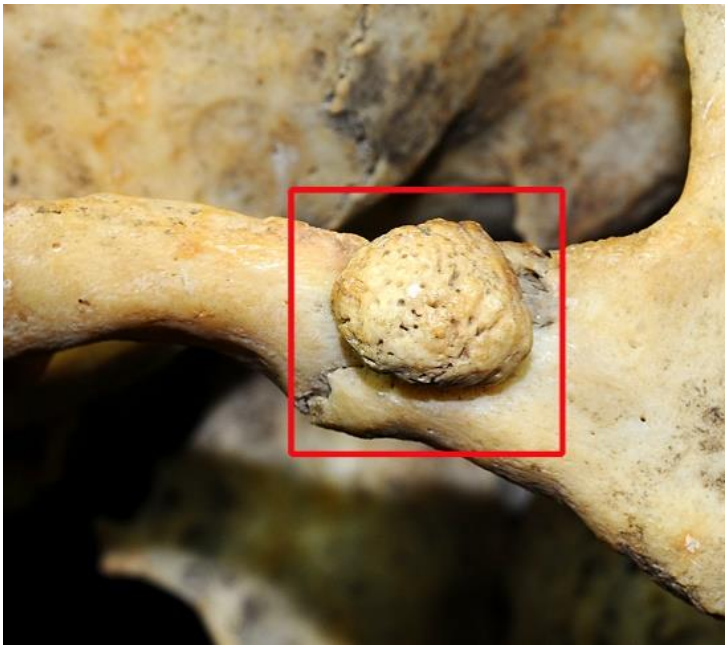

Figure 5.2 – Osteoma on the right zygomatic arch

In order to test the intra-individual variability samples were taken along the entire skeleton, including long, flat, irregular and sesamoid bones (Fig. 5.3), for a total of forty-nine samples. Different portions of long bones were sampled (e.g. diaphysis, and proximal and distal metaphysis) since different mechanical loads to which the different parts of the bones are subjected may result in regional variation of bone microarchitecture (see paragraph 2.4).

Since cervical vertebrae and ilia primarily consist of spongy bone, they were sectioned in both longitudinal and transversal planes so as to verify the presence of Haversian systems.

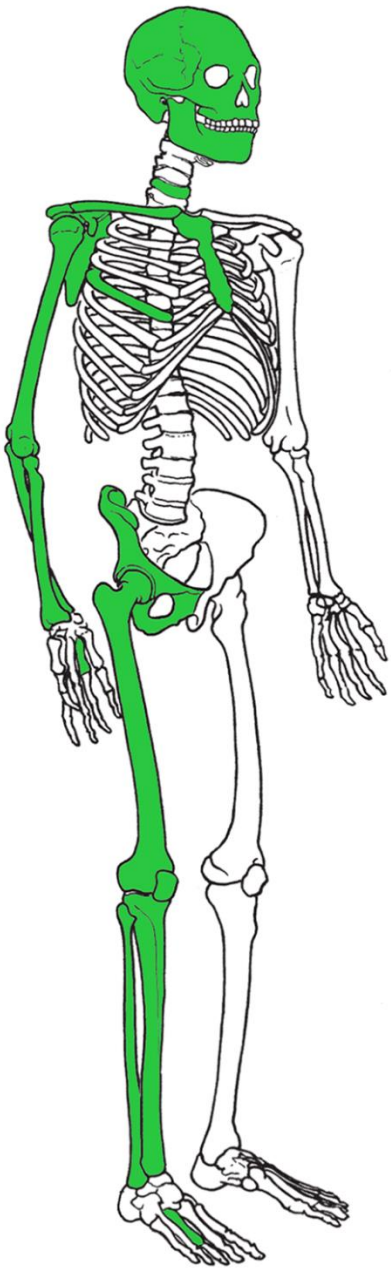

Long bones	Humerus (PM, D, DM)
	Ulna (PM, D, DM)
	Radius (PM, D, DM)
	Clavicle (medial end, D, lateral end)
	Femur (neck, PM, D, DM)
	Tibia (PM, D, DM)
	Fibula (PM, D, DM)
	Metacarpal (base, shaft, head)
	Metatarsal (base, shaft, head)
Flat bones	Glabella
	Zygomatic process of frontal bone
	Parietal (middle portion)
	Occipital
	Petrous (Temporal bone)
	Scapula superior border
	Scapula acromion
	Sternum
	Rib (head, body)
	Iliac crest (longitudinal, transversal)
	Ischiopubic ramus
	Iliopubic ramus
Sesamoid	Patella (sagittally)
Irregular bones	Gonion (mandible)
	Mental protuberance (mandible)
	Mandibular condyle (mandible)
	Cervical vertebra (longitudinal, transversal, spinous process)

Figure 5.3 – Study sample for the assessment of intraspecies variability: human adult skeleton. PM = proximal metaphysis; D = diaphysis; DM = distal metaphysis (adapted from White and Folkens 2005)

With regard to the human juvenile (HJ), the length of long bones, as well as the development and eruption of the dentition, suggested an age ranging between seven and eight years (Maresh 1970; Ubelaker 1979). Sex was not estimated as sexual dimorphism

is not that evident at that age (Christensen *et al.* 2014; Sauer and Lackey 2000). The skeleton showed no evident sign of pathological conditions. Given the excellent preservation for an archaeological skeleton (Fig. 5.4), it was decided to minimize the destructiveness of the sampling (English Heritage 2013), taking only the posterior portion of some bones (Fig. 5.5). In the absence of the entire transverse section human juvenile samples were used to test the intra-individual histomorphometric variability rather than the histomorphological variability (see paragraph 4.1, aim 2).

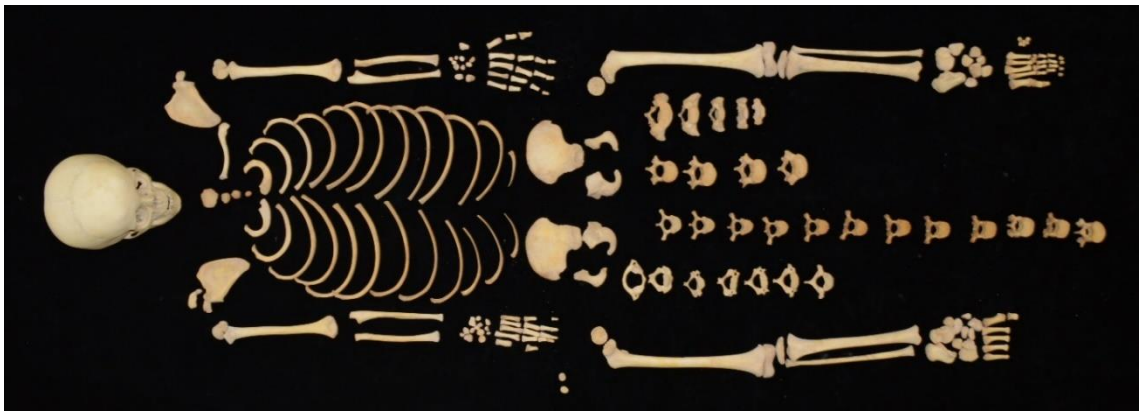

Figure 5.4 – Study sample: an archaeological human juvenile skeleton (HJ)

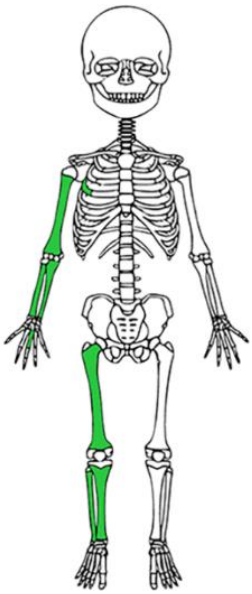

Long bones	Humerus (PM, D, DM)
	Ulna (PM, D, DM)
	Radius (PM, D, DM)
	Femur (PM, D, DM)
	Tibia (PM, D, DM)
	Fibula (PM, D, DM)
	Metacarpal (base, shaft, head)
Flat bones	Occipital
	Rib (body)

Figure 5.5 – Study sample for the assessment of intraspecies variability: human juvenile skeleton. PM = proximal metaphysis; D = diaphysis; DM = distal metaphysis)

The use of archaeological material for histological investigations was authorized by an agreement between LABANOF laboratory (Milan, Italy) and the Lombardia archaeological superintendency.

The remaining individuals (HA2-HA18 and HF) along with HA1 were utilized to test the both the intra-species and the inter-species histomorphological and histomorphometric variability (see chapter 4, aims 1-4).

In order to achieve these aims it was decided to reduce the types of bone to sample and increase the number of individuals. The criterion for selection of the bones to sample was based on previous studies (Skedros *et al.* 2003; Skedros *et al.* 2004; Shaffler and Burr 1984) which demonstrated a higher rate of remodeling in bones involved in the locomotion (limb bones). In addition, both in human and nonhuman, ribs are known to exhibit remodeling given the increased loading cycles due to thoracic breathing motion (Skedros *et al.* 2003; Currey 1981; Parfitt 2002).

Therefore, the choice fell on the following bones: humerus, radius, ulna, femur, tibia, metatarsal and rib (Table 5.2).

For each bone, the mid-diaphysis was sampled since it is mainly composed of compact bone, and this makes it more resistant to postmortem degradation, compared to the epiphysis or to flat and irregular bones which are characterized by a prevalence of cancellous bone (Haglund and Sorg 1997). Moreover, with regard to the gross morphology, the inter-species skeletal variation is more evident at the articular surfaces of the epiphyses of long bones which are generally more sculpted in quadrupeds compared to humans. Therefore, in case of fragmented skeletal remains, the discrimination between human and nonhuman is more challenging in case of diaphyseal fragments as they generally lack distinctive features (Komar and Buikstra 2008; France 2011). In addition, the results of the analysis of the intra-individual histomorphological variability on the human adult (HA1) and the juvenile pig (PJ1) showed a higher rate of remodeling at the mid-diaphysis of long bones compared to the proximal and distal metaphysis.

Fibula was excluded for the impossibility to collect enough samples from the available skeletal material. Metatarsal was chosen instead of metacarpal since the majority of the human skeletons came from a cemetery, and the presence of socks increased the availability of metatarsal bones compared to metacarpal bones.

With regard to flat bones, rib was chosen since the histomorphological analysis on the human adult (HA1) and the pig juvenile (PJ1) revealed a higher rate of remodeling compared to the other flat bones. Moreover, especially when fragmented, determining the human or nonhuman origin of a rib fragment by macroscopic analysis can be particularly challenging (Hillson 2003).

Bone		n° of cross-sections (HUMAN)	n° of cross-sections (*Sus scrofa*)
Long bones	Humerus	6	6
	Ulna	6	6
	Radius	6	6
	Femur	6	6
	Tibia	6	6
	Metacarpal	6	6
Flat bones	Rib	6	6
Total		42	42

Table 5.2 – Study sample for the assessment of the intra- and inter-species histomorphological and histomorphometric variability.

As stated above, human skeletal material was obtained from different sources (archaeological, autopsy and cemeterial). Both cemeterial and autopsy specimens were collected from unknown and/or unclaimed individuals in agreement with local legislation (DPR 10.09.90 n° 285, art. 43) which allows to use for research and teaching unclaimed remains.

Autopsy bone samples were obtained from fresh cadavers of unknown individuals with soft tissues still adhering and had to be macerated prior to being utilized for the histological analyses (see paragraph 5.2.1). Bone sampling was part of the normal procedure to determine the biological profile and chronological age was obtained after the identification of the individuals.

On the contrary, cemeterial samples were obtained from fully skeletonized individuals which did not require any particular preparation. The chronological age of the individuals was obtained from death certificates (Cattaneo *et al.* 2018), except for individuals HA14-HA18 for which no demographic data was available. For these individuals, given the availability of few skeletal elements, age was estimated by microscopic analysis on the femoral diaphysis (Kerley 1965; Kerley and Ubelaker 1978).

The rationale for the choice of the human individuals to be sampled was based on the availability and the condition of the skeletal elements. Permission to destroy part of the specimens was given after meetings with the director of the collection during which the number of skeletons and of bones to be sampled was concorded: 63 bones to be sampled from 14 individuals. The type of bone was selected according to the criteria previously stated and the number of individuals, bones, sections within the bone and number of osteons examined per section was considered in line or greater with respect to previous investigations. However, it was attempted to sample individuals of different ages in order to have a wide overview of the morphological and metric variability that human bone may exhibit at histological level.

5.1.2 PIG SPECIMENS

All the nonhuman samples (Table 5.3) came from pigs (*Sus scrofa*) that died a natural death in Italian farms. No obvious sign of pathological conditions was observed on the skeletons of the animals.

Prior to being used for this research, the carcasses of these animals were stored in refrigerated cells at -4°C. According to literature (Lander *et al.* 2014; Tersigni 2007) the

freezing process does not significantly affect bone microarchitecture. Both the Haversian canals and osteocyte lacunae do not experience modifications in term of size although microcracks originating from the boundary of the Haversian systems may be observed through SEM analysis. Nonetheless, in these investigations bones were frozen at -20°C, which is considerably lower than the temperature employed in this research.

	individual	n° of bones sampled	n° of thin sections	Source	Sex	Age
PIG SAMPLES	PJ1	19	40	Farm	n.d	11-13 months
	PJ2	7	7	Farm	n.d	11-13 months
	PJ3	7	7	Farm	n.d	11-13 months
	PJ4	7	7	Farm	n.d	11-13 months
	PJ5	7	7	Farm	n.d	11-13 months
	PJ6	7	7	Farm	n.d	11-13 months
	PN1	7	7	Farm	n.d	newborn
	PN2	7	7	Farm	n.d.	newborn

Table 5.3 – Details of the nonhuman study sample (PJ= pig juvenile; PN= pig newborn)

The choice to utilize juvenile pigs refers to the fact that they are generally slaughtered by the year of age. Therefore, the odds of dealing with bones of adult pigs in forensic contexts should be quite low.

Unfortunately, information on the exact age of the animals were not available, thus an assessment of teeth eruption (McCance *et al.* 1961) and of the epiphyseal fusion of long bones (Bull and Payne 1982; Barone 1976) was performed in order to estimate the age of the animals.

The crown formation of mandibular third molars was complete (Fig. 5.6) in all the individuals, indicating an age ranging between twelve and thirteen months, whereas the

fusion of the acetabulum and the distal epiphyses of the humerus was still not complete, suggesting an age slightly inferior to twelve months.

Figure 5.6 – Juvenile pig (PJ1) – the crown formation of mandibular third molar is complete, suggesting an age ranging between twelve and thirteen months

Like the human adult HA1, the juvenile pig PJ1 (Fig. 5.7) was used to test the intra-individual, the intra-species and inter-species histomorphological and histomorphometric variability (see chapter 4).

A total of forty samples were taken along the entire skeleton (Fig. 5.8) and in different portion of the same bone (proximal metaphysis, diaphysis, distal metaphysis).

Figure 5.7 – Study sample: the skeleton of a juvenile pig

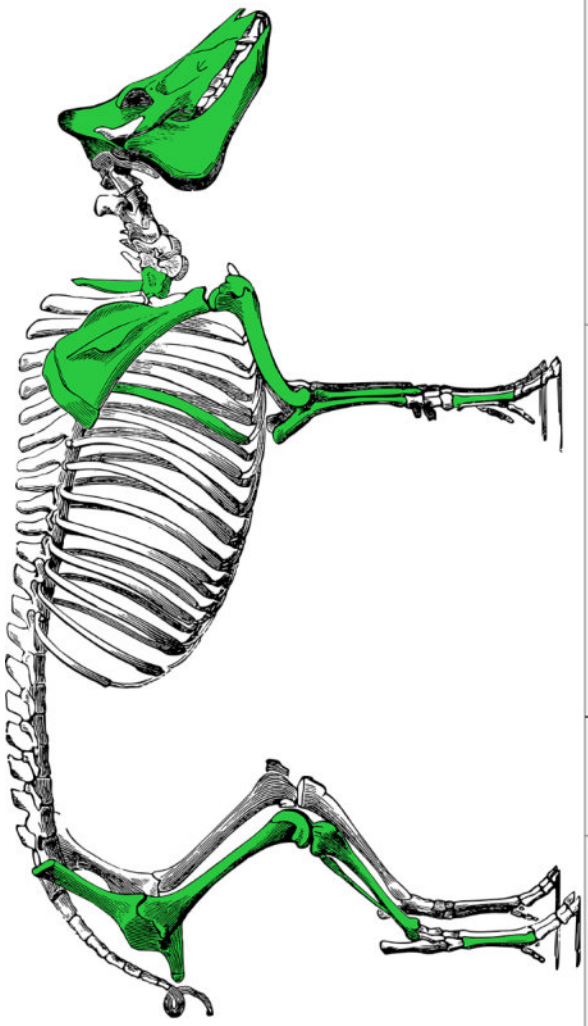

Long bones	Humerus (PM, D, DM)
	Ulna (PM, D, DM)
	Radius (PM, D, DM)
	Femur (PM, D, DM)
	Tibia (PM, D, DM)
	Fibula (PM, D, DM)
	Metacarpal (base, shaft, head)
	Metatarsal (base, shaft, head)
Flat bones	Zygomatic process of frontal bone
	Parietal (middle portion)
	Occipital
	Petrous (Temporal bone)
	Scapula superior border
	Scapula acromion
	Rib (head, body)
	Iliopubic ramus
	Ischiopubic ramus
Sesamoid	Patella (sagittally)
Irregular bones	Gonion (mandible)
	Mental protuberance (mandible)
	Mandibular condyle (mandible)
	Cervical vertebra (longitudinal, transversal, spinous process)

Figure 5.8 – Study sample for the assessment of intraspecies variability: pig juvenile skeleton. PM = proximal metaphysis; D = diaphysis; DM = distal metaphysis (adapted from Theobald 1899)

The other juvenile pigs (PJ2-PJ6) were employed to test both the intra- and inter-species histomorphological and histomorphometric variability. Just like the human individuals, samples were taken from the diaphysis of the following bones: humerus, radius, ulna, femur, tibia, metatarsal and rib (Table 5.2).

5.2 SPECIMEN PREPARATION

5.2.1 MACERATION

With the exception of the archaeological and cemeterial skeletons, all the other samples were taken from modern bones, with soft tissues still adhering to bone surface.

All pig bones were obtained from the whole body of the animals (Fig. 5.9). The first step consisted in disarticulating the body with a sharp knife and a scalpel, removing also the majority of soft tissues.

Once disjointed, the body parts were stored in plastic boxes labeled with their contents.

Figure 5.9 – Study sample: juvenile pig (PJ1)

Afterwards, bones had to be macerated in order to remove the remaining soft tissues.

Since there are currently no guidelines on how to macerate bones prior undertaking a histological analysis, the choice fell on the technique which is less aggressive to bones

and possesses fewer health and safety issues (Mairs *et al.* 2004; Nawrocki 2007; King and Birch 2015; Yin *et al.* 2010; Uhre *et al.* 2015): the maceration in water (Fig. 5.10). If on the one hand this represent the safest maceration technique, on the other hand it is also the one that require most time-consuming. In fact, before immersing the body parts of the animals in water, most of the soft tissues had to be manually removed.

Figure 5.10 – Study sample: maceration in water of a juvenile pig (PJ1)

The remaining soft tissues were daily removed with the use of scalpel and forceps. A scouring pad was used to remove the periosteum (Fig. 5.11). The total process took up to three-four weeks for each pig.

Figure 5.11 – Study sample: removal of soft tissues from a juvenile pig (PJ1)

Although the outer surface of the bones was completely clean, the inside of the bones contained a large amount of fat which could have hindered the preparation of bone thin sections. According to literature, bone degreasing can be accomplished by soaking the bones in a solution of water and ammonia (Fenton *et al.* 2003) or water and detergent (Mairs *et al.* 2004). In addition, water and acetone or water and bleach solutions (Urbanová 2005) have been employed but Christensen and colleagues (2014) suggested that these solutions can be detrimental to bone tissue.

Hence, bones were degreased in a solution of water and detergent (Mairs *et al.* 2004) at room temperature (20-25 °C), changing the water every 48 hours until the solution showed no fat residues. Although this is the least aggressive method reported in the literature, it is also the slowest one. Indeed, depending on the bone size, the process took up to fifteen days to be completed. Small holes were made on the epiphyses of long bones with a 5mm trephine in order to allow the degreasing solution to penetrate inside the bone

and speed up the process. The same procedure was followed to macerate and degrease fresh human bone samples.

5.2.2 ASSESSMENT OF THE PRESERVATION OF BONE HISTOLOGICAL STRUCTURE

The principal concern of using archaeological skeletons for histological investigations lay with the possibility that microstructural changes of bone tissue had occurred during burial due to microbiological attack. Under certain temperature and pH conditions, bone's mineral phase undergo dissolution exposing the collagen to microbial enzymes such as collagenase, an enzyme that digest bone collagen and paves the way for microbial attack (Jans *et al.* 2004; Dixon *et al.* 2008; Müller *et al.* 2011; Booth and Madgwick 2016). As a consequence, microscopic focal destruction (MFD) (Jans *et al.* 2004) can easily hinder the analysis of bone microscopic structure. A sample from each skeleton was taken in order to ascertain the preservation of the histological structure (Fig. 5.12). No signs of MFD were found and the preservation of the histological bone structure was excellent (Oxford Histological Index 5) (Hedges *et al.* 1995).

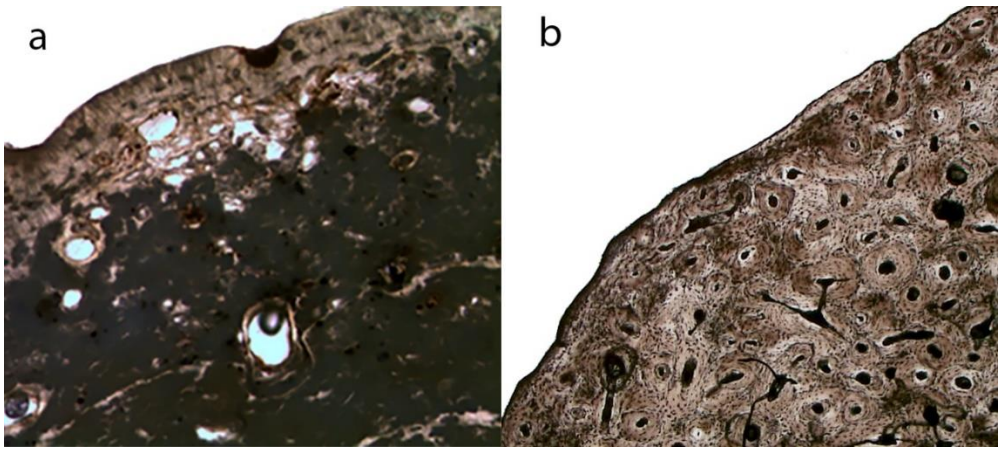

Figure 5.12 - a) example of "MFD" from the cross section of an archaeological femur; b) femoral cross section from the archaeological human adult skeleton (HA1), x25

5.2.3 THIN SECTION PREPARATION

The method used in this study to produce bone thin sections was based on the procedure commonly used at LABANOF (Laboratory of Forensic Anthropology and Odontology) for histological investigations of bone tissue (Cattaneo *et al.* 1999; Cattaneo *et al.* 2009; Caccia *et al.* 2016).

Complete cross-sections of approximately 5 mm were obtained from each bone by making two parallel cuts, perpendicular to the long axis of the bone using a hack-saw.

As previously stated (see paragraph 4.1.1), the only exception to this regarded the human juvenile skeleton, for which, only the posterior portion of some bones was taken.

With regard to the human fetus, prior to cutting, the mold of each bone was prepared using Xirid Push (Flockcart, Milan, Italy), a bi-component rubber paste. Bones were then cut with a rotatory tool to minimize the sampling thickness and avoid damaging the remaining bone portions. The mold of each bone was then used to reconstruct the missing portions by using a synthetic paste.

Each bone sample was ground and then polished using a Struer DAP-7 grinding wheel for geologist equipped with different Buehler® abrasive papers up to 4000 grit (Fig. 5.13).

The smoothed face of the bone samples was glued to the slides using Pertex® mounting medium (HistoLab, Göteborg, Sweden). Once the mounting medium dried, the other face of the bones was ground down to approximately 70-100 μm. The slides were then polished with 2400 and 4000 grit silicon carbide abrasive papers in order to remove surface scratches.

Figure 5.13 – Cross-sections preparation: Struer DAP-7 grinding wheel for geologist

5.3 HISTOLOGICAL ANALYSIS

The histological analyses were performed using an Axio Scope.A1® polarized light microscope connected to a Tucsen's TrueChrome II HD® camera (Fig. 5.14). Photos and measurements were taken using IScapture® software. Different images for each slide were photo-merged using Adobe Photoshop CS®. All the images were taken for illustrative purposes only, as all the observations and measurements were performed directly with the microscope and its relative software.

Qualitative observations of bone tissue were performed at 25X, 100X and 200X magnification, whereas measurements of structures were taken at 100X, 200X and 400X magnification. Calibration at each magnification was established with a stage micrometer. Polarized light was used in both histomorphological and histomorphometric analysis since it aided the recognition of the boundary of the structures, the nature of bone matrix as well as the orientation of the collagen fibres.

Figure 5.14 – The "Axio Scope.A1" polarized light microscope used for the histological analyses

5.3.1 HISTOMORPHOLOGICAL ANALYSIS

A qualitative histomorphological analysis was carried out on ninety-one human and eighty-nine pig cross sections. This analysis aimed at assessing the variability of the microstructural architecture in different parts of the skeleton. In fact, as outlined in the previous chapters, several factors such as posture and locomotion can influence the

mechanical strain that each bone (as well as different regions within the same bone) experience during the life of the individual.

In this research bone tissue microstructure was described according to the classification system and definitions of Francillon-Viellot and colleagues (1990) and Enlow and Brown (1956).

First, the presence of primary (woven, parallel-fibered, fibro-lamellar, or circumferential lamellar bone) and/or secondary bone (Haversian bone) was assessed (for definitions see paragraph 2.2). Second, the presence or absence and the orientation of the vascular canals were evaluated (avascular tissue, longitudinal, circumferential, reticular, or radial vascular canals). When secondary bone was present, a distinction was made according to the secondary osteons arrangement (Francillon-Viellot *et al.* 1990; Cuijpers 2006), distinguishing between irregular and dense Haversian bone, characterized respectively by few isolated and scattered, and tightly packed secondary osteons. Furthermore, the presence of "drifting osteons" or "osteon banding" was verified (for definitions see paragraph 2.2). Finally, the location of the tissue types within the section was reported (e.g. anterior aspect, periosteal surface).

Finally, since human and pig are characterized by different posture and locomotion, the anatomical terminology to describe the two mammals is different (Fig. 5.15).

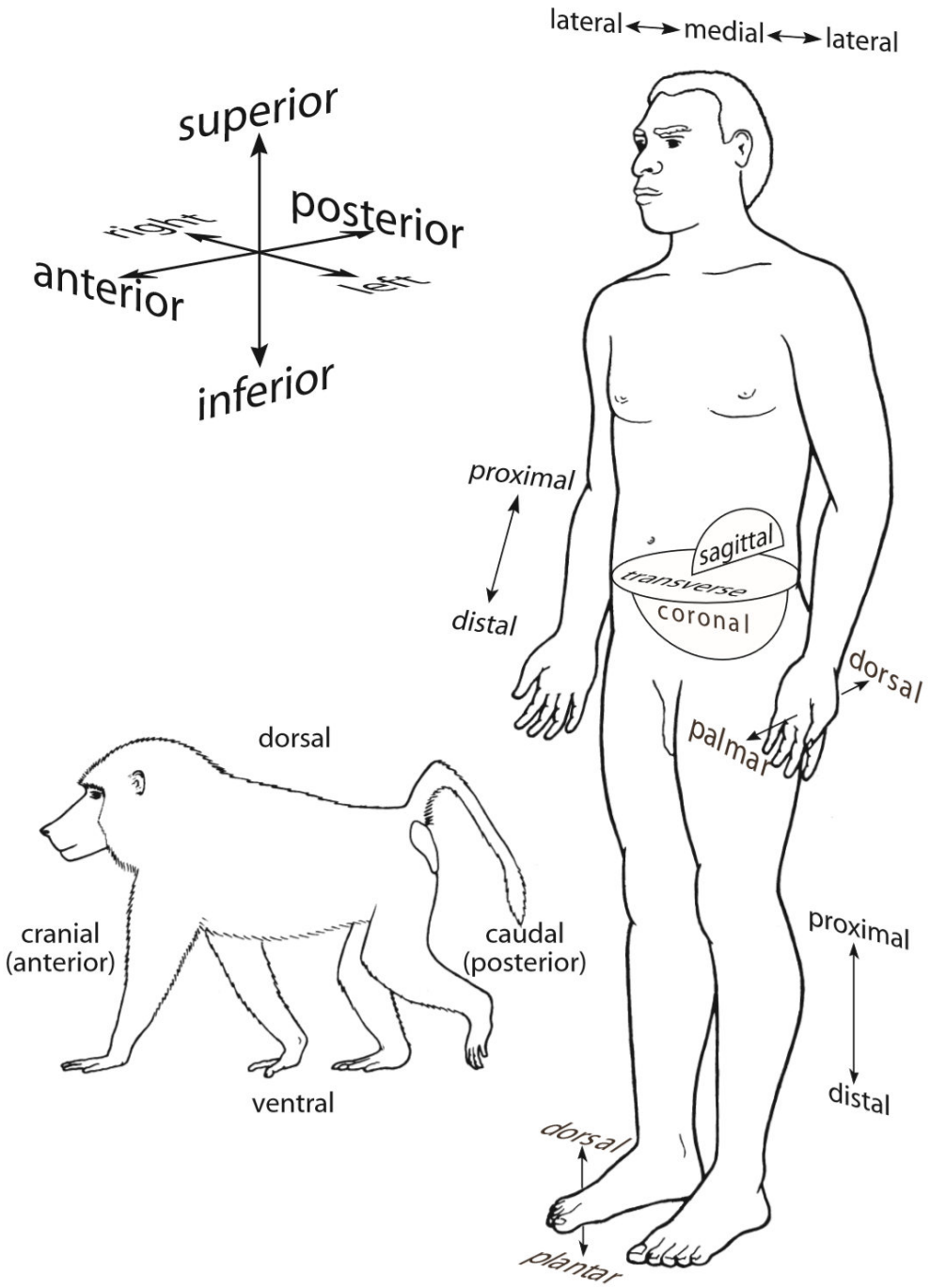

Figure 5.15 – Directional terms and planes for human and quadrupedal mammals (from White and Folkens 2005)

5.3.2 HISTOMORPHOMETRIC ANALYSIS

A histomorphometric analysis was performed on each section which showed the presence of remodeling, and therefore of secondary osteons. The choice of the osteons to measure was in accordance with the following criteria commonly used in histomorhometric studies (Qiu *et al.* 2003; Martin *et al.* 1996; Skedros *et al.* 2011): a)mature osteon (the Haversian canal area must be smaller than ¼ of the osteon area); b)not in resorption phase; c)with a well-defined and complete cement line; d)absence of Volkmann's canals crossing the osteon; e) the ratio between the Haversian canal maximum and minimum diameter must be inferior to 2:1. Criterion "e" was chosen in order to minimize the bias that may be introduced when measuring osteons which are not transversely sectioned. Therefore, when the ratio between the maximum and minimum diameter of the Haversian canal was higher than 2:1, the secondary osteon was excluded from the analysis.

The list of measurements (Table 5.4) for the histomorphometric analysis was made following previous investigations on species discrimination by the quantification of the size of bone structures (Dittman 2003; Urbanová and Novotny 2005; Martiniaková *et al.* 2006a; Cattaneo *et al.* 2009), namely maximum and minimum diameter, area and perimeter of secondary osteons and Haversian canals (Fig. 5.16). In addition, osteon circularity was added since recent research on the possibility to use the shape of osteons to discriminate between species showed promising results (Crescimanno and Stout 2012; Dominguez and Crowder 2012; Keenan *et al.* 2017). The index of circularity was determined for each osteon using the following formula (Crescimanno and Stout 2012):

$$Circularity = 4\,\pi\,(\frac{area}{perimeter^2})$$

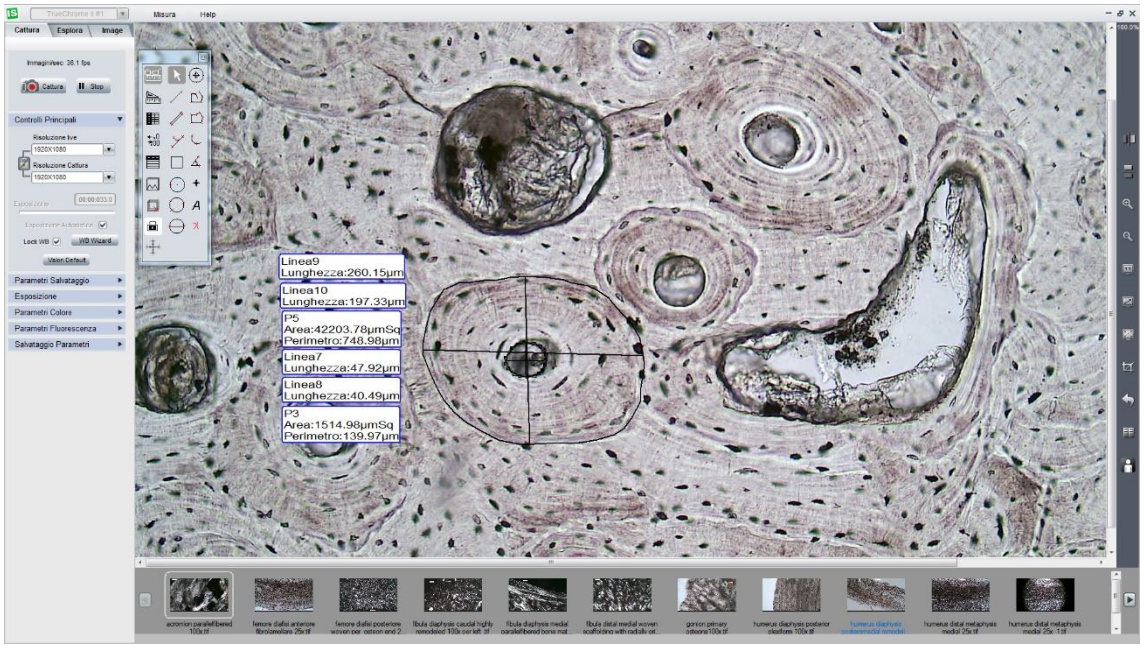

Figure 5.16 – Measurement of osteon and Haversian canals parameters using IScapture® software.

Finally, as previously stated in paragraph 4.3, an exploratory research was undertaken in order to ascertain the possibility to use the size of osteocyte lacunae to discriminate between human and pig secondary osteons with similar dimensions. Therefore, a histomorphometric analysis on osteocyte lacunae was performed from a total of one hundred and thirty-six secondary osteons, equally divided between human (HA1) and pig (PJ1). Osteons were selected according to criteria stated above. In addition, the osteons had to be characterized by a dark appearance under polarized light (Fig. 5.17) and the area of the osteons had to range between 17000 μm^2 and 45000 μm^2.

As regards the areas of the secondary osteons, the range 17000-45000 μm^2 was chosen since the majority of the osteons of individuals HA1 and PJ1, fell within this range. The criterion for the choice of osteons with a dark appearance under polarized light related to the relationship in lamellar bone between the arrangement of collagen fibres and the orientation of osteocyte lacunae. Marotti (1979) in fact, argued that “the major axis of

each lacuna is always parallel to the length of the collagen fibres; the intermediate and minor axes are respectively parallel and perpendicular to the surfaces of the lamellae which enclose the lacunae". The dark appearance of a secondary osteon under polarized light implies that its collagen fibres are mainly longitudinally directed, whereas an osteon which shows birefringence consists of collagen fibres which alternate between longitudinal and transverse direction (Frasca *et al.* 1977). This means that in cross-sections of birefringent osteons, several osteocyte lacunae may not be intersected according to their major axis. Therefore, dark osteons should be preferred for morphometric analysis of osteocyte lacunae.

After the selection of the osteons, the total number of lacunae per osteons was counted and the following measurements were taken: minimum and maximum diameter, area and perimeter of nine lacunae divided between outer, intermediate and inner lacunae. The focal plane chosen for each lacuna corresponded to its largest area. As regards the rationale behind the decision to divide the osteon in three layers, a previous investigation by Ardizzoni (2001) demonstrated that human osteocyte lacunae decrease in size from the cement line towards the Haversian canal. Therefore, one of the aims of this research was to verify if this trend can be seen even in pig bones.

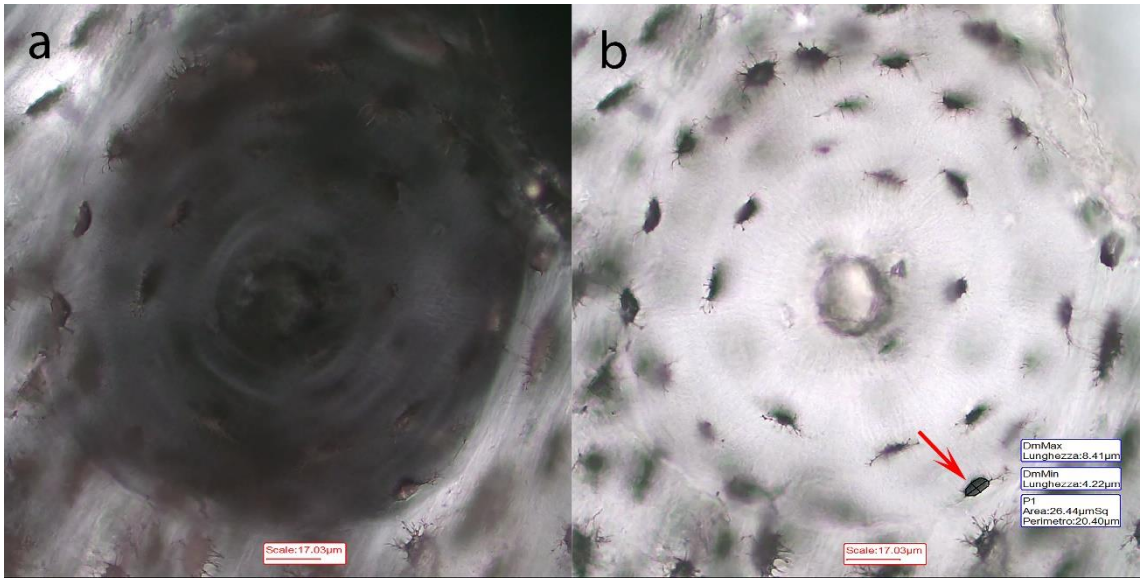

Figure 5.17 - Pig secondary osteon: a) dark appearance under polarized light (dark morphotype); b) measurement of osteocyte lacunae, x200

Structure	Parameter to measure/assess
Osteon	Minimum diameter (µm)
	Maximum diameter (µm)
	Area (µm^2)
	Perimeter (µm)
	Circularity (ratio)
Haversian canal	Minimum diameter (µm)
	Maximum diameter (µm)
	Area (µm^2)
	Perimeter (µm)
Osteocyte lacunae	Minimum diameter (µm)
	Maximum diameter (µm)
	Area (µm^2)
	Perimeter (µm)

Table 5.4 – List of parameters that were measured/assessed during the histomorphometric analysis

5.4 STATISTICAL ANALYSIS

The histomorphometric analyses involved the measurement of 3553 secondary osteons (2503 from human bones and 1050 from pig bones) and 1242 osteocyte lacunae (equally divided between human and pig). For each secondary osteon, nine parameters were measured, thus reaching a total of 31977 individual measurements. For each osteocyte lacuna, four parameters were measured, for a total of 4968 individual measurements.

Statistical analysis of the results was computed using SPSS 22 software (SPSS Inc., Chicago, IL, USA). The descriptive statistics of the mean value, the standard deviation of the mean, the minimum value and the maximum value were obtained for the data set of all cross-sections of human and pig bones, for each of the parameters measured. Shapiro-Wilks test was performed to assess the distribution of data for each variable in each dataset.

Generally, with non-normal distribution a non-parametric test such as Kruskal-Wallis should be preferred rather than the one-way analysis of variance (ANOVA). Nonetheless, several studies on the effect of non-normality on F-test (ANOVA) robustness pointed out that F-test is robust, since Type I error performance do not seem to be affected by non-normal distribution (Lix *et al.* 1996; Glass *et al.* 1972; Harwell *et al.* 1992; Blanca *et al.* 2017). According to Blanca and colleagues (2017), F-test is robust when distribution is characterized by values of skewness and kurtosis that range between -1 and 1. Therefore, since the values of skewness and kurtosis of the distribution of data in each dataset was within that range, ANOVA test could be performed.

In addition, since the histomorphometric analysis considered several variables, a multivariate analysis of variance (MANOVA) seemed, at first, the most appropriate test.

However, as suggested by Tabachnick and Fidell (2012), in order to perform the MANOVA test, the dependent variables cannot be too correlated to each other ($r < .90$). A Pearson correlation test indicated a high correlation between some of the variables (e.g. diameters and area), thus ANOVA test was chosen to analyze the data.

When more than two groups were tested, and results showed statistically significant differences ($p < .05$), Tukey post-hoc test was carried out in order to verify which of the specific group differed.

In addition, Intraclass Correlation Coefficient (ICC) was calculated repeating measurements of thirty secondary osteons and thirty osteocyte lacunae by two trained operators and by the same operator after twenty-four, forty-eight and seventy-two hours in order to test the inter-rater and intra-rater reliability. This index measures both the degree of correlation and agreement between measurements. For each variable an intraclass correlation coefficient was obtained. This value ranges between 0 and 1, with values less than 0.5 indicating poor reliability, values between 0.5 and 0.75 indicating good reliability, and values greater than 0.90 representing excellent reliability (Portney and Watkins 2000; Koo and Li 2016).

CHAPTER 6
RESULTS

This chapter presents the results of the histomorphological and histomorphometric analyses of human and pig bone. Paragraphs 6.1 and 6.2 describe the extent of intra-individual variability from a qualitative and quantitative perspective, whereas paragraphs 6.3, 6.4 and 6.5 focus on the intra- and inter-species variability. The results of the exploratory research on osteocyte lacunae are presented in paragraph 6.6.

Photo-merged images of the human cross-sections are presented in Appendix A, whereas the descriptive statistics of osteon and Haversian canal parameters for each human and pig bone are provided in Appendix B.

As previously stated in paragraph 5.4, a Pearson correlation test indicated a high correlation between the maximum diameter, minimum diameter, area and perimeter of both the osteon and the Haversian canal (see Table 6.1 and Figure 6.1). Therefore, in the next chapters, results will be presented and discussed in terms of osteon size and Haversian canal size rather then considering each single variable.

	1	**2**	**3**	**4**
1. On.Dm (max)	-			
2. On.Dm (min)	.880**	-		
3. On.Ar	.957**	.949**	-	
4. On.Pm	.977**	.945**	.986**	-
	5	6	7	8
5. HC.Dm (max)	-			
6. HC.Dm (min)	.902**	-		
7. HC.Ar	.947**	.954**	-	
8. HC.Pm	.973**	.955**	.979**	-

****. Correlation is significant at the 0.01 level (2-tailed).**

Table 6.1 - Pearson Correlations among osteon and Haversian canal variables

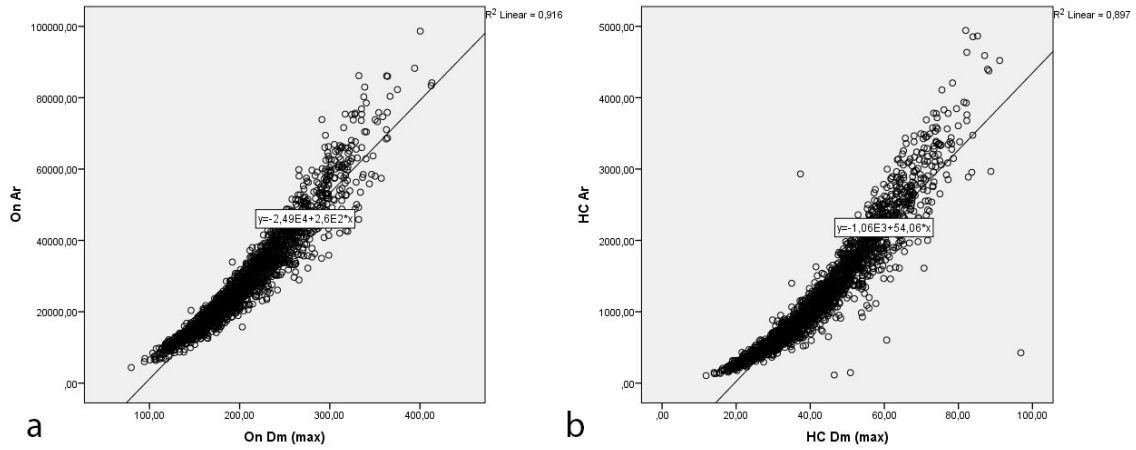

Figure 6.1 – Scatterplots showing the correlation between (a) osteon maximum diameter and area, and between (b) Haversian canal maximum diameter and area

6.1 INTRA-INDIVIDUAL HISTOMORPHOLOGICAL VARIABILITY

6.1.1 ADULT HUMAN SKELETON (HA1)

A qualitative histomorphological analysis was carried out on forty-nine cross-sections from an adult human skeleton in order to evaluate the presence of primary and secondary bone and to assess the arrangement of the vascular canals. Different portions of the same bone were analyzed as to verify the variability of bone microstructural architecture (see Chapter 4 for the details of the bone samples and the methodological approach).

Overall, no histological sections showed primary non-lamellar bone (Table 6.2). Long bones exhibited a higher rate of remodeling compared to flat and irregular bones, which showed a prevalence of lamellar tissue (see Appendix A for the whole slide images of each cross-section).

The **humerus** exhibited Haversian bone as well as some areas of primary lamellar bone in the outer and inner surfaces. Following the length of the bone, the differences between the three portions sampled regarded mainly the density of secondary osteons, which were more scattered and isolated in the proximal metaphysis and more tightly packed proceeding towards the distal end of the bone.

The proximal metaphysis was characterized by a rather uniform tissue consisting in scattered secondary osteons without organization and immersed in a lamellar matrix. In the posterolateral aspect of the bone, close to the periosteum, the osteons were organized in circumferential rows. In the posteromedial aspect of the bone, close to the endosteum, large areas of inner circumferential lamellae with longitudinal vascular canals and resorption spaces were observed.

The humeral diaphysis was characterized by a combination of dense and irregular Haversian bone. The former, consisted in tightly packed osteons with no organization and it was located at the medial and lateral aspect; the latter was located at the anterior and posterior aspect and it consisted in scattered osteons without organization. A thin layer of outer circumferential lamellae with longitudinal vascular canals was present along the entire section. The anterior and posterior aspect of the bone exhibited several large resorption spaces.

The distal metaphysis of the humerus exhibited dense Haversian bone at the anterior and posterior aspect, whereas the lateral and medial aspect were characterized by scattered secondary osteons organized in circumferential rows. Some cases of linear arrangement of secondary osteons (Fig. 6.2) surrounded by lamellar tissue were observed (rows of four to five osteons).

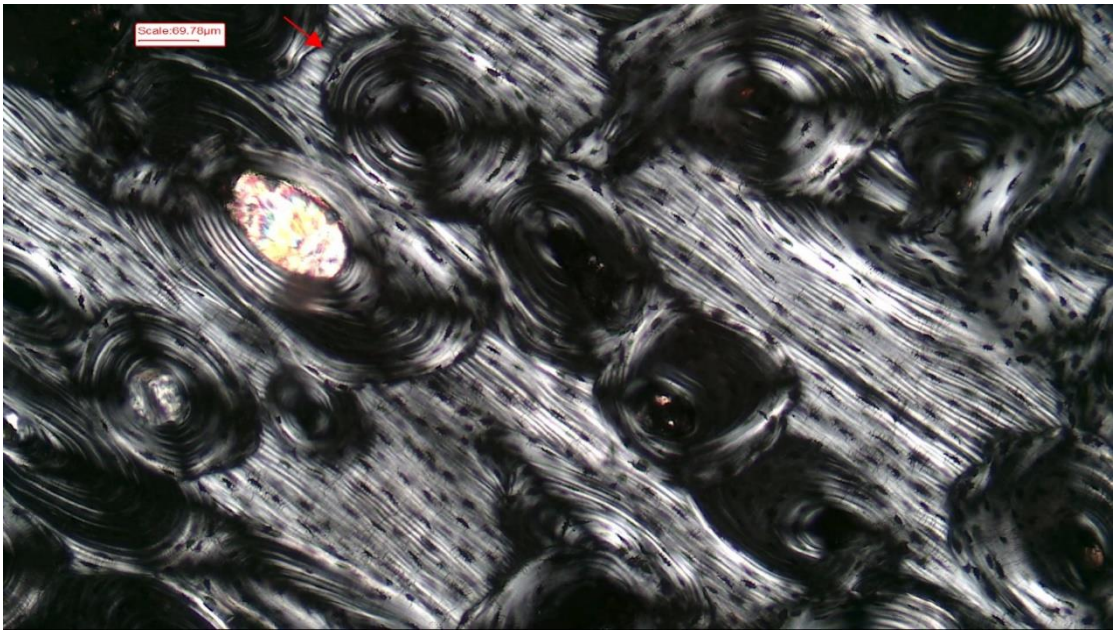

Figure 6.2 – Humerus (distal metaphysis). Linear band of secondary osteons, x100. Polarized light

The **ulna** exhibited Haversian bone with remnants of primary lamellar bone at the periosteal and endosteal surfaces. Unlike the humerus, the density of secondary osteons seemed to decrease from the proximal metaphysis towards the distal metaphysis. The former consisted almost entirely in dense osteons, which were organized in circumferential rows at the medial and lateral aspect, especially close to the periosteum.

The ulnar diaphysis was mainly characterized by scattered secondary osteons without organization, with the exception of the lateral aspect exhibiting a high number of tightly packed secondary osteon. At the posteromedial aspect of the bone a large layer of outer circumferential lamellae was observed. Proceeding towards the medial aspect, close to the periosteum, secondary osteons are arranged in circumferential rows. Several drifting osteons were identified observing the section by polarized light (Fig. 6.3).

The distal metaphysis appeared uniform, consisting in isolated secondary osteons without organization and immersed in abundant lamellar matrix. Several resorption spaces were observed around the medullary cavity.

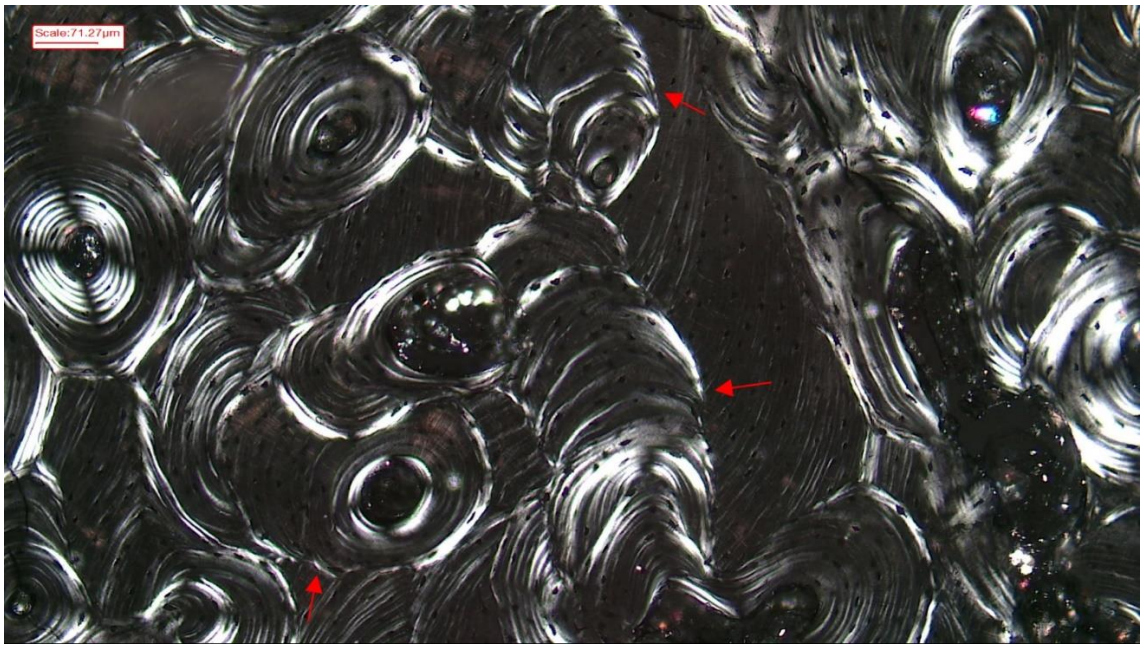

Figure 6.3 – Ulna (diaphysis). Drifting osteons at the posterior aspect, x100. Polarized light

The **radius** exhibited Haversian bone. Like the ulna, the density of secondary osteons seemed to decrease proceeding distally.

The proximal metaphysis consisted almost entirely of tightly packed secondary osteons without organization, except for the posterior portion in which they were organized in circumferential rows. Remnants of primary lamellar bone were present in form of inner and outer circumferential lamellae.

The radial diaphysis exhibited extensive areas of tightly packed secondary osteons organized in circumferential rows. The lateral aspect was characterized by more isolated osteons with no organization immersed in abundant lamellar matrix. Close to the

endosteum, a large area of avascular lamellar tissue was observed (Fig. 6.4), whereas at the posterior aspect, close to the periosteum, a large area of outer circumferential lamellae with longitudinal vascular canals was present (Fig. 6.5). Several resorption spaces were noted around the medullary cavity.

The distal metaphysis of the radius exhibited a uniform tissue characterized by isolated secondary osteons without organization in abundant lamellar matrix. Layers of outer and inner circumferential lamellae were present in the entire section.

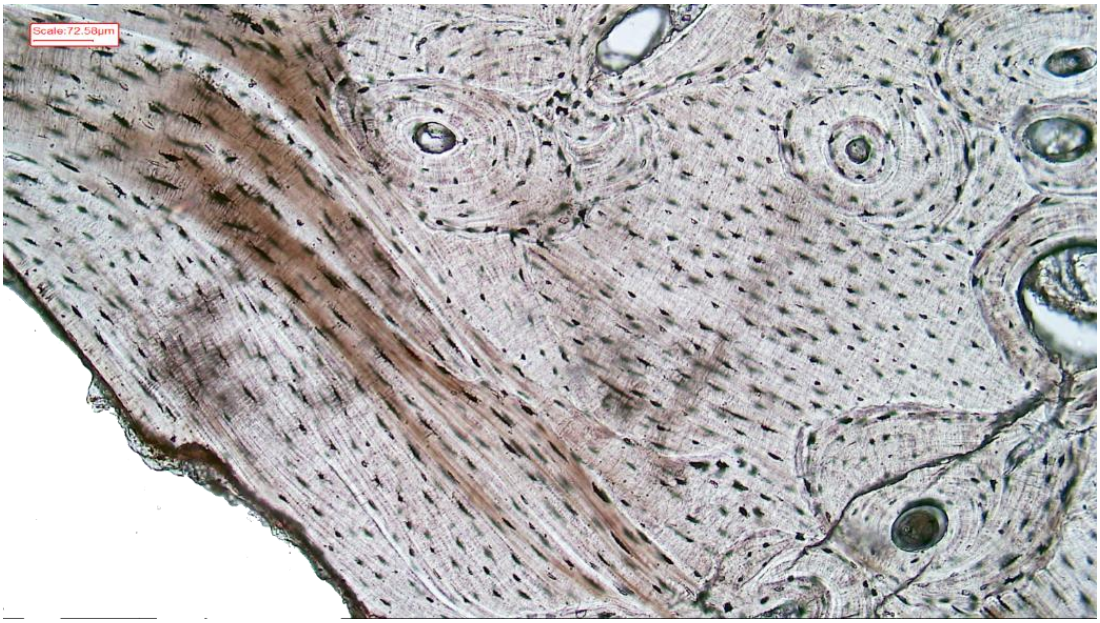

Figure 6.4 – Radius (diaphysis). Avascular lamellar tissue at the lateral aspect, x100

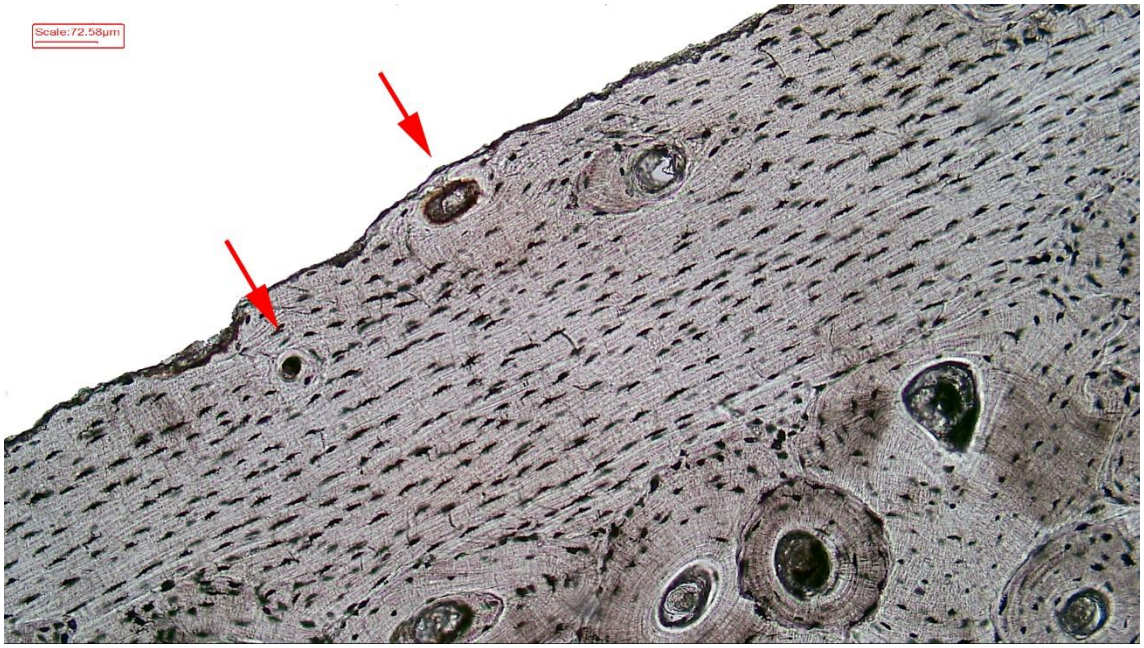

Figure 6.5 – Radius (diaphysis). Lamellar tissue with few longitudinal vascular canals (red arrows) at the posterior aspect, x100

The **clavicle** was characterized by Haversian bone with some difference in osteon density and organization between shaft and the medial and lateral portion.

The medial portion exhibited mainly isolated osteons without organization, except for the superior aspect which showed tightly packed secondary osteons. At the posteroinferior aspect, close to the endosteum, remnants of primary lamellar bone with longitudinal vascular canals were observed.

The shaft was characterized by tightly packed secondary osteons organized in circumferential rows, especially at the posterior aspect (Fig. 6.6). Several drifting osteons were observed at the inferior aspect (Fig. 6.7).

The lateral end exhibited dense osteons without a particular organization, except for the superior aspect which is characterized by isolated secondary osteons. Several resorption spaces were present along the entire section.

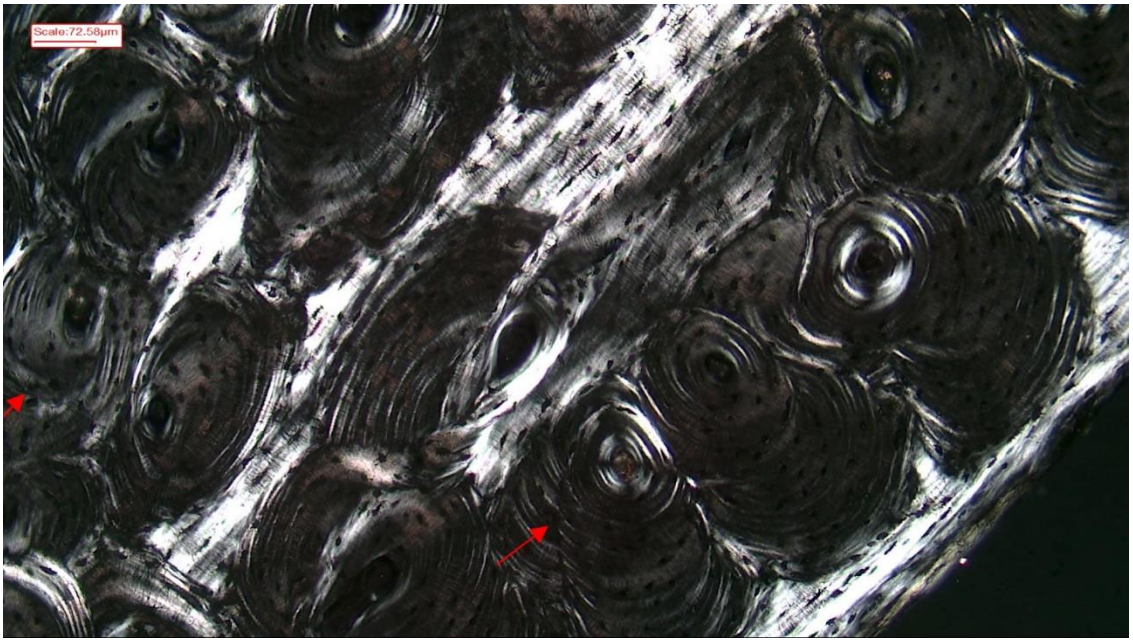

Figure 6.6 – Clavicle (shaft). Dense osteons organized in circumferential rows at the posterior aspect, x100. Polarized light

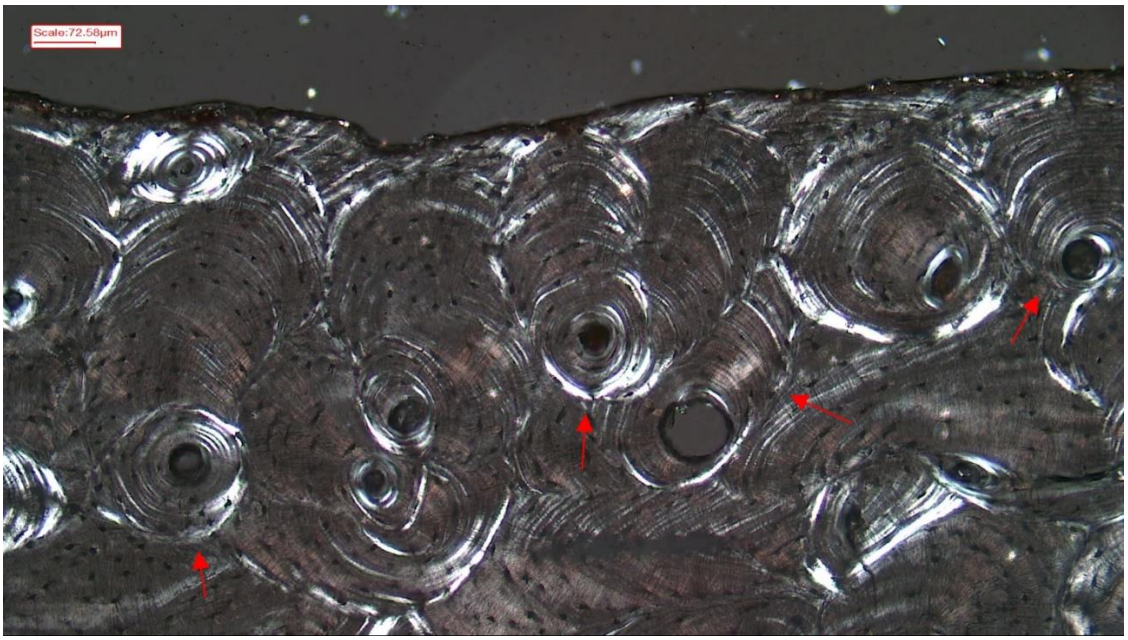

Figure 6.7 – Clavicle (shaft). Several drifting osteons at the inferior aspect, x100. Polarized light

The **femur** was composed mainly of tightly packed secondary osteons. Like the ulna and the radius, the density of secondary osteons seemed to decrease towards the distal metaphysis.

The femoral neck exhibited mainly dense osteons, which were organized in circular rows at the periosteal surface. Several resorption spaces were observed at the anterior aspect. The trabeculae were generally characterized by lamellar tissue although occasional small osteons were present.

The proximal metaphysis exhibited a rather uniform tissue composed of tightly packed secondary osteons without organization. Several resorption spaces were observed around the medullary cavity, especially at the anterior and posterior aspect.

With regard to the diaphysis, it mainly consisted of dense osteons. At the lateral and posteromedial aspect secondary osteons were more scattered and organized in circumferential rows with some linear bands of osteons surrounded by lamellar tissue.

The distal metaphysis exhibited isolated secondary osteons with no organization in abundant lamellar matrix (Fig. 6.8). A thin layer of outer circumferential lamellae with longitudinal vascular canals was observed at the outer surface of the bone.

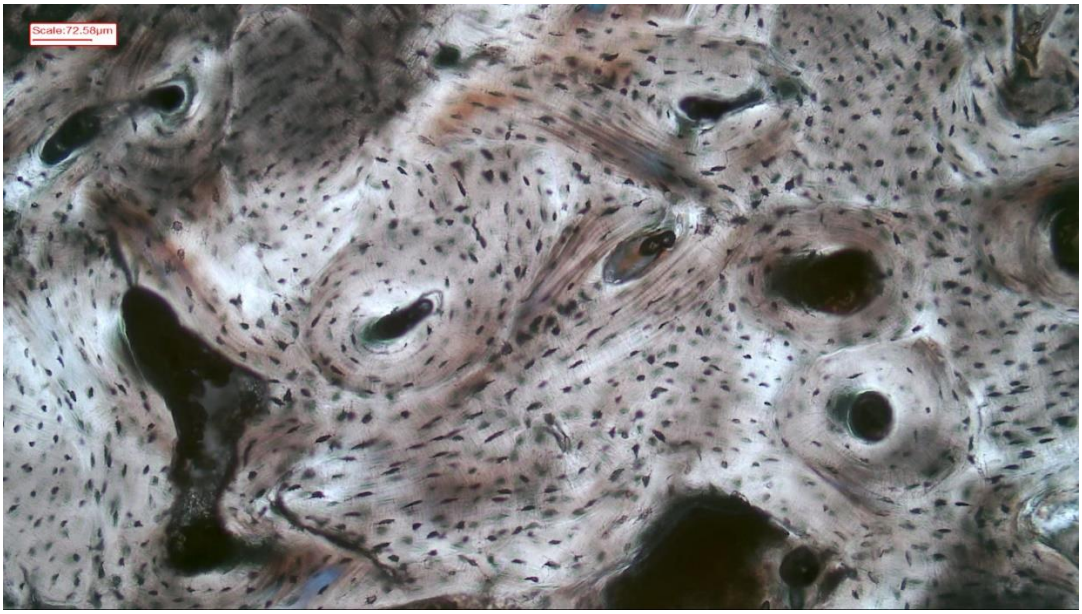

Figure 6.8 – Femur (distal metaphysis). Isolated secondary osteons, x100

The **tibia** exhibited Haversian bone with remnants of primary lamellar bone at the outer and inner surface.

The proximal metaphysis was characterized by tightly packed secondary osteons at the anterior and posterior aspect, whereas at the medial and lateral aspect, secondary osteons are more scattered and immersed in a lamellar matrix. Resorption spaces were present along the entire section, and radial vascular canals were observed at the lateral aspect (Fig. 6.9).

The tibial diaphysis exhibited dense osteons, except for the posterior aspect in which secondary osteons were more scattered in abundant lamellar matrix. At the anterior aspect, close to the periosteum, osteons were organized in circumferential rows. Thin layers of outer and inner circumferential lamellae with longitudinal vascular canals were observed, especially at the lateral aspect.

The distal metaphysis was characterized by dense osteons at the anterior and lateral aspect, whereas at the posterior and medial aspect, osteons were more scattered in a lamellar matrix. Several resorption spaces were observed along the entire section (Fig. 6.10).

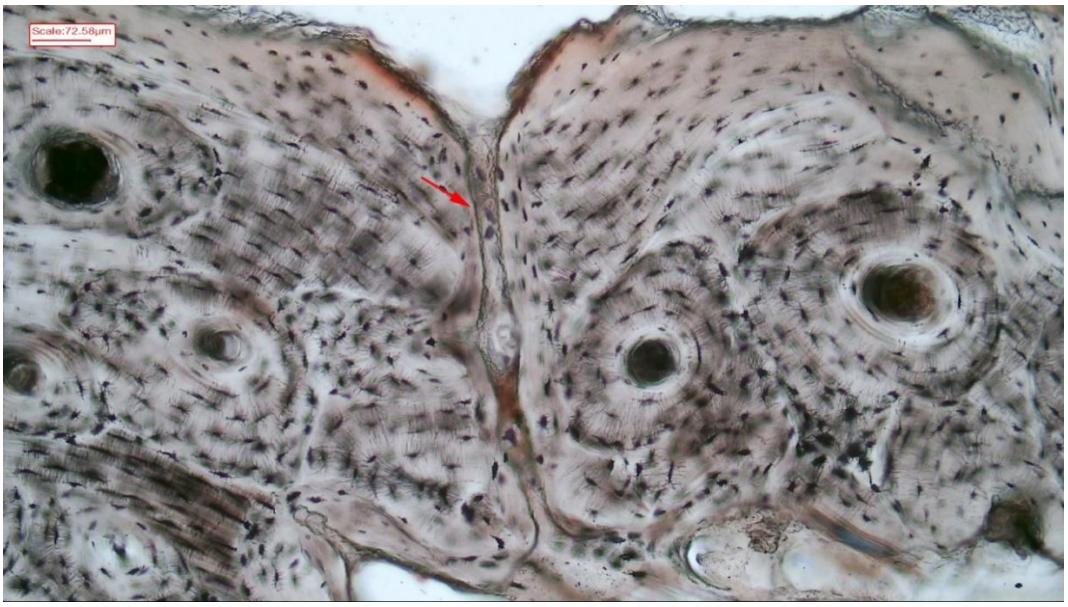

Figure 6.9 – Tibia (proximal metaphysis). Radial vascular canal at the lateral aspect, x100

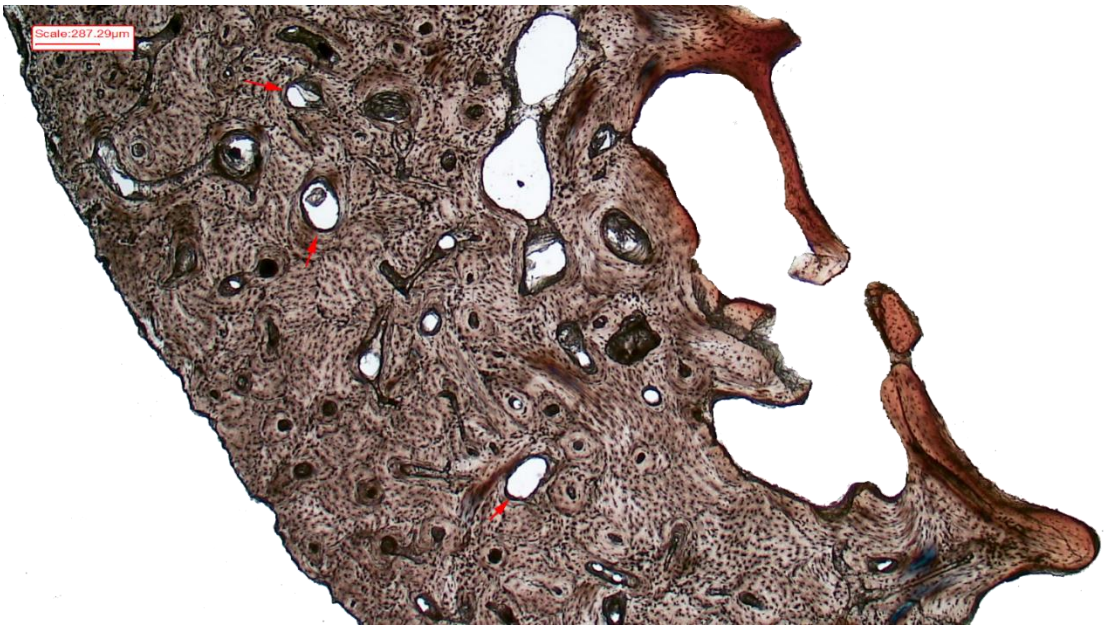

Figure 6.10 – Tibia (distal metaphysis). Resorption spaces at the posterolateral aspect, x25

The **fibula** was characterized by Haversian bone, mainly in form of isolated secondary osteons. The osteon density seemed to decrease proceeding distally.

The proximal metaphysis exhibited mainly isolated secondary osteons in a lamellar matrix, except for the lateral portion in which osteons were tightly packed. Several Volkmann's canals and longitudinal vascular canals were present along the entire section.

The fibular diaphysis consisted mainly of isolated secondary osteons with abundant interstitial lamellae, except for the medial aspect in which osteons are tightly packed and organized in circumferential rows, especially close to the periosteum. Several Volkmann's canals and resorption spaces were present along the entire section.

The distal metaphysis exhibited a rather uniform tissue characterized by isolated secondary osteons immersed in a lamellar matrix. At the posterior aspect, close to the endosteum, a large area of lamellar tissue with radial vascular canals were observed (Fig. 6.11)

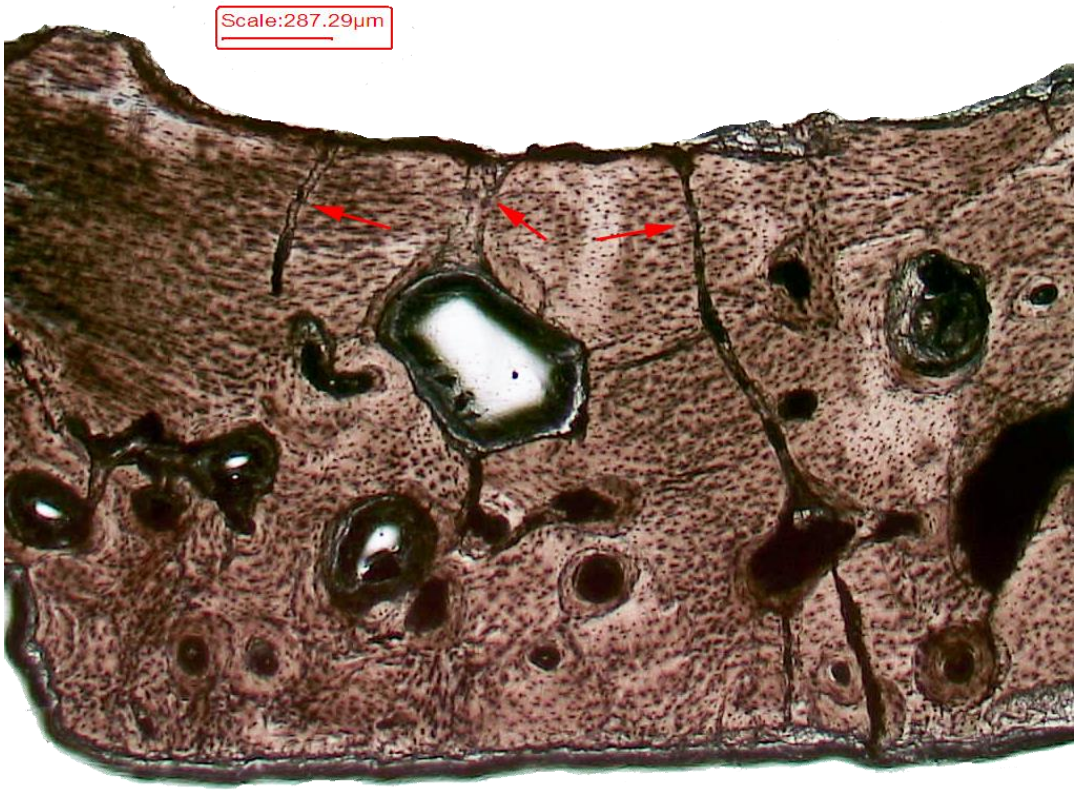

Figure 6.11 – Fibula (distal metaphysis). Lamellar tissue with radial vascular canals at the posterior aspect, x25

The **metacarpal** was characterized by a low osteon density exhibiting scattered secondary osteons immersed in large areas of lamellar tissue.

The metacarpal head showed isolated secondary osteons organized in circumferential rows, especially close to the periosteal surface. Close to the endosteum thick layers of inner circumferential lamellae with longitudinal vascular canals were observed.

The metacarpal body exhibited a similar pattern of scattered secondary osteons organized in circumferential rows (Fig. 6.12). In addition, several drifting osteons were observed by polarized light, especially at the medial aspect (Fig. 6.13).

The base of the metacarpal showed a tissue entirely composed of lamellar tissue without any secondary osteon.

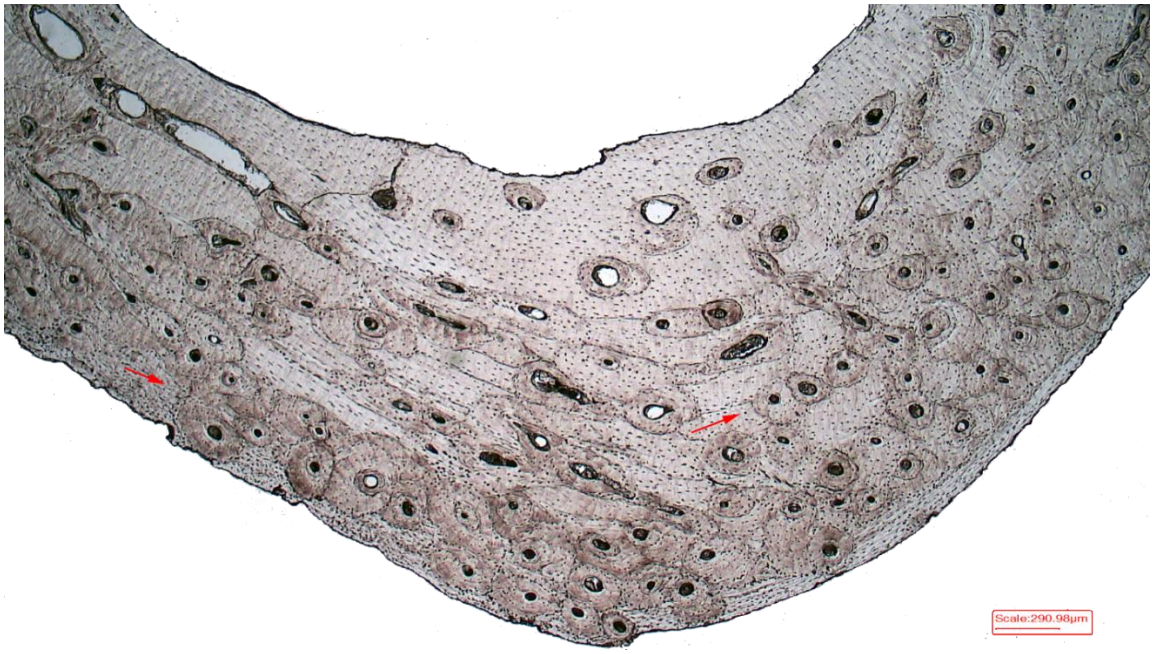

Figure 6.12 – Metacarpal (shaft). Scattered secondary osteons organized in circumferential rows and immersed in a lamellar matrix at the medial aspect, x25

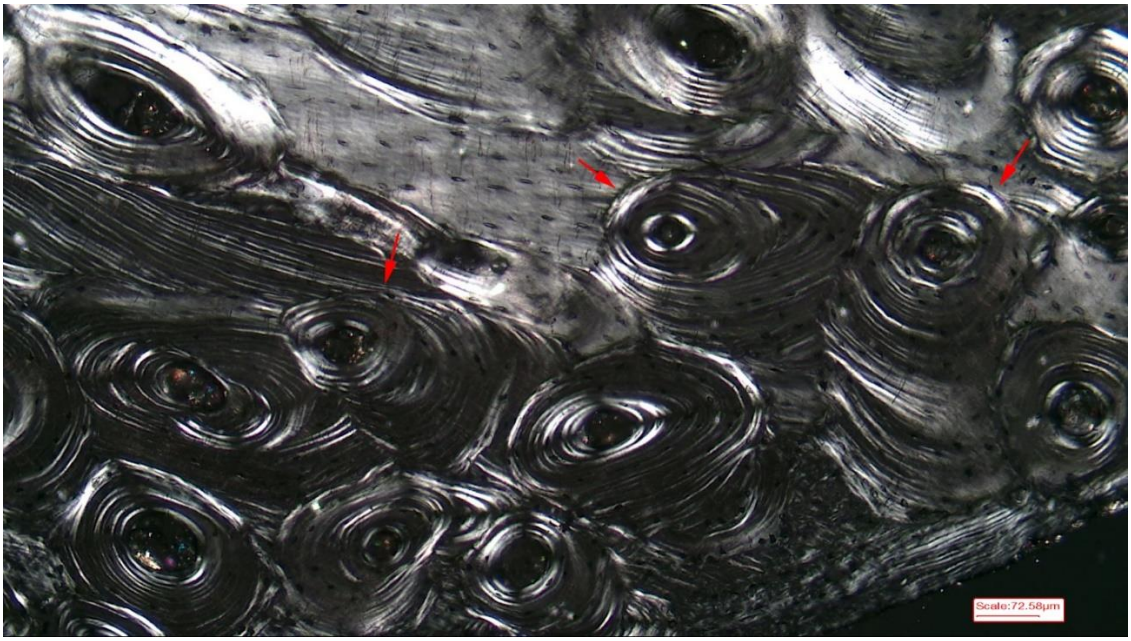

Figure 6.13 – Metacarpal (shaft). Drifting osteons at the medial aspect, x100. Polarized light

The **metatarsal** exhibited a higher osteon density compared to the metacarpal.

The head of the metacarpal consisted mostly of lamellar tissue, except for the dorsal aspect which showed isolated secondary osteons in a lamellar matrix. Several resorption spaces were present, especially at the plantar and lateral aspects.

The shaft of the metatarsal was characterized by tightly packed secondary osteons, except for the dorsolateral aspect in which osteons are more scattered. Several resorption spaces were observed, especially at the lateral aspect.

The base of the metatarsal showed scattered secondary osteons with no organization in a lamellar matrix. The trabeculae consisted of lamellar tissue without any osteon.

The **rib** was characterized by tightly packed secondary osteons in the body whereas the rib's head showed isolated osteons without organization. At the anterior aspect of the rib's head several drifting osteons were observed (Fig. 6.14).

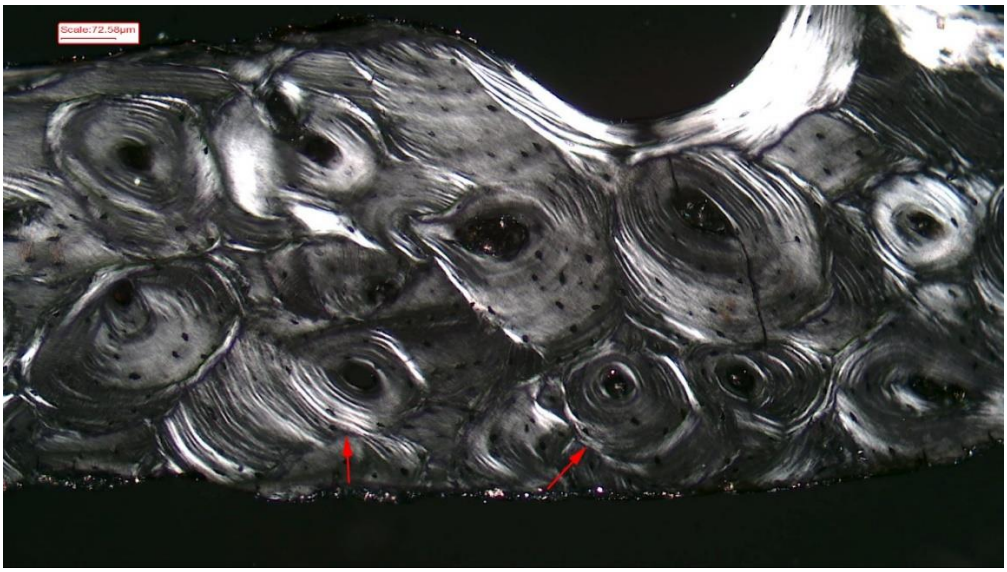

Figure 6.14 – Rib (head). Drifting osteons at the anterior aspect, x100. Polarized light

The **sternum** exhibited mainly isolated secondary osteons in a lamellar matrix, except for the anterior aspect in which secondary osteons were tightly packed.

The **scapula** showed a higher osteon density in the superior border compared to the acromion, in which secondary osteons were more isolated with abundant interstitial lamellae.

With regard to the **ox coxae**, the iliac crest consisted in a uniform tissue composed of scattered secondary osteons without organization. Several resorption spaces were observed.
The ischiopubic ramus showed isolated secondary osteons in a lamellar matrix, whereas the iliopubic ramus exhibited a higher osteon density.

With regard to the **cranium**, a general prevalence of lamellar tissue with some areas of scattered or dense osteons was observed. The parietal and frontal bone (glabella) exhibited large areas of lamellar tissue with isolated secondary osteons. The zygomatic process of the frontal bone was characterized solely by lamellar tissue with longitudinal vascular canals. The occipital showed the highest rate of remodeling, exhibiting an alternation of areas of tightly packed secondary osteons and areas in which the osteons were more scattered. Petrous exhibited mainly lamellar tissue with a high number of osteocyte lacunae and reticular vascular canals (Fig. 6.15).

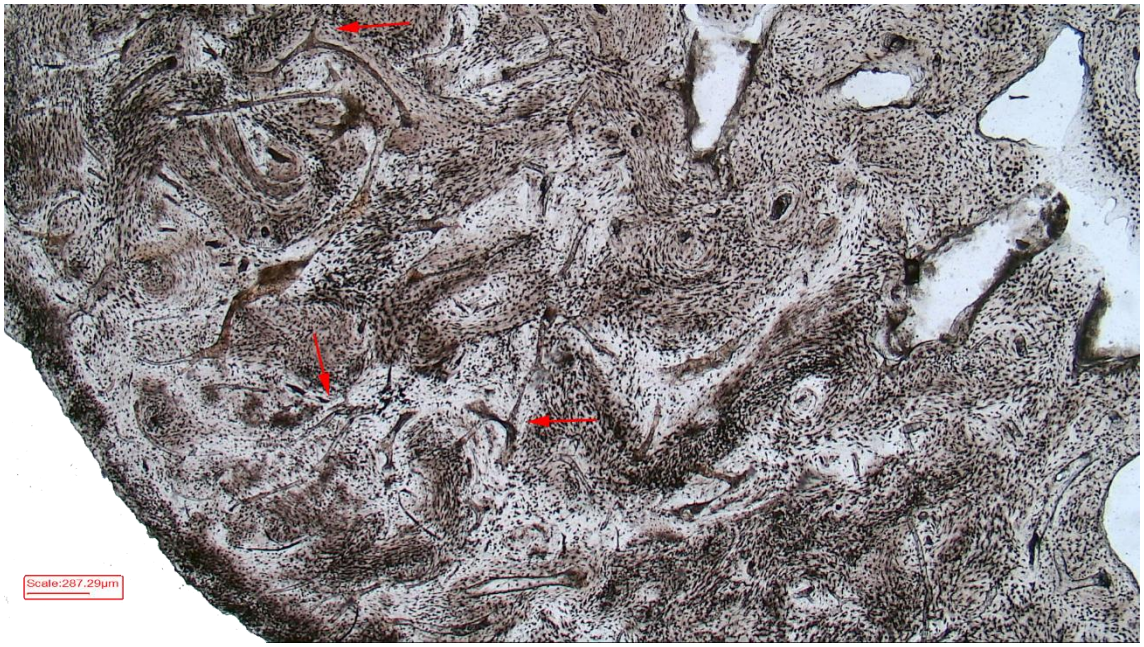

Figure 6.15 – Petrous. Lamellar tissue with reticular vascular canals, x25

The **mandible** was characterized by a rather uniform tissue consisting of isolated secondary osteons in abundant lamellar matrix. Gonion and mental protuberance exhibited exclusively isolated osteons without organization, except for a small area of the mental protuberance in which osteons are organized in circumferential rows, showing some linear bands of three to four osteons surrounded by lamellar tissue. The mandibular condyle was characterized by lamellar tissue with longitudinal vascular canals, except for some scattered secondary osteons at the superior aspect.

The longitudinal section of the **cervical vertebra** exhibited isolated osteons at the posterior portion of the vertebral body and thightly packed osteons in the spinous process. The transversal section showed exclusively lamellar tissue.

The patella was characterized by lamellar tissue with longitudinal vascular canals without any secondary osteons.

Table 6.2 – Results of the histomorphological analysis on the adult human skeleton HA1

Bone tissue type	Bone	Primary bone				Secondary bone								Vascularization				
		Non-lamellar		Lamellar (outer and inner circumferential lamellae)		Scattered secondary osteons without organization		Scattered secondary osteons organized in circumferential rows		Dense secondary osteons without organization		Dense secondary osteons organized in circumferential rows		Avascular	Longitudinal vascular canals	Circumferential vascular canals	Reticular vascular canals	Radial vascular canals
		Periosteal layer	Endosteal layer	Periosteal layer	Endosteal layer	Periosteal layer	Endosteal layer	Periosteal layer	Endosteal layer	Periosteal layer	Endosteal layer	Periosteal layer	Endosteal layer					
Long bones	Humerus – proximal metaphysis				✓	✓	✓	✓							✓			
	Humerus - diaphysis			✓		✓	✓			✓	✓				✓			
	Humerus – distal metaphysis					✓	✓			✓	✓							
	Ulna – proximal metaphysis							✓		✓	✓							
	Ulna – diaphysis			✓		✓	✓	✓		✓	✓							
	Ulna – distal metaphysis					✓	✓											✓
	Radius – proximal metaphysis									✓	✓	✓						
	Radius – diaphysis			✓	✓	✓						✓		✓	✓			
	Radius – distal metaphysis			✓		✓	✓											
	Clavicle – medial end			✓	✓	✓	✓			✓					✓			
	Clavicle – diaphysis			✓								✓						
	Clavicle – lateral end						✓			✓	✓							
	Femur - neck										✓	✓	✓					
	Femur – proximal metaphysis									✓	✓							
	Femur – diaphysis								✓	✓	✓	✓						
	Femur – distal metaphysis				✓	✓	✓								✓			
	Tibia proximal metaphysis					✓	✓			✓	✓							
	Tibia – diaphysis			✓	✓					✓	✓	✓			✓			
	Tibia – distal metaphysis			✓	✓	✓	✓			✓	✓	✓			✓			
	Fibula – proximal metaphysis					✓	✓			✓								
	Fibula – diaphysis						✓			✓	✓	✓						
	Fibula – distal metaphysis			✓		✓	✓											✓
	Metacarpal – proximal end			✓	✓													
	Metacarpal – shaft			✓	✓		✓					✓	✓					

Bone tissue type	Bone	Primary bone				Secondary bone								Vascularization				
		Non-lamellar		Lamellar (outer and inner circumferential lamellae)		Scattered secondary osteons without organization		Scattered secondary osteons organized in circumferential rows		Dense secondary osteons without organization		Dense secondary osteons organized in circumferential rows		Avascular	Longitudinal vascular canals	Circumferential vascular canals	Reticular vascular canals	Radial vascular canals
		Periosteal layer	Endosteal layer	Periosteal layer	Endosteal layer	Periosteal layer	Endosteal layer	Periosteal layer	Endosteal layer	Periosteal layer	Endosteal layer	Periosteal layer	Endosteal layer					
	Metacarpal – distal end			✓	✓							✓	✓					
	Metatarsal – proximal end					✓	✓											
	Metatarsal – shaft						✓			✓	✓							
	Metatarsal – distal end			✓	✓	✓	✓											
Flat bones	Temporal bone – zygomatic process			✓	✓										✓			
	Frontal bone – glabella					✓	✓								✓			
	Temporal bone - petrous			✓	✓	✓									✓		✓	
	Parietal			✓		✓	✓								✓			
	Occipital					✓	✓											
	Rib – head					✓	✓								✓			
	Rib – body				✓		✓			✓								
	Sternum					✓	✓			✓					✓			
	Scapula – superior border			✓	✓					✓	✓							
	Scapula – acromion					✓	✓	✓										
	Ilium – iliac spine					✓	✓											
	Iliac crest – transversal					✓	✓								✓			
	Iliac crest – longitudinal					✓	✓											
	Iliopubic ramus					✓	✓											
Irregular bones	Mandible – gonion					✓	✓											
	Mandible – mental protuberance			✓		✓	✓								✓			
	Mandibular condyle			✓										✓	✓			
	Cervical vertebra – longitudinal				✓	✓												
	Cervical vertebra – transversal			✓	✓										✓			
Sesamoid	Patella			✓	✓										✓			

CONCLUDING REMARKS

The histomorphological analysis of the adult human skeleton (HA1) pointed out the absence of both woven and fibro-lamellar bone. With regard to the Haversian bone, approximately seventy percent of the cross-sections exhibited scattered secondary osteons without organization. About half of the sections were characterized by primary circumferential lamellar bone in the form of inner and/or outer circumferential lamellae, respectively located at the endosteal and periosteal surfaces. Overall, except for the trabeculae which showed avascular or poorly vascularized lamellar tissue, long bones exhibited a higher variability. Approximately fifty percent of long bones were characterized by an alternation within the same cross section of areas consisting in tightly packed secondary osteons (dense Haversian bone) and areas characterized by isolated secondary osteons immersed in abundant lamellar matrix (irregular Haversian bone). Some distinctive features have been noted, such as avascular lamellar tissue in the lateral aspect of the radial diaphysis, and lamellar tissue with radial vascular canals at the lateral aspect of the proximal metaphysis of the tibia and at the posterior aspect of the distal metaphysis of the fibula.

Conversely, flat and irregular bones exhibited a greater uniformity, with over eighty percent of the cross-sections showing a single pattern of osteon organization. Overall, flat bones were characterized by scattered secondary osteons with abundant interstitial lamellae, except for the rib, the sternum, the superior border of the scapula, the iliopubic ramus and the occipital which exhibited a higher osteon density, with tightly packed secondary osteons and scarce interstitial lamellae.

Petrous bone was characterized by a distinctive tissue consisting in lamellar tissue with a large network of reticular and longitudinal vascular canals and a higher cellularity (lacunar density), which were not noted in any other section.

With regard to irregular bones, the most frequent pattern was lamellar tissue with small areas of scattered secondary osteons, except for the spinous process of the cervical vertebra which exhibited a higher osteon density.

Finally, short bones (patella) was characterized by lamellar tissue with longitudinal vascular canals and the total absence of secondary osteons.

The use of polarized light allowed the observation of several “drifting osteons” in the ulna, the clavicle, the metacarpal and the rib.

In addition, linear rows of up to five secondary osteons surrounded by lamellar tissue were noted in the femoral diaphysis, in the distal metaphysis of the humerus and in the mandible.

Comparing the different portions of the same bone, the principal difference concerns the density and the organization of secondary osteons. Overall, in long bones, the density of secondary osteons seemed to decrease proceeding from the proximal metaphysis towards the distal metaphysis, except for the humerus which showed an opposite trend. Flat and irregular bones showed a higher homogeneity with a similar bone microarchitecture in different portions of the same bone, except for the scapula in which the acromion was characterized by scattered secondary osteons in abundant lamellar matrix whereas in the superior border, the osteons were tightly packed with scarce interstitial lamellae.

6.1.2 JUVENILE PIG SKELETON (PJ1)

A qualitative histomorphological analysis was carried out on forty-one cross-sections from a juvenile pig skeleton as to assess the presence of primary and secondary bone and to assess the arrangement of the vascular canals. Like the analysis on the adult human skeleton, different portion of the same bone were sampled as to verify the variability of bone microstructural architecture (see Chapter 5 for the details of the bone samples and the methodological approach).

Overall, pig bones were mainly characterized by primary bone (woven or fibrolamellar) although several areas of Haversian bone were observed, especially in long bones at the endosteal surface (Table 6.3).

The **humerus** exhibited mainly fibrolamellar tissue with a low/moderate remodeling (scattered secondary osteons) at the endosteal surface.

The proximal metaphysis showed a rather uniform tissue characterized by fibrolamellar bone.

The humeral diaphysis exhibited fibrolamellar tissue at the periosteal surface, whereas scattered secondary osteons were observed close to the endosteum and in the middle cortex at the medial and caudal aspect (Fig. 6.16). Several resorption spaces were present in the middle cortex. An area of radially oriented fibrolamellar bone was noted at the caudal aspect (Fig. 6.17).

The distal metaphysis was characterized by fibrolamellar bone at the middle cortex, and few scattered secondary osteons at the endosteal surface. The periosteal surface consisted of a woven scaffolding with radially oriented resorption spaces and vascular canals.

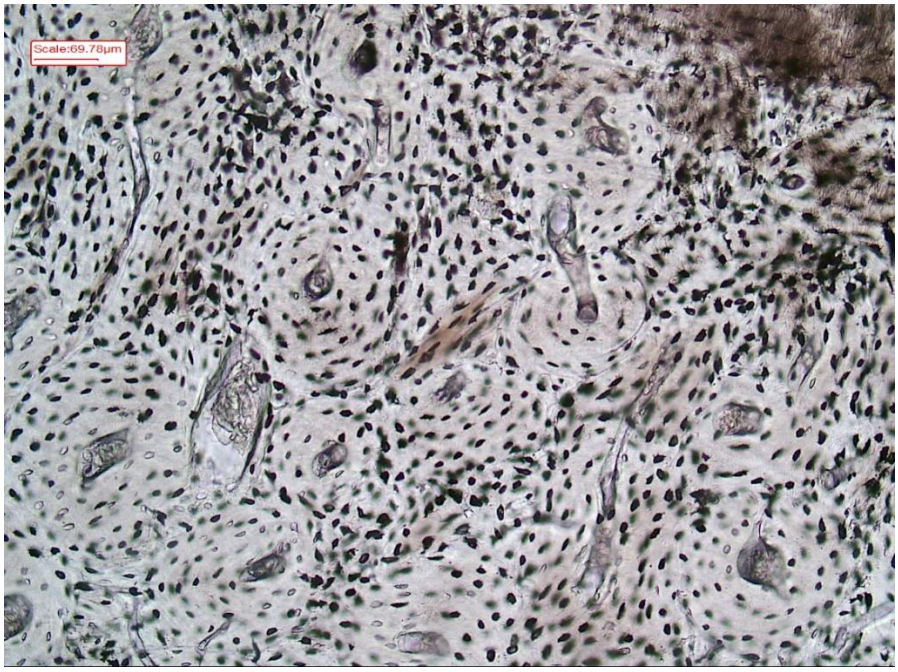

Figure 6.16 – Pig humerus (diaphysis). Secondary osteons at the caudal aspect, x100

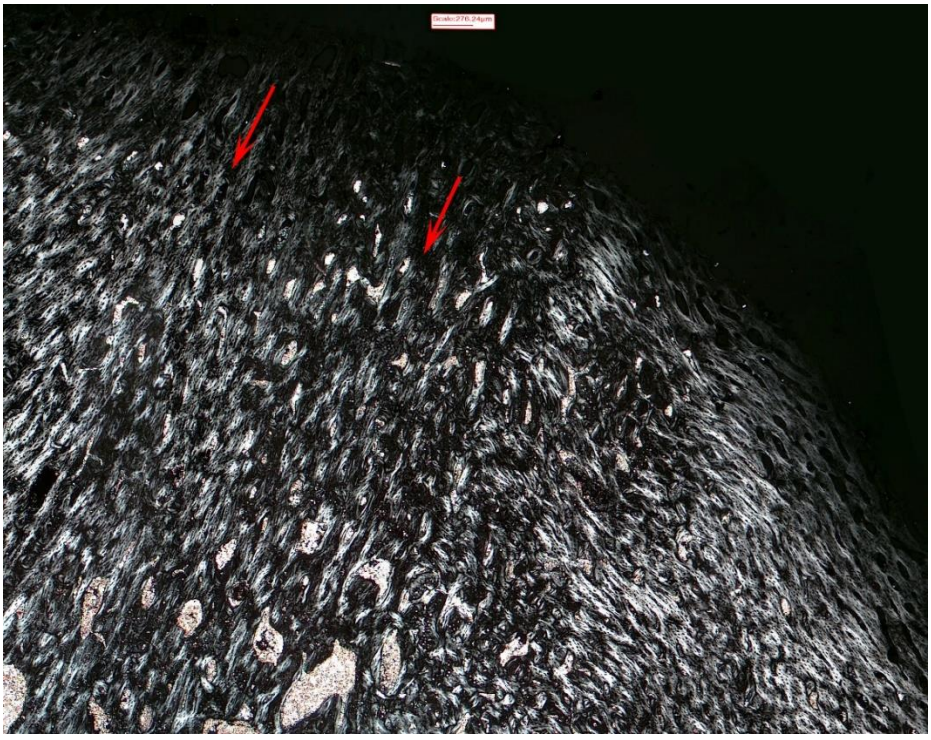

Figure 6.17 – Pig humerus (diaphysis). Radially oriented fibrolamellar tissue at the cranial aspect, x25. Polarized light

The **ulna** exhibited mainly fibrolamellar and woven bone although large areas of secondary osteons were present, especially in the diaphysis.

The proximal metaphysis exhibited a reticular pattern (Fig. 6.18) at the caudal aspect and fibrolamellar bone at the medial aspect. Proceeding towards the dorsal aspect the tissue was characterized by a woven scaffolding with primary osteons. Moderate to high remodeling was observed at the cranial and lateral aspect close the endosteum.

The ulnar diaphysis showed a reticular pattern at the caudal aspect, close to the periosteum. At the endosteal surface, few scattered secondary osteons were noted. At the lateral aspect, fibrolamellar bone was present close to the periosteum, whereas moderate to high remodeling was observed proceeding towards the endosteal surface. At the craniolateral aspect, the entire cortex was characterized by tightly packed secondary osteons (Fig. 6.19). At the craniomedial aspect, the periosteal surface exhibited a thin layer of fibrolamellar bone, while the middle cortex and the endosteal surface showed tightly packed secondary osteons. The medial aspect mainly consisted of fibrolamellar tissue with few scattered secondary osteons at the endosteal surface.

The distal metaphysis exhibited a highly vascularized tissue characterized by reticular and radial vascular canals in a woven matrix. No secondary osteons were observed.

Figure 6.18 – Pig ulna (proximal metaphysis). Reticular pattern at the caudal aspect. Periosteal surface, x25

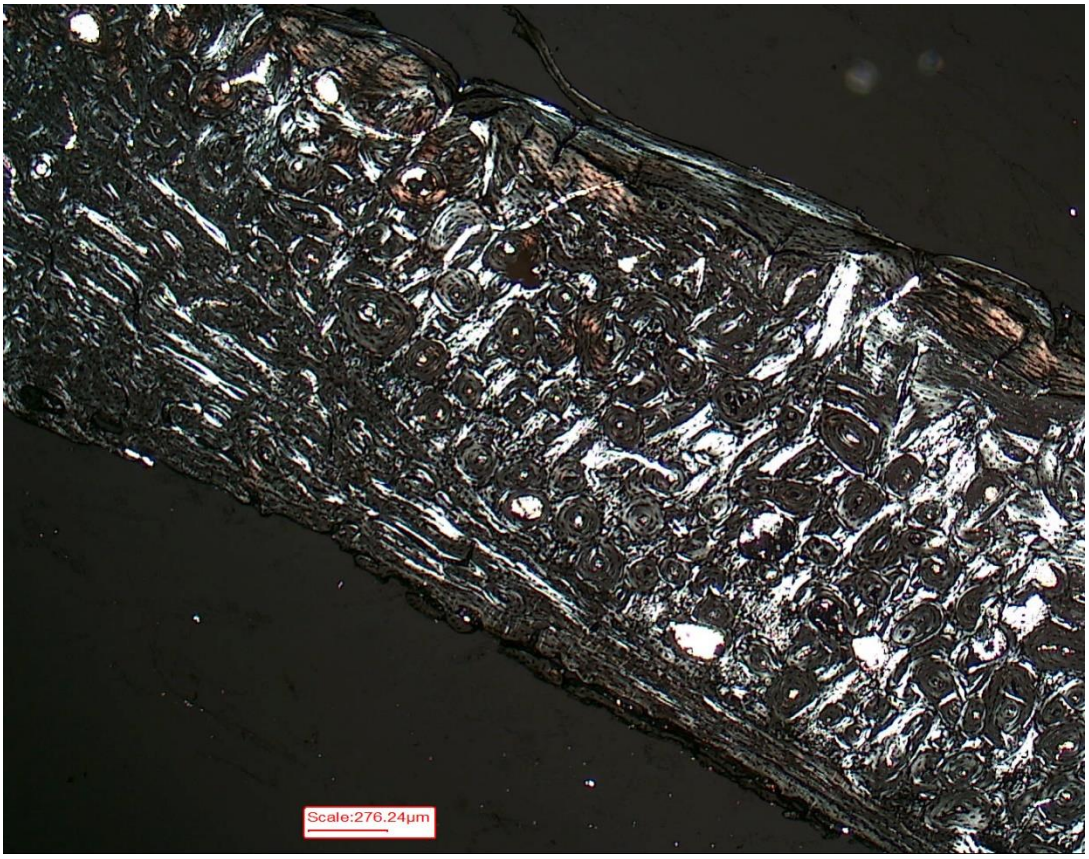

Figure 6.19 – Pig ulna (diaphysis). Transition from fibrolamellar bone (left) to dense Haversian bone (right) at the craniolateral aspect, x25. Polarized light

The **radius** was mainly characterized by fibrolamellar tissue although moderate to high remodeling was observed at the endosteal surface, especially in the diaphysis.

The proximal metaphysis exhibited fibrolamellar bone at the cranial and medial aspect. Scattered secondary osteons were present close to the endosteum at the medial aspect. The caudal and lateral aspects were characterized by woven bone at the periosteal surface and tightly packed secondary osteons at the endosteal surface.

Overall, the radial diaphysis showed a high rate of remodeling. The cranial aspect was characterized by fibrolamellar bone at the periosteal surface and scattered secondary osteons towards the endosteum. The lateral aspect mainly consisted of woven bone with primary osteons except for an area of scattered secondary osteons close to the endosteum (Fig. 6.20). Extensive remodeling characterized by tightly packed secondary osteons was observed at the caudal aspect (Fig. 6.21), whereas at the medial aspect, the periosteal surface exhibited woven bone with radially oriented primary osteons close to the periosteum, and moderate to high remodeling towards the endosteum. At the cranial aspect, close to the endosteum, a linear arrangement of longitudinal vascular canals was observed, whereas the medial and lateral aspects exhibited several resorption spaces.

The distal metaphysis showed a highly vascularized tissue characterized by longitudinal, radial and reticular vascular canals along the entire section.

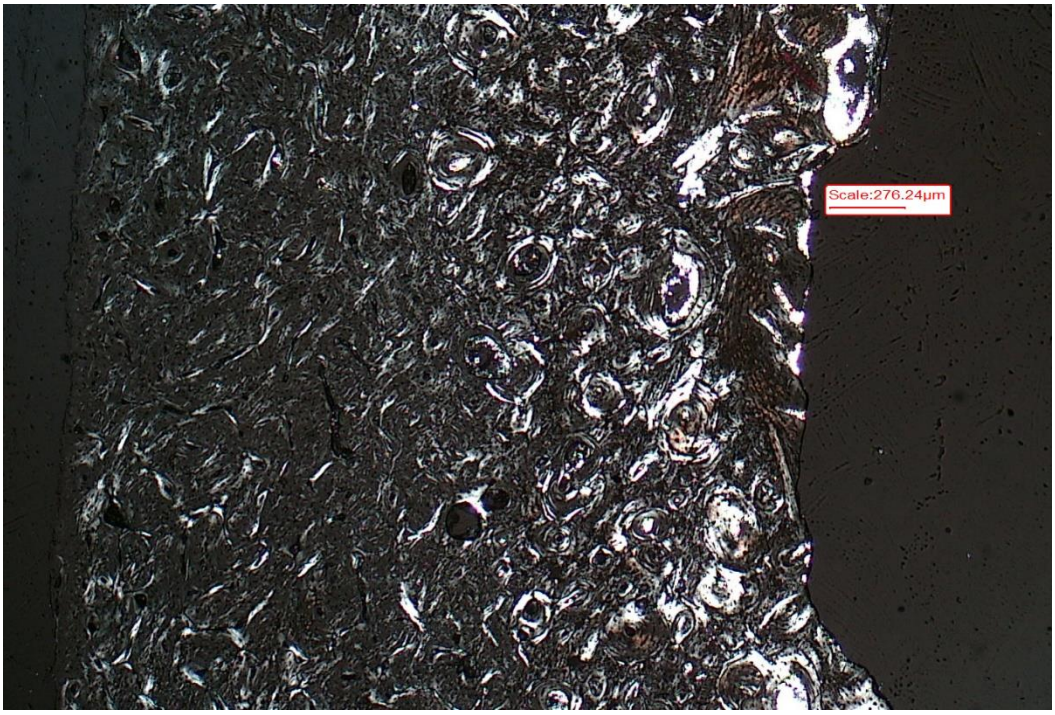

Figure 6.20 – Pig radius (diaphysis), lateral aspect. Woven bone with primary osteon at the periosteal surface (left) and scattered secondary osteons at the endosteal surface (right), x25. Polarized light

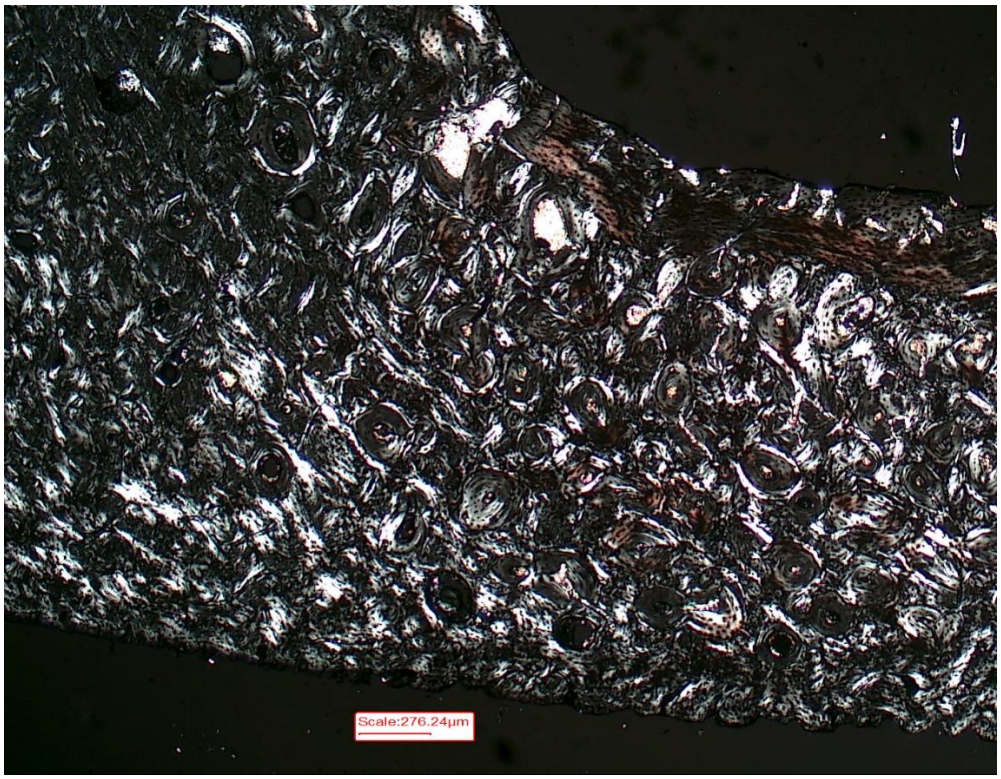

Figure 6.21 – Pig radius (diaphysis) – Extensive remodeling at the caudal aspect, x25. Polarized light

The **femur** showed a prevalence of fibrolamellar bone although moderate to high remodeling was observed at the endosteal surface.

The proximal metaphysis consisted almost entirely of fibrolamellar bone, except for small areas of scattered secondary osteons at the caudal aspect, close to the endosteum. Several resorption spaces were observed around the medullary cavity.

The femoral diaphysis exhibited solely fibrolamellar bone at the cranial (Fig. 6.22), medial and lateral aspects. On the contrary, the caudal aspect exhibited moderate to high remodeling (Fig. 6.23).

The distal metaphysis showed a highly vascularized tissue characterized by longitudinal and reticular vascular canal in a woven matrix. Several resorption spaces were observed.

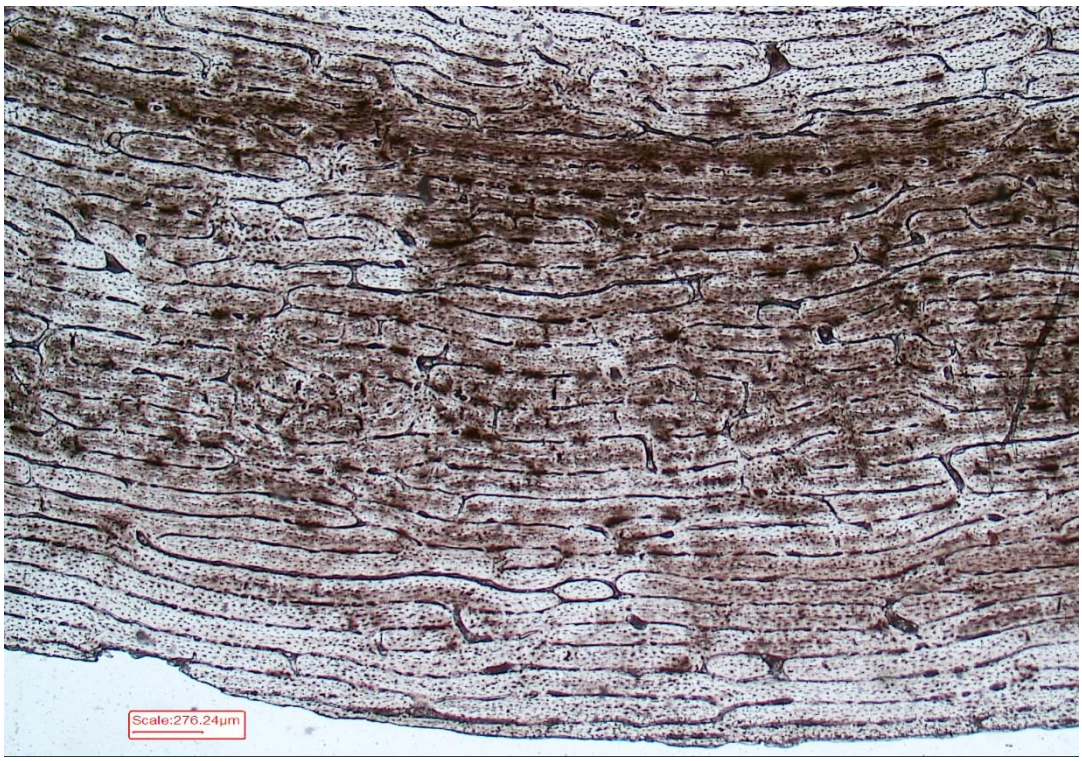

Figure 6.22 – Pig femur (diaphysis) – Fibrolamellar bone at the cranial aspect, x25

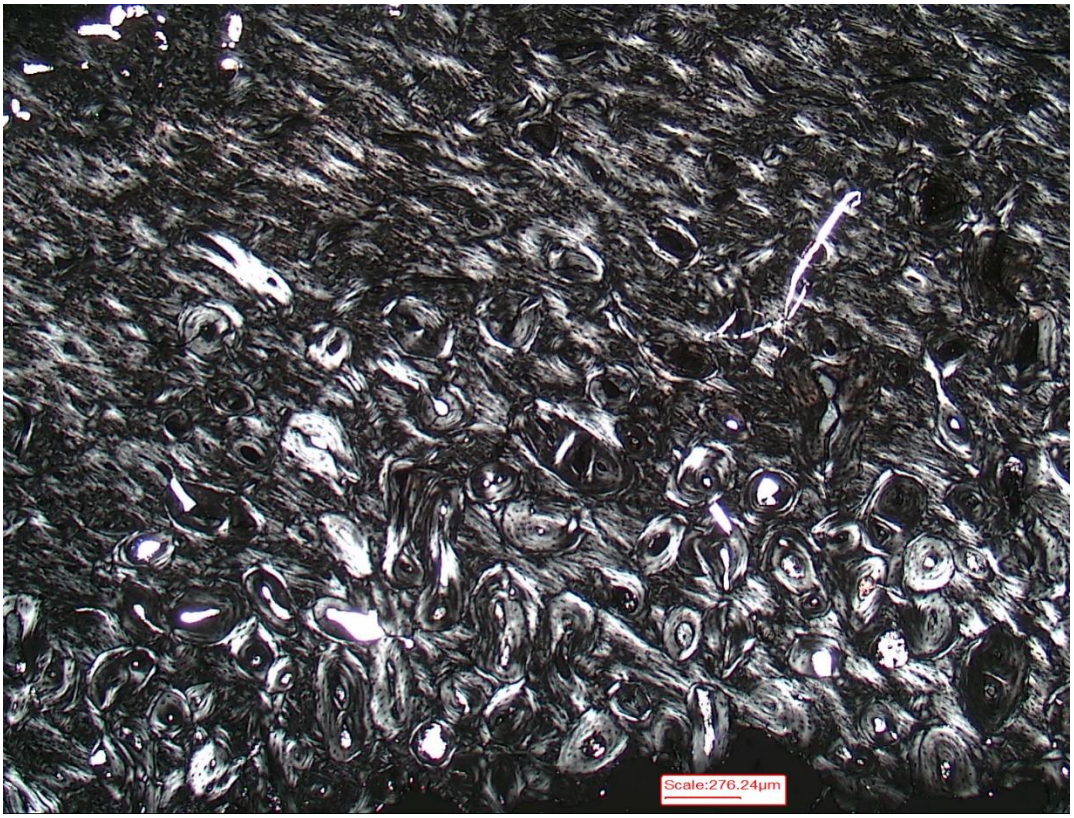

Figure 6.23 – Pig femur (diaphysis). Caudal aspect: woven bone at the periosteal surface (up) and moderate remodeling at the endosteal surface (down), x25

The **tibia** exhibited a prevalence of fibrolamellar bone although moderate remodeling was observed, especially in the diaphysis.

The proximal metaphysis was characterized exclusively by fibrolamellar bone with primary osteons with no evidence of remodeling.

The tibial diaphysis exhibited mainly fibrolamellar bone with primary osteons, except for the lateral aspect characterized by scattered secondary osteons at the endosteal surface and an area of parallel-fibered bone with a row of longitudinal vascular canals (Fig. 6.24). At the cranial aspect osteons were arranged in linear bands (Fig. 6.25)

The distal metaphysis exhibited a highly vascularized tissue characterized by reticular vascular canals. Few scattered secondary osteons were observed at the lateral aspect, close to the endosteum.

Figure 6.24 – Pig tibia (diaphysis) – Parallel-fibered bone with a linear arrangement of longitudinal vascular canals at the lateral aspect, x100

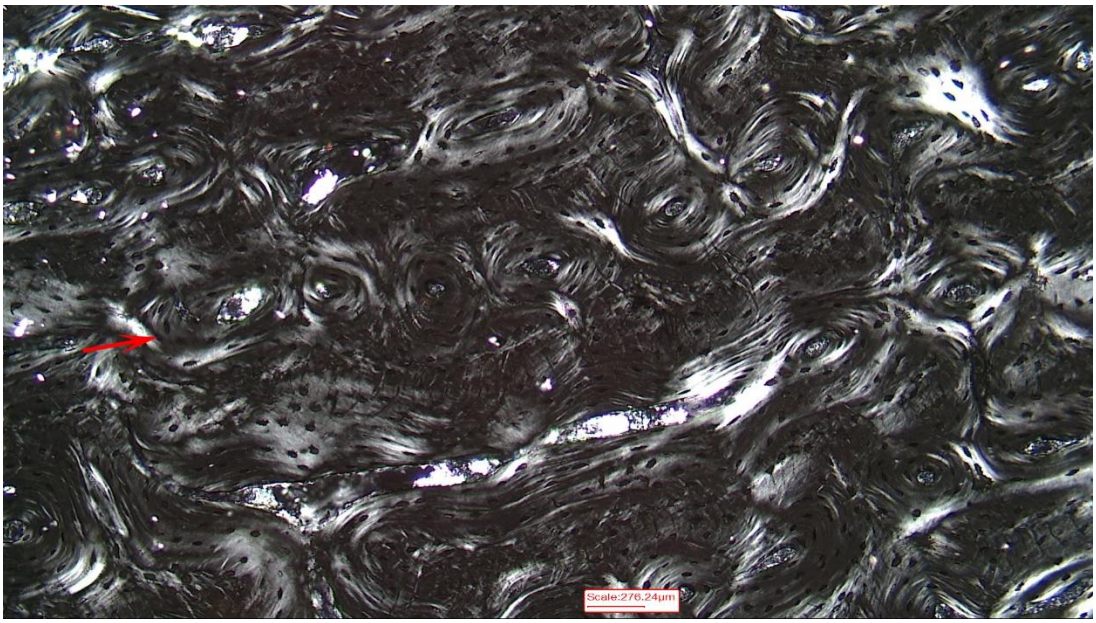

Figure 6.25 – Pig tibia (diaphysis) – Osteon banding at the cranial aspect, x25. Polarized light

The **fibula** showed a prevalence of woven bone although extensive remodeling was observed in the diaphysis.

The proximal metaphysis consisted mainly of parallel-fibered and woven bone. Several large vascular canals (mainly radial) and primary osteons were observed along the entire section.

The diaphysis exhibited tightly packed secondary osteons at the caudal aspect (Fig. 6.26), whereas the lateral and cranial aspects were characterized by more scattered osteons.

The distal metaphysis consisted of a woven scaffolding without any sign of remodeling. An area of radially oriented primary osteons was observed at the medial aspect (Fig. 6.27).

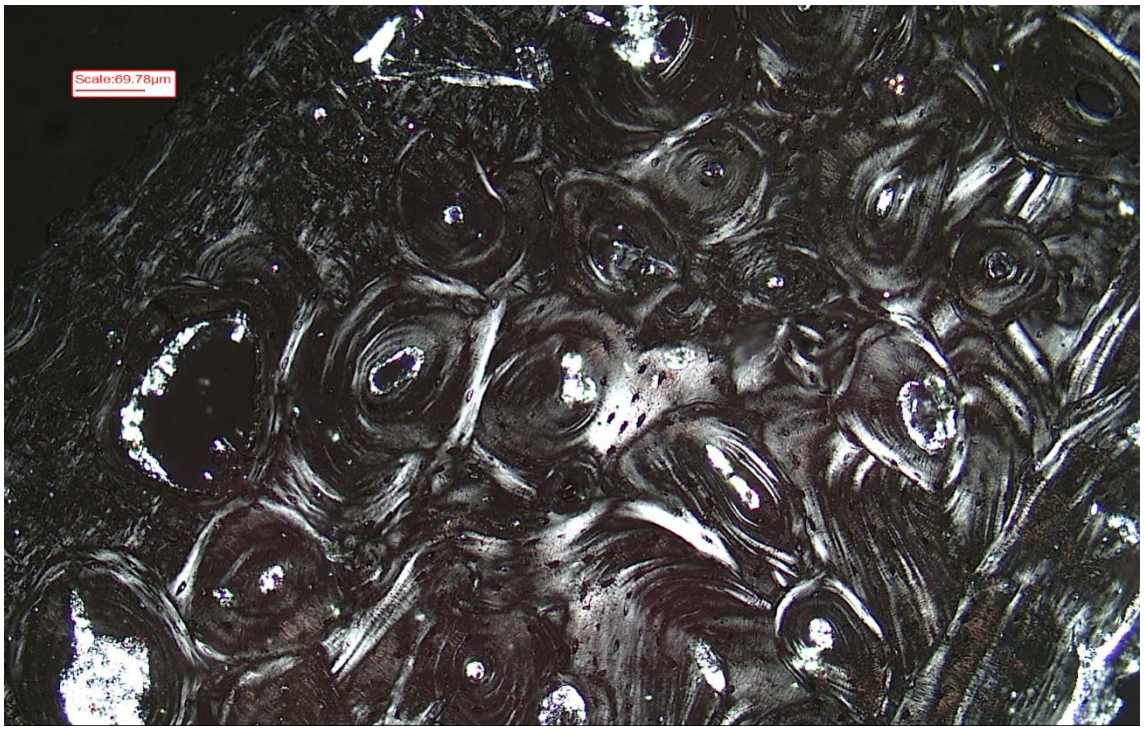

Figure 6.26 – Fibula (diaphysis) – Caudal aspect: woven bone at the periosteal surface (left) and highly remodeled bone at the middle cortex, x100. Polarized light

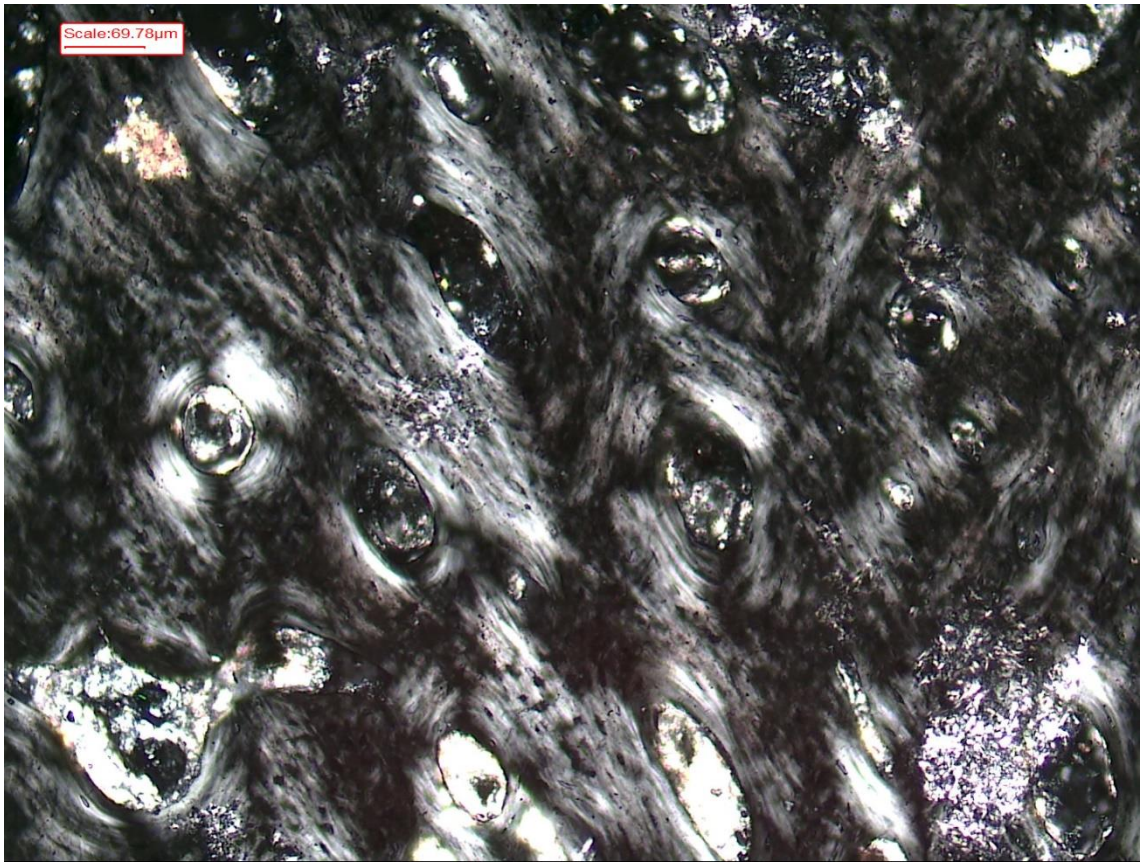

Figure 6.27 – Pig fibula (distal metaphysis) – Woven bone with radially oriented primary osteons at the medial aspect, x100. Polarized light

The **metacarpal** was mainly characterized by fibrolamellar tissue and areas of secondary osteons, especially in the body.

The head of the metacarpal exhibited mainly fibrolamellar bone with primary osteons. At the medial and lateral aspects, scattered secondary osteons were observed. The periosteal surface of the lateral aspect was characterized by woven bone with primary osteons.

The body of the metacarpal exhibited fibrolamellar bone at the periosteal surface, except for the caudal aspect, which was characterized by woven bone with primary osteons (Fig. 6.28). At the lateral portion, an area of tightly packed secondary osteons in the middle cortex was sandwiched between two layers of fibrolamellar bone (Fig. 6.29).

The base of the metacarpal consisted entirely of fibrolamellar bone with no remodeling.

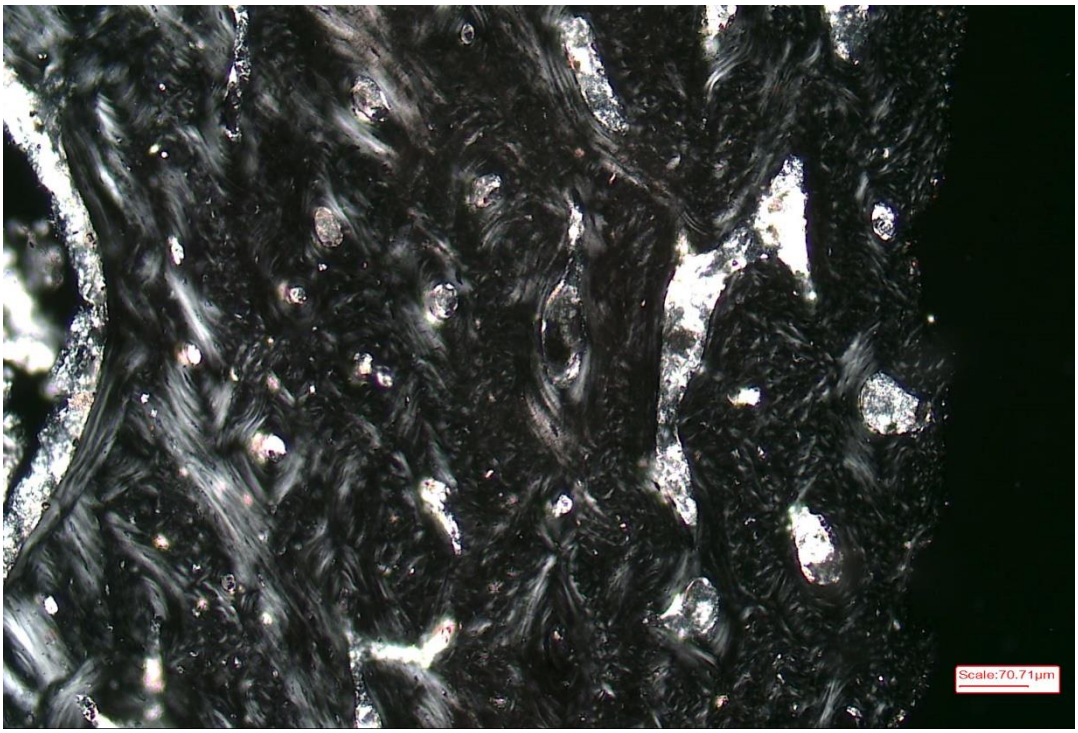

Figure 6.28 – Pig metacarpal (body) – Woven bone with primary osteons, x100. Polarized light

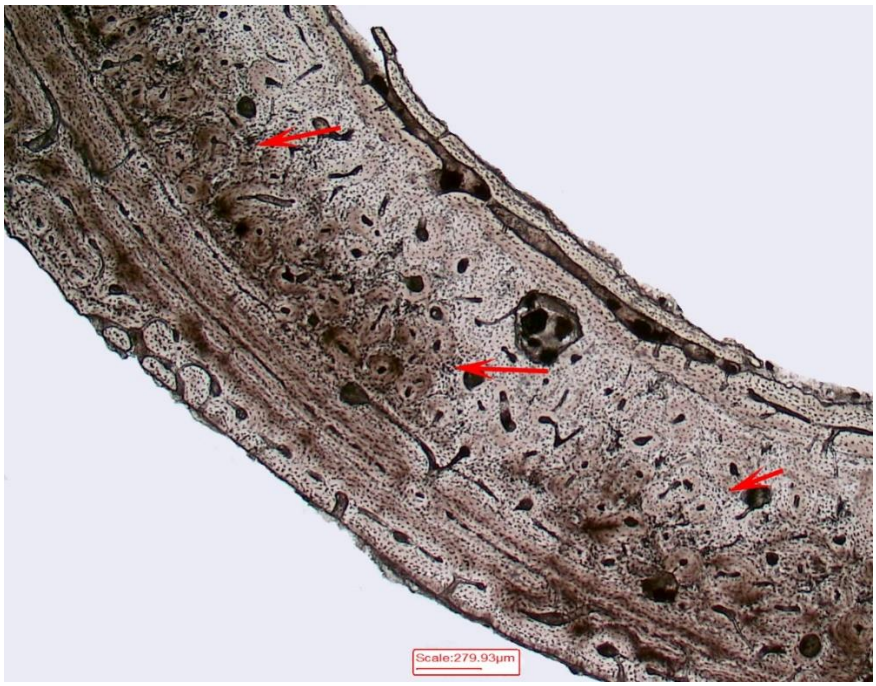

Figure 6.29 – Pig metacarpal (body) – Lateral portion: areas of Haversian bone (red arrows) between two layers of fibrolamellar bone

The **metatarsal** showed a prevalence of fibrolamellar and woven bone, although a high number of secondary osteons were observed in the body.

The head of the metatarsal exhibited solely fibrolamellar bone with primary osteons and no remodeling.

The body was characterized by woven bone with primary osteons at the periosteal surface, whereas a high rate of remodeling was observed at the middle cortex and at the endosteal surface along the entire section (Fig. 6.30).

The base of the metacarpal consisted exclusively of woven bone with primary osteons.

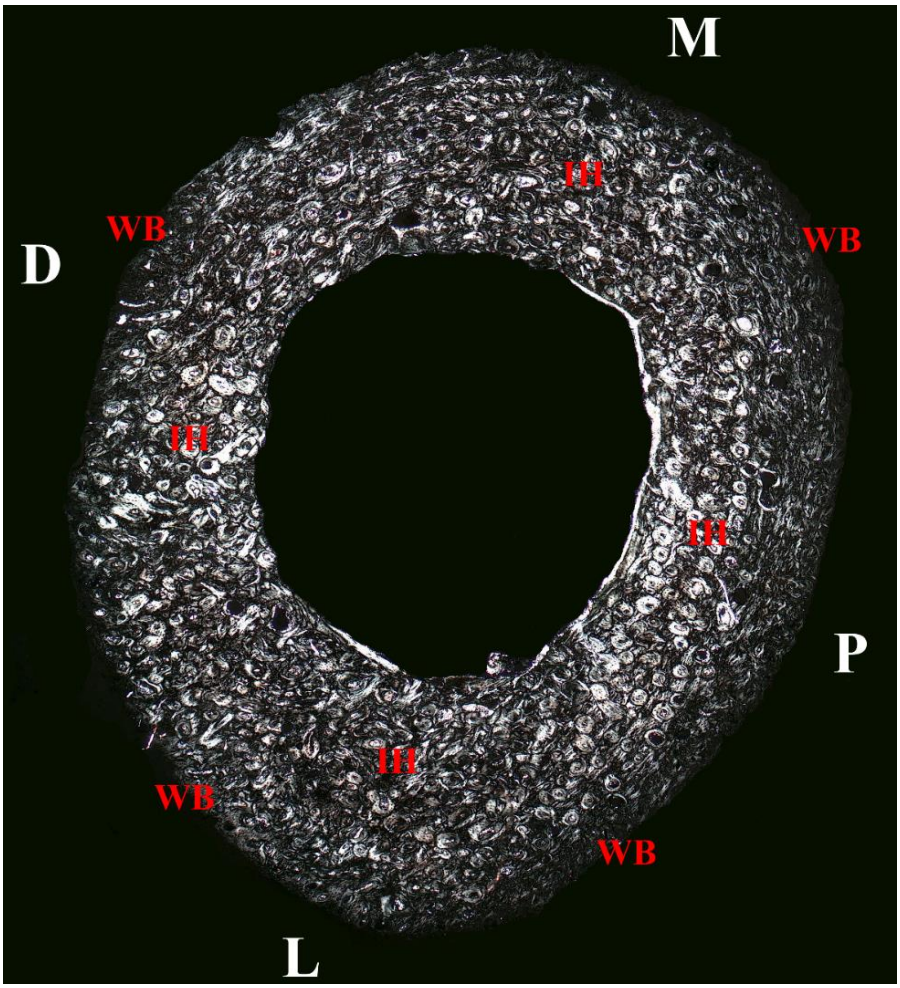

Figure 6.30 – Pig metatarsal (body) – Woven bone (WB) at the periosteal surface and irregular Haversian bone (IH) at the middle cortex and at the endosteal surface, x25. Polarized light

The **rib** consisted mainly of woven bone although moderate remodeling was observed in the body.

The head of the rib consisted exclusively in a woven scaffolding with primary osteons. The body exhibited a similar tissue, although scattered secondary osteons were present at the cranial aspect.

The **sternum** exhibited an alternation of woven and parallel-fibered bone whereas, the superior border of the scapula and the acromion were characterized by parallel-fibered bone (Fig. 6.31).

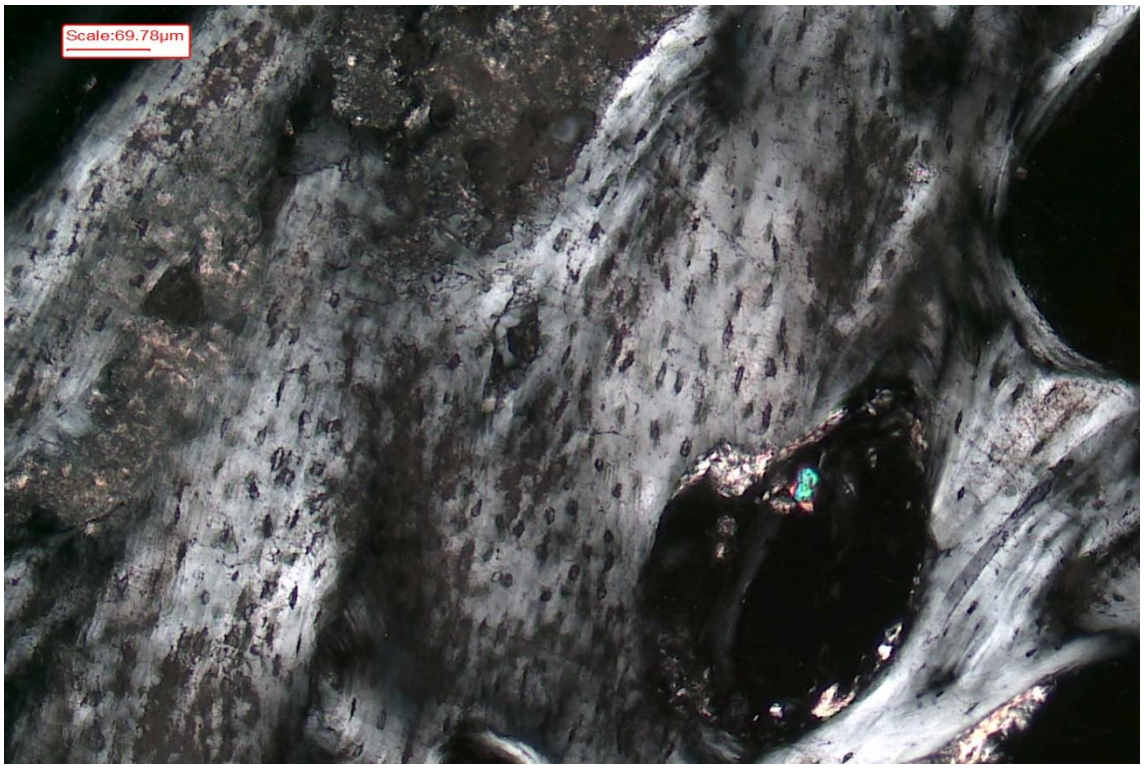

Figure 6.31 – Pig scapula (acromion) – Parallel-fibered bone, x100. Polarized light

With regard to the **ox coxae**, the ischiopubic ramus exhibited mainly parallel-fibered bone with primary osteons and a few scatted secondary osteons at the lateral aspect.

The iliopubic ramus showed a prevalence of fibrolamellar bone, although moderate to high remodeling was present, close to the endosteum, at the medial and ventral aspects (Fig. 6.32). A woven scaffolding with radially oriented primary osteons was observed at the ventral aspect, close to the periosteum.

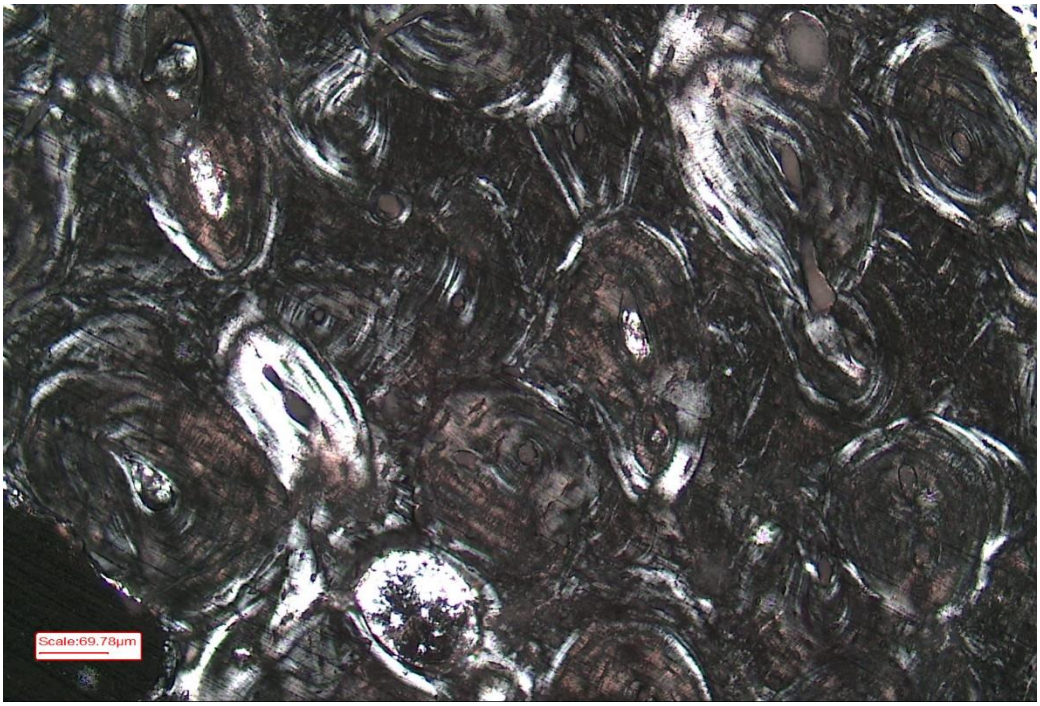

Figure 6.32 – Pig iliopubic ramus – Tightly packed secondary osteons at the anterior aspect, 100x. Polarized light

With regard to the **cranium**, the parietal, the occipital and the temporal were characterized by a similar tissue consisting of woven bone with primary osteons and longitudinal vascular canals.

All the cross-sections of the **mandible** (mental protuberance, gonion and mandibular condyle) were characterized by the same pattern consisting in a woven scaffolding with few primary osteons and no remodeling (Fig. 6.33).

Figure 6.33 – Pig mandible (gonion) – woven bone with primary osteons, x100

The **cervical vertebra** was characterized by a uniform tissue consisting of parallel-fibered bone with few primary osteons (Fig. 6.34).

The **patella** exhibited a rather uniform tissue consisting of parallel fibered bone.

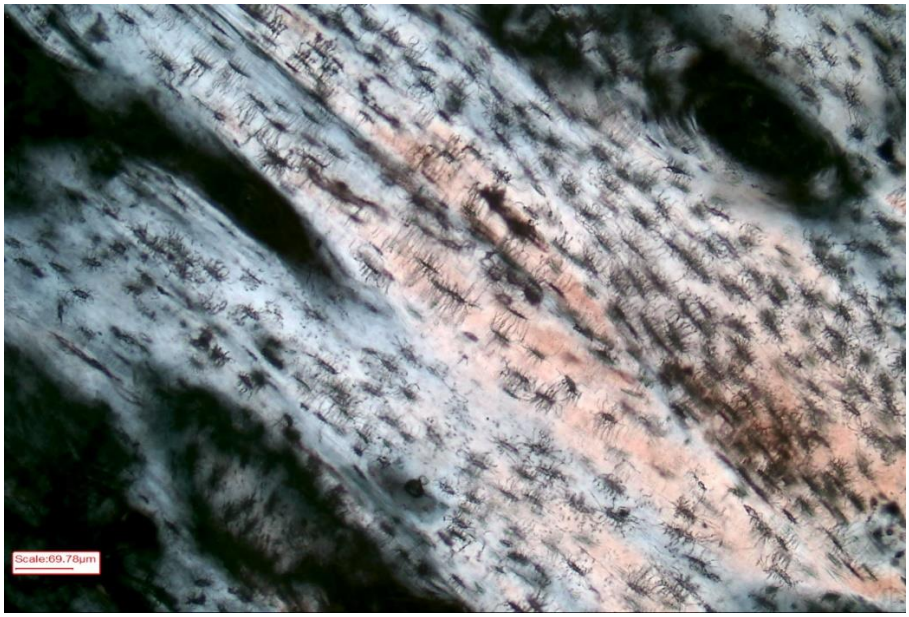

Figure 6.34 – Pig cervical vertebra (spinous process) – Parallel-fibered bone, x100. Polarized light

CONCLUDING REMARKS

The histomorphological analysis of the juvenile pig skeleton (PJ1) indicated a prevalence of primary bone, consisting of woven or fibrolamellar bone. Nonetheless, especially in the diaphysis of long bones, moderate to high remodeling was observed.

Areas characterized by secondary osteons were generally observed at the endosteal surface, though several cross-sections of the limbs such as those of the diaphysis of the humerus, ulna, radius, femur, fibula, metacarpal and metatarsal exhibited remodeling also at the middle cortex.

Overall, the bones of the forelimbs were characterized by a higher rate of remodeling, consisting often in medium-to-large areas of secondary osteons, whereas in the bones of the hindlimbs, secondary osteons were generally confined in small areas.

As regards the localization of secondary osteons within the section, in the hindlimbs, remodeling regarded mainly the caudal and lateral aspects, whereas in the forelimbs, secondary osteons had a wider distribution across the section, although they were more frequently observed at the lateral and medial aspects.

No drifting osteons nor embedded and double-zonal osteons were noted.

Several “anomalous” secondary osteons were observed. These were characterized by two or three longitudinal vascular canals within the wall of the osteon (Fig. 6.35).

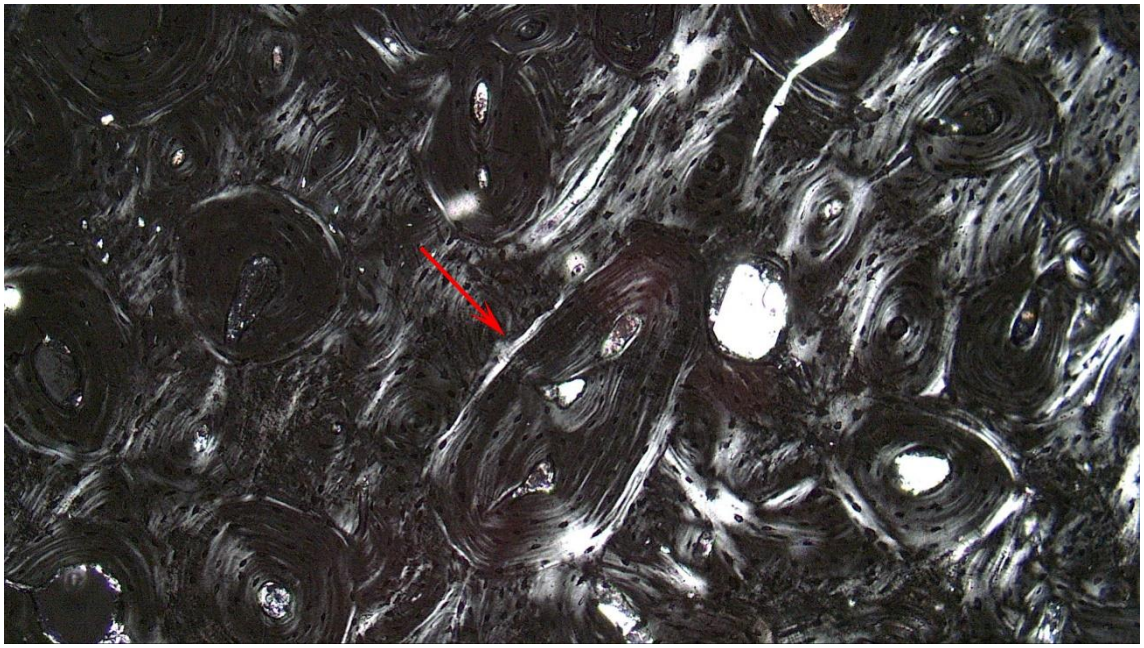

Figure 6.35 – Anomalous secondary osteon in the proximal metaphysis of the ulna, x100. Polarized light.

Osteon banding was observed exclusively in the tibial diaphysis, although linear arrangement of longitudinal vascular canals were present at the endosteal surface in the radial and tibial diaphyses.

Table 6.3 – Results of the histomorphological analysis on the juvenile pig skeleton PJ1

	Bone	Primary bone									Secondary bone					
		Woven			Fibrolamellar			Parallel-fibered			Scattered secondary osteons			Dense secondary osteons without organization		
		Periosteal layer	Middle cortex	Endosteal layer	Periosteal layer	Middle cortex	Endosteal layer	Periosteal layer	Middle cortex	Endosteal layer	Periosteal layer	Middle cortex	Endosteal layer	Periosteal layer	Middle cortex	Endosteal layer
Long bones	Humerus – proximal metaphysis				✓	✓	✓						✓			
	Humerus - diaphysis				✓	✓	✓					✓	✓			
	Humerus – distal metaphysis	✓				✓	✓						✓			
	Ulna – proximal metaphysis	✓	✓	✓	✓	✓	✓						✓			
	Ulna – diaphysis				✓	✓	✓						✓	✓	✓	✓
	Ulna – distal metaphysis	✓	✓	✓												
	Radius – proximal metaphysis	✓			✓	✓	✓						✓			✓
	Radius – diaphysis	✓			✓					✓			✓		✓	✓
	Radius – distal metaphysis				✓	✓	✓									
	Femur – proximal metaphysis				✓	✓	✓						✓			
	Femur – diaphysis				✓	✓	✓					✓	✓			✓
	Femur – distal metaphysis	✓	✓	✓												
	Tibia proximal metaphysis				✓	✓	✓									
	Tibia – diaphysis				✓	✓	✓			✓			✓			
	Tibia – distal metaphysis				✓	✓	✓						✓			
	Fibula – proximal metaphysis	✓	✓	✓				✓	✓	✓						
	Fibula – diaphysis	✓										✓	✓		✓	✓
	Fibula – distal metaphysis	✓	✓	✓												
	Metacarpal – proximal end	✓			✓	✓	✓						✓			
	Metacarpal – shaft	✓			✓	✓									✓	
	Metacarpal – distal end				✓	✓	✓									
	Metatarsal – proximal end				✓	✓	✓									
	Metatarsal – shaft	✓										✓	✓		✓	✓
	Metatarsal – distal end	✓	✓	✓												

	Bone	Primary bone									Secondary bone					
		Woven			Fibrolamellar			Parallel-fibered			Scattered secondary osteons			Dense secondary osteons without organization		
		Periosteal layer	Middle cortex	Endosteal layer	Periosteal layer	Middle cortex	Endosteal layer	Periosteal layer	Middle cortex	Endosteal layer	Periosteal layer	Middle cortex	Endosteal layer	Periosteal layer	Middle cortex	Endosteal layer
Flat bones	Temporal bone – zygomatic process	✓	✓	✓												
	Temporal bone - petrous	✓	✓	✓												
	Parietal	✓	✓	✓												
	Occipital	✓	✓	✓												
	Rib – head	✓	✓	✓												
	Rib – body	✓	✓	✓									✓			
	Sternum	✓	✓					✓	✓	✓						
	Scapula – superior border							✓	✓	✓						
	Scapula – acromion							✓	✓	✓						
	Iliopubic ramus	✓			✓	✓	✓						✓			
	Ischiopubic ramus							✓	✓	✓			✓			
Irregular bones	Mandible – gonion	✓	✓	✓												
	Mandible – mental protuberance	✓	✓	✓												
	Mandibular condyle	✓	✓	✓												
	Cervical vertebra – longitudinal							✓	✓	✓						
	Cervical vertebra – transversal							✓	✓	✓						
Sesamoid bones	Patella							✓	✓	✓						

6.2 INTRA-INDIVIDUAL HISTOMORPHOMETRIC VARIABILITY

Prior to undertaking the histomorphometric analyses, Intraclass Correlation Coefficient (ICC) was computed repeating measurements of thirty osteons and Haversian canals by the same operator and by two trained operators after twenty-four, forty-eight and seventy-two hours in order to test the intra- and inter-rater reliability (Table 6.4).

	Intraclass Correlation Coefficient (ICC) Intra-rater reliability	**Intraclass Correlation Coefficient (ICC) Inter-rater reliability**
On.Dm$_{max}$	0.957	0.874
On.Dm$_{min}$	0.979	0.925
On.Ar	0.995	0.997
On.Pm	0.988	0.990
HC.Dm$_{max}$	0.874	0.973
HC.Dm$_{min}$	0.782	0.889
HC.Ar	0.832	0.969
HC.Pm	0.886	0.983

Table 6.4 – Histomorphometric analysis of osteons and Haversian canals: Intraclass correlation coefficient (ICC) for intra-rater and inter-rater reliability

The Intraclass Correlation Coefficient (ICC), indicated an excellent agreement between the observations of the same observer as well as those of the two observers. The minimum correlation coefficient regarded the measurement of the Haversian canal minimum diameter, even though the agreement remains excellent (Portney and Watkins 2000; Koo and Li 2016).

6.2.1 ADULT HUMAN SKELETON (HA1)

The histomorphometric analysis of the human adult individual (HA1) involved the measurement of 1317 secondary osteons and Haversian canals.

The descriptive statistics of the mean value, standard deviation, minimum and maximum value for osteon and Haversian canal parameters in long, flat and irregular bones are shown respectively in Table 6.5 and Table 6.6 (see Appendix B for the descriptive statistics of bone).

Osteons were generally bigger in irregular bones compared to long and flat bones, with a mean area respectively of 33020,97(±16192,20) μm^2, 29385,27(±13268,86) μm^2 and 21786,36(±10926,12) μm^2.

Similarly, the highest mean value for the Haversian canal area was observed in irregular bones (1888,53±946,08 μm^2), followed by long bones (1626,35±784,76 μm^2) and flat bones (1418,59±743,42 μm^2). Osteon circularity was higher in long bones (0,90±0,04) compared to flat bones (0,89±0,04) and irregular bones (0,87±0,05).

HUMAN ADULT (HA1) – OSTEON						
Bone type		**On.Dm$_{max}$ (µm)**	**On.Dm$_{min}$ (µm)**	**On.Ar (µm^2)**	**On.Pm (µm)**	**On.Cr**
Long bones (n=1028)	Mean	216,79	166,77	29385,27	623,8	0,90
	SD	54,36	40,08	13268,86	144,65	0,04
	Min	100,77	73,98	7122,36	310,65	0,69
	Max	413,23	321,01	86173,82	1137,03	0,98
Flat bones (n=254)	Mean	192,40	139,50	21786,36	536,81	0,89
	SD	53,71	37,41	10926,12	138,27	0,04
	Min	84,54	64,26	4472,39	249,95	0,72
	Max	351,42	248,99	60628,03	924,58	0,97
Irregular bones (n=35)	Mean	240,50	165,62	33020,97	669,60	0,87
	SD	70,79	42,73	16192,20	180,04	0,05
	Min	124,09	80,58	9017,82	361,57	0,78
	Max	384,96	260,74	68078,28	1004,43	0,94
Total (n=1317)	Mean	212,61	161,41	27998,45	607,97	0,90
	SD	55,82	41,11	13305,33	148,98	0,04
	Min	84,54	64,26	4472,39	249,95	0,69
	Max	413,23	321,01	86173,82	1137,03	0,98

Table 6.5 - Descriptive statistics of osteon parameters for the human adult individual HA1

HUMAN ADULT (HA1) – HAVERSIAN CANAL					
Bone type		**HC.Dm$_{max}$ (µm)**	**Hc.Dm$_{min}$ (µm)**	**HC.Ar (µm^2)**	**HC.Pm (µm)**
Long bones (n=1028)	Mean	50,18	38,4	1626,35	146,25
	SD	13,53	10,6	784,76	36,29
	Min	17,01	13,83	231,56	56,43
	Max	101,42	71,72	3592,42	245,09
Flat bones (n=254)	Mean	48,66	34,34	1418,59	137,91
	SD	14,96	9,5	743,42	37,69
	Min	17,5	14,39	219,14	55,08
	Max	91,3	61,61	3930,87	230,57
Irregular bones (n=35)	Mean	54,77	40,55	1888,53	159,35
	SD	15,36	10,04	946,08	40,77
	Min	31,21	22,5	572,68	90,52
	Max	86,37	60,16	3890,45	236,55
Total (n=1317)	Mean	49,99	37,66	1592,26	144,93
	SD	13,91	10,52	787,31	36,94
	Min	17,01	13,83	219,14	55,08
	Max	101,42	71,72	3930,87	245,09

Table 6.6 - Descriptive statistics of Haversian canal parameters for the human adult individual HA1

ANOVA test revealed that both the sizes of osteon and Haversian canal were statistically significantly different between the three groups (Table 6.7).

Tukey post-hoc test indicated that the size of the osteon was statistically significantly higher in long bones (p=0.000, Cohen's d=0.592, 95% CI for Cohen's d: 0.453 – 0.11731) and irregular bones (p=0.000, Cohen's d=0.962, 95% CI for Cohen's d: 0.6 – 1.324) compared to flat bones. There was no statistically significant difference between long and irregular bones.

The size of the Haversian canal was statistically significantly higher in long bones (p=0.000, Cohen's d=0.267, 95% CI for Cohen's d: 0,13 – 0,405) and irregular bones (p=0.003, Cohen's d=0.61, 95% CI for Cohen's d: 0.253 – 0.967) compared to flat bones. There was no statistically significant difference between long and irregular bones.

Osteon circularity was statistically significantly higher in long bones (p=0.000, Cohen's d=0.743, 95% CI for Cohen's d: 0.405 – 1.082) and in flat bones (p=0.017, Cohen's d=0.484, 95% CI for Cohen's d: 0.129 – 0.84) compared to irregular bones. There was a statistically significant difference in osteon circularity also between long and flat bones (p=0.006, Cohen's d=0.25, 95% CI for Cohen's d: 0.112 – 0.388).

HUMAN ADULT – LONG VS FLAT VS IRREGULAR BONES									
	On.Dm (max)	**On.Dm (min)**	**On.Ar**	**On.Pm**	**HC.Dm (max)**	**Hc.Dm (min)**	**HC.Ar**	**HC.Pm**	**On.Cr**
Sig.									
Between groups	.000	.000	.000	.000	.036	.000	.000	.000	.000
Long vs flat	.000	.000	.000	.000	.261	.000	.000	.003	.006
Long vs irregular	.032	.985	.231	.156	.132	.452	.125	.95	.000
Flat vs irregular	.000	.001	.000	.000	.039	.003	.003	.004	.017

Table 6.7 – Human adult skeleton HA1 - Results of ANOVA and Tukey post-hoc test on osteon and Haversian canal parameters

As regards the differences between different portions of the same bone, in the **humerus** (Table 6.8 – 6.9), Haversian canals were smaller in the proximal metaphysis (1613,96±666,31 μm^2) and in the distal metaphysis (1601,17±779,32 μm^2) compared to the diaphysis (2063,91±958,44 μm^2).

HUMAN ADULT (HA1) – HUMERUS (OSTEON)						
Bone portion		**On.Dm$_{max}$ (μm)**	**On.Dm$_{min}$ (μm)**	**On.Ar (μm^2)**	**On.Pm (μm)**	**On.Cr**
Proximal metaphysis (n=50)	Mean	251,85	183,55	37057,52	712,34	0,89
	St.dev	49,73	32,48	12530,4	124,51	0,05
	Min	170,15	119,85	15605,15	467,6	0,76
	Max	339,63	260,5	68174,21	680,36	0,97
Diaphysis (n=36)	Mean	224,56	167,31	31538,02	655,78	0,88
	St.dev	61,94	35,30	13877,72	164,18	0,05
	Min	111,2	79,75	7122,36	310,65	0,71
	Max	357,15	233,87	57431,27	948,73	0,97
Distal metaphysis (n=50)	Mean	238,14	168,43	31488,5	657,1	0,89
	St.dev	52,35	33,20	11970,5	123,12	0,05
	Min	129,42	109,6	12335,59	404,68	0,77
	Max	383,91	256,74	62365,56	957,81	0,96
Total (n=136)	Mean	239,58	173,69	33549,04	677,03	0,89
	St.dev	54,81	34,11	12892,33	137,29	0,05
	Min	111,2	79,75	7122,36	310,65	0,71
	Max	383,91	260,5	68174,21	957,81	0,97

Table 6.8 – Humerus (HA1) - descriptive statistics of osteon parameters

HUMAN ADULT (HA1) – HUMERUS (HAVERSIAN CANAL)					
Bone portion		**HC.Dm$_{max}$ (µm)**	**Hc.Dm$_{min}$ (µm)**	**HC.Ar (µm^2)**	**HC.Pm (µm)**
Proximal metaphysis (n=50)	Mean	54,76	36,72	1613,96	150,91
	St.dev	13,51	9,06	666,31	31,59
	Min	30,4	22,72	639,89	92,89
	Max	101,42	59,43	3293,42	245,09
Diaphysis (n=36)	Mean	55,49	42,67	2063,91	163
	St.dev	12,21	12,21	958,44	42,33
	Min	23,13	17,54	388,63	75,37
	Max	83,89	64,36	3474,24	222,33
Distal metaphysis (n=50)	Mean	51,73	37,13	1601,17	147,07
	St.dev	14,54	10,54	779,32	37,11
	Min	20,94	16,98	290,24	66,2
	Max	90,99	60,76	3386,43	232,17
Total (n=136)	Mean	53,84	38,45	1728,36	152,70
	St.dev	14,55	10,74	812,78	36,98
	Min	20,94	16,98	290,24	66,2
	Max	101,42	64,36	3474,24	245,09

Table 6.9 – Humerus (HA1) - descriptive statistics of Haversian canal parameters

ANOVA and Tukey post-hoc test revealed that the size of Haversian canals was statistically significantly lower in the proximal metaphysis (p=0.028, Cohen's d=0.562, 95% CI for Cohen's d: 0.125 – 0.998) and in the distal metaphysis (p=0.023, Cohen's d=0.539, 95% CI for Cohen's d: 0.103 – 0.975) compared to the diaphysis. There was no statistically significant difference between the proximal and distal metaphysis, as well as in osteon circularity between the three groups (Table 6.10).

HUMERUS – ANOVA and Tukey's post hoc test									
	On.Dm (max)	**On.Dm (min)**	**On.Ar**	**On.Pm**	**HC.Dm (max)**	**Hc.Dm (min)**	**HC.Ar**	**HC.Pm**	**On.Cr**
Sig.									
Between groups	.072	.035	.052	.072	.427	.021	.014	.131	.412
Proximal vs diaphysis	.058	.072	.119	.140	.971	.029	.028	.291	.407
Proximal vs distal metaphysis	.416	.066	.076	.107	.553	.980	.996	.860	.631
Diaphysis vs distal metaphysis	.487	.987	1.000	.999	.465	.045	.023	.120	.897

Table 6.10 – Humerus (HA1) - Results of ANOVA and Tukey post-hoc test on osteon and Haversian canal parameters

With regard to the **radius** (Table 6.11 – 6.12), osteons were smaller in the proximal metaphysis (28406,51±11610,9 μm^2) and in the distal metaphysis (29198,18±9798,13 μm^2) compared to the diaphysis (36387,9±13310,31 μm^2).

Haversian canals were smaller in the proximal metaphysis (1262,43±588,42 μm^2) and in the diaphysis (1088,72±436.73 μm^2) compared to the distal metaphysis (2042,44±742,52μm^2).

HUMAN ADULT (HA1) – RADIUS (OSTEON)						
Bone portion		**On.Dm$_{max}$ (µm)**	**On.Dm$_{min}$ (µm)**	**On.Ar (µm^2)**	**On.Pm (µm)**	**On.Cr**
Proximal metaphysis (n=37)	Mean	220,14	166,91	28406,51	615,91	0,90
	St.dev	54,31	37,76	11610,9	136,69	0,03
	Min	135,43	99,46	9862,24	371,11	0,82
	Max	343,04	258,06	52504,79	865,10	0,96
Diaphysis (n=50)	Mean	244,56	188,69	36387,9	699,86	0,90
	St.dev	49,81	44,39	13310,31	137,2	0,04
	Min	132,16	87,20	8705,67	353,69	0,76
	Max	350,25	266,23	66297,41	960,50	0,96
Distal metaphysis (n=43)	Mean	217,13	169,64	29198,18	621,9	0,92
	St.dev	43,76	31,34	9798,13	105,96	0,04
	Min	141,16	112,31	13132,28	415,57	0,78
	Max	298,28	254,03	55050,21	850,25	0,97
Total (n=130)	Mean	228,54	176,19	31738,13	650,18	0,91
	St.dev	50,52	39,57	12242,89	132,59	0,04
	Min	132,16	87,20	8705,67	353,69	0,76
	Max	350,25	266,23	66297,41	960,50	0,97

Table 6.11 – Radius (HA1) - descriptive statistics of osteon parameters

HUMAN ADULT (HA1) – RADIUS (HAVERSIAN CANAL)					
Bone portion		**HC.Dm$_{max}$ (µm)**	**Hc.Dm$_{min}$ (µm)**	**HC.Ar (µm^2)**	**HC.Pm (µm)**
Proximal metaphysis (n=37)	Mean	46,14	34,8	1262,43	131,22
	St.dev	11,57	8,58	588,42	30,45
	Min	27,99	18,07	421,72	78,78
	Max	78,21	53,49	2752,39	201,84
Diaphysis (n=50)	Mean	43,68	30,58	1088,72	122,27
	St.dev	10,82	6,6	436,73	25,94
	Min	20,47	14,43	245,44	58,45
	Max	70,72	44,53	2246,42	179,64
Distal metaphysis (n=43)	Mean	56,55	43,5	2042,44	165,54
	St.dev	11,87	10,12	742,52	30,17
	Min	34,43	22,72	804,48	109,34
	Max	78,11	63,38	3558,33	217,45
Total (n=130)	Mean	48,64	36,05	1453,62	139,13
	St.dev	12,64	10,05	725,42	34,22
	Min	20,47	14,43	245,44	58,45
	Max	78,21	63,38	3558,33	217,45

Table 6.12 – Radius (HA1) - descriptive statistics of Haversian canal parameters

ANOVA and Tukey post-hoc test indicated that the size osteons was statistically significantly lower in the proximal metaphysis (p=0.006, Cohen's d=0.633, 95% CI for Cohen's d: 0.197 – 1.068) and in the distal metaphysis (p=0.011, Cohen's d=0.608, 95% CI for Cohen's d: 0.191 – 1.025) compared to the diaphysis. There was no statistically significant difference between the proximal and distal metaphysis (Table 6.13).

The size of the Haversian canal was statistically significantly lower in the proximal metaphysis (p=0.000, Cohen's d=1.154, 95% CI for Cohen's d: 0.68 – 1.629) and in the diaphysis (p=0.000, Cohen's d=1.596, 95% CI for Cohen's d: 1.128 – 2.064) compared to the distal metaphysis. No statistically significant difference was observed between the proximal metaphysis and the diaphysis.

RADIUS – ANOVA and Tukey's post hoc test									
	On.Dm (max)	**On.Dm (min)**	**On.Ar**	**On.Pm**	**HC.Dm (max)**	**Hc.Dm (min)**	**HC.Ar**	**HC.Pm**	**On.Cr**
Sig.									
Between groups	.015	.015	.002	.003	.000	.000	.000	.000	.004
Proximal vs diaphysis	.061	.028	.006	.008	.580	.059	.372	.325	.926
Proximal vs distal metaphysis	.960	.947	.952	.976	.000	.000	.000	.000	.028
Diaphysis vs distal metaphysis	.023	.050	.011	.011	.000	.000	.000	.000	.005

Table 6.13 – Radius (HA1) - Results of ANOVA and Tukey post-hoc test on osteon and Haversian canal parameters

In the ulna (Table 6.14 - 6.15), osteons were bigger in the proximal metaphysis (35655,79±14025,38 μm^2) and in the diaphysis (34389,81±18876,18 μm^2) compared to the distal metaphysis (24417,89±10373,38 μm^2). Osteons were more circular in the proximal metaphysis (0,92±0,03) and in the distal metaphysis (0,91±0,03) compared to the diaphysis (0,88±0,05).

HUMAN ADULT (HA1) – ULNA (OSTEON)						
Bone portion		**On.Dm$_{max}$ (µm)**	**On.Dm$_{min}$ (µm)**	**On.Ar (µm^2)**	**On.Pm (µm)**	**On.Cr**
Proximal metaphysis (n=49)	Mean	235,72	184,86	35655,79	682,35	0,92
	St.dev	49,96	40,4	14025,38	140,54	0,03
	Min	131,46	107,41	13935,79	430,15	0,85
	Max	329,86	257,28	60651,89	925,33	0,97
Diaphysis (n=37)	Mean	234,67	180,66	34389,81	678,73	0,88
	St.dev	72,45	51,14	18876,18	196,75	0,05
	Min	119,93	96,86	9117,10	358,75	0,70
	Max	413,23	321,01	84195,76	1137,03	0,95
Distal metaphysis (n=41)	Mean	198,8	152,74	24417,89	566,52	0,91
	St.dev	47,43	35,54	10373,38	127,97	0,03
	Min	116,01	88,79	8462,18	340,74	0,82
	Max	306,74	234,86	48178	827,19	0,96
Total (n=127)	Mean	223,49	173,27	31658,98	643,9	0,90
	St.dev	58,81	44,44	15374,18	163,29	0,04
	Min	116,01	88,79	8462,18	340,74	0,70
	Max	423,23	321,01	84195,76	1137,03	0,97

Table 6.14 – Ulna (HA1) - descriptive statistics of osteon parameters

HUMAN ADULT (HA1) – ULNA (HAVERSIAN CANAL)					
Bone portion		**HC.Dm$_{max}$ (µm)**	**Hc.Dm$_{min}$ (µm)**	**HC.Ar (µm^2)**	**HC.Pm (µm)**
Proximal metaphysis (n=49)	Mean	49,71	37,53	1583,04	143,73
	St.dev	12,38	10,7	760,63	760,63
	Min	24,42	20,91	506,94	83,17
	Max	77,11	61,58	3581,22	219,56
Diaphysis (n=37)	Mean	56,96	41,95	1966,5	160,25
	St.dev	19,92	11,68	933,71	45,43
	Min	24,79	17,87	424,67	76,02
	Max	124,52	58,57	3479,59	280,12
Distal metaphysis (n=41)	Mean	49,1	38,3	1613,47	145,24
	St.dev	12,63	11,31	791,87	36,21
	Min	23,04	16,01	388,61	76,44
	Max	79	63,01	3251,05	217,50
Total (n=127)	Mean	51,63	39,06	1704,58	149,03
	St.dev	15,3	11,26	834,96	38,95
	Min	23,04	16,01	388,61	76,02
	Max	124,52	63,01	3581,22	280,12

Table 6.15 – Ulna (HA1) - descriptive statistics of Haversian canal parameters

ANOVA and Tukey post-hoc test revealed that the size of the osteon was statistically significantly higher in the proximal metaphysis (p=0.001, Cohen's d=0.899, 95% CI for Cohen's d: 0.464 – 1.334) and in the diaphysis (p=0.009, Cohen's d=0.664, 95% CI for Cohen's d: 0.208 – 1.121) compared to the distal metaphysis. Osteon circularity was statistically significantly higher in the proximal metaphysis (p=0.000, Cohen's d=1.004, 95% CI for Cohen's d: 0.552 – 1.457) and in the distal metaphysis (p=0.000, Cohen's d=0.737, 95% CI for Cohen's d: 0.278 – 1.196) compared to the diaphysis. There was no statistically significant difference between the proximal metaphysis and the diaphysis (Table 6.16).

ULNA – ANOVA and Tukey's post hoc test									
	On.Dm (max)	**On.Dm (min)**	**On.Ar**	**On.Pm**	**HC.Dm (max)**	**Hc.Dm (min)**	**HC.Ar**	**HC.Pm**	**On.Cr**
Sig.									
Between groups	.004	.001	.001	.001	.040	.172	.075	.112	.000
Proximal vs diaphysis	.996	.892	.917	.994	.073	.169	.087	.125	.000
Proximal vs distal metaphysis	.007	.001	.001	.002	.980	.944	.983	.981	.502
Diaphysis vs distal metaphysis	.017	.012	.009	.005	.059	.324	.146	.204	.000

Table 6.16 – Ulna (HA1) - Results of ANOVA and Tukey post-hoc test on osteon and Haversian canal parameters

The **femur** (Table 6.17 – 6.18) showed a general uniformity in the size of the osteon and Haversian canal. The only statistically significant difference concerned the osteon area between the proximal metaphysis (24683,9±8367,31 μm^2) and the distal metaphysis (30872,51±12324,9 μm^2, p=0.021, Cohen's d=0.589, 95% CI for Cohen's d: 0.164 – 1.013; Table 6.19)

HUMAN ADULT (HA1) – FEMUR (OSTEON)						
Bone portion		**On.Dm$_{max}$ (µm)**	**On.Dm$_{min}$ (µm)**	**On.Ar (µm^2)**	**On.Pm (µm)**	**On.Cr**
Neck (n=45)	Mean	202,16	153,05	25600,7	593,45	0,89
	St.dev	41,77	29,13	9425,44	121,21	0,04
	Min	122,06	87,95	9352,86	370,46	0,76
	Max	277,61	206,85	45473,82	848,20	0,96
Proximal metaphysis (n=50)	Mean	199,29	160,47	24683,9	578,68	0,90
	St.dev	35,12	31,44	8367,31	96,56	0,04
	Min	137,71	107,33	10899,50	390,40	0,82
	Max	303,14	234,41	46537,87	808,24	0,98
Diaphysis (n=44)	Mean	200,66	151,49	25521,31	583,40	0,90
	St.dev	46,93	37,83	10883,85	125,74	0,03
	Min	131	79,06	9934,30	382,99	0,82
	Max	336,27	229,83	57658,22	893,60	0,97
Distal metaphysis (n=44)	Mean	230,76	171,02	30872,51	645,46	0,89
	St.dev	57,79	34,41	12324,9	140,82	0,05
	Min	124,97	79,36	8427,61	349,13	0,71
	Max	367,60	244,27	61261,59	960,65	0,97
Total (n=183)	Mean	207,93	159,06	26604,58	599,59	0,89
	St.dev	47,23	33,84	10492,91	123,20	0,04
	Min	122,06	79,06	8427,61	349,13	0,71
	Max	367,60	244,27	61261,59	960,65	0,98

Table 6.17 – Femur (HA1) - descriptive statistics of osteon parameters

HUMAN ADULT (HA1) – FEMUR (HAVERSIAN CANAL)					
Bone portion		**HC.Dm$_{max}$ (µm)**	**Hc.Dm$_{min}$ (µm)**	**HC.Ar (µm^2)**	**HC.Pm (µm)**
Neck (n=45)	Mean	49,36	36,76	1496,92	141,59
	St.dev	12,5	9,99	699,12	33,51
	Min	22,74	17,27	418,80	78,55
	Max	73,60	53,32	3020,71	202,42
Proximal metaphysis (n=50)	Mean	46,04	34,57	1305,07	131,76
	St.dev	11,88	8,04	578,7	29,84
	Min	22,66	15,15	310,20	66,96
	Max	83,39	54,42	3094,25	211,20
Diaphysis (n=44)	Mean	48,12	38,39	1640	147,43
	St.dev	13,08	10,05	749,58	34,93
	Min	21,55	21,65	429,52	76,02
	Max	77,23	57,24	3139,21	207,74
Distal metaphysis (n=44)	Mean	50,39	35,57	1529,3	142,83
	St.dev	15,74	11,37	850,74	40,35
	Min	19,98	18,54	305,33	67,04
	Max	81,00	66,62	3566,13	224,67
Total (n=183)	Mean	48,40	36,26	1485,85	140,57
	St.dev	13,32	9,90	725,92	34,90
	Min	19,98	15,15	305,33	66,96
	Max	83,39	66,62	3566,13	224,67

Table 6.18 – Femur (HA1) - descriptive statistics of Haversian canal parameters

FEMUR – ANOVA and Tukey's post hoc test									
	On.Dm (max)	**On.Dm (min)**	**On.Ar**	**On.Pm**	**HC.Dm (max)**	**Hc.Dm (min)**	**HC.Ar**	**HC.Pm**	**On.Cr**
Sig.									
Between groups	.003	.026	.019	.037	.426	.288	.157	.167	.271
Proximal vs diaphysis	.999	.565	.980	.998	.876	.249	.119	.135	.999
Proximal vs distal metaphysis	.006	.419	.021	.042	.394	.961	.437	.414	.942
Diaphysis vs distal metaphysis	.013	.034	.076	.084	.858	.544	.891	.926	.908
Neck vs proximal metaphyisi	.990	.699	.973	.934	.619	.702	.568	.514	.332
Neck vs diaphysis	.999	.996	1.000	.980	.972	.867	.789	.860	.299
Neck vs distal metaphysis	.019	.056	.078	.184	.984	.941	.997	.998	.698

Table 6.19 – Femur (HA1) - Results of ANOVA and Tukey post-hoc test on osteon and Haversian canal parameters

In the **tibia** (Table 6.20 – 6.21), osteons were smaller in the diaphysis (29574,32±15616,75 μm^2) and in the distal metaphysis (26974,41±10482,21 μm^2) compared to the proximal metaphysis (38318,25±11601,89 μm^2). Osteon circularity was lower in the distal metaphysis (0,90±0,03) compared to the diaphysis (0,92±0,02).

HUMAN ADULT (HA1) – TIBIA (OSTEON)						
Bone portion		**On.Dm$_{max}$ (µm)**	**On.Dm$_{min}$ (µm)**	**On.Ar (µm^2)**	**On.Pm (µm)**	**On.Cr**
Proximal metaphysis (n=46)	Mean	251,33	195,49	38318,25	717,92	0,91
	St.dev	42,75	31,65	11601,89	110,29	0,03
	Min	163,85	130,64	16704,25	465,38	0,84
	Max	348,94	268,33	64909,04	958,17	0,97
Diaphysis (n=43)	Mean	206,3	166,36	29574,32	617,95	0,92
	St.dev	53,48	44,59	15616,75	157,91	0,02
	Min	126,17	101,75	11128,40	389,39	0,84
	Max	327,75	302,79	75311,94	1009,65	0,97
Distal metaphysis (n=49)	Mean	210,6	161,53	26974,41	602	0,90
	St.dev	46,81	37,82	10482,21	125,51	0,03
	Min	114,55	89,06	8879,52	357,60	0,83
	Max	304,19	244,14	47423,68	831,03	0,95
Total (n=138)	Mean	222,84	174,35	31565,81	645,61	0,91
	St.dev	51,54	40,85	13474,83	140,84	0,03
	Min	114,55	89,06	8879,52	357,60	0,83
	Max	348,94	302,79	75311,94	1009,65	0,97

Table 6.20 – Tibia (HA1) - descriptive statistics of osteon parameters

HUMAN ADULT (HA1) – TIBIA (HAVERSIAN CANAL)					
Bone portion		**HC.Dm$_{max}$ (µm)**	**Hc.Dm$_{min}$ (µm)**	**HC.Ar (µm^2)**	**HC.Pm (µm)**
Proximal metaphysis (n=46)	Mean	50,26	38,91	1604,51	145
	St.dev	13,24	11,83	791,1	36,98
	Min	21,19	15,74	3179,47	64,02
	Max	78,53	61,04	545,94	208,33
Diaphysis (n=43)	Mean	49,62	39,55	1731,87	150,89
	St.dev	13,16	9,66	824,9	36,91
	Min	27,91	21,65	545,94	87,12
	Max	78,16	61,86	3491,29	219,07
Distal metaphysis (n=49)	Mean	53,3	42,42	1844,89	156,66
	St.dev	10,91	8,62	693,51	29,79
	Min	32,46	28,13	782,08	103,47
	Max	77,59	59,61	3238,88	210,40
Total (n=138)	Mean	51,14	40,36	1729,55	150,98
	St.dev	12,45	10,15	769,87	34,66
	Min	21,19	15,74	298,52	64,02
	Max	78,53	61,86	3491,29	219,07

Table 6.21 – Tibia (HA1) - descriptive statistics of Haversian canal parameters

ANOVA and Tukey post-hoc test indicated the size of the osteon was statistically significantly lower in the diaphysis (p=0.004, Cohen's d=0.639, 95% CI for Cohen's d: 0.213 – 1.065) and in the distal metaphysis (p=0.000, Cohen's d=1.028, 95% CI for Cohen's d: 0.6 – 1.456) compared to the proximal metaphysis. There was no statistically significant difference between the diaphysis and the distal metaphysis.

Osteon circularity was statistically significantly lower in the distal metaphysis (p=0.009, Cohen's d=0.775, 95% CI for Cohen's d: 0.35 – 1.199) compared to the diaphysis (Table 6.22).

TIBIA – ANOVA and Tukey's post hoc test									
	On.Dm (max)	**On.Dm (min)**	**On.Ar**	**On.Pm**	**HC.Dm (max)**	**Hc.Dm (min)**	**HC.Ar**	**HC.Pm**	**On.Cr**
Sig.									
Between groups	.000	.000	.000	.000	.313	.200	.317	.263	.009
Proximal vs diaphysis	.000	.001	.004	.001	.968	.952	.715	.702	.678
Proximal vs distal metaphysis	.000	.000	.000	.000	.462	.212	.284	.231	.080
Diaphysis vs distal metaphysis	.903	.817	.588	.832	.337	.366	.762	.704	.009

Table 6.22 – Tibia (HA1) - Results of ANOVA and Tukey post-hoc test on osteon and Haversian canal parameters

In the **fibula** (Table 6.23 – 6.24), osteons were smaller in the proximal metaphysis (11885,34±4661,31μm^2) and in the distal metaphysis (25095,26±7509,45μm^2) compared to the diaphysis (35354,56±15416,09 μm^2).

Haversian canals were bigger in the diaphysis (1679,99±810,42 μm^2) and in the distal metaphysis (1819,7±857,46 μm^2) compared to the proximal metaphysis (1203,48±784,76 μm^2).

HUMAN ADULT (HA1) – FIBULA (OSTEON)						
Bone portion		**On.Dm$_{max}$ (µm)**	**On.Dm$_{min}$ (µm)**	**On.Ar (µm^2)**	**On.Pm (µm)**	**On.Cr**
Proximal metaphysis (n=32)	Mean	136,12	109,6	12433,08	409,6	0,91
	St.dev	25,57	20,23	4482,49	73,82	0,04
	Min	100,77	83,33	7253,73	317,75	0,79
	Max	208,95	148,49	23524,8	591,78	0,95
Diaphysis (n=42)	Mean	224,94	186,5	35354,56	677,89	0,91
	St.dev	56,18	46,05	15416,09	159,08	0,03
	Min	113,10	96,88	9734,61	370,24	0,86
	Max	315,54	278,45	65870,96	925,91	0,97
Distal metaphysis (n=33)	Mean	196,09	159,33	25095,26	576,07	0,93
	St.dev	33,77	34,65	7509,45	92,75	0,03
	Min	123,02	38,28	10858,59	384,72	0,85
	Max	259,36	206,91	38224,70	748,68	0,97
Total (n=107)	Mean	186,72	153,25	24809,29	558,55	0,92
	St.dev	57,6	48,87	14464,88	166,68	0,03
	Min	74,43	38,28	4436,91	249,83	0,79
	Max	315,54	278,45	65870,96	925,91	0,97

Table 6.23 – Fibula (HA1) - descriptive statistics of osteon parameters

HUMAN ADULT (HA1) – FIBULA (HAVERSIAN CANAL)					
Bone portion		**HC.Dm$_{max}$ (µm)**	**Hc.Dm$_{min}$ (µm)**	**HC.Ar (µm^2)**	**HC.Pm (µm)**
Proximal metaphysis (n=35)	Mean	40,6	32,38	1223,59	122,25
	St.dev	15,24	11,31	802,3	42,56
	Min	17,01	13,83	231,56	56,43
	Max	76,47	55,23	3084,87	203,34
Diaphysis (n=42)	Mean	47,99	39,84	1679,99	147,21
	St.dev	12,74	10,55	810,42	37,25
	Min	23,27	19,08	402,26	73,64
	Max	76,78	58,64	3312,08	217,05
Distal metaphysis (n=33)	Mean	52,34	41,6	1819,7	152,56
	St.dev	19,46	11,11	857,46	38,55
	Min	23,32	21,50	445,10	76,76
	Max	130,18	60,96	3401,04	222,40
Total (n=110)	Mean	46,79	37,94	1570,28	140,55
	St.dev	16,30	11,57	849,51	41,10
	Min	17,01	13,83	231,56	56,43
	Max	130,18	60,96	3401,04	222,40

Table 6.24 – Fibula (HA1) - descriptive statistics of Haversian canal parameters

ANOVA and Tukey post-hoc test revealed that the size of the osteon was statistically significantly lower in the proximal metaphysis (p=0.000, Cohen's d=1.985, 95% CI for Cohen's d: 1.438 – 2.532) and in the distal metaphysis (p=0.000, Cohen's d=0.816, 95% CI for Cohen's d: 0.341 – 1.29) compared to the diaphysis. There was also a statistically significant difference in the size of the osteon between the proximal and distal metaphysis (p=0.000, Cohen's d=2.128, 95% CI for Cohen's d: 1.533 – 2.723).

The size of the Haversian canal was statistically significantly higher in the diaphysis (p=0.033, Cohen's d=0.596, 95% CI for Cohen's d: 0.138 – 1.055) and in the distal metaphysis (p=0.007, Cohen's d=0.751, 95% CI for Cohen's d: 0.259 – 1.243) compared to the proximal metaphysis. There was no statistically significant difference between diaphysis and the distal metaphysis (Table 6.25).

FIBULA – ANOVA and Tukey's post hoc test									
	On.Dm (max)	**On.Dm (min)**	**On.Ar**	**On.Pm**	**HC.Dm (max)**	**Hc.Dm (min)**	**HC.Ar**	**HC.Pm**	**On.Cr**
Sig.									
Between groups	.000	.000	.000	.000	.02	.002	.011	.005	.014
Proximal vs diaphysis	.000	.000	.000	.000	.062	.013	.052	.021	.533
Proximal vs distal metaphysis	.000	.000	.000	.000	.024	.003	.012	.007	.012
Diaphysis vs distal metaphysis	.011	.008	.000	.001	.853	.805	.746	.829	.107

Table 6.25 – Fibula (HA1) - Results of ANOVA and Tukey post-hoc test on osteon and Haversian canal parameters

The **clavicle** (Table 6.26 – 6.27) showed no secondary osteon in its lateral end. There was no statistically significant difference between the shaft and the medial end in terms of osteon and Haversian canal size.

HUMAN ADULT (HA1) – CLAVICLE (OSTEON)						
Bone portion		**On.Dm$_{max}$ (µm)**	**On.Dm$_{min}$ (µm)**	**On.Ar (µm^2)**	**On.Pm (µm)**	**On.Cr**
Shaft (n=44)	Mean	217,29	181,37	32666,70	644,77	0,92
	St.dev	61,59	45,40	17008,90	168,07	0,03
	Min	113,70	90,64	7637,73	320,10	0,84
	Max	393,78	286,13	74180,58	1025,29	0,97
Medial (n=26)	Mean	221,57	164,68	28303,78	619,20	0,89
	St.dev	58,33	38,75	11890,90	132,43	0,06
	Min	110,21	103,93	8896,08	365,79	0,69
	Max	388,03	274,03	62318,32	936,19	0,96
Total (n=70)	Mean	218,88	175,17	31046,18	635,27	0,91
	St.dev	60,01	43,53	15363,21	155,28	0,04
	Min	110,21	90,64	7637,73	320,10	0,69
	Max	393,78	286,13	74180,58	1025,29	0,97

Table 6.26 – Clavicle (HA1) - descriptive statistics of osteon parameters

HUMAN ADULT (HA1) – CLAVICLE (HAVERSIAN CANAL)					
Bone portion		**HC.Dm$_{max}$ (µm)**	**Hc.Dm$_{min}$ (µm)**	**HC.Ar (µm^2)**	**HC.Pm (µm)**
Shaft (n=44)	Mean	50,05	40,50	1686,44	150,30
	St.dev	10,41	10,41	664,41	29,59
	Min	26,53	25,83	633,56	92,86
	Max	71,33	58,63	3183,36	208,22
Medial (n=26)	Mean	55,91	38,74	1711,91	153,92
	St.dev	14,15	9,16	715,79	34,69
	Min	29,22	19,98	450,94	81,65
	Max	85,42	54,64	3421,49	220,94
Total (n=70)	Mean	52,23	39,85	1695,90	151,64
	St.dev	12,18	8,92	678,89	31,38
	Min	26,53	19,98	450,94	81,65
	Max	85,42	58,63	3421,49	220,94

Table 6.27 – Clavicle (HA1) - descriptive statistics of Haversian canal parameters

Osteon circularity was statistically significantly lower in the medial end (0,89±0,06, p=0.004, Cohen's d=0.69, 95% CI for Cohen's d: 0.191 – 1.188) compared to the shaft (0,92±0,03; Table 6.28).

CLAVICLE – ANOVA test									
	On.Dm (max)	**On.Dm (min)**	**On.Ar**	**On.Pm**	**HC.Dm (max)**	**Hc.Dm (min)**	**HC.Ar**	**HC.Pm**	**On.Cr**
Sig.									
Shaft vs medial	.776	.122	.254	.509	.051	.430	.881	.644	.004

Table 6.28 – Clavicle (HA1) - Results of ANOVA on osteon and Haversian canal parameters

The **metacarpal** showed no secondary osteons in its base. No statistically significant difference between the shaft and the head was observed in terms of osteon and Haversian canal size (Table 6.29 – 6.30 – 6.31).

HUMAN ADULT (HA1) – METACARPAL (OSTEON)						
Bone portion		**On.Dm$_{max}$ (µm)**	**On.Dm$_{min}$ (µm)**	**On.Ar (µm^2)**	**On.Pm (µm)**	**On.Cr**
Head (n=44)	Mean	216,17	150,33	25827,43	598,11	0,87
	St.dev	49,05	32,83	9880,35	119,41	0,04
	Min	132,63	85,94	9376,72	361,31	0,79
	Max	329,03	223,08	48724,39	878,08	0,96
Shaft (n=43)	Mean	196,86	146,40	23152,17	561	0,88
	St.dev	46,90	31,73	9284,02	120,26	0,04
	Min	125,65	85,40	10221,63	380,88	0,76
	Max	310,04	208,88	49300,97	839,87	0,95
Total (n=87)	Mean	206,63	148,39	24505,17	579,77	0,88
	St.dev	48,69	32,17	9628,85	120,58	0,04
	Min	125,65	85,40	9376,72	361,31	0,76
	Max	329,03	223,08	49300,97	878,08	0,96

Table 6.29 – Metacarpal (HA1) - descriptive statistics of osteon parameters

HUMAN ADULT (HA1) – METACARPAL (HAVERSIAN CANAL)					
Bone portion		**HC.Dm$_{max}$ (µm)**	**Hc.Dm$_{min}$ (µm)**	**HC.Ar (µm^2)**	**HC.Pm (µm)**
Head (n=44)	Mean	52,47	40,46	1685,93	149,59
	St.dev	14,29	11,74	818,65	37,45
	Min	26,75	19,30	474,31	79,90
	Max	79,49	71,72	3592,42	228,99
Shaft (n=43)	Mean	49,31	40,96	1716,71	149,67
	St.dev	12,58	10,81	815,62	36,56
	Min	26,05	19,85	425,62	79,22
	Max	74,02	62,08	3528,14	218,42
Total (n=87)	Mean	50,91	40,71	1716,71	149,67
	St.dev	13,49	11,23	815,62	36,56
	Min	26,05	19,30	425,62	79,22
	Max	79,49	71,72	3592,42	228,99

Table 6.30 – Metacarpal (HA1) - descriptive statistics of Haversian canal parameters

METACARPAL – ANOVA test									
	On.Dm (max)	**On.Dm (min)**	**On.Ar**	**On.Pm**	**HC.Dm (max)**	**Hc.Dm (min)**	**HC.Ar**	**HC.Pm**	**On.Cr**
Sig.									
Head vs shaft	.064	.572	.197	.152	.278	.835	.724	.984	.108

Table 6.31 – Metacarpal (HA1) - Results of ANOVA on osteon and Haversian canal parameters

The **metatarsal** showed no statistically significant differences in osteon size and Haversian canal size between the head, the shaft and the base (Table 6.32 – 6.33 – 6.34).

HUMAN ADULT (HA1) – METATARSAL (OSTEON)						
Bone portion		**On.Dm$_{max}$ (µm)**	**On.Dm$_{min}$ (µm)**	**On.Ar (µm^2)**	**On.Pm (µm)**	**On.Cr**
Head (n=4)	Mean	206,65	156,60	23951,92	577,28	0,88
	St.dev	39,55	28,38	7950,02	90,14	0,03
	Min	157,31	126,55	14955,04	474,61	0,83
	Max	252,41	185,85	31932,97	670,25	0,92
Shaft (n=39)	Mean	199,14	164,91	27165,60	590,39	0,92
	St.dev	50,05	37,96	14272	147,12	0,03
	Min	117,26	106,46	10565,92	372,93	0,85
	Max	332,25	283,11	86173,82	1088,39	0,97
Base (n=9)	Mean	189,53	139,23	20382,33	536,34	0,87
	St.dev	38,41	32,81	6201,17	96,71	0,06
	Min	109,04	73,98	7456,58	321,55	0,77
	Max	241,92	188,97	28343,96	637,07	0,94
Total (n=52)	Mean	198,06	159,83	25744,36	580,03	0,91
	St.dev	47,01	37,22	12976,49	135,98	0,04
	Min	109,04	73,98	7456,58	321,55	0,77
	Max	332,25	283,11	86173,82	1088,39	0,97

Table 6.32 – Metatarsal (HA1) - descriptive statistics of osteon parameters

HUMAN ADULT (HA1) – METATARSAL (HAVERSIAN CANAL)					
Bone portion		**HC.Dm$_{max}$ (µm)**	**Hc.Dm$_{min}$ (µm)**	**HC.Ar (µm^2)**	**HC.Pm (µm)**
Head (n=4)	Mean	50,16	35,30	1374,73	139,13
	St.dev	12,11	5,70	477,96	26,70
	Min	35,22	26,98	745,07	102,20
	Max	63,90	39,38	1888,98	166,03
Shaft (n=39)	Mean	50,39	41,78	1816,20	151,63
	St.dev	14,30	11,49	894,24	39,24
	Min	23,73	20,48	431,46	75,72
	Max	74	63,67	3586,09	218,93
Base (n=9)	Mean	47,80	33,08	1288,32	132,55
	St.dev	11,32	6,07	560,39	28,67
	Min	37,10	28,01	639,89	92,76
	Max	67,33	45,74	2445,59	182,83
Total (n=52)	Mean	49,93	39,78	1690,88	147,36
	St.dev	13,49	10,89	840,82	37,10
	Min	23,73	20,48	431,46	75,72
	Max	74	63,67	3586,09	218,93

Table 6.33 – Metatarsal (HA1) - descriptive statistics of Haversian canal parameters

METATARSAL – ANOVA and Tukey's post hoc test									
	On.Dm (max)	**On.Dm (min)**	**On.Ar**	**On.Pm**	**HC.Dm (max)**	**Hc.Dm (min)**	**HC.Ar**	**HC.Pm**	**On.Cr**
Sig.									
Between groups	.805	.174	.360	.570	.878	.065	.176	.349	.000
Head vs shaft	.952	.902	.885	.982	.999	.474	.571	.797	.052
Head vs base	.823	.711	.891	.873	.956	.934	.984	.953	.936
Shaft vs base	.850	.151	.341	.540	.867	.075	.206	.353	.001

Table 6.34 – Metatarsal (HA1) - Results of ANOVA and Tukey post-hoc test on osteon and Haversian canal parameters

In **rib**, no statistically significant difference between the body and the head was observed in terms of osteon and Haversian canal size (Table 6.35 – 6.36).

HUMAN ADULT (HA1) – RIB (OSTEON)						
Bone portion		**On.Dm$_{max}$ (µm)**	**On.Dm$_{min}$ (µm)**	**On.Ar (µm^2)**	**On.Pm (µm)**	**On.Cr**
Head (n=5)	Mean	174,35	103,66	14216,88	458,36	0,83
	St.dev	35,56	19,23	4606,21	78,66	0,06
	Min	132,42	80,65	8803,55	370,99	0,77
	Max	213,55	133,80	19810,19	536,35	0,93
Body (n=48)	Mean	177,98	138,40	20279,75	511,05	0,91
	St.dev	51,64	40,94	11030,51	140,45	0,03
	Min	94,92	68,30	6661,35	298,84	0,80
	Max	328,22	248,99	48832,50	853,92	0,97
Total (n=53)	Mean	177,63	135,12	19707,78	506,08	0,90
	St.dev	50,09	40,60	10714,75	136,19	0,04
	Min	94,92	68,30	6661,35	298,84	0,77
	Max	328,22	248,99	48832,50	853,92	0,97

Table 6.35 –Rib (HA1) - descriptive statistics of osteon parameters

HUMAN ADULT (HA1) – RIB (HAVERSIAN CANAL)					
Bone portion		**HC.Dm$_{max}$ (µm)**	**Hc.Dm$_{min}$ (µm)**	**HC.Ar (µm^2)**	**HC.Pm (µm)**
Head (n=5)	Mean	43,73	28,13	1042,23	121,65
	St.dev	10,30	8,61	508,49	28,66
	Min	33,74	16,65	568,79	95,22
	Max	56,54	36,02	1761,88	160,19
Body (n=48)	Mean	39,49	31,43	1063,24	116,98
	St.dev	10,27	9,31	583,51	30,85
	Min	17,50	14,39	219,14	55,08
	Max	69,73	50,90	2922,83	199,99
Total (n=53)	Mean	39,89	31,12	1061,26	117,42
	St.dev	10,25	9,22	572,43	30,42
	Min	17,50	14,39	219,14	55,08
	Max	69,73	50,90	2922,83	199,99

Table 6.36 – Rib (HA1) - descriptive statistics of Haversian canal parameters

Osteon circularity was statistically significantly lower in the head (0,83±0,06, p=0.000, Cohen's d=2.399, 95% CI for Cohen's d: 1.371 – 3.427) compared to the body (0,91±0,03; Table 6.37).

RIB – ANOVA test									
	On.Dm (max)	**On.Dm (min)**	**On.Ar**	**On.Pm**	**HC.Dm (max)**	**Hc.Dm (min)**	**HC.Ar**	**HC.Pm**	**On.Cr**
Sig.									
Head vs body	.879	.068	.232	.416	.384	.453	.939	.747	.000

Table 6.37 – Rib (HA1) - Results of ANOVA on osteon and Haversian canal parameters

6.2.2 JUVENILE HUMAN SKELETON

The histomorphometric analysis of the human juvenile individual (HJ1) involved the measurement of 139 secondary osteons and Haversian canals (see Appendix B for the descriptive statistics of each bone).

As shown in Table 6.38, osteons were generally bigger in long bones compared to flat bones, with a mean area respectively of 37792,68(±13372,18) μm^2 and 28801,04(±15657,26) μm^2.

Similarly, Haversian canals area were bigger in long bones compared with flat bones, with a mean area respectively of (1360,79±737,02) μm^2 and (1256,88±743,41) μm^2 (Table 6.39).

HUMAN JUVENILE (HJ) - OSTEON						
Bone type		**On.Dm$_{max}$ (μm)**	**On.Dm$_{min}$ (μm)**	**On.Ar (μm^2)**	**On.Pm (μm)**	**On.Cr**
Long bones (n=126)	Mean	248,47	189,32	37792,68	713,43	0,91
	St.dev	48,80	39	13372,18	129,86	0,04
	Min	125,2	101,35	12130,57	400,9	0,78
	Max	393,98	286,47	79907,9	1072,89	0,98
Flat bones (n=13)	Mean	222,32	158,51	28801,04	613,67	0,89
	St.dev	72,49	50,95	15657,26	171,96	0,05
	Min	109,81	95,91	8796,25	342,14	0,79
	Max	391,31	239,72	59016,14	943,79	0,97
Total (n=139)	Mean	246,02	186,44	36951,74	704,1	0,90
	St.dev	51,70	41,04	13791	136,73	0,04
	Min	109,81	95,91	8796,25	342,14	0,78
	Max	393,98	286,47	79907,9	1072,89	0,98

Table 6.38 - Descriptive statistics of osteon parameters for the human juvenile individual HJ

HUMAN JUVENILE (HJ) HAVERSIAN CANAL					
Bone type		**HC.Dm$_{max}$ (µm)**	**Hc.Dm$_{min}$ (µm)**	**HC.Ar (µm^2)**	**HC.Pm (µm)**
Long bones (n=126)	Mean	47,01	33,60	1360,79	133,34
	St.dev	15,24	10,15	737,02	37,50
	Min	22,89	13,96	336,99	70,81
	Max	94,14	57,01	3692,74	230,85
Flat bones (n=13)	Mean	50,25	29,60	1256,88	134,62
	St.dev	16,66	9,88	743,41	39,62
	Min	30,71	21,64	599,95	90,64
	Max	79,06	59,09	3317,28	216,6
Total (n=139)	Mean	47,31	33,23	1351,07	133,46
	St.dev	15,35	10,16	735,53	37,56
	Min	22,89	13,96	336,99	70,81
	Max	94,14	59,09	3692,74	230,85

Table 6.39 - Descriptive statistics of osteon parameters for the human juvenile individual HJ

ANOVA test revealed that the size of osteon was statistically significantly different between long and flat bones (p=0.025, Cohen's d=0.662, 95% CI for Cohen's d: 0.086 – 1.238). The size of the Haversian canal and osteon circularity showed no statistically significant differences (Table 6.40).

HUMAN JUVENILE – LONG VS FLAT BONES									
Bone type	**On.Dm (max)**	**On.Dm (min)**	**On.Ar**	**On.Pm**	**HC.Dm (max)**	**Hc.Dm (min)**	**HC.Ar**	**HC.Pm**	**On.Cr**
Sig.									
Between groups	.083	.009	.025	.012	.470	.083	.527	.908	.726

Table 6.40 – Results of ANOVA on osteon and Haversian canal parameters for the human juvenile individual HJ

Concerning the differences between different portions of the same bone, comparisons were possible exclusively for the humerus and the ulna, since they represented the only

bones which exhibited remodeling if different portions of the bone. ANOVA test revealed that, in the humerus, the size of the Haversian canal was statistically significantly lower in the diaphysis (1296,06±597μm^2, p=0.009, Cohen's d=1.048, 95% CI for Cohen's d: 0.267 – 1.828) compared to the distal metaphysis (2073,68±959,48μm^2).

There was no statistically significant difference in the size of the osteon and in the osteon circularity between the diaphysis and the distal metaphysis (Table 6.41).

HUMERUS – ANOVA test									
	On.Dm (max)	**On.Dm (min)**	**On.Ar**	**On.Pm**	**HC.Dm (max)**	**Hc.Dm (min)**	**HC.Ar**	**HC.Pm**	**On.Cr**
Sig.									
Diaphysis vs distal metaphysis	.363	.955	.625	.619	.005	.067	.009	.003	.931

Table 6.41 - Humerus (HJ) - Results of ANOVA on osteon and Haversian canal parameters

In the ulna, no statistically significant difference between the proximal metaphysis and the diaphysis was observed in terms of osteon and Haversian canal size (Table 6.42).

ULNA – ANOVA test									
	On.Dm (max)	**On.Dm (min)**	**On.Ar**	**On.Pm**	**HC.Dm (max)**	**Hc.Dm (min)**	**HC.Ar**	**HC.Pm**	**On.Cr**
Sig.									
Proximal vs diaphysis	.559	.626	.878	.700	.126	.252	.108	.139	.171

Table 6.42 - Ulna (HJ) - Results of ANOVA on osteon and Haversian canal parameters

6.2.3 JUVENILE PIG SKELETON

The histomorphometric analysis of the juvenile pig skeleton (PJ1) involved the measurement of 301 secondary osteons and Haversian canals in long and flat bones (see Appendix B for the descriptive statistics of each bone). No secondary osteons were found in irregular bones.

As shown in Table 6.43, osteons were generally bigger in long bones compared to flat bones, with a mean area respectively of 24979,68(±11227,73) μm^2, and 20169,2(±12203,69) μm^2.

Similarly, Haversian canals (Table 6.44) were bigger in long bones compared to flat bones, with a mean area respectively of 848,68(±473,15) μm^2 and (752,04±380,25) μm^2.

JUVENILE PIG SKELETON (PJ1)						
Bone type		**On.Dm$_{max}$ (μm)**	**On.Dm$_{min}$ (μm)**	**On.Ar (μm^2)**	**On.Pm (μm)**	**On.Cr**
Long bones (n=288)	Mean	195,77	155,74	24979,68	571,65	0,91
	St.dev	45,17	38,84	11227,73	128,24	0,04
	Min	103,26	72,72	5143,44	271,17	0,77
	Max	321,39	269,96	67185,16	934,65	0,98
Flat bones (n=13)	Mean	172,03	137,95	20169,2	497,17	0,93
	St.dev	56,74	45,94	12203,69	161,90	0,02
	Min	79,74	69,51	4362,82	242,54	0,89
	Max	247,62	228,69	46015,83	769,89	0,98
Total (n=301)	Mean	194,74	154,97	24771,92	568,44	0,91
	St.dev	45,87	39,25	11292,3	130,43	0,04
	Min	79,74	69,51	4362,82	242,54	077
	Max	321,39	269,96	67185,16	934,65	0,98

Table 6.43 - Descriptive statistics of osteon parameters for the juvenile pig skeleton (PJ1)

JUVENILE PIG SKELETON (PJ1)					
Bone type		**HC.Dm$_{max}$ (μm)**	**Hc.Dm$_{min}$ (μm)**	**HC.Ar (μm^2)**	**HC.Pm (μm)**
Long bones (n=288)	Mean	38,01	25,49	848,68	108
	St.dev	10,97	7,45	473,15	27,92
	Min	17,89	9,36	220,11	56,2
	Max	78,92	58,29	3425,88	211,41
Flat bones (n=13)	Mean	34,28	25,31	752,04	100,97
	St.dev	11,2	5,33	380,25	25,7
	Min	21,85	17,46	378,87	72,66
	Max	54,19	34,74	1508,16	148,75
Total (n=301)	Mean	37,85	25,48	844,50	107,7
	St.dev	10,98	7,37	469,41	27,82
	Min	17,89	9,36	220,11	56,2
	Max	78,92	58,29	3425,88	211,41

Table 6.44 - Descriptive statistics of Haversian canal parameters for the juvenile pig skeleton (PJ1)

ANOVA test revealed that there were no statistically significant differences in the size of osteon and Haversian canal between long and flat bones (Table 6.45).

JUVENILE PIG – LONG VS FLAT BONES									
Bone type	**On.Dm (max)**	**On.Dm (min)**	**On.Ar**	**On.Pm**	**HC.Dm (max)**	**Hc.Dm (min)**	**HC.Ar**	**HC.Pm**	**On.Cr**
Sig.									
Between groups	.175	.110	.152	.044	.171	.791	.478	.337	.190

Table 6.45 – Pig juvenile skeleton PJ1 - Results of ANOVA and Tukey post-hoc test on osteon and Haversian canal parameters

As regards the differences between different portions of the same bone, in the **radius**, osteons were smaller in the proximal metaphysis (26423,71±8620,42 μm^2) compared to the diaphysis (33667,22±12834,89 μm^2; Table 6.46).

Similarly, Haversian canals were smaller in the proximal metaphysis (718,10±241,48 μm^2) compared to the diaphysis (1042,97±580,6 μm^2; Table 6.47).

PIG JUVENILE (PJ1) – RADIUS (OSTEON)						
Bone portion		**On.Dm$_{max}$ (µm)**	**On.Dm$_{min}$ (µm)**	**On.Ar (µm^2)**	**On.Pm (µm)**	**On.Cr**
Proximal metaphysis (n=38)	Mean	200,85	162,16	26423,71	592,94	0,92
	St.dev	34,49	32,09	8620,40	97,56	0,03
	Min	121,50	101,82	10689,61	383,14	0,84
	Max	271,75	221,86	41372,51	756,21	0,96
Diaphysis (n=29)	Mean	228,68	183,89	33667,22	664,62	0,93
	St.dev	44,46	41,88	12834,89	128,87	0,02
	Min	142,53	115,26	13202,89	417,58	0,86
	Max	319,27	269,96	61705,71	924,65	0,96
Total (n=67)	Mean	212,90	171,56	29558,96	623,67	0,92
	St.dev	41,21	37,94	11163,43	116,88	0,03
	Min	121,50	101,82	10689,61	383,14	0,84
	Max	319,27	269,96	61705,71	924,65	0,96

Table 6.46 - Radius (PJ1) - descriptive statistics of osteon parameters

PIG JUVENILE (PJ1) – RADIUS (HAVERSIAN CANAL)					
Bone portion		**HC.Dm$_{max}$ (µm)**	**Hc.Dm$_{min}$ (µm)**	**HC.Ar (µm^2)**	**HC.Pm (µm)**
Proximal metaphysis (n=38)	Mean	35,37	23,75	718,10	101,11
	St.dev	7,98	4,58	241,48	17,15
	Min	21,68	13,55	302,41	69,02
	Max	55,09	31,76	1261,27	137,77
Diaphysis (n=29)	Mean	40,51	29,37	1042,97	119,12
	St.dev	11,65	8,90	580,06	30,84
	Min	26,05	14,56	408,57	75,84
	Max	64,39	56,02	2871,21	196,04
Total (n=67)	Mean	37,60	26,18	858,71	108,91
	St.dev	9,99	7,30	449,15	25,48
	Min	21,68	13,55	302,41	69,02
	Max	64,39	56,02	2871,21	196,04

Table 6.47 - Radius (PJ1) - descriptive statistics of Haversian canal parameters

ANOVA test revealed that the size of the osteon was statistically significantly lower in the proximal metaphysis ($p=0.007$, Cohen's $d=0.681$, 95% CI for Cohen's d: 0.184 – 1.177) compared to the diaphysis. In addition, the size of the Haversian canal was

statistically significantly lower in the proximal metaphysis (p=0.003, Cohen's d=0.77, 95% CI for Cohen's d: 0.269 – 1.27) compared to the diaphysis (Table 6.48).

There was no statistically significant difference in osteon circularity between the proximal metaphysis and the diaphysis.

RADIUS – ANOVA test									
	On.Dm (max)	**On.Dm (min)**	**On.Ar**	**On.Pm**	**HC.Dm (max)**	**Hc.Dm (min)**	**HC.Ar**	**HC.Pm**	**On.Cr**
Sig.									
Proximal vs diaphysis	.005	.019	.007	.012	.036	.001	.003	.003	.399

Table 6.48 – Radius (PJ1) - Results of ANOVA on osteon and Haversian canal parameters

In the **ulna**, osteons were bigger in the proximal metaphysis (29920,29±12363,53 μm^2) compared to the diaphysis (21595,44±7110,81 μm^2; Table 6.49).

Similarly, Haversian canals were bigger in the proximal metaphysis (1007,68±518,79 μm^2) compared to the diaphysis (774,24±433,28 μm^2; Table 6.50)

PIG JUVENILE (PJ1) – ULNA (OSTEON)						
Bone portion		**$On.Dm_{max}$ (µm)**	**$On.Dm_{min}$ (µm)**	**On.Ar (μm^2)**	**On.Pm (µm)**	**On.Cr**
Proximal metaphysis (n=28)	Mean	211,80	173,66	29920,29	624,78	0,92
	St.dev	48,57	42,61	12363,53	136,34	0,03
	Min	117,93	102,22	9718,58	368,12	0,80
	Max	288,94	252,18	47942,30	811,50	0,96
Diaphysis (n=26)	Mean	182,95	144,81	21595,44	538,19	0,91
	St.dev	32,34	30,90	7110,81	95,56	0,03
	Min	111,11	73,36	6777,25	306,90	0,83
	Max	245,85	215,14	34293,83	713,33	0,98
Total (n=54)	Mean	197,91	159,77	25912,03	583,09	0,91
	St.dev	43,67	39,83	10924,73	125,24	0,03
	Min	111,11	73,36	6777,25	306,90	0,80
	Max	288,94	252,18	47942,30	811,50	0,98

Table 6.49 - Ulna (PJ1) - descriptive statistics of osteon parameters

PIG JUVENILE (PJ1) – ULNA (HAVERSIAN CANAL)					
Bone portion		**HC.Dm$_{max}$ (μm)**	**Hc.Dm$_{min}$ (μm)**	**HC.Ar (μm^2)**	**HC.Pm (μm)**
Proximal metaphysis (n=28)	Mean	41,90	28,95	1007,68	118,36
	St.dev	13,10	7,49	518,79	30,76
	Min	22,18	14,04	321,40	67,04
	Max	78,92	43,25	2658,89	201,56
Diaphysis (n=26)	Mean	34,78	24,91	774,24	101,01
	St.dev	9,04	6,10	443,28	25,62
	Min	17,89	15,06	224,01	56,93
	Max	63,52	39,09	2260,06	175,41
Total (n=54)	Mean	38,47	27	895,28	110,01
	St.dev	11,78	7,09	493,62	29,47
	Min	17,89	14,04	224,01	56,93
	Max	78,92	43,25	2658,89	201,56

Table 6.50 - Ulna (PJ1) - descriptive statistics of Haversian canal parameters

ANOVA test indicated that the size of the osteon was statistically significantly higher in the proximal metaphysis (p=0.004, Cohen's d=0.818, 95% CI for Cohen's d: 0.262 – 1.373) compared to the diaphysis (Table 6.51). There was no statistically significant difference in the Haversian canal area between the proximal metaphysis and the diaphysis.

ULNA – ANOVA test									
	On.Dm (max)	**On.Dm (min)**	**On.Ar**	**On.Pm**	**HC.Dm (max)**	**Hc.Dm (min)**	**HC.Ar**	**HC.Pm**	**On.Cr**
Sig.									
Proximal vs diaphysis	.014	.007	.004	.010	.025	.035	.082	.029	.531

Table 6.51 – Ulna (PJ1) - Results of ANOVA on osteon and Haversian canal parameters

With regard to the **tibia**, osteons were smaller in the distal metaphysis (18050,06±6158,18 μm^2) compared to the diaphysis (30469,25±11066,06 μm^2).

PIG JUVENILE (PJ1) – TIBIA (OSTEON)						
Bone portion		**On.Dm$_{max}$ (μm)**	**On.Dm$_{min}$ (μm)**	**On.Ar (μm^2)**	**On.Pm (μm)**	**On.Cr**
Proximal metaphysis (n=9)	Mean	184,06	146,72	23864,10	537,18	0,92
	St.dev	63,33	55,30	18845,03	191,22	0,02
	Min	117,56	87,71	8046,79	330,41	0,88
	Max	311,98	263,87	67185,16	934,65	0,97
Diaphysis (n=32)	Mean	218,18	173,21	30469,25	634,01	0,92
	St.dev	46,69	34,10	11066,06	120,63	0,03
	Min	141,24	118,02	13521,38	422,23	0,85
	Max	310,99	269,29	57883,43	891,29	0,98
Distal metaphysis (n=10)	Mean	166,66	132,82	18050,06	492,60	0,91
	St.dev	30,62	24,39	6158,18	86,14	0,02
	Min	139,69	90,12	10947,71	394,16	0,85
	Max	220,85	166,95	29496,63	638,39	0,94
Total (n=51)	Mean	202,05	160,62	26868,50	589,19	0,92
	St.dev	51,35	40,10	12847,07	140,88	0,03
	Min	117,56	87,71	8046,79	330,41	0,85
	Max	311,98	269,29	67185,16	934,65	0,98

Table 6.52 – Tibia (PJ1) - descriptive statistics of osteon parameters

PIG JUVENILE (PJ1) – TIBIA (HAVERSIAN CANAL)					
Bone portion		**HC.Dm$_{max}$ (μm)**	**Hc.Dm$_{min}$ (μm)**	**HC.Ar (μm^2)**	**HC.Pm (μm)**
Proximal metaphysis (n=9)	Mean	36,87	25,33	881,53	110,42
	St.dev	6,95	7,03	404,31	24,76
	Min	28,89	14,23	368,15	78,44
	Max	52,77	36,39	1512,06	150,37
Diaphysis (n=32)	Mean	43,03	28,74	1077,53	123,60
	St.dev	9,84	5,73	390,86	22,59
	Min	29,61	19,36	554,67	85,64
	Max	62,51	44,68	2117,86	171,03
Distal metaphysis (n=10)	Mean	37,61	22,99	750,09	103,69
	St.dev	9,73	4,67	277,33	21,82
	Min	20,09	17,26	292,67	62,81
	Max	51,32	32,58	1214,52	131,87
Total (n=51)	Mean	40,88	27,01	978,74	117,37
	St.dev	9,63	6,15	391,30	23,90
	Min	20,09	14,23	292,67	62,81
	Max	62,51	44,68	2117,86	171,03

Table 6.53 – Tibia (PJ1) - descriptive statistics of Haversian canal parameters

ANOVA revealed that the size of the osteon was statistically significantly lower in the distal metaphysis (p=0.018, Cohen's d=1.211, 95% CI for Cohen's d: 0.427 – 1.996) compared to the diaphysis. There was no statistically significant difference between the proximal and distal metaphysis and between the diaphysis and the proximal metaphysis. No statistically significant difference was observed in the size of Haversian canal between the three groups.

TIBIA – ANOVA and Tukey's post hoc test									
	On.Dm (max)	**On.Dm (min)**	**On.Ar**	**On.Pm**	**HC.Dm (max)**	**Hc.Dm (min)**	**HC.Ar**	**HC.Pm**	**On.Cr**
Sig.									
Between groups	.008	.008	.018	.008	.115	.021	.046	.041	.519
Proximal vs diaphysis	.148	.151	.323	.129	.202	.272	.356	.286	.956
Proximal vs distal metaphysis	.706	.695	.550	.737	.984	.656	.727	.798	.779
Diaphysis vs distal metaphysis	.012	.011	.018	.012	.260	.023	.051	.051	.486

Table 6.54 – Tibia (PJ1) - Results of ANOVA and Tukey post-hoc test on osteon and Haversian canal parameters

In the metacarpal, no statistically significant difference between the shaft and the base was observed in terms of osteon and Haversian canal size.

PIG JUVENILE (PJ1) – METACARPAL (OSTEON)						
Bone portion		**On.Dm$_{max}$ (µm)**	**On.Dm$_{min}$ (µm)**	**On.Ar (µm^2)**	**On.Pm (µm)**	**On.Cr**
Head (n=32)	Mean	174,13	136,67	19113,99	505,47	0,90
	St.dev	37,68	28,08	7132,37	101,40	0,04
	Min	103,26	82,68	6549,83	300,25	0,80
	Max	240	188,50	32038,64	659,14	0,97
Base (n=15)	Mean	182,80	141,69	20752,87	524,15	0,91
	St.dev	37,74	32,57	9359,89	103,38	0,02
	Min	144,38	102,49	12985,22	417,10	0,85
	Max	291,83	225,72	48617,74	812,09	0,94
Total (n=47)	Mean	176,89	138,27	19637,04	511,43	0,91
	St.dev	37,51	29,32	7844,86	101,29	0,03
	Min	103,26	82,68	6549,83	300,25	0,80
	Max	291,83	225,72	48617,74	812,09	0,97

Table 6.55 - Metacarpal (PJ1) - descriptive statistics of osteon parameters

PIG JUVENILE (PJ1) – METACARPAL (HAVERSIAN CANAL)					
Bone portion		**HC.Dm$_{max}$ (µm)**	**Hc.Dm$_{min}$ (µm)**	**HC.Ar (µm^2)**	**HC.Pm (µm)**
Head (n=32)	Mean	33,69	24,34	657,62	96,25
	St.dev	7,86	6,10	244,91	18,32
	Min	18,89	13,22	220,11	56,20
	Max	54	35,37	1141,96	135,60
Base (n=15)	Mean	40,25	24,47	874,19	109,30
	St.dev	14,37	8,33	591,32	33,78
	Min	20,18	13,88	251,28	61,36
	Max	77,38	45,44	2664,73	196
Total (n=47)	Mean	35,79	24,39	726,73	100,42
	St.dev	10,68	6,80	396,55	24,73
	Min	18,89	13,22	220,11	56,20
	Max	77,38	45,44	2664,73	196

Table 6.56 - Metacarpal (PJ1) - descriptive statistics of Haversian canal parameters

METACARPAL – ANOVA test									
	On.Dm (max)	**On.Dm (min)**	**On.Ar**	**On.Pm**	**HC.Dm (max)**	**Hc.Dm (min)**	**HC.Ar**	**HC.Pm**	**On.Cr**
Sig.									
Shaft vs base	.466	.590	.510	.561	.049	.953	.081	.092	.505

Table 6.57 – Metacarpal (PJ1) - Results of ANOVA on osteon and Haversian canal parameters

6.3 INTRA- AND INTER-SPECIES HISTOMORPHOLOGICAL VARIABILITY

After evaluating the intra-individual variability, a total of eighty-four cross-sections, equally divided between human and pig were analyzed. The samples were taken from several individuals in order to test the intra- and inter-species variability of bone tissue (see Chapter 4 for details on the study sample).

6.3.1 ADULT HUMANS

Overall, the differences between the different individuals mainly concerned the organization of the secondary osteons, although remnants of primary lamellar bone were frequently observed. No fibro-lamellar bone nor woven bone were noted in the human specimens.

Humeri were generally characterized by tightly packed secondary osteons, although, areas of scattered secondary osteons were observed at the posterior aspect. In particular, the individual HA3 (73 years) exhibited a large area of lamellar tissue with scattered

secondary osteons at the posteromedial aspect (Fig. 6.36). Drifting osteons were observed in all the individuals.

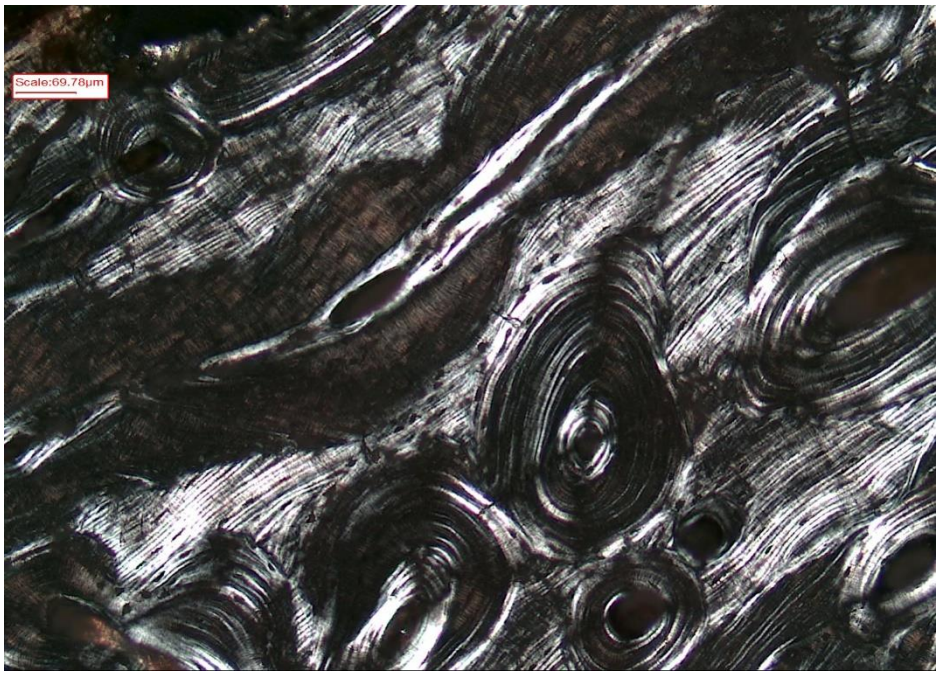

Figure 6.36 – HA3 – Scattered secondary osteons in abundant lamellar matrix at the posteromedial aspect of the humerus, x100. Polarized light

Radii exhibited tightly packed secondary osteons at the medial and lateral aspects, whereas at the anterior and posterior aspects osteons were more scattered at the periosteal surface, with an increasing density proceeding towards the endosteum. Individual HA1 showed thicker layers of inner and outer circumferential lamellae (Fig. 34-35) compared to the other individuals.

Ulnae were mainly characterized by irregular Haversian bone (scattered osteons), especially at the anterior and medial aspects. The posterior and lateral aspects exhibited a higher osteon density, especially at the periosteal surface. Few drifting osteons were observed in all the individuals, except for the individual HA5 (84 years).

Femora consisted almost entirely of tightly packed secondary osteons, except for the individual HA14 (39-57) which exhibited large areas of lamellar tissue with scattered secondary osteons, especially at the anterior and posterior aspects (Fig. 6.37).

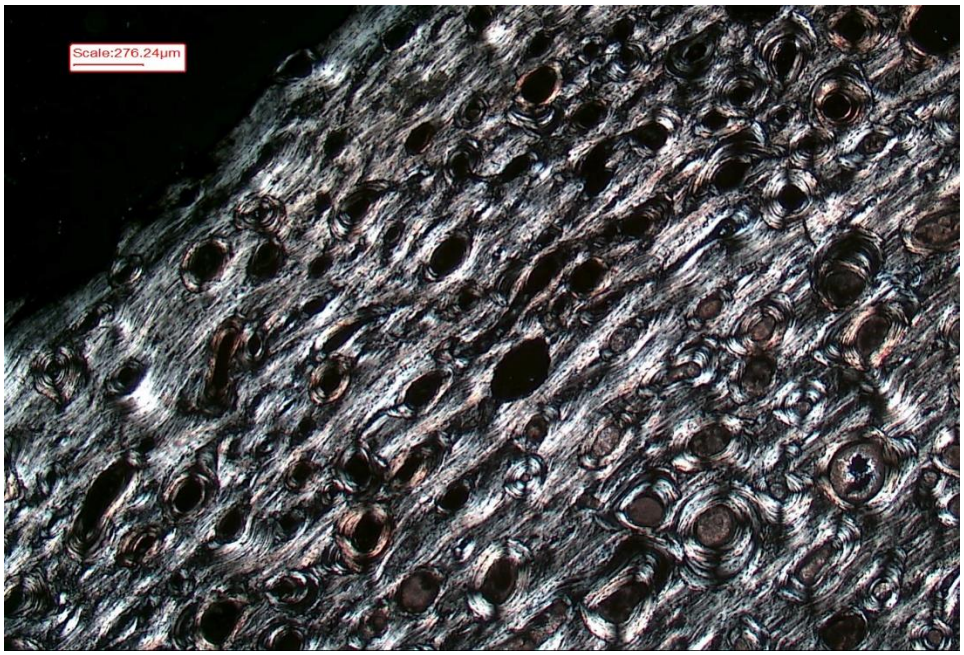

Figure 6.37 – HA14 – Scattered secondary osteons in abundant lamellar matrix at the anterior aspect of the femur, x25. Polarized light

Tibiae were generally characterized by tightly packed secondary osteons at the anterior, posterior and medial aspects, and more scattered osteons at the lateral aspect (especially at the periosteal surface). Individuals HA12 and HA13, exhibited more scattered secondary osteons immersed in abundant lamellar matrix, especially at the medial and lateral aspects. In addition, they showed a higher number of drifting osteons compared to the other individuals.

Metatarsals exhibited mainly scattered secondary osteons in abundant lamellar matrix, except for the plantar aspect which consisted of tightly packed secondary osteons. Individuals HA1 and HA7 showed a higher osteon density compared to the other

individuals, especially at the plantar, dorsal and medial aspects. Drifting osteons were observed exclusively in individuals HA2 and HA6.

Ribs exhibited a prevalence of scattered secondary osteons in abundant lamellar matrix in most of the individuals, although individuals HA1 and HA8 showed mainly tightly packed secondary osteons.

6.3.2 JUVENILE PIGS

Humeri were characterized mainly by fibro-lamellar bone, although moderate to high remodeling was observed especially at the medial and lateral aspects. Generally, secondary osteons were observed at the endosteal surface, though in PJ5, evidence of remodeling were noted also at the middle cortex. PJ1 and PJ2 exhibited a lower rate of remodeling compared to the other individuals.

Radii showed moderate to high remodeling, especially at the caudal aspect, though areas of scattered secondary osteons were observed also in the cranial, medial and lateral aspects. The periosteal surface generally consisted of fibro-lamellar bone, whereas remodeling mainly regarded the endosteal surface, though PJ1, PJ2 and PJ3 exhibited secondary osteons also in the middle cortex.

Ulnae were characterized by fibro-lamellar bone although moderate to high remodeling was observed in all the individuals, especially at the cranial, medial and lateral aspects. In PJ2, PJ3 and PJ5, at the cranial aspect, the entire cortex was characterized by tightly packed secondary osteons (Fig. 6.38). The medial aspect was often characterized by a reticular pattern of vascular canals which was not observed in the human specimens (Fig.

6.39), except for the petrous bone in the individual HA1 (see paragraph 5.1). Finally, a single drifting osteon was observed in PJ3 (Fig. 6.40).

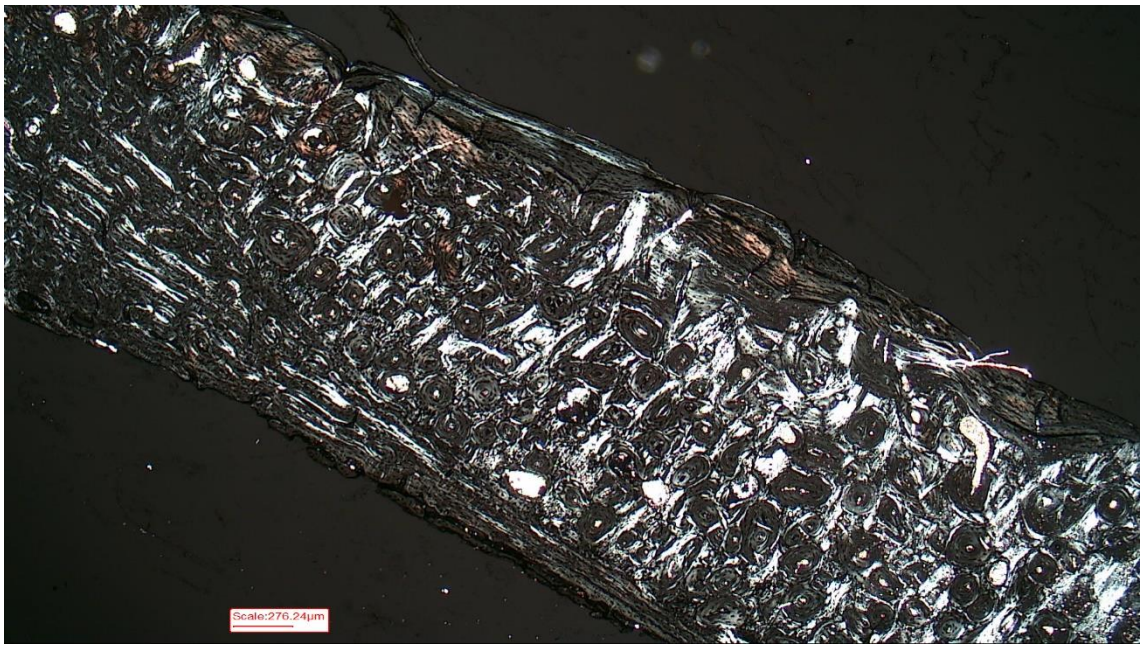

Figure 6.38 – PJ2 – Extensive remodeling through the entire cortex at the craniolateral aspect of the ulna, x25. Polarized light

Figure 6.39 – PJ6 – Reticular pattern at the medial aspect of the ulna, x25

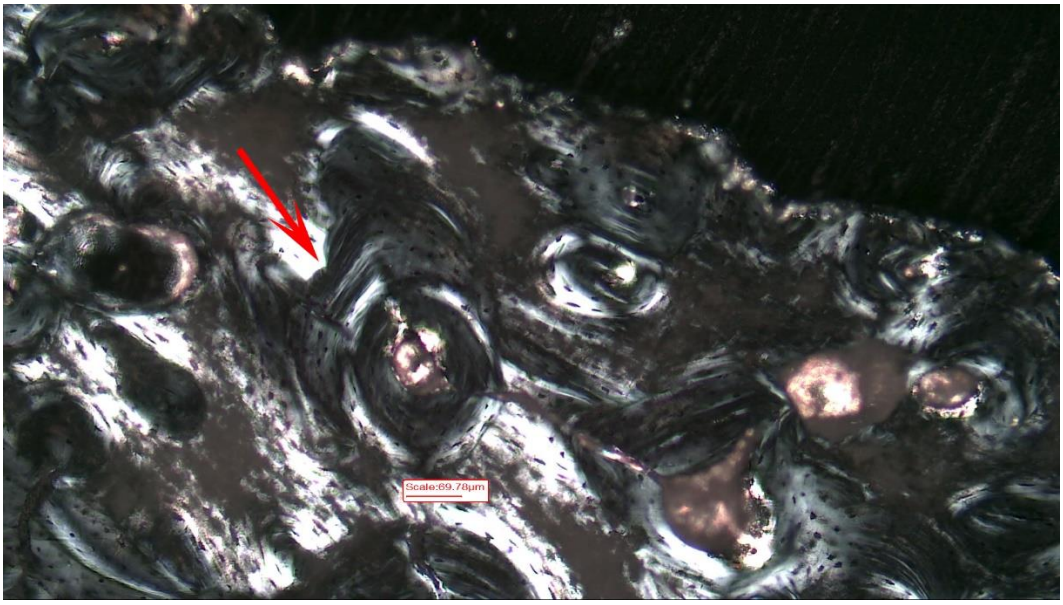

Figure 6.40 – PJ3 - Drifting osteon at the anterior aspect of the ulna, x100. Polarized light

Femora showed a prevalence of fibro-lamellar bone, especially at the periosteal and at the middle cortex. Low to moderate remodeling was observed at the endosteal surface, especially at the cranial and lateral aspects.

At the caudal aspect, close to the periosteum, an area characterized by radially oriented fibro-lamellar bone was observed in all the individuals, except for PJ1.

Tibiae mainly consisted of fibro-lamellar bone although moderate to high remodeling was observed close to the endosteum, especially at the cranial aspect. In PJ2, PJ4 and PJ5 aspect, the remodeling process involved also the middle cortex.

PJ5 exhibited the highest rate of remodeling which was noted in the entire section and consisted generally of scattered secondary osteons. At the posterior aspect, close to the endosteum, a multi-branching vascular network was observed (Fig. 6.41).

Finally, PJ3 exhibited multiple rows of primary osteons (osteon banding) at the middle cortex (Fig. 6.42).

Figure 6.41 – PJ5 – Multi-branching vascular network at the posterior aspect of the tibia, x100

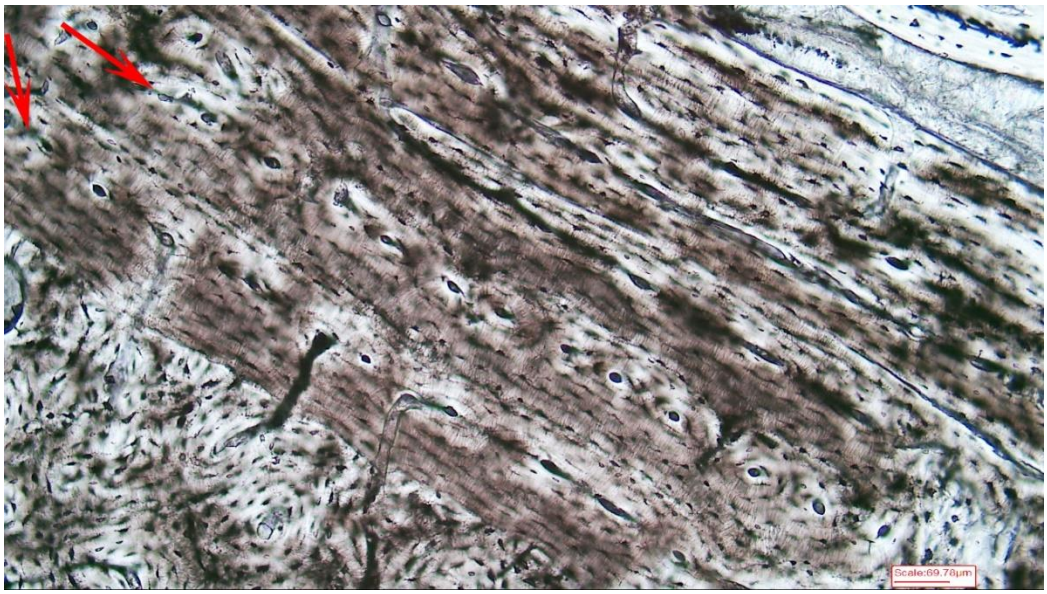

Figure 6.42 – PJ3 – Multiple rows of primary osteons (osteon banding) at the middle cortex of the tibia, x100

Metatarsals were characterized by either fibro-lamellar or a woven scaffolding (often radially oriented) at the periosteal surface, whereas the middle cortex and endosteal surface experienced moderate to high rate of remodeling in the entire cross-sections.

Ribs consisted entirely of fibro-lamellar bone at the caudal aspect, whereas the rest of the section exhibited moderate to high remodeling, especially at the endosteal surface. PJ2, PJ5 and PJ6 showed the presence of secondary osteons also in the middle cortex. Finally, PJ5, exhibited multiple rows of primary osteons at the dorsal aspect.

6.3.3 HUMAN FOETUS VS PIG NEWBORN

Overall, both the human foetus and pig newborn were characterized by an immature bone tissue without any sign of remodeling (Table 6.58).

However, pig bones were characterized by early stages of fibro-lamellar formation, whereas human bones were entirely characterized by a more immature woven scaffolding with the initial formation of few primary osteons (Fig. 6.43)

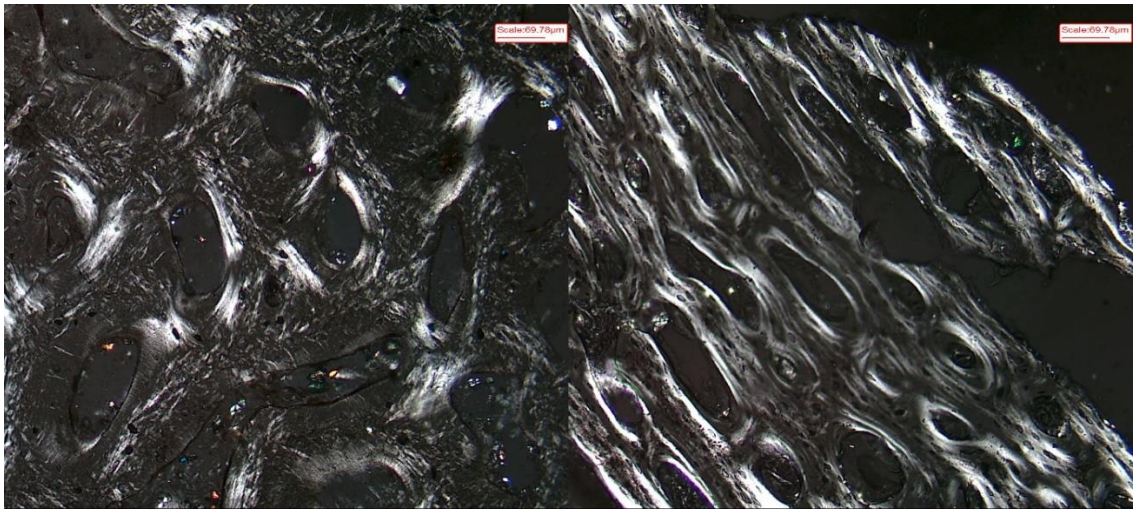

Figure 6.43 – Woven scaffolding in the human foetus (left) and early stages of fibro-lamellar formation in the pig newborn (right), x100. Polarized light

	HUMAN FOETUS (HF)	PIG NEWBORN (PN1, PN2)
	Tissue type	**Tissue type**
Humerus	Woven scaffolding with few primary osteons and radial vascular canals	Woven scaffolding at the periosteal surface; fibro-lamellar at the middle cortex
Radius	Woven scaffolding with few primary osteons	Woven scaffolding at the periosteal surface; fibro-lamellar at the middle cortex
Ulna	Woven scaffolding with few primary osteons	Radially oriented woven scaffolding at the periosteal surface; initial formation of fibro-lamellar bone at the middle cortex
Femur	Woven scaffolding with few primary osteons; several vascular canals	Fibro-lamellar with several primary osteons
Tibia	Woven scaffolding with initial formation of primary osteons	Initial formation of fibro-lamellar bone
Metatarsal	Radially oriented woven scaffolding	Radially oriented woven scaffolding at the periosteal surface; initial formation of fibro-lamellar bone at the middle cortex
Rib	Woven scaffolding with initial formation of primary osteons	Woven scaffolding with numerous primary osteons

Table 6.58 – Results of the histomorphological analysis on the human foetus (HF) and pig newborns (PN1, PN2)

Unlike all the other human bones, metatarsal exhibited a radially oriented woven scaffolding (Fig. 6.44). Similarly, humerus showed several radial vascular canals originating from both the periosteal and endosteal surface (Fig. 6.45).

Figure 6.44 – Human foetus – Radially oriented woven scaffolding in the metatarsal, x25

Figure 6.45 – Human foetus – Radial vascular canals in the humerus, x100

With regard to pig newborn, all the cross-section exhibited the initial formation of a fibro-lamellar bone, except for the rib which was characterized by a high number of primary osteons immersed in a woven matrix (Fig. 6.46).

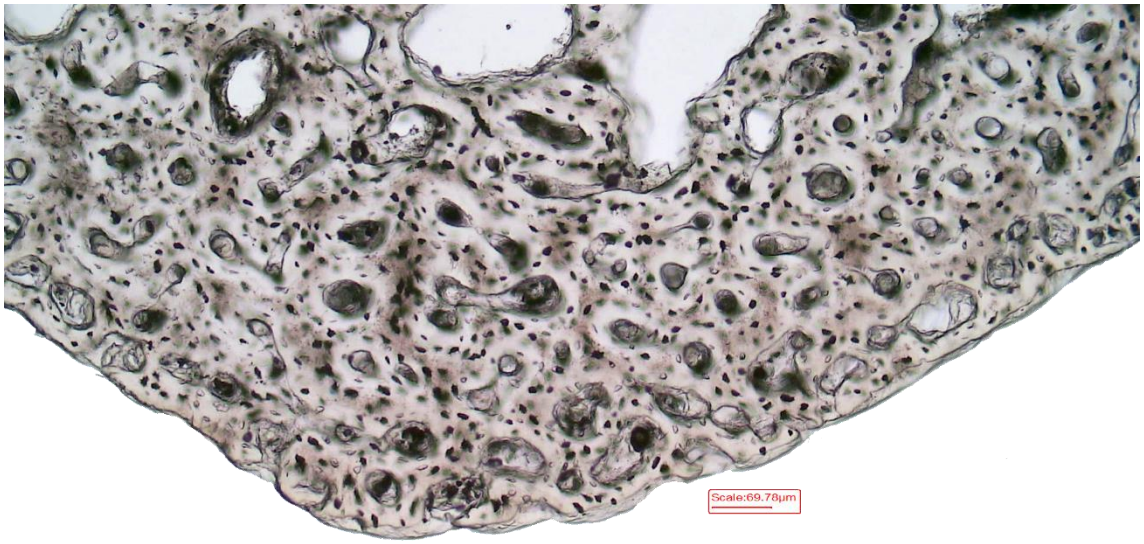

Figure 6.46 – Pig newborn (rib) – Numerous primary osteons immersed in a woven matrix, x100

CONCLUDING REMARKS

Overall, with regard to adult human and juvenile pig, the intra-species variability in bone microarchitecture seemed to concern mainly the extent of remodeling which take place in the different aspects of each bone and the arrangement of secondary osteons.

Adult human bones were generally characterized by Haversian bone in the entire cross-sections, although remnants of primary lamellar bone were frequently observed. No fibro-lamellar bone nor woven bone were noted in the human specimens.

On the contrary, these types of tissues represented the main component of pig microarchitecture, although most of the pig samples exhibited areas of remodeling which resembled those of human bone.

Generally, the periosteal surface differs significantly bewteen the two species given the presence of fibro-lamellar or woven bone in pigs and circumferential lamellar bone or

Haversian bone in humans. Nonetheless, especially radius, ulna, tibia and metatarsal were the bones which showed the highest rate of remodeling in pigs, which often involved also the middle cortex. In such areas, the differences between the two species are less marked and distinguishing between human and pig may not be straightforward. However, pig bone exhibited some peculiarities which were not observed in any of the human specimens.

Several sections showed “anomalous” Haversian systems characterized by two or more longitudinal vascular canals within the walls of the osteon (Fig. 6.47). These particular structures have never been observed in human samples. Moreover, in some pig bones, such as the tibia and the rib, multiple linear arrangement of more than ten primary osteons have been noted. Finally, a reticular pattern of vascular canals was frequently found in pig bone, whereas it was absent in human bone.

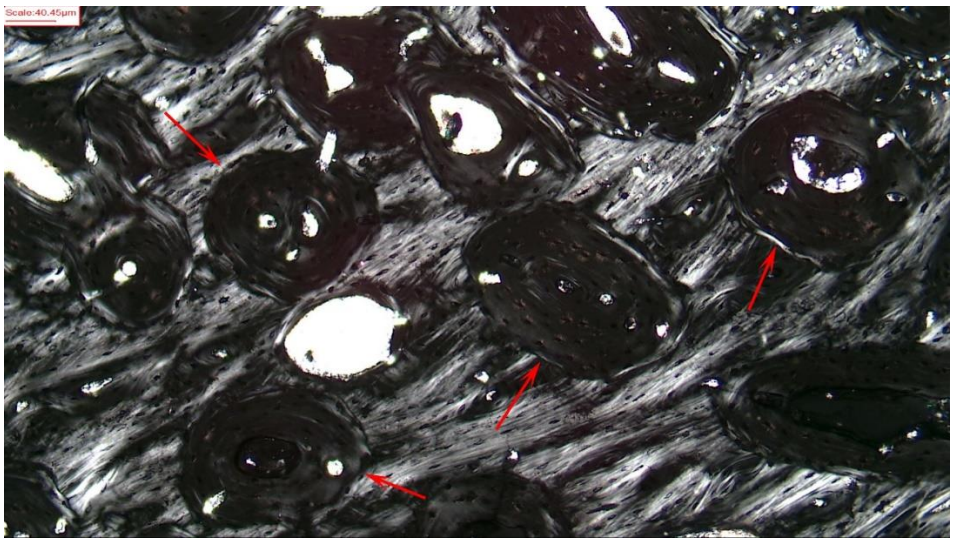

Figure 6.47 – PJ2 – Anomalous secondary osteons at the middle cortex of the ulna, x100. Polarized light

As regard human foetus and pig newborn, the main differences between the two consisted in the type of bone tissue rather than in the rate of remodeling, since the latter was absent in all the cross-sections.

Human bone was characterized by an immature tissue consisting of a woven scaffolding with the initial formation of primary osteons, whereas pig bone exhibited an early stage of fibro-lamellar formation although, especially at the periosteal surface, remnants of a more immature woven scaffolding was observed in most of the cross-sections.

6.4 INTRA-SPECIES HISTOMORPHOMETRIC VARIABILITY

This section provides the result of the histomorphometric analysis of osteon and Haversian canal parameters. ANOVA and Tukey post-hoc test were employed in order to verify whether there are significant quantitative differences between the same bones in different individuals.

6.4.1 ADULT HUMANS

In **humeri**, osteons were generally bigger in HA2 compared to HA1, HA7 and HA13, with a mean area respectively of 44131,93(±12126,76) μm^2, 31538,02(±13887,72) μm^2, 30481,16(±7552,74) μm^2, and 31171,11(±10745,72) μm^2.

The size of the Haversian canals was bigger in HA1 and HA2 compared to HA6 and HA13 with a mean area respectively of 2063,91(±958,44) μm^2, 1939,9(±750,08) μm^2, 1197,6(±545,53) μm^2, and 1322,04(±760,64) μm^2.

ANOVA and Tukey post-hoc test (Fig. 6.48) revealed that the size of the osteon was statistically significantly higher in the individual HA2 compared to individuals HA1 and HA13($p<0.01$), whereas Haversian canal size was statistically significantly lower in HA6 and HA13 compared to HA1 and HA2 ($p<0.01$).

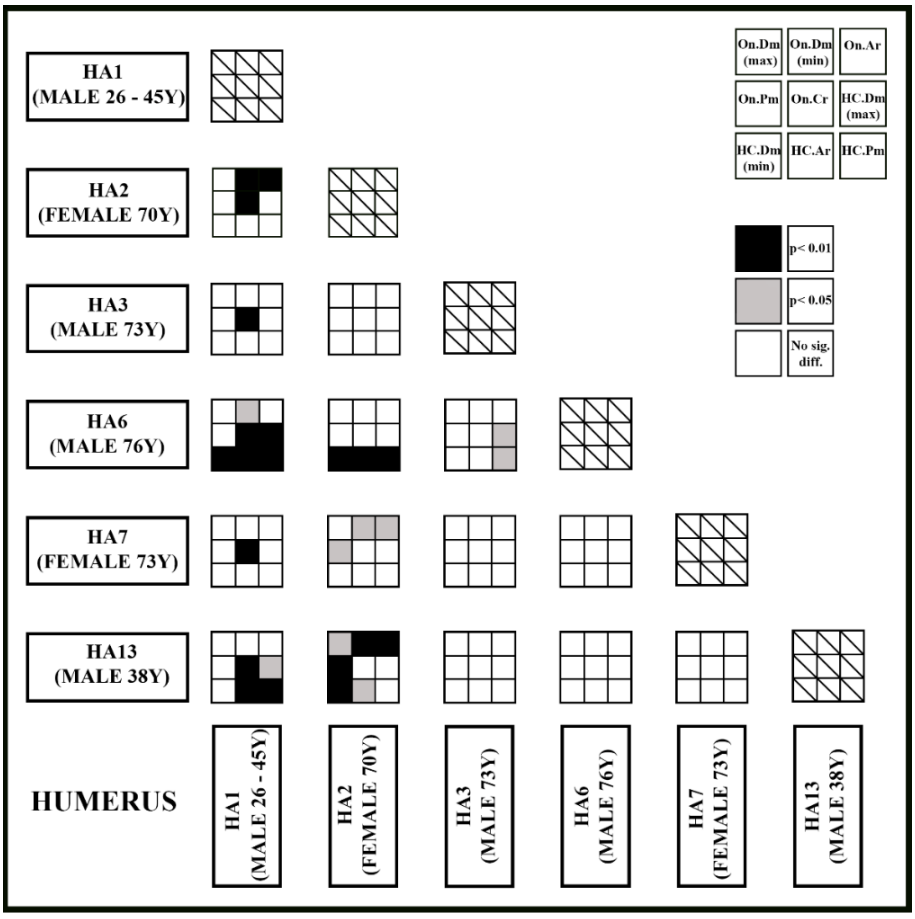

Figure 6.48 – Humerus (human) – results of Tukey post-hoc test on osteon and Haversian canal parameters in different individuals

In **radii**, osteon size resulted similar between the six individuals, with a mean area of 36021,84(±14196,65) μm^2, whereas Haversian canals were generally smaller in HA1 and HA7 compared to HA3, HA4 and HA13, with a mean area respectively of 1088,72(±436,73) μm^2, 1268,94(±648,6) μm^2, 2092,2(±873,11) μm^2, 1902(±687,72)

μm^2 and 1738,85(±896,56) μm^2. Moreover, the mean value of osteon circularity in HA1 (0,90±0,04) was considerably lower compared to the other individuals, in which it ranged between 0,94 and 0,96(±0,02).

ANOVA and Tukey post-hoc test (Fig. 6.49) revealed that the size of the Haversian canals was statistically significantly lower in HA1 compared to HA3, HA4 and HA13 ($p<0.01$). Similarly, Haversian canals were statistically significantly smaller in HA7 compared to HA4 ($p<0.01$) and HA3 ($p<0.05$).

In addition, osteon circularity was statistically significantly lower in HA1 compared to all the other individuals ($p<0.01$).

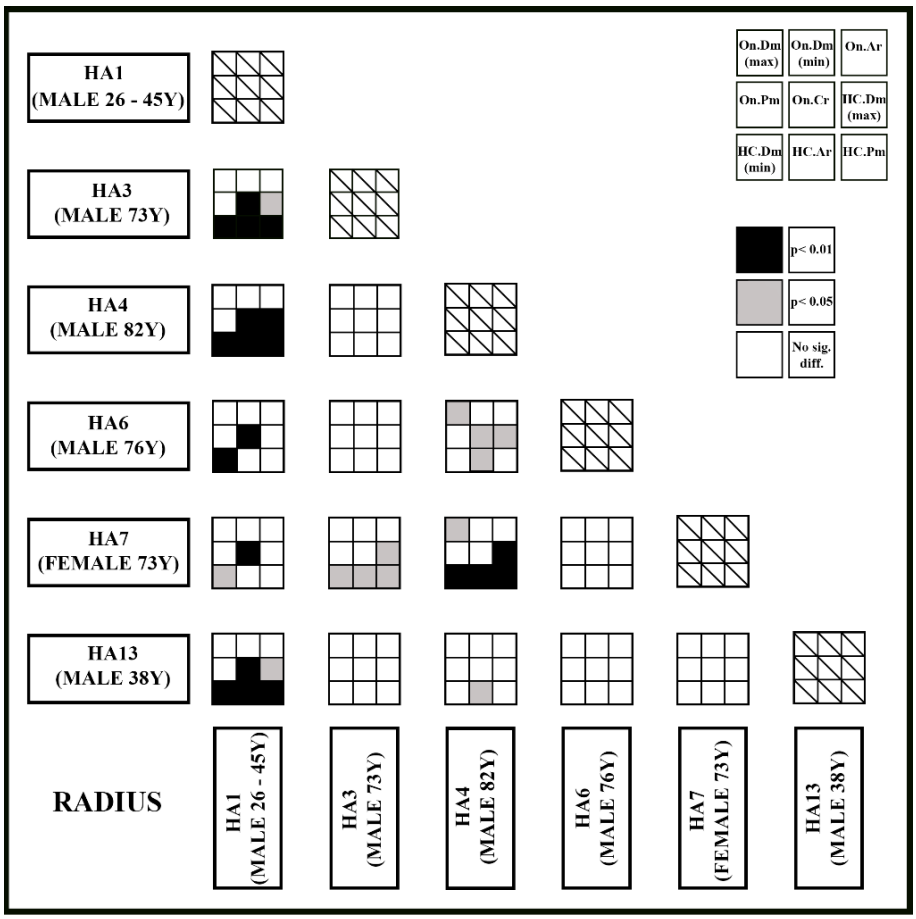

Figure 6.49 - Radius (human) – results of Tukey post-hoc test on osteon and Haversian canal parameters in different individuals

Ulnae showed a general uniformity in terms of osteon and Haversian canal size, with a mean value respectively of 34027,8(±13789,54) μm^2 and 1748,99(±775,61) μm^2. However, Haversian canal were bigger in HA4 (2135,8±693,7 μm^2) compared to HA5 (1422,18±557,54 μm^2) and HA6 (1554,3±601,68 μm^2).

ANOVA and Tukey post-hoc test (Fig. 6.50) confirmed that the size of the Haversian canals was statistically significantly bigger in HA4 compared to HA5 ($p<0.01$) and HA6 ($p<0.05$). In addition, osteons were less circular in HA1 compared to all the other individuals ($p<0.01$).

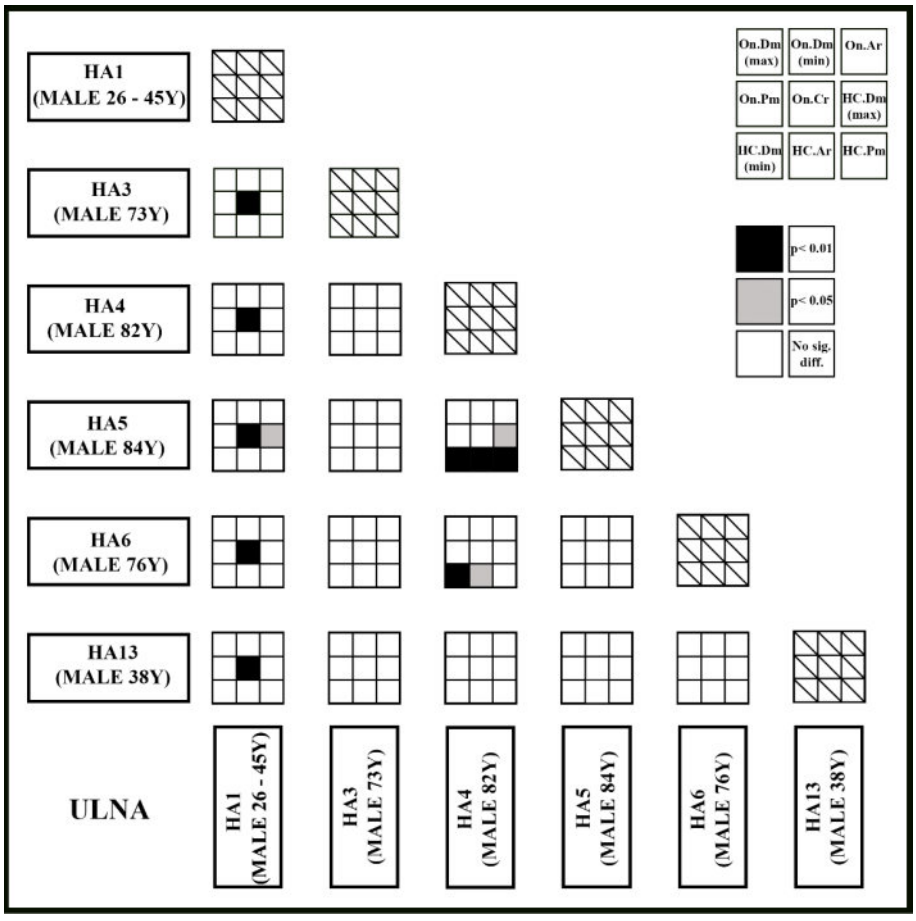

Figure 6.50 - Ulna (human) – results of Tukey post-hoc test on osteon and Haversian canal parameters in different individuals

Femora showed a high variability in terms of osteon and Haversian canal size between the different individuals. The mean value of the osteon area ranged from 25521,31(±10883,85) μm^2 in HA1 to 52493,21(±16778,71) μm^2 in HA14.

The size of Haversian canals ranged from 1463,03(±568) μm^2 in HA18 to 2280,93(±908,62) μm^2 in HA14.

ANOVA and Tukey post-hoc test (Fig. 6.51) revealed that the size of osteons was statistically significantly smaller in HA1 compared to all the other individuals except for HA16, whereas in HA14 and HA15 osteons were statistically significantly bigger compared to the other individuals ($p<0.01$).

On the contrary, Haversian canals were characterized by a lower intra-species variability except for the individual HA14 in which the mean value of the Haversian canal area was statistically significantly higher compared to all the other individuals (2280,93±908,62 μm^2).

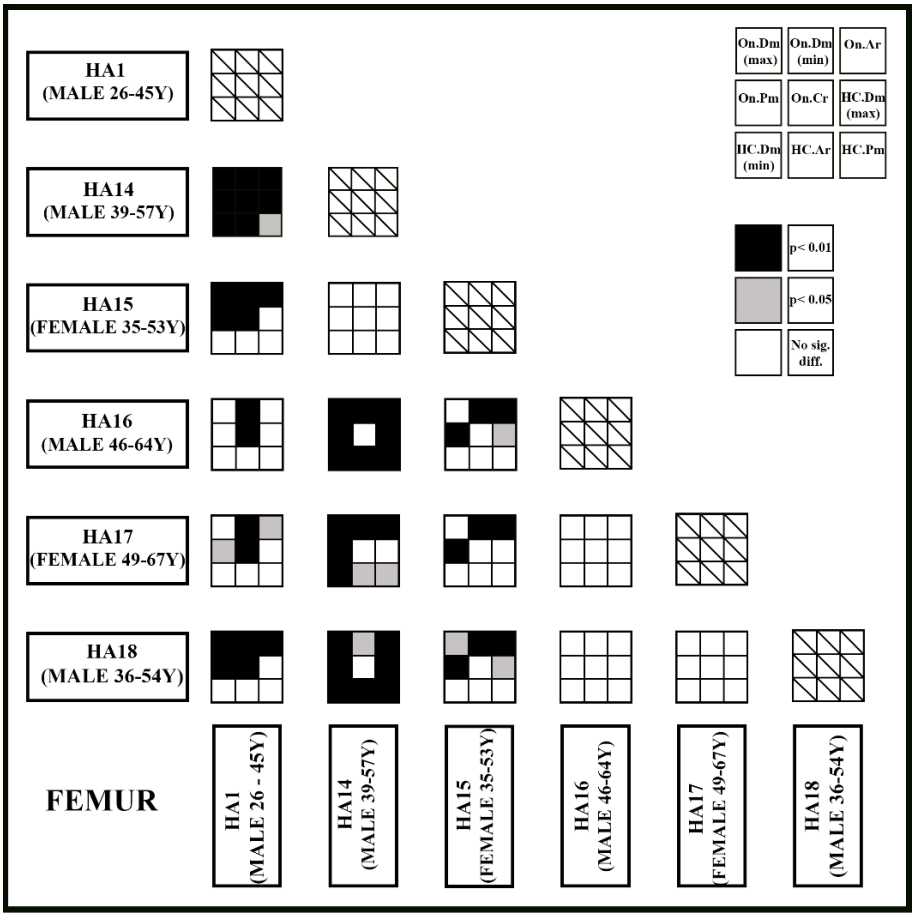

Figure 6.51 - Femur (human) – results of Tukey post-hoc test on osteon and Haversian canal parameters in different individuals

In **tibiae**, the area of the osteon ranged from 29574,32(±15616,75) μm^2 in HA1 to 45422,64(±14180,92) μm^2 in HA2, whereas the area of Haversian canal ranged from 1442,63(±805,15) μm^2 in HA7 to 2040,14(±1011,22) μm^2.

ANOVA and Tukey post-hoc test (Fig. 6.52) revealed that the size of osteons was statistically significantly smaller in HA1 compared to HA2, HA3 and HA13 ($p<0.01$), whereas in HA2 it was statistically significantly bigger compared to HA7 ($p<0.05$) and HA6 ($p<0.01$). There was also a statistically significant difference in osteon circularity between HA1 (0,92±0,02) and all the other individuals ($p<0.01$).

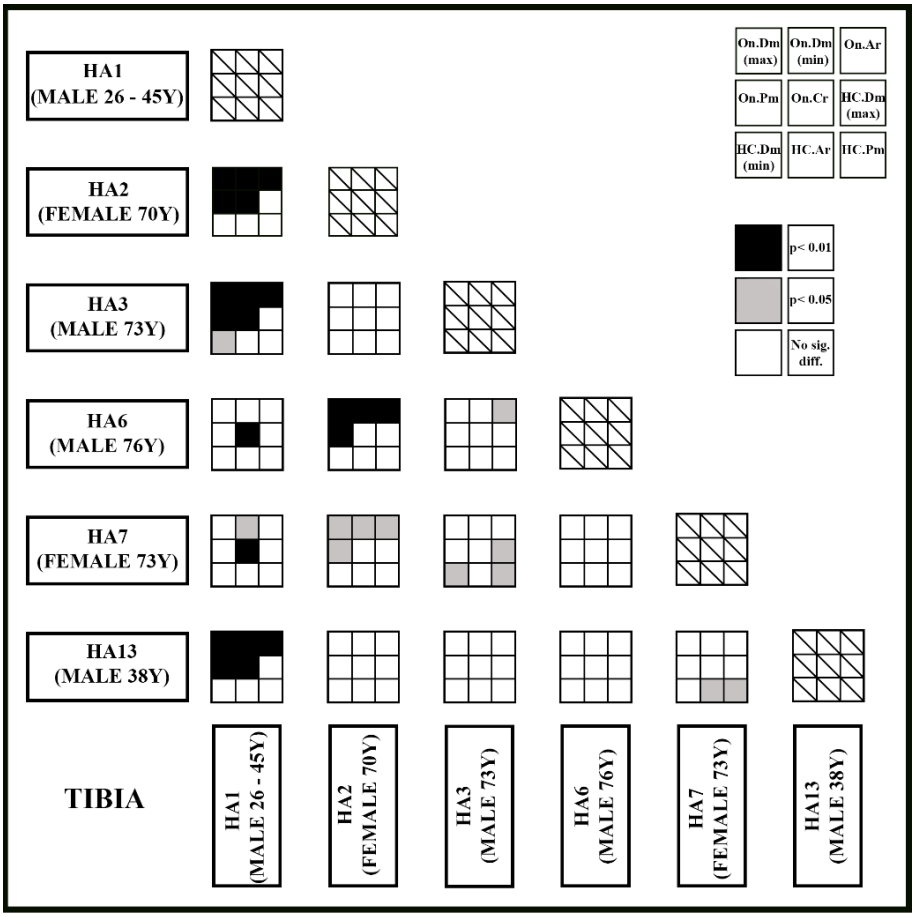

Figure 6.52 - Tibia (human) – results of Tukey post-hoc test on osteon and Haversian canal parameters in different individuals

Metatarsals showed a general uniformity in terms of osteon and Haversian canal size, with a mean value respectively of 27146,28 (±13696,98) μm^2 and 1618,57 (±759,69) μm^2. However, there was a statistically significant difference in osteon size between HA13 (38126,5±21884,48 μm^2) and the other individuals (Fig. 6.53). In addition, osteon circularity in HA1 was statistically significantly lower compared to all the other individuals ($p<0.01$).

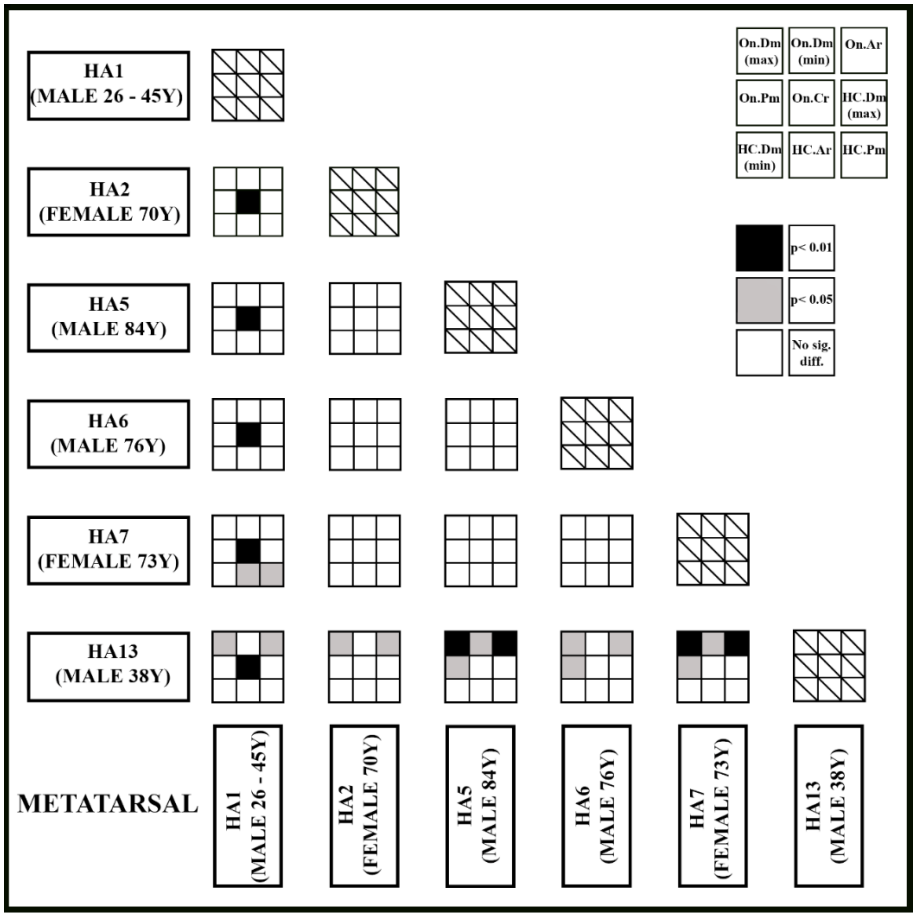

Figure 6.53 - Metatarsal (human) – results of Tukey post-hoc test on osteon and Haversian canal parameters in different individuals

Ribs showed a general uniformity in terms of osteon and Haversian canal size, with a mean value respectively of 24597,93 (±13080,86) μm^2 and 1163,28 (±694,36) μm^2. However, there was a statistically significant difference in osteon size between HA1 (20279,75±11030,5 μm^2) and HA8 (33366,27±17808,65; $p<0.05$). In addition, osteon circularity in HA1 (0,91±0,03) was statistically significantly lower compared to HA10, HA11 and HA12 ($p<0.01$).

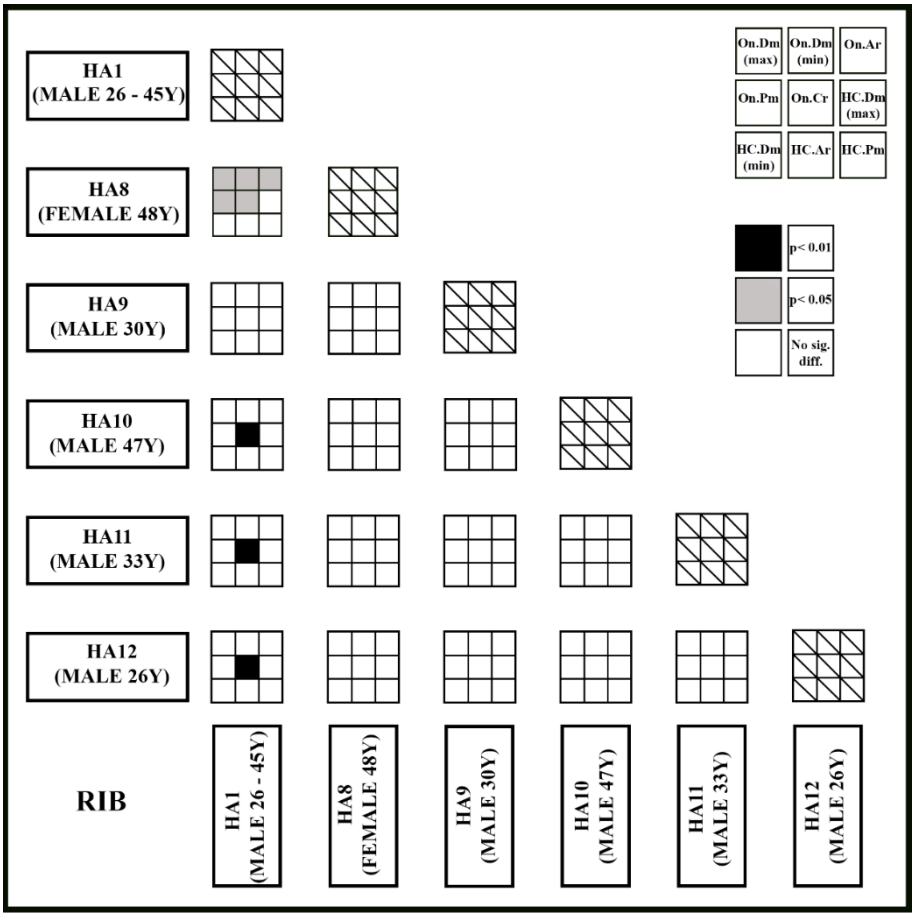

Figure 6.54 - Rib (human) – results of Tukey post-hoc test on osteon and Haversian canal parameters in different individuals

6.4.2 JUVENILE PIGS

Humeri showed a general uniformity in terms of osteon and Haversian canal size, with a mean value respectively of 21285,58 (±8606,82) μm^2 and 696,36 (±428,18) μm^2.

However in PJ1, Haversian canals were statistically significantly bigger compared to PJ3 and PJ6 ($p<0.05$).

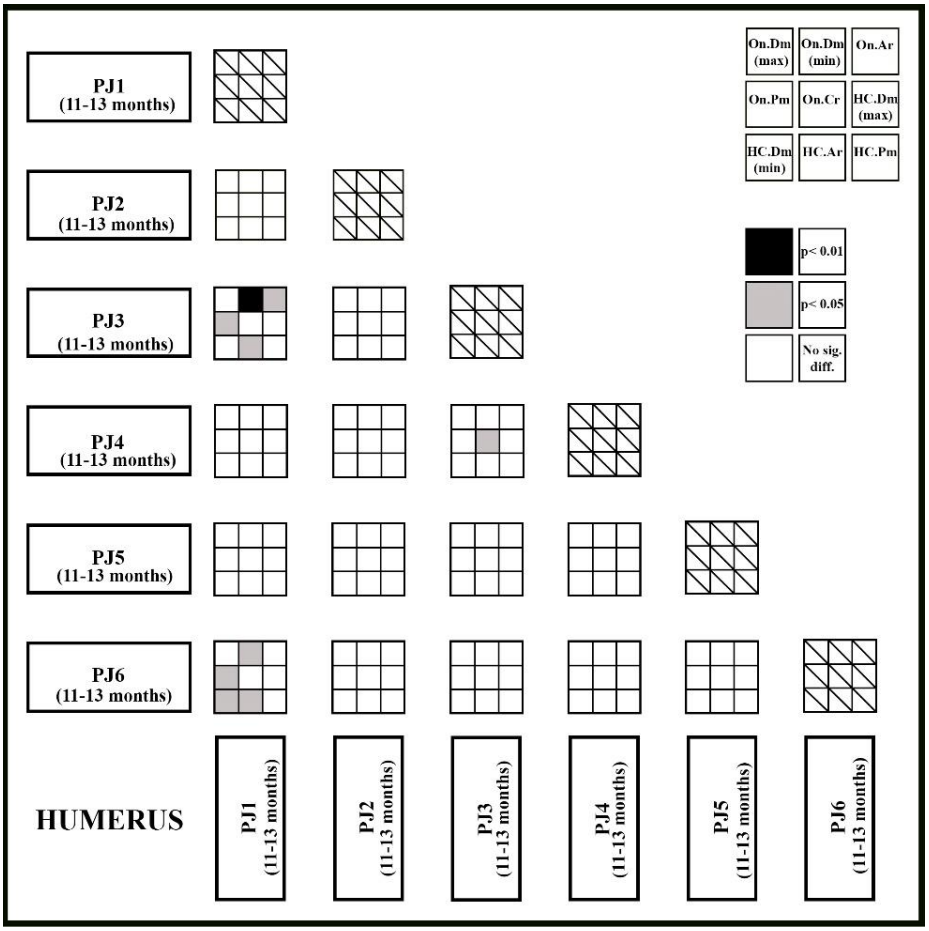

Figure 6.55 - Humerus (pig) – results of Tukey post-hoc test on osteon and Haversian canal parameters in different individuals

In **radii**, the area of the osteon ranged from 21415,04(±6274,16) μm^2 in PJ4 to 33667,22(±12834,88) μm^2 in PJ1, whereas the area of Haversian canal ranged from 659,75(±341,09) μm^2 in PJ5 to 2244,31(±747,81) μm^2.

ANOVA and Tukey post-hoc test (Fig. 6.56) revealed that the size the Haversian canal was statistically significantly bigger in PJ6 (2244,31±747,81 μm^2) compared to all the other individuals ($p<0.01$). Moreover, osteon area in PJ1 was statistically significantly higher (33667,22±12834,88 μm^2) compared to PJ4 and PJ5 ($p<0.01$).

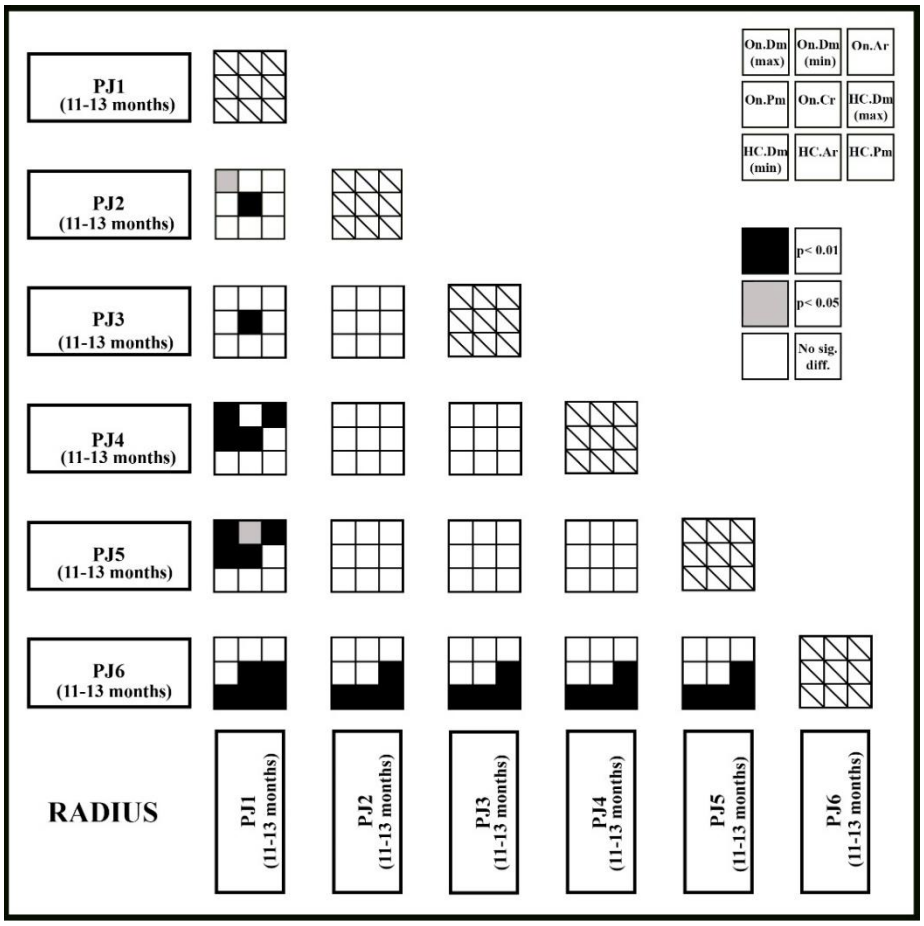

Figure 6.56 - Radius (pig) – results of Tukey post-hoc test on osteon and Haversian canal parameters in different individuals

Ulnae showed a high variability in terms of osteon and Haversian canal size between the different individuals. The mean value of the osteon area ranged from 18160,85(±6933) μm^2 in PJ5 to 27743,24(±8103,03) μm^2 in PJ2.

The size of Haversian canals ranged from 774,24(±443,28) μm^2 in PJ1 to 1793,18(±1513,04) μm^2 in PJ4.

ANOVA and Tukey post-hoc test (Fig. 6.57) revealed that the size of osteons was statistically significantly higher in PJ2 (27743,24±8103,03 μm^2) compared to PJ1, PJ3 and PJ5, whereas in PJ4 Haversian canals were statistically significantly bigger (1782,18±1513,04 μm^2) compared to all the individuals, except for PJ6.

Finally, osteon circularity was lower in PJ1 (0,91±0,03) compared to the other individuals ($p<0.01$).

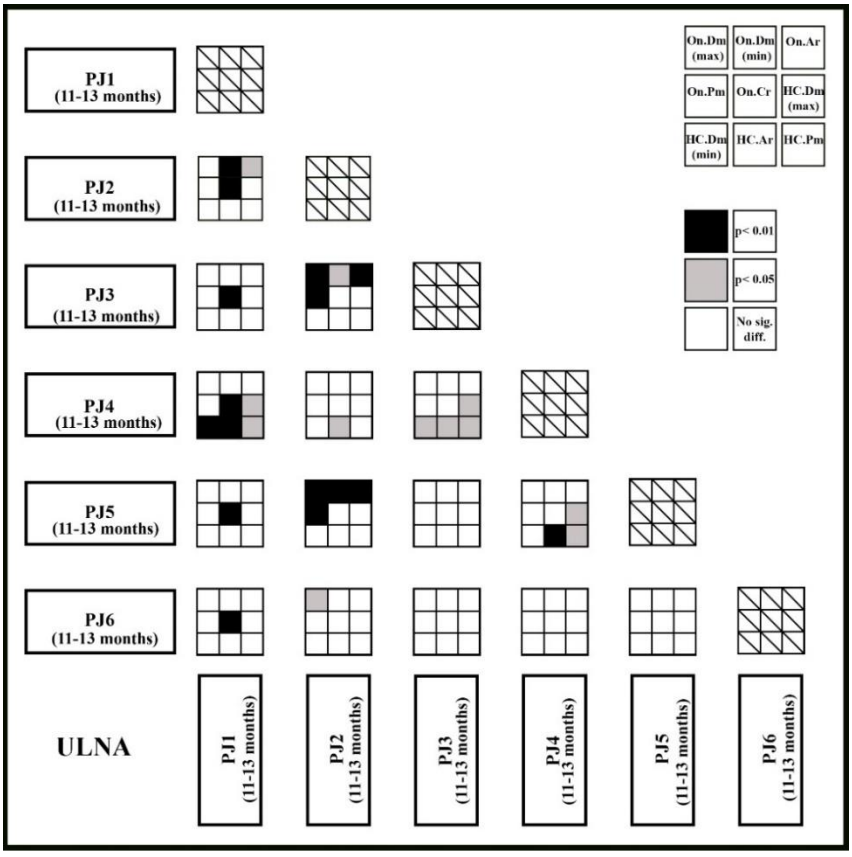

Figure 6.57 – Ulna (pig) – results of Tukey post-hoc test on osteon and Haversian canal parameters in different individuals

Femora showed a general uniformity in terms of osteon and Haversian canal size, with a mean value respectively of 19689,23(±8110,47) μm^2 and 639,82(±623,49) μm^2. However in PJ1, osteons were statistically significantly bigger (34840,8±10336,5 μm2) compared to all the other individuals ($p<0.01$; Fig. 6.58).

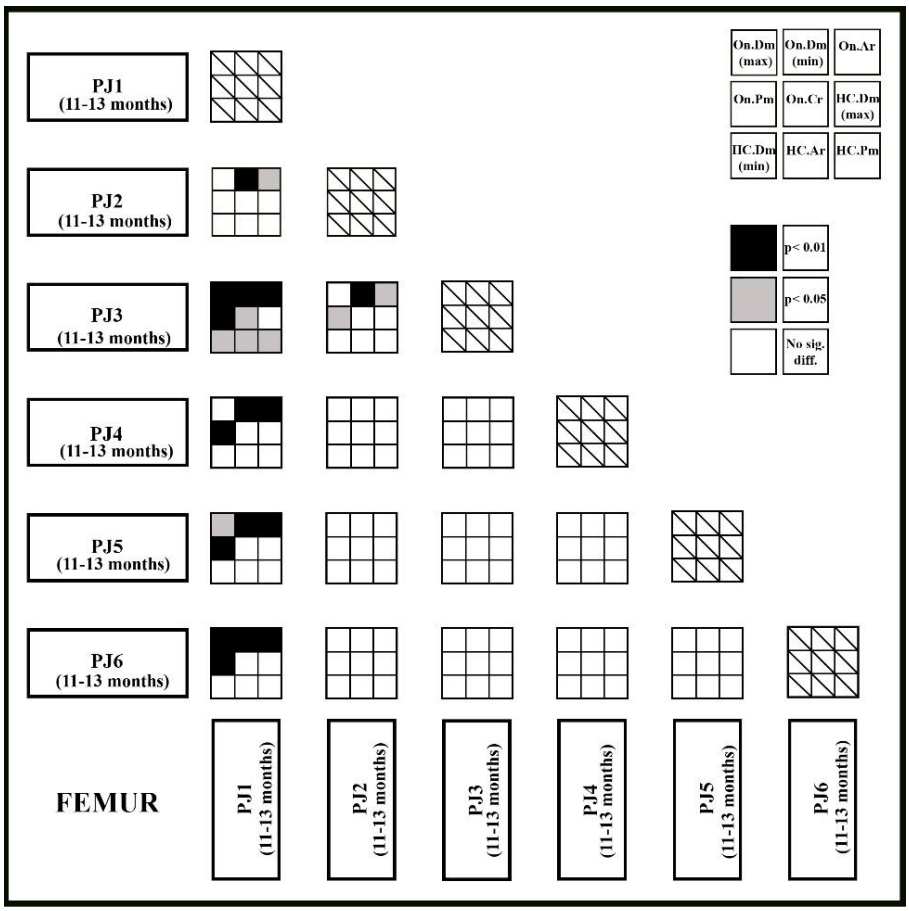

Figure 6.58 – Femur (pig) – results of Tukey post-hoc test on osteon and Haversian canal parameters in different individuals

Like femora, **tibiae** showed a low variability in terms of osteon and Haversian canal size, with a mean value respectively of 20814,85(±8735,55) μm^2 and 752,46(±423,11) μm^2. However in PJ1, both the osteon and the Haversian canal were statistically significantly bigger compared to all the other individuals ($p<0.01$; Fig. 6.59).

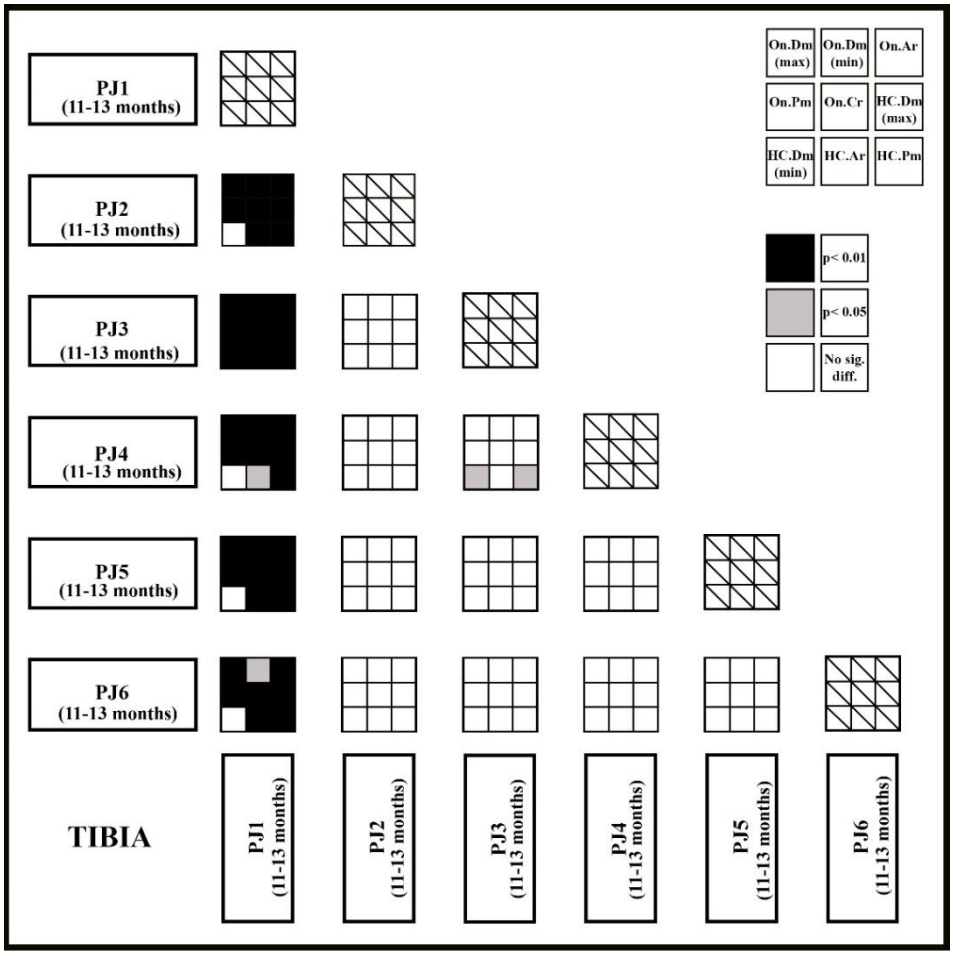

Figure 6.59 – Tibia (pig) – results of Tukey post-hoc test on osteon and Haversian canal parameters in different individuals

Metatarsals were characterized by a general uniformity in terms of osteon and Haversian canal size, with a mean value respectively of 18183,87(±6915,57) μm^2 and 679,48(±383,17) μm^2.

The only exception regarded PJ1 in which both the osteon and the Haversian canal was generally bigger compared to the other individuals (Fig. 6.60). On the contrary, osteon circularity was lower in PJ1 compared to the other individuals ($p<0.01$).

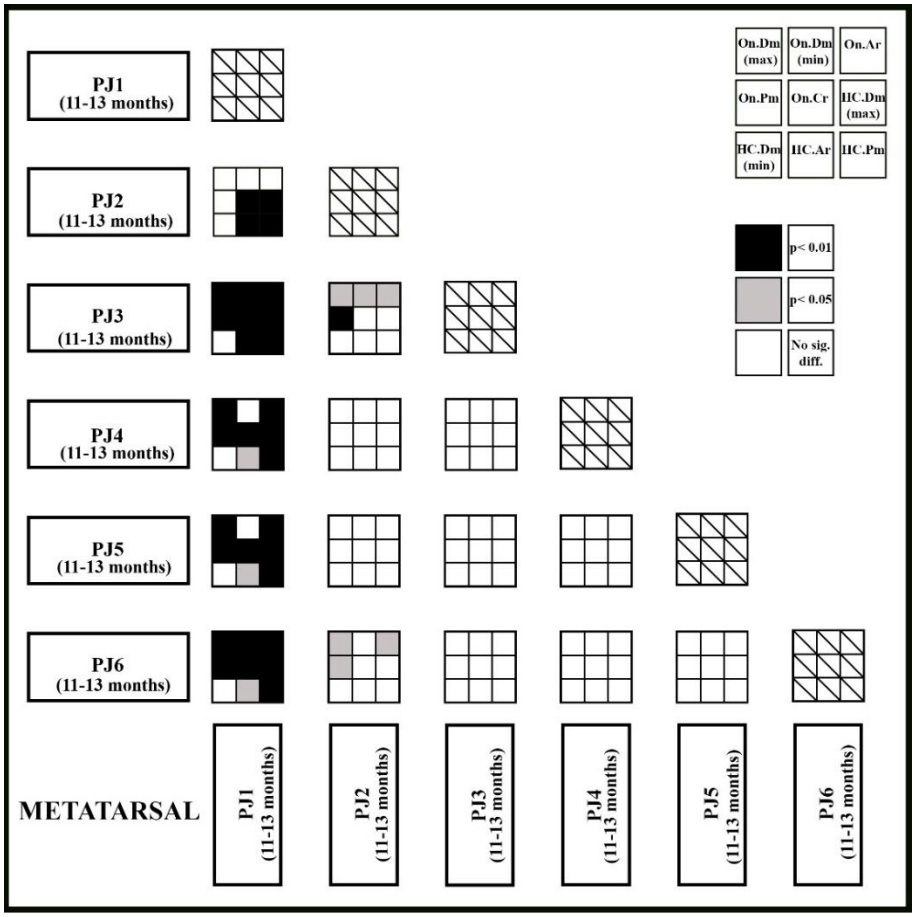

Figure 6.60 – Metatarsal (pig) – results of Tukey post-hoc test on osteon and Haversian canal parameters in different individuals

Ribs, showed a low variability in terms of osteon and Haversian canal size, with a mean value respectively of 17835,94(±8321,39) μm^2 and 663,28(±415,28) μm^2.

The only exception was represented by PJ3 (Fig. 6.61), in which the size of osteons (23886,15±11244,21μm^2) was statistically significantly bigger compared to PJ2 ($p<0.05$) and PJ6 ($p<0.01$).

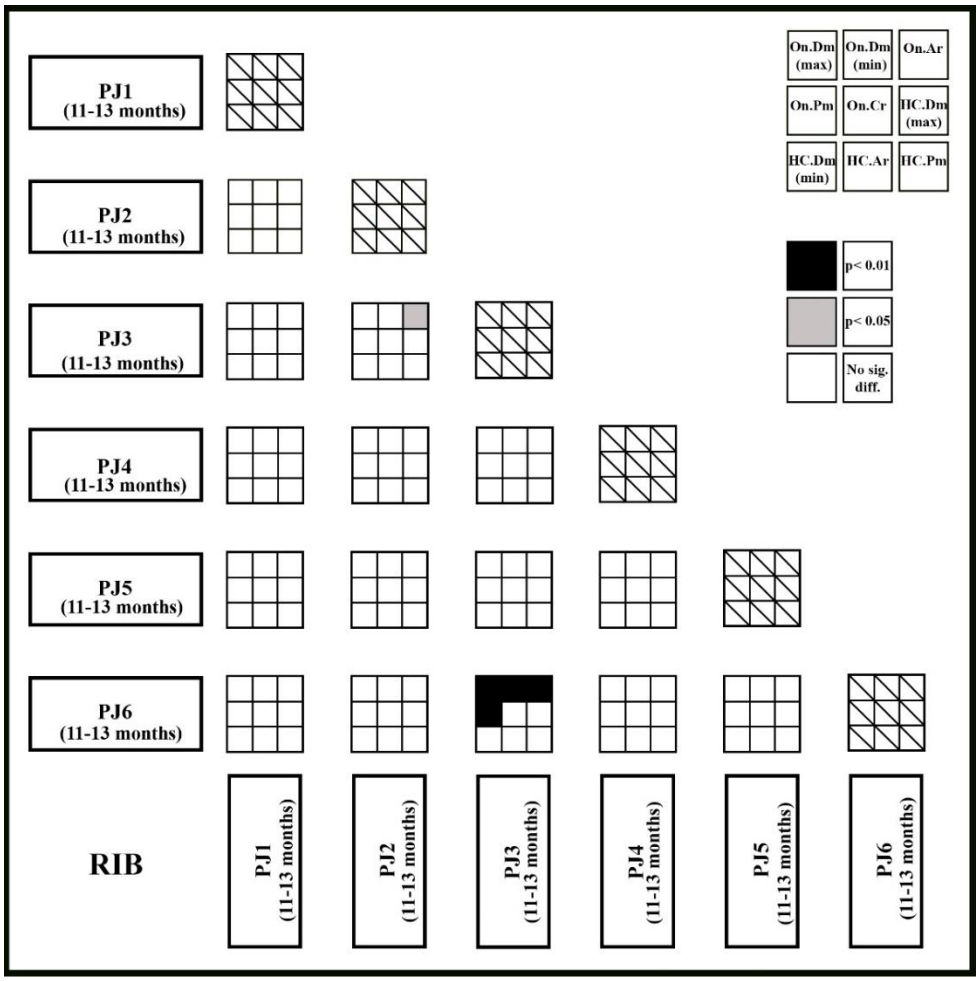

Figure 6.61 – Rib (pig) – results of Tukey post-hoc test on osteon and Haversian canal parameters in different individuals

6.5 INTER-SPECIES HISTOMORPHOMETRIC VARIABILITY

The histomorphometric analysis consisted in the measurements of a total of 2064 secondary osteons and Haversian canals (1246 from adult human bones and 818 from juvenile pig bones) from eighty-four cross-sections, equally divided between human and pig (see Chapter 4 for the details of the sample).

Tables 6.59 and 6.60 show the descriptive statistics of the osteon and Haversian canals parameters in human and pig long bones.

Overall, human osteons seemed bigger compared with pig osteons, with a mean area respectively of 34838,43(±14545,47) μm^2 and 21988,54(±9155,87) μm^2. Osteon circularity seemed generally higher in pig bones (0,95±0,03) compared to human bones (0,94±0,03).

The disparity between human and pig seemed even larger when comparing the Haversian canals size. The mean value of human Haversian canal was considerably higher (1666,63±785,02 μm^2) compared to that of pig (828,56±623,63 μm^2).

HUMAN VS PIG (LONG BONES)						
Bone type		**On.Dm$_{max}$ (µm)**	**On.Dm$_{min}$ (µm)**	**On.Ar (µm^2)**	**On.Pm (µm)**	**On.Cr**
HUMAN (n=1123)	Mean	228,38	187,41	34838,43	666,40	0,94
	St.dev	50,03	40,64	14545,47	139,50	0,03
	Min	111,20	79,06	7122,36	310,65	0,71
	Max	413,23	335,66	98668,16	1137,36	0,99
PIG (n=733)	Mean	180,55	149,52	21988,54	528,88	0,95
	St.dev	38,74	31,69	9155,87	108,31	0,03
	Min	103,52	73,36	6777,25	306,90	0,77
	Max	321,39	272,70	61705,71	924,65	0,99

Table 6.59 - Descriptive statistics of osteon parameters for human and pig long bones

HUMAN VS PIG (LONG BONES)					
Bone type		**HC.Dm$_{max}$ (µm)**	**Hc.Dm$_{min}$ (µm)**	**HC.Ar (µm^2)**	**HC.Pm (µm)**
HUMAN (n=1123)	Mean	50,28	41,09	1666,63	145,31
	St.dev	12,49	10,20	785,02	34,46
	Min	19,54	14,43	114,20	58,45
	Max	96,86	73,12	4865,38	252,24
PIG (n=733)	Mean	35,05	27,42	828,56	100,96
	St.dev	12,29	9,67	623,63	34,45
	Min	14,03	11,03	131,97	103,45
	Max	81,98	77,33	4943,29	42,51

Table 6.60 - Descriptive statistics of Haversian canal parameters for human and pig long bones

ANOVA test (Table 6.61)revealed that the size of human osteons was statistically significantly higher compared to the size of pig osteons (p=0.000, Cohen's d=1.012, 95% CI for Cohen's d: 0.914 – 1.111). In addition, a statistically significant difference in the size of Haversian canals was observed between human and pig (p=0.000, Cohen's d=1.155, 95% CI for Cohen's d: 1.055 – 1.255).

Osteon circularity was statistically significantly higher in pig bones (p=0.000) compared to human bones although the effect size was small (Cohen's d=0.333, 95% CI for Cohen's d: 0.24 – 0.427).

HUMAN VS PIG LONG BONES – ANOVA test									
	On.Dm (max)	**On.Dm (min)**	**On.Ar**	**On.Pm**	**HC.Dm (max)**	**Hc.Dm (min)**	**HC.Ar**	**HC.Pm**	**On.Cr**
Sig.									
HUMAN VS PIG	.000	.000	.000	.000	.000	.000	.000	.000	.000

Table 6.61 – Human vs pig (long bones) - Results of ANOVA on osteon and Haversian canal parameters

With regard to flat bones, a similar trend was observed. The mean value of the area of human secondary osteons was considerably higher (24770,86±13167,55 μm^2) compared to that of pig (17793,84±8361,56 μm^2; Table 6.62). Similarly, human Haversian canals were bigger compared to pig Haversian canals, with a mean area respectively of 1170,08 (±695,61) μm^2 and 659,95(±416,58) μm^2 (Table 6.62).

Osteon circularity seemed higher in pig bones (0,95±0,03) compared to human bones (0,94±0,03).

HUMAN VS PIG (FLAT BONES)						
Bone type		**On.Dm$_{max}$ (μm)**	**On.Dm$_{min}$ (μm)**	**On.Ar (μm^2)**	**On.Pm (μm)**	**On.Cr**
HUMAN (n=123)	Mean	195,67	153,73	24770,86	561,15	0,93
	St.dev	53,98	42,76	13167,55	148,45	0,04
	Min	94,92	68,30	6661,35	299,84	0,69
	Max	337,66	301,12	80254,14	1017,20	0,99
PIG (n=86)	Mean	164,71	132,71	17793,84	474,67	0,95
	St.dev	38,85	31,50	8361,56	108,27	0,02
	Min	79,74	69,51	4362,82	242,54	0,87
	Max	293,77	237,32	57282,99	876,98	0,98

Table 6.62 - Descriptive statistics of osteon parameters for human and pig flat bones

HUMAN VS PIG (FLAT BONES)					
Bone type		**HC.Dm$_{max}$ (μm)**	**Hc.Dm$_{min}$ (μm)**	**HC.Ar (μm^2)**	**HC.Pm (μm)**
HUMAN (n=123)	Mean	41,60	33,80	1170,08	121,17
	St.dev	12,28	9,79	695,61	33,57
	Min	17,50	14,39	219,14	55,08
	Max	83,93	74,93	4854,18	250,84
PIG (n=86)	Mean	31,38	24,96	659,95	90,87
	St.dev	10,35	7,69	416,58	27,66
	Min	11,88	9,79	105,67	38,41
	Max	63,75	48,11	2267,85	172,21

Table 6.63 - Descriptive statistics of Haversian canal parameters for human and pig flat bones

ANOVA test (Table 6.64) indicated that the size of human osteons was statistically significantly higher compared to the size of pig osteons (p=0.000, Cohen's d=0.61, 95% CI for Cohen's d: 0.328 – 0.891). Moreover, a statistically significant difference in the size of Haversian canals was found between human and pig (p=0.000, Cohen's d=0.854, 95% CI for Cohen's d: 0.567 – 1.142). Finally, osteon circularity was statistically significantly higher in pig compare to human (p=0.000, Cohen's d=0.601, 95% CI for Cohen's d: 0.32 – 0.883).

HUMAN VS PIG FLAT BONES – ANOVA test									
	On.Dm (max)	**On.Dm (min)**	**On.Ar**	**On.Pm**	**HC.Dm (max)**	**Hc.Dm (min)**	**HC.Ar**	**HC.Pm**	**On.Cr**
Sig.									
HUMAN VS PIG	.000	.000	.000	.000	.000	.000	.000	.000	.000

Table 6.64 – Human vs pig (flat bones) - Results of ANOVA on osteon and Haversian canal parameters

Although the mean values of both osteon and Haversian canal parameters showed statistically significant differences between human and pig (p<0.01), the analysis of the data showed some extent of overlap (Fig. 6.62).

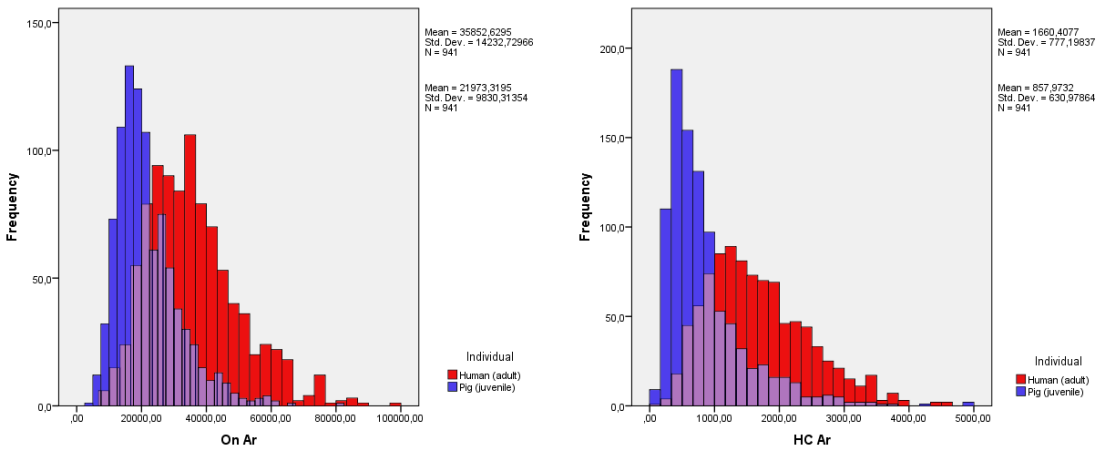

Figure 6.62 – Histograms showing the overlap in the size of osteon (left) and the size of Haversian canals (right) between human and pig

A discriminant function analysis was performed to ascertain the possibility to use osteon and Haversian canal parameters to discriminate between human and pig. The statistical analysis showed significant differences between human and pig measurements in both long ($P<0.001$; Wilks' $\lambda=0.636$; $\chi^2=830.451$; df=2) and flat bones ($P<0.001$; Wilks' $\lambda=0.753$; $\chi^2=56.355$; df=2), thus permitting canonical discriminant function (D), based on two selected variables to be employed in determining whether an osteon was likely to be human or pig in origin:

Equation for long bones	$D= -4.837 + 0.004 (On.Pm) + 0.076 (HC.Dm_{min})$
Equation for flat bones	$D= -4,413 + 0.003 (On.Pm) + 0.102 (HC.Dm_{min})$

A positive value of D indicates a human origin whereas a negative values indicates a nonhuman origin (*Sus scrofa*).

The models correctly classified 80,9% of cases for long bones and 73,3% for flat bones (Table 6.65).

Classification table					
Long bones			**Predicted**		
			Individual		**Percentage Correct**
	Observed		Human	*Sus scrofa*	
	Individual	Human	944	174	84,4
		Sus scrofa	177	543	75,4
	Overall Percentage				80,9
Flat bones			**Predicted**		
			Individual		**Percentage Correct**
	Observed		Human	*Sus scrofa*	
	Individual	Human	97	24	80,2
		Sus scrofa	30	51	63,0
	Overall Percentage				73,3

Table 6.65 – Classification table of the discriminant function analysis models for long and flat bones

6.6 EXPLORATORY RESEARCH: HISTOMORPHOMETRIC ANALYSIS OF OSTEOCYTE LACUNAE IN HUMAN AND PIG

Like for the previous histomorphometric analysis on secondary osteons, Intraclass Correlation Coefficient (ICC) was computed repeating measurements of thirty osteocyte lacunae by the same operator and by two trained operators after twenty-four, forty-eight and seventy-two hours in order to test the intra- and inter-rater reliability.

The Intraclass Correlation Coefficient (ICC), indicated an excellent agreement between the observations of the same observer as well as those of the two observers (Table 6.66). The minimum correlation coefficient regarded the measurement of minimum diameter, even though the agreement remains excellent.

	Intraclass Correlation Coefficient (ICC) Intra-rater reliability	**Intraclass Correlation Coefficient (ICC) Inter-rater reliability**
Lc.Dm$_{max}$	.995	.984
Lc.Dm$_{min}$	.897	.762
Lc.Ar	.996	.976
Lc.Pm	.991	.916

Table 6.66 – Histomorphometric analysis of osteocyte lacunae: Intraclass correlation coefficient (ICC) for intra-rater and inter-rater reliability.

The results of the histomorphometric analysis on 1242 osteocyte lacunae are shown in Table 6.67.

Overall, pig lacunae seemed generally smaller than human lacunae, with a mean area respectively of 39,6 (±15,52) μm^2 and 45,06 (±17,42) μm^2 (P<0,001, Cohen's d=0,33, 95% CI for Cohen's d: 0,172 – 0,491). Cohen's d effect size implied that the area of approximately 62% of pig osteocyte lacunae was smaller than the average area in human.

Maximum area did not exceed 97,52 μm^2 in pig, whereas it reached 126,91 μm^2 in human. Conversely, the smallest lacuna (11,42 μm^2) was found in pig, whereas in human it was never smaller than 14,12 μm^2.

	Lc.Dm$_{max}$ (μm)		**Lc.Dm$_{min}$ (μm)**		**Lc.Pm (μm)**		**Lc.Ar (μm^2)**		**Lc.N**	
	Sus scrofa	Human	Sus scrofa	Human	Sus scrofa	Human	Sus scrofa	Human	Sus scrofa	Human
Max	19,05	24,21	11,24	11,59	42,27	52,18	97,52	126,91	77	97
Min	5,28	6,53	2,55	2,6	14,26	16,24	11,42	14,12	23	24
Mean	11,04	12,82	5,15	5,16	26,06	29,6	39,60	45,07	46,91	48,97
St. Dev.	2,58	3,17	1,15	1,18	5,38	6,48	15,52	17,42	13,57	15,49

Table 6.67 – Descriptive statistics of human and pig osteocyte lacunae.

The difference in the average value of maximum diameter between the two specimens was statistically significant (p<0,001, Cohen's d=0,62, 95% CI for Cohen's d: 0,454 – 0,778). Likewise, a statistically significant difference was found between human and pig in the average value of the perimeter (P<0,001, Cohen's d=0,61, 95% CI for Cohen's d: 0,447 – 0,771). Cohen's d effect size indicated that the maximum diameter and perimeter of approximately 73% of pig osteocyte lacunae were smaller than the average maximum diameter and perimeter in human.

Conversely, the number of lacunae per osteon and the minimum diameter did not show a statistically significant difference between the two specimens (P>0,05).

With regard to the differences between inner, intermediate and outer osteocyte lacunae, results (Table 6.68) indicated that, both in human and pig, their size decreased from the cement line towards the Haversian canal.

Inner lacunae								
	Lc.Dm$_{max}$ (μm)		**Lc.Dm$_{min}$ (μm)**		**Lc.Pm (μm)**		**Lc.Ar (μm^2)**	
	Sus scrofa	Human	Sus scrofa	Human	Sus scrofa	Human	Sus scrofa	Human
Max	18,65	18,28	7,83	8,26	41,64	42,87	86,27	112,1
Min	5,28	6,53	2,55	2,6	14,26	16,24	11,42	14,12
Mean	9,90	11,42	4,56	4,57	23,37	26,46	31,28	35,32
St. Dev.	2,07	2,643	0,99	0,92	4,26	5,33	11,66	12,20
Intermediate lacunae								
	Lc.Dm$_{max}$ (μm)		**Lc.Dm$_{min}$ (μm)**		**Lc.Pm (μm)**		**Lc.Ar (μm^2)**	
	Sus scrofa	Human	Sus scrofa	Human	Sus scrofa	Human	Sus scrofa	Human
Max	18,31	23,11	11,24	11,59	38,19	50,43	68,67	90,76
Min	5,28	6,86	2,67	3,07	16,6	17,44	16,03	16,87
Mean	10,61	12,13	5,09	4,88	25,13	28,03	36,80	38,74
St. Dev.	2,15	2,99	1,09	0,92	4,47	5,85	12,46	11,72
Outer lacunae								
	Lc.Dm$_{max}$ (μm)		**Lc.Dm$_{min}$ (μm)**		**Lc.Pm (μm)**		**Lc.Ar (μm^2)**	
	Sus scrofa	Human	Sus scrofa	Human	Sus scrofa	Human	Sus scrofa	Human
Max	19,05	24,21	9,03	9,51	42,27	52,18	97,52	126,91
Min	6,2	9,11	3,14	3,45	15,79	22,57	16,99	24,79
Mean	12,5977	14,92	5,79	6,04	29,68	34,57	50,73	61,14
St. Dev.	2,683512	2,74	1,04	1,12	5,27	5,17	15,23	15,24

Table 6.68 - Descriptive statistics of human and pig osteocyte lacunae divided between inner, intermediate and outer.

ANOVA analyses showed that all the variables demonstrated significant differences in relation to their position within the osteon (Tables 6.69 – 6.70). In human, the mean area of outer lacunae was 61,14 (±15,24) μm^2, decreasing up to 35,32 (±12,20) μm^2 in inner lacunae; the mean area in pig ranges from 50,73 (±15,23) μm^2 for the more external osteocyte lacunae to 31,28 (±11,66) μm^2 for the more internal ones.

OSTEOCYTE LACUNAE – HUMAN – ANOVA AND TUKEY'S POST HOC TESTS				
	$Lc.Dm_{max}$	**$Lc.Dm_{min}$**	**Lc.Pm**	**Lc.Ar**
Between groups	.000	.000	.000	.000
Internal vs intermediate	.031	.007	.010	.027
Internal vs outer	.000	.000	.000	.000
Intermediate vs outer	.000	.000	.000	.000

Table 6.69 – Results of ANOVA test and post-hoc tests for statistical significance of the size variation of inner, intermediate and outer osteocyte lacunae in human bone.

OSTEOCYTE LACUNAE – PIG – ANOVA AND TUKEY'S POST HOC TESTS				
	$Lc.Dm_{max}$	**$Lc.Dm_{min}$**	**Lc.Pm**	**Lc.Ar**
Between groups	.000	.000	.000	.000
Internal vs intermediate	.006	.000	.000	.000
Internal vs outer	.000	.000	.000	.000
Intermediate vs outer	.000	.000	.000	.000

Table 6.70 – Results of ANOVA test and post-hoc tests for statistical significance of the size variation of inner, intermediate and outer osteocyte lacunae in pig bone.

CHAPTER 7 – DISCUSSION

This chapter will discuss the findings presented in Chapter 6. The extent of intra-individual and intra-species variability, from both a qualitative and quantitative perspective, are discussed in sections 7.1, 7.2 and 7.3, 7.4, respectively. Section 7.5 discusses the main differences between human and pig (*Sus scrofa*) bone microarchitecture in the context of species discrimination.

7.1 INTRA-INDIVIDUAL HISTOMORPHOLOGICAL VARIABILITY

7.1.1 HUMAN ADULT (HA1)

The histomorphological analysis on 49 cross-sections from an adult human individual (HA1) highlighted the absence of woven bone which was somewhat expected since it is typically found in embryonic bone, during repair processes and in response to pathological conditions, such as bone tumors (Martin and Burr 1989; Hillier and Bell 2007). Although bone tissue was mainly characterized by Haversian bone, some extent of variation was observed throughout the skeleton, especially in the pattern of osteon organization. Compared to flat bones, long bones showed a higher variability of bone microarchitecture in different bones, in different portions of the same bone and even in different parts of the same section.

The cross-sections of long bones, in fact, were frequently characterized by different rates of remodeling, exhibiting an alternation of areas consisting in tightly packed secondary

osteons (dense Haversian bone) and areas characterized by scattered secondary osteons immersed in abundant lamellar matrix (irregular Haversian bone).

According to Enlow (1975), the sites of muscle insertion experience a higher rate of remodeling. The author argued that the formation of secondary osteons helps the muscle to have a firm attachment to the bone even when muscle attachments migrate during growth. In addition, several investigations on mammals (Currey 2003; Weiner *et al.* 1999; McFarlin *et al.* 2008; Romanus 1974; Lanyon *et al.* 1979, 1982; Carter *et al.* 1980) demonstrated that mechanical stress (e.g. muscle pull) influences the rate of Haversian remodeling.

The findings of the histomorphological analysis on the adult human individual (HA1) were in accordance with these investigations.

In the **humerus**, in fact, osteon density seemed to increase from the proximal metaphysis towards the distal metaphysis, especially at the anterior and posterior aspects. This may be explained by the large attachments for *brachialis* and *triceps brachii* muscles at the distal diaphysis (Fig. 7.1), respectively at the anterior and posterior aspects of the bone.

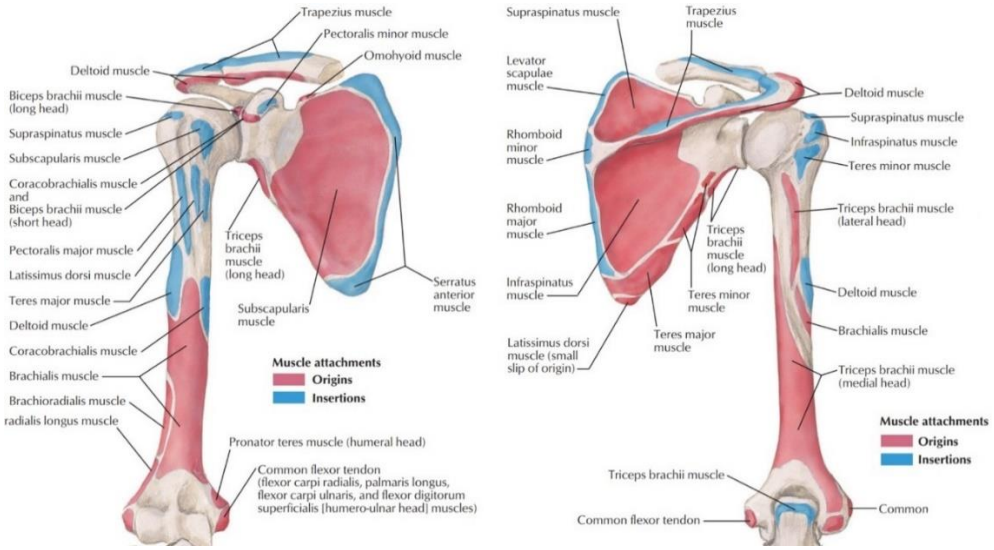

Figure 7.1 – Muscles attachments in the shoulder and axilla (adapted from Netter 2014)

On the contrary, the **ulna** and the **radius** showed the opposite pattern, with a higher osteon density at the proximal metaphysis compared to the distal metaphysis. This may be due to the attachments of the *pronator teres* and *supinator* muscles, respectively (Fig. 7.2). Similarly, the lateral aspect of the ulna and the medial aspect of the radius exhibited a high rate of remodeling which may be due to the interosseous membrane which connects the two bones.

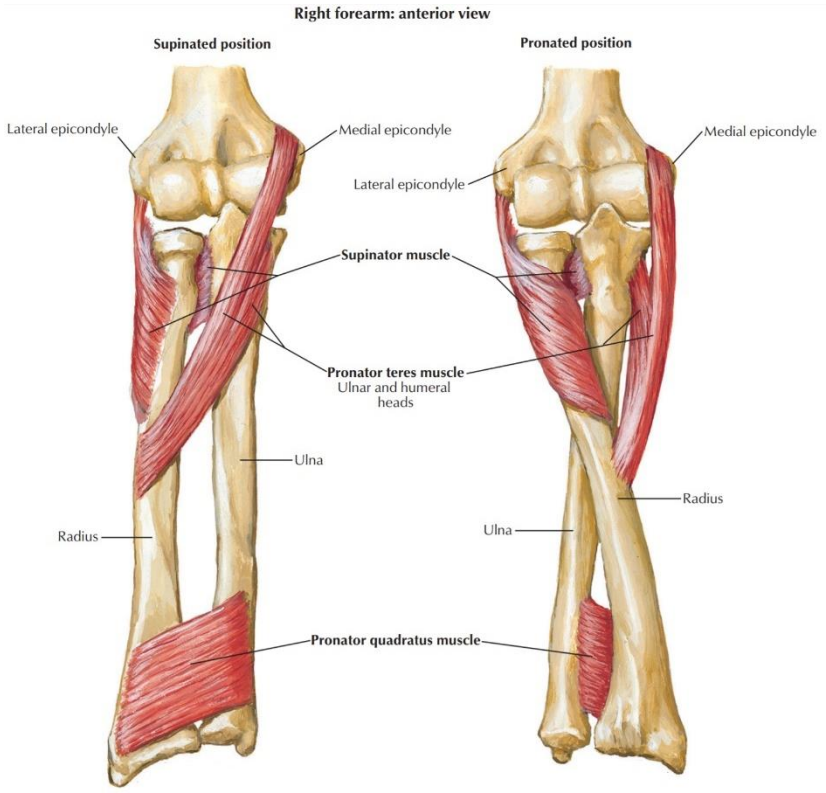

Figure 7.2 – Muscles attachments in the forearm (adapted from Netter 2014)

A higher osteon density was noted also in the shaft and in the lateral end of the **clavicle** compared to the medial end, which was characterized by scattered secondary osteons in a lamellar matrix. The shaft and the lateral end, in fact, are the sites of attachment of

deltoid and *trapezoid* muscles (Fig. 7.1) and this may explain this disparity in the rate of Haversian remodeling.

With regard to the lower limb, the **femur** was mainly composed by tightly packed secondary osteons, especially in the proximal metaphysis and the diaphysis. Osteons were more scattered in the distal metaphysis. This may be explained by the attachment of the large muscles of the leg such as the *vastus medialis*, the *vastus intermedius* and the *vastus lateralis* (Fig. 7.3).

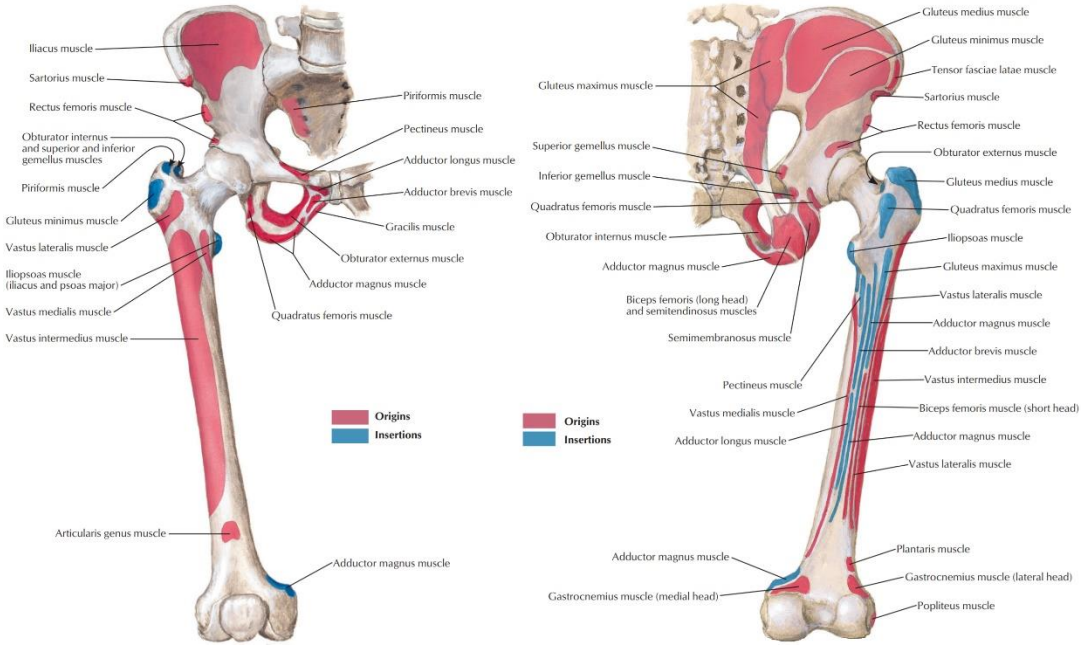

Figure 7.3 – Muscles attachments of hip and tigh (adapted from Netter 2014)

Similarly, **tibia** showed a higher remodeling at the anterolateral aspect of the diaphysis, which may be a consequence of the attachments of *tibialis anterior* and *quadriceps femoris* muscles.

Like the femur, the **fibula** exhibited a higher osteon density in the proximal metaphysis and the diaphysis compared to the distal metaphysis and this may be due to the fact that

most of the muscles attachments on the fibula are located in the upper three-quarters of the bone (Fig. 7.4).

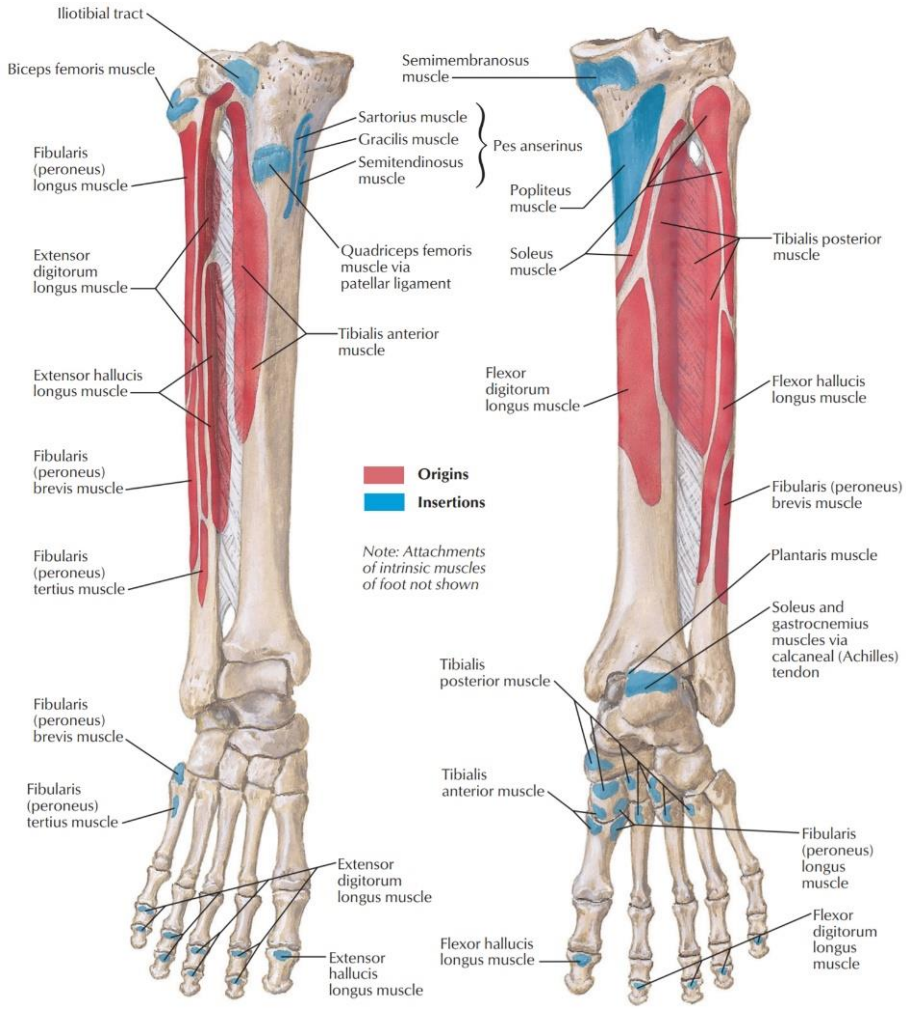

Figure 7.4 – Muscles attachments of the leg (adapted from Netter 2014)

The variation observed in different portions of long bones should be taken into account for the implications that it may have on the reliability of histological age-at-death estimation methods, which refer to precise locations on specific bones. If the site and/or bones is not determinable, such methods may not be exploitable. However, it is not possible to exclude that, with increasing age, the remodeling may increase also in the sites were osteon density is low.

With regard to flat bones, although they were generally characterized by scattered osteons, some exceptions have been observed. The superior border of the **scapula**, the **sternum**, the **iliopubic ramus** and the **rib** exhibited large areas characterized by tightly packed secondary osteons which may be a consequence of muscles attachments, such as those of the *levator scapulae* (scapula), *pectoralis major* (sternum), *pectineus* (iliopubic ramus) and *internal intercostal* and *transverse thoracis* (rib).

Similarly, the dense Haversian bone in the spinous process of the **cervical vertebra** may be related to the attachment of the *serratus posterior superior*.

In addition to these disparities in the rate of Haversian remodeling, some distinctive features were observed along the skeleton.

Several sections, especially those of irregular bones and the cranium, consisted mostly of lamellar tissue with different patterns of vascularization, ranging from longitudinal, to circumferential (mandible, cervical vertebra) and reticular (petrous) vascular canals. The lower rate of remodeling may be explained by the fact that these bones are not directly involved in locomotion and are subjected very little stress compared to long bones (Currey 2002). Accordingly, these bones may be less prone to develop microcracks and require a lower rate of Haversian remodeling which is known to act as a repair mechanism (Martin 2002; Currey 2002; Skedros *et al.* 2003).

Similarly, large areas of lamellar tissue (generally remnants of primary lamellar bone) were observed in long bones, such as radius (diaphysis), fibula (distal metaphysis) and metacarpal (body). Areas of lamellar tissue without evidence of remodeling are frequently found also in other mammals, such as cat (*Felis catus)*, dog (*Canis lupus*), horse (*Equus ferus)* and non-human primates. In case of fragmentary remains the presence solely of

lamellar tissue with no distinctive features can make the discrimination between these species particularly challenging.

Moreover, the metaphysis of the humerus, the diaphysis of the femur and the mental protuberance of the mandible exhibited linear rows of maximum five secondary osteons surrounded by lamellar tissue. Linear arrangements of more than five primary or secondary osteons are frequently found in sheep, miniature swine, equids and nonhuman primates (Mulhern and Ubelaker 2001; Brits *et al*. 2014; Cuijpers 2009). In agreement with literature in human samples rows of maximum five secondary osteons were observed (Mulhern and Ubelaker 2001).

The use of polarized light during the analysis allowed the observation of numerous drifting osteons, especially in the rib, the shaft of the clavicle, the diaphysis of the ulna and the body of the metacarpal. Although the stimulus that trigger their formation is still unknown, drifting osteons are the most common type of osteon in human juvenile bones (Stout and Crowder 2012; Crowder 2005; Robling and Stout 1999).

However, the finding of drifting osteons in an adult skeleton is not surprising since, according to literature, their presence in older individuals is also attested (Robling and Stout 1999).

7.1.2 *SUS SCROFA*

The histomorphological analysis on 41 cross-sections from a juvenile pig (PJ1) highlighted some extent of variability in the different bones of the skeleton, in different portions of the same bone and even in different aspects of the same cross-section.

Like in human, long bones in pig exhibited a higher variation in bone microarchitecture compared to flat and irregular bones.

Overall, the predominant type of tissue in pig bone was fibro-lamellar, which is typical of fast-growing animals whose bones need to grow quickly in diameter (Currey 2002). Weight-bearing bones (limb bones), which are also involved in locomotion, are known to experience high stress and/or repeated stress cycles which can damage the bone and lead to fatigue failure. It has been suggested by several authors (Frost 1973; Lanyon *et al.*1979; Martin and Burr 1982; Carter *et al*. 1981) that Haversian remodeling may prevent fatigue failure by limiting the propagation of microcracks in bone.

Consistently with these hypotheses, the histomorphological analysis on the juvenile pig (PJ1) revealed that Haversian remodeling was present almost exclusively in long bones.

At the surface on bones which do not have to sustain high loads, such as those of the cranium, strains are generally lower, and this may have an influence on the rate of remodeling (Currey 2002). However, it has to be taken into account that osteons are generally oriented following the the direction of the principal mechanical strains (e.g. longitudinal in long bones). Flat bones, such as those of the cranium, are known to experience bidirectional loading and therefore their osteons can have different orientations (Currey 2002; van Oers 2008). Thus, in cross section, a number of Haversian systems may have not been cutted transversely and this may have hindered their observation.

Nonetheless, rib showed evidence of Haversian remodeling and this may be due to the increasing loading cycles provoked by the contraction and relaxation of the muscles of the thorax during respiration (Skedros *et al.* 2003; Qiu *et al*. 2010). Moreover, as suggested by Currey (1981), ribs require a lower safety factor than limb bones and are able to bear the reduction in strenght provoked by the Haversian remodeling.

In addition, the bones of the forelimb exhibited a higher rate of Haversian remodeling compared to those of the hindlimb. This was an expected finding since in quadrupeds the center of gravity tends to be closer to the forelimbs and this may imply higher vertical forces in the forelimb compared to the hindlimb (Thorup *et al.* 2007*;* Von Wachenfelt *et al.* 2010).

With regard to the localization of Haversian remodeling within the section, in the hindlimbs, remodeling regarded mainly the caudal and lateral aspects, whereas in the forelimbs, secondary osteons had a wider distribution across the section, although they were more frequently observed at the lateral and medial aspects.

Without *in vivo* measurements of the principal strains imposed on pig bones during stance and locomotion, making inferences about why some regions experience remodeling and others do not, represents a complicated task. However, it has been suggested that the presence or absence of remodeling in the different regions may serve to maintain adequate safety-factors-to-failure throughout the volume of bone (Lanyon *et al.*1979; Riggs *et al.*1993; Skedros *et al.*1994). Accordingly, it can be hypothesized that these particular regions experience higher strains and be more prone to develop microcracks, requiring a higher rate of Haversian remodeling in order to maintain bone structural integrity.

Drifting osteons were not observed in any of the cross-sections, whereas a high number of “anomalous” osteons were noted along the skeleton. These Haversian systems were

characterized by two or more longitudinal canals within the boundary of the osteon. Their presence is quite surprising considering that vascular canals reduce the strength and stiffness of bone by increasing its porosity. The more obvious hypothesis is that their formation may be related to the necessity of a more efficient blood supply. The fibrolamellar bone that is replaced by Haversian bone, in fact, consists of a wide network of vascular canals which may be more efficient in providing blood and nutrients to bone (Currey 1960). However, in literature no information on these structures has been provided and further research is needed in order to understand how and why they form. Nonetheless, at least in the study sample of this research, these types of osteons were never observed in the human specimens and they may represent a distinctive feature of nonhuman bone which can aid species discrimination.

7.2 INTRA-INDIVIDUAL HISTOMORPHOMETRIC VARIABILITY

7.2.1 HUMAN

The histomorphometric analysis on the human adult individual HA1 revealed that the size of both Haversian systems and Haversian canals were statistically significantly higher in long and irregular bones compared to flat bones. Although literature does not provide an explanation for the variation in the size of osteons and Haversian canals in long and flat bones, this may be due to the smaller cross-sectional areas of the latter, as well as differences in the habitual loading. Flat bones may be less prone to fatigue microdamage requiring a lower rate of Haversian remodeling. Moreover, since Haversian canals make bone lose strength and stiffness by increasing the porosity of the bone (Martin 1991), a

reduction in the size of the canals may help to minimize the effect of porosity on bending and torsional strength.

In addition, Dominguez and colleagues (2016) demonstrated a correlation in ribs between the size of osteons, the age of the specimen and the cortical area. With increasing age, the cortical area decreases and this may limit the size of forming osteons.

The differences observed in different portions of each bone were consistent with the hypothesis that cortical thickness determines the size of osteons.

Indeed, in the proximal metaphysis, which is characterized by a thinner cortex compared to that of the diaphysis and distal metaphysis, osteons were statistically significantly smaller. Moreover, the diaphysis of long bones showed systematically higher standard deviations probably due to a larger area of cortical bone compared to that of the metaphyses, allowing a higher variability in terms of the size of osteons. On the contrary, in flat bones, as well as in metatarsals and metacarpals, the cross-sectional area is rather uniform along the length of the bone, and this could explain why in these bones there is a lower variability in terms of the size of osteons.

With regard to the human juvenile individual (HJ), the osteon size was statistically significantly greater in long bones compared to flat bones. Like the adult human, this disparity in the size of osteons between long and flat bones may be a consequence of the different cross-sectional areas. Haversian remodeling was observed mainly at the diaphysis of long bones. Nonetheless, since only the posterior portion of bones were sampled, the presence of remodeling in the other aspects, as well as some extent of variability in the size of osteons and Haversian canals cannot be excluded.

Statistical analysis on the variation in the size of osteon and Haversian canal between the adult and the juvenile individuals was not performed since two individuals would not

have been representative of any intra-specific variability. Nonetheless, the juvenile individual was characterized by bigger osteons and smaller Haversian canals compared to the adult individual. These data are in agreement with previous studies on age-related changes in the size of Haversian systems in human, which pointed out an increase with age in the size of Haversian canals and a decrease in the size of Haversian systems (Britz *et al.* 2009; Mulhern and Van Gerven 1997; Currey 1964; Evans 1976; Thompson 1980).

7.2.2 *SUS SCROFA*

The histomorphometric analysis on the pig juvenile individual PJ1 showed no statistically significant differences in the size of osteons and Haversian canals between long and flat bones.

Although the current literature does not provide explanations, this homogeneity in the size of the secondary osteons may be a consequence of the function and/or the pattern of the mechanical stress of the bones of the skeleton.

Previous investigations on the reaction of bone to mechanical stress in rats, demonstrated that compact bone does not react to continuous stimuli (Heřt *et al*. 1969; 1972). On the contrary, intermittent loading provides the stimulus that triggers the activation of remodeling.

The fact that the pig came from an intensive farm, and therefore had a reduced mobility during life, may have had an influence in the pattern of Haversian remodeling (Young *et al.* 1986).

7.3 INTRA-SPECIES HISTOMORPHOLOGICAL VARIABILITY

7.3.1 HUMAN

Overall, the different cross-sections of each bone from different individuals were characterized by a general homogeneity. Nonetheless, some extent of intra-species variability in bone microarchitecture was present and involved mainly the amount of primary lamellar bone as well as the pattern of osteon organization.

In particular, the humerus of individual HA3 (73 years), the radius of individual HA1 (26-45 years) and the femur of individual HA14 (39-57 years) exhibited large areas characterized by thick layers of primary lamellar tissue (circumferential lamellae) at the periosteal surface. Usually this type of primary bone is replaced by Haversian bone during life and, in mature individuals is generally reduced to a thin layer of lamellae (Eriksen 1991; Currey 2002; Zoetis *et al.* 2003). Although these patterns are somehow surprising given the age of the individuals, the absence or low rate of Haversian remodeling in those regions represent an exception which may be a consequence of pathological conditions, even though not visible macroscopically. Indeed, there are several pathological conditions which can alter the microscopic appearance of cortical bone in human (e.g. osteomalacia, osteoporosis, diabetes mellitus, Paget's disease, osteogenesis imperfecta, trauma, immobilization, hyperparathyroidism). These long-standing conditions are known to modify bone histological appearance by decreasing or increasing the rate of Haversian remodeling. Diabetes mellitus, for example, causes a reduction in the remodeling rate and therefore a decrease in the normal number of secondary osteons and osteon fragments.

With regard to the pattern of osteon organization, areas characterized by tightly packed secondary osteons were generally found at the sites of muscle attachments (Enlow 1975;

Bradley 1959; Romanus 1974; Lanyon *et al.* 1979, 1982; Carter *et al.* 1980). According to Currey (2002) the Haversian remodeling at the site of muscle attachments function as an anchoring mechanism which allow muscles to maintain a firm attachment to the bone, especially when the muscle insertion migrates during the growth of the individual. Again, this finding highlights the implications that this variation may have on the reliability of histological age-at-death estimation methods, which refer to precise locations on specific bones. Applying those methods in different portion of the bone may lead to biased estimations.

Humeri showed a higher osteon density at the anterior, medial and lateral aspects which may be related to the muscle attachments of the *brachialis* and *triceps brachii* muscles. Similarly, the posterior and lateral aspects of **ulnae**, which are the site of attachments of the *flexor digitorum profundus* and the *extensor pollicis longus* respectively, showed a higher osteon density compared to the rest of the section.

Radii exhibited tightly packed secondary osteons at the medial and lateral aspect which may be a consequence of the attachments of the *extensor pollicis brevis* and *pronator teres*. **Femora and tibiae** consisted almost entirely of tightly packed secondary osteons, probably due to the attachments of the large muscles of the leg and their direct involvement in the locomotion. In **metatarsals**, a higher osteon density was observed at the plantar aspect, and this may be due to an increased loading and contact with the ground (Skedros *et al.*2003). This may result in an increase in microcracks requiring a higher rate of remodeling.

Finally**, ribs** exhibited mainly scattered secondary osteons in a lamellar matrix. Although flat bones are generally characterized by lamellar tissue with absent or low rate of remodeling, ribs, due to the loading cycles imposed by the contraction and relaxation of

the muscles of the thorax during respiration experience moderate to high remodeling (Skedros *et al.* 2003; Qiu *et al*. 2010).

7.3.2 *SUS SCROFA*

Overall, the analysis of the cross-sections of each bone from different pigs highlighted a low histomorphological intra-species variability. Generally, the different regions of each bone (cranial, caudal, medial and lateral) exhibited similar microscopic morphology in the different individuals.

Humeri showed a prevalence of fibro-lamellar tissue although moderate to high remodeling was observed at the medial and lateral aspect. This is probably a consequence of attachments of the *teres major* and the medial and lateral heads of the *triceps brachii* muscle which is an extensor of the elbow and support the weight of the body by keeping the limbs in extension.

In **radii** and **ulnae**, the sites of muscle attachments are located on the radial tuberosity (*biceps brachii*) and on the olecranon process (*triceps brachii*), respectively. Nonetheless, radial and ulnar diaphysis exhibited moderate to high rate of remodeling in all the aspects of the bone, except for the medial aspect of the ulna which was generally characterized by a large network of reticular vascular canals. Therefore, the presence of Haversian remodeling may be a consequence of the higher vertical forces imposed to these two bones since in pig, the center of gravity tends to be closer to the forelimbs (Thorup *et al.* 2007*;* Von Wachenfelt *et al.* 2010). This implies higher stress and/or repeated stress cycles which can damage the bone and lead to fatigue failure. Haversian remodeling

limits the propagation of microcracks improving the fatigue strength of the bone (Currey 2002; Frost 1973; Lanyon *et al.*1979; Martin and Burr 1982; Carter *et al*. 1981)

The shaft of **femora**, despite being the site of attachments of *vastus medialis*, *vastus intermedius* and *vastus lateralis* muscles, exhibited a prevalence of fibro-lamellar bone and a low rate of remodeling in all the pigs. Although surprising, the reasons for this may be twofold: on the one hand, the center of gravity closer to the forelimbs may reduce the vertical forces that the femur has to sustain; on the other hand, since the pigs came from an intensive farm, their mobility during life must be considerably limited. Several authors have argued that an increased muscular activity accelerate the rate of Haversian remodeling (Johnson 1966; Bradley 1959; Romanus 1974; Lanyon *et al*. 1979, 1982; Carter *et al*. 1980). Therefore, a reduced mobility of the pigs may have affected their bone microstructure. However, this reduced rate of Haversian remodeling and a prevalence of fibrolamellar bone represents a benefit since it make the pig's femur easily distinguishable from human bone by histomorphological analysis.

With regard to **tibiae**, the insertion of *tibialis cranialis* muscle may be responsible for the moderate to high remodeling observed at the cranial aspect of the bone.

Metatarsals were characterized by a high rate of remodeling at all the aspects of the bone. This extensive remodeling may be related to the insertion of *peroneus longus* muscle, as well as an increased loading which the more distal bones are known to experience (Skedros *et al.*2003).

Finally, **ribs** experienced moderate to high remodeling (except at the caudal aspect), probably due to the contraction and relaxation of the muscles of the thorax during respiration (Skedros *et al.* 2003; Qiu *et al*. 2010). As suggested by Currey (1981), ribs

require a lower safety factor than limb bones and are able to bear the reduction in strenght provoked by the Haversian remodeling.

Nevertheless, this general homogeneity in the histological appearance may be due to the fact that all the pigs were juveniles between 11 and 13 months of age. It is likely that older pigs would have shown a higher rate of remodeling which would have replaced the existing fibro-lamellar tissue (Currey 1959; Currey 2002; Martin and Burr 1989).

7.4 INTRA-SPECIES HISTOMORPHOMETRIC VARIABILITY

7.4.1 HUMAN

The results of ANOVA and Tukey post-hoc tests revealed that the bones of the upper limbs showed a higher variability in the size of Haversian canals, whereas the bone of the lower limbs were characterized by a higher variability in the size of osteons.

Overall, the individual which showed more statistically significant differences with the rest of the study sample was the archaeological one (HA1).

Unfortunately, no demographic information is available from the archaeological report of the site were HA1 individual was recovered. However, these differences in osteon morphometry may be related to different activity patterns compared to modern populations, as well as different diet and health condition (Bourrin *et al.* 1992; Turner *et al.* 2001; Brandao-Burch *et al.* 2005). Pathological conditions, in fact, are known to affect bone microstructure in several ways. Diabetes mellitus, for example, is known to results a decrease in the the normal rate of Haversian remodeling (Hillier and Bell 2007).

If we consider only the modern individuals, the intra-species histomorphometric variability is considerably lower and regards mainly the femur and the tibia. A higher

variability in terms of size of osteons and Haversian canals in these bones may be a consequence of a different load history of the lower limbs (due to locomotion) compared to the upper limbs.

Nevertheless, by comparing the data of the present research with those reported in literature, some differences in the size of osteons and Haversian canals have been noted (Table 7.1).

According to literature, the mean value of the area of Haversian systems in human ribs ranges from 28442±16606 μm^2 (Pfeiffer 1998) to 44000±18000 μm^2 (Qiu *et al.* 2003). These values are considerably higher compared to those obtained in the present study (24597,93±13080,86 μm^2).

Similarly, the mean value of the area of the Haversian canal in human femora ranges from 2100±656 μm^2 (Mulhern and Van Gerven 1997) to 3667,4±3901 μm^2 (Pfeiffer *et al.* 2006), whereas in the present research a significantly lower mean value was obtained (1704,86±796,41 μm^2).

	Studies	**On.Ar**	**HC.Ar**
FEMUR	Mulhern and Van Gerven 1997	33118,87 (±3239,81) μm^2	2100 (±656) μm^2
	Pfeiffer *et al.* 2006	44533 (±22443) μm^2	3667,4 (±3901) μm^2
	Our data	38003,91 (±15886,51) μm^2	1704,86 (±796,41) μm^2
RIB	Pfeiffer 1998	28442 (±16606) μm^2	1886 (±3119) μm^2
	Qiu *et al.* 2003	44000 (±18000) μm^2	2000 (±1000) μm^2
	Our data	24597,93 (±13080,86) μm^2	1163,28 (±694,36) μm^2

Table 7.1 – Human bone - comparison of the mean values of osteon and Haversian canal area with those reported in literature

These differences may have several explanations. First, some of these studies were carried out on ancient populations whose bone microarchitecture may differ from that of the more recent ones due to different health conditions or activity patterns. Moreover, in these investigations the age of the specimens was not provided and the disparities in the size of the osteons and Haversian canals may be due to age differences.

Several authors suggested that, with increasing age, there is a decrease in the size of secondary osteons and an increase in the size of the Haversian canals. It has been suggested that this increase in the size of Haversian canals is more evident in females than in males (Britz *et al.* 2009; Jowsey 1966; Mulhern and Van Gerven 1997; Currey 1964; Evans 1976; Burr *et al.* 1990).

This may be explained by the fact a high number of small osteons and therefore of cement lines, enhances the ability of bone to attenuate microcracks propagation and consequently improves the bone fatigue strength (Gibson *et al*. 2006; O'Brien *et al*. 2005). In addition, with increasing age, bone becomes rarefied and the formation of smaller resorption spaces, and therefore of smaller secondary osteons, decrease the chance of catastrophic failure (Britz *et al.* 2009; Moyle *et al.* 1978).

Although the sample size of the present research is not sufficiently large to verify age- and sex-related change in osteon and Haversian canal morphometry, the results of ANOVA and post-hoc test do not agree with previous investigations. The only exception regarded the metatarsals, in which the older individuals had statistically significantly smaller osteons compared to the 38-year individual (HA13).

On the contrary, in humeri, the size of osteons in the 70-year female individual (HA2) was statistically significantly higher compared to the 38-year male individual. Similarly,

the size of Haversian canals in HA2 was statistically significantly lower compared to HA13.

Nonetheless, it has to be taken into account that the previous investigations on age-related changes in the morphometry of Haversian systems focused mainly on the femur. Other bones, especially those not directly involved in locomotion, might respond differently with increasing age.

7.4.2 *SUS SCROFA*

A general homogeneity in the size of osteons and Haversian canal was observed in the pig specimens.

Overall, the main differences regarded PJ1 and were particularly marked in the bones of the hindlimb. On the contrary, even in PJ1, the bones of the forelimb showed limited or no significant differences with all the other pigs.

Given the lack of precise information on the life of the animals and the environment in which they lived, trying to give an explanation for the differences observed between some of them is not straightforward.

In addition, although literature provides several *in vivo* studies on the correlation between the principal strains imposed during stance and locomotion, and the rate of remodeling in various mammals, no data on pigs are available.

Overall, the literature on the Haversian remodeling in pigs is extremely scarce and investigations on the intra-species histomorphometric variability have never been undertaken.

Nevertheless, by comparing the data of the present research with those reported in literature (Table 7.2), osteons result considerably smaller compared to those measured by Martiniaková and colleagues (2006a) and Urbanová and Novotny (2005) but rather bigger compared to those reported by Morris (2007). The only exception regards the humerus in which osteons were considerably smaller compared to those measured by Morris (2007). However, in all these studies no information was provided on the age of the specimens as well as on the number of osteons that were measured.

With regard to the Haversian canal area, the mean values obtained in this research are in accordance with those reported in literature.

The disparity in the size of osteons may be due to several factors, such as different sample sizes, different age of the specimens and different mechanical environments.

	Studies	**On.Ar**	**HC.Ar**
FEMUR	Urbanová and Novotny 2005	33118,87 (±3239,81) μm^2	826,45 (±66,88) μm^2
	Martiniaková *et al.* 2006a	28031,80 (±10004,39) μm^2	1015,21 (±539,63) μm^2
	Morris 2007	13900 (±650) μm^2	645 (±341) μm^2
	Our data	19689,23 (±8110,47) μm^2	639,82 (±623,49) μm^2
HUMERUS	Morris 2007	25100 (±166) μm^2	775 (±560) μm^2
	Our data	21285,58 (±8606,82) μm^2	696,36 (±428,18) μm^2
RIB	Morris 2007	11300 (±570) μm^2	602 (±469) μm^2
	Our data	17835,94 (±8321,39) μm^2	663,28 (±415,28) μm^2

Table 7.2 – Pig bone - comparison of the mean values of osteon and Haversian canal area with those reported in literature

7.5 DISCRIMINATION BETWEEN HUMAN AND PIG (*Sus scrofa)* BY HISTOLOGICAL ANALYSIS

7.5.1 HISTOMORPHOLOGY

The histomorphological analysis on the cross-sections of human and pig (*Sus scrofa*) bones highlighted a marked difference in bone microarchitecture of the two species.

As shown in paragraph 6.3.3, in the human foetus and pig newborns these differences regarded the type of bone tissue rather than the rate of remodeling, since the latter was absent in all the cross-sections.

Human foetal bone was characterized by an immature tissue consisting of a woven scaffolding with the initial formation of primary osteons, whereas pig bone exhibited an early stage of fibro-lamellar formation although, especially at the periosteal surface, remnants of a more immature woven scaffolding were observed in most of the cross-sections.

The radial vascular canals found in the humerus of the human foetus and the radially oriented woven scaffolding found in the metatarsal may be a signature of a high-speed osteogenesis (Goldman *et al.* 2009). Several authors, in fact, demonstrated that this type of bone is characterized by a very fast bone deposition typical of growing individuals (de Margerie *et al.* 2004; de Ricqlès 1977).

Adult human cortical bone showed a prevalence of Haversian bone, although, especially flat bones, exhibited a prevalence of lamellar tissue with low (or sometimes absent) remodeling.

Flat and irregular bones in juvenile pig (hereafter “pig”) were frequently characterized by areas of parallel-fibered bone which, in normal transmitted light, resembles the lamellar

tissue found in human. However, with the aid of polarized light these two types of tissues were easily distinguishable since parallel-fibered bone appears entirely dark or bright and does not show the alternation of bright and dark lamellae typical of lamellar tissue.

The periosteal surface differed significantly between the two species, since in pig bone, it was characterized by either fibro-lamellar or a more immature woven scaffolding, whereas in human bone, it exhibited low-to-high remodeling although remnants of primary circumferential lamellar bone was frequently observed.

Proceeding towards the endosteal surface, several pig bones, especially those of the limbs, were characterized by a low-to-high rate of remodeling (Haversian bone).

A proximal-to-distal increase in the rate of Haversian remodeling was observed in all the pig specimens. In fact, humerus and femur exhibited a considerably lower number of secondary osteons compared to the ulna, radius, tibia and metatarsal. The more distal bones are probably more prone to develop microcracks due to an increase in loading and contact with the ground. Consequently, a higher rate of remodeling helps to maintain bone structural integrity by limiting microcrack propagation. A similar “proximal-to-distal” trend in Haversian remodeling was observed by Skedros and colleagues (2003) during their investigation on Rocky Mountain mule deer.

Moreover, in several cross-sections, except for those of the femur, the Haversian remodeling regarded also the middle cortex. At the cranial aspect of the ulna, three out five cross-sections showed the presence of secondary osteons across the entire cortex. In case of fragmented remains from that specific bone region, a discrimination between human and nonhuman exclusively by a histomorphological analysis may not be straightforward. Similarly, in radii and tibiae, Haversian remodeling was observed at the endosteal surface and in the middle cortex at the caudal and cranial aspects, respectively.

In metatarsals, except for the periosteal surface, all the cross-sectional area exhibited extensive remodeling. In case of degraded bone fragments where the periosteal surface is compromised or absent, the presence of secondary osteons can lead to wrong diagnoses. Furthermore, it has to be taken into account that in the present research exclusively juvenile pigs were employed. It is likely that, with increasing age, those pigs would have shown a higher rate of remodeling which probably would have characterize larger areas of cortical bone. Indeed, previous studies on nonhuman mammals exhibiting fibro-lamellar bone, demonstrated that, with increasing age, this type of tissue is generally either partially or completely replaced with Haversian bone (Currey 1959; Currey 2002; Martin and Burr 1989).

In addition, some distinctive features were noted in both human and pig bone. Several drifting osteons were observed in the majority of the human samples, whereas in pig bone a single drifting osteon was noted at the anterior aspect of the ulna. A recent study by McCullough and colleagues (2015) evaluated the presence of drifting osteons across mammal species. The authors found drifting osteons only in seven nonhuman species: bear (n=1), rabbit (n=1), panther (n=1), dog (n=3), and pig (n=1).

Thus, considering the results obtained by McCullough and colleagues and those of the present research, the presence of several drifting osteons in a bone fragment may allow to successfully rule out the nonhuman origin. Nevertheless, the age of the animals was unknown, thus further research is needed in order to assess the presence or absence of drifting osteons during the lifespan of the most common mammals.

Moreover, the limb bones in pig showed several “anomalous” Haversian systems characterized by two or more longitudinal vascular canals within the wall of the osteon.

No information was found in literature on this type of Haversian systems. Whether they are due to a pathology or they are formed under normal conditions, these structures were observed exclusively in pig bone. Further investigations should aim at verifying whether these “anomalies” are present also in other mammals since they may represent an easily identifiable structure which can aid species discrimination.

Furthermore, in pig, at the proximal and distal metaphysis of long bones a reticular pattern of vascular canals was frequently observed. This type of vascular arrangement is generally considered a nonhuman characteristic and it is often found in rat (*Rattus rattus)*, horse (*Equus ferus*), as well as in several carnivores (Enlow and Brown 1958; Cuijpers 2006). In the human specimens of the present research, this particular arrangement of vascular canals was observed exclusively in the petrous bone of the individual HA1. As shown in Fig. 7.5, the pattern of vascularization observed in the human petrous bone closely resembled that observed in pig. Although this reticular pattern in human seems to be an exclusive peculiarity of petrous bone, this should be taken into account when the histological appearance of an unknown bone fragment exhibits this type of vascular arrangement.

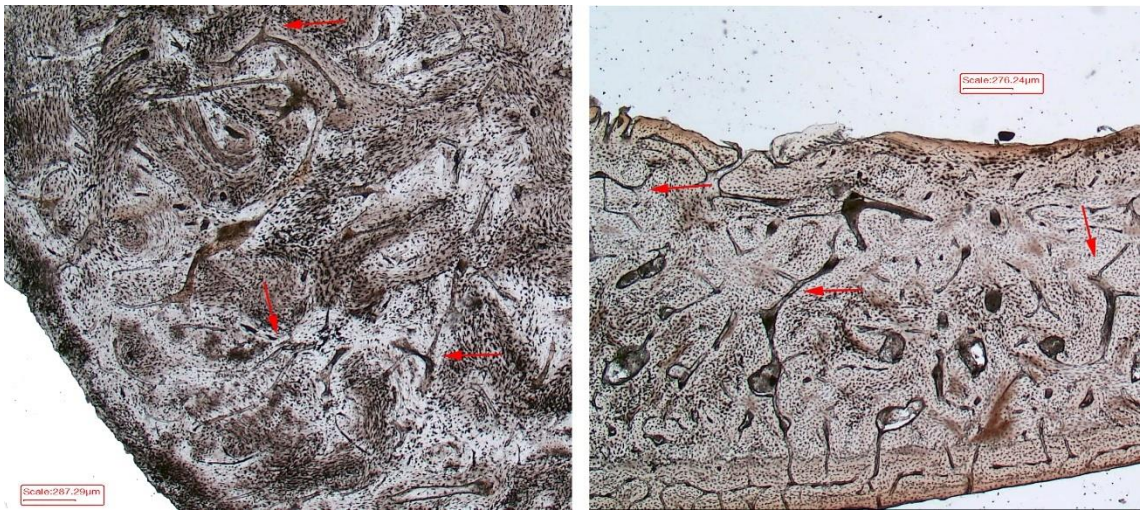

Figure 7.5 – Reticular arrangement of vascular canals in human (left) and pig (right), x25

With regard to “osteon banding”, generally considered a nonhuman characteristic consisting in rows of more than five primary or secondary osteons, it was observed exclusively in the tibial diaphysis of a single pig.

In accordance with literature (Cuijpers 2009; Mulhern and Ubelaker 2001), in human the samples, single rows of maximum five secondary osteons were noted in the metaphysis of the humerus, the diaphysis of the femur and the mental protuberance of the mandible

7.5.2 HISTOMORPHOMETRY

The results of the histomorphometric analysis revealed a statistically significant difference between human and pig in terms of both the size of osteon and Haversian canal (Table 7.3).

	On.Ar (μm^2)		**HC.Ar (μm^2)**	
	Human	*Sus scrofa*	Human	*Sus scrofa*
Long bones	34838,43 (±14545,47)	21988,54 (±9155,87)	1666,63 (±785,02)	828,56 (±623,63)
Flat bones	24770,86 (±13167,55	17793,84 (±8361,56	1170,08 (±695,61)	659,95 (±416,58)

Table 7.3 – Mean values for osteon and Haversian canal area in human and pig

Although the reasons behind these differences could be multiple and much more complex, a number of investigations which studied the possible correlation between strain and osteon morphometry, observed an inverse relation between the size of osteons and the strain magnitude. According to Frost (1990), in fact, osteons are generally larger close to the endosteum, a region which experiences a lower strain magnitude compared to the periosteal side of the cortex. Similarly, Skedros and colleagues (1994; 2001; 2007), during their investigations on the heel bone of hoofed animals, found larger osteons at the

tension cortex, which is characterized by a lower strain magnitude, compared to the higher strained compression cortex. According to van Oers and colleagues (2008), the formation of small osteons have some benefits: on the one hand, the creation of a small cavity (cutting cone) when forming a new osteon has a minor effect on bone strength, on the other hand, several small osteons are able to reduce damage accumulation more efficiently than few large osteons, given the higher number of cement lines which act as barriers to crack propagation.

Whether it is due to strain magnitude or a mechanism to maintain bone structural integrity, it is clear that such small osteons represent a benefit in the context of species discrimination.

The results of the discriminant function analysis, in fact, demonstrated that the histomorphometric analysis is a reliable technique in distinguishing between human and pig bone. The percentage of correct classification obtained in this thesis (Table 6.65) is in line with previous studies on species discrimination (Cattaneo *et al.* 2009; Martiniakova 2006a; Urbanová and Novotny 2005).

However, it is important to consider that the human samples of this thesis mainly consisted in adult/elderly individuals and in literature, it is well known that, with increasing age, there is a decrease in the size of secondary osteons and an increase in the size of the Haversian canal (Thompson 1980; Jowsey 1966; Currey 1964; Evans 1976). Therefore, with younger individuals it is likely that the difference in the size of Haversian canals between human and pig would have been smaller, whereas the difference in the size of secondary osteons would have been even larger.

This results, however, highlight the importance of conducting similar studies on a wide range of bones in order to have a better understanding of the variability of the size of osteon and Haversian canal in different species.

With regard to the histomorphometric analysis on osteocyte lacunae, the statistical analysis showed minimal differences between human and pig in the number of lacunae per osteons as well as in the minimum diameter. On the contrary, a significant difference ($p<0,001$) has been observed in the maximum diameter, perimeter and area. The Cohen's d effect size for these three parameters were respectively medium (.61, .62) and small (.33). This implies that the area of approximately 62% of pig osteocyte lacunae was smaller than the average area in human, whereas the maximum diameter and perimeter of approximately 73% of pig osteocyte lacunae were smaller than the average maximum diameter and perimeter in the human skeleton. This results demonstrated a good potential of osteocyte lacunae to discriminate between the two species although an overlap between human and pig exists. Further research on a wider sample should be undertaken in order to verify its applicability for species discrimination.

With regard to the difference between the dimensions of osteocyte lacunae based on their position within the osteon (inner, intermediate and outer lacunae), the results obtained are in agreement with a previous investigation by Ardizzoni (2001) who pointed out that human osteocyte lacunae close to the Haversian canal are generally smaller compared to the ones which are closer to the cement line. Moreover, the same patterm was observed in pig bone.

As hypothesized in previous studies (Qiu *et al.* 2003; Ardizzoni 2001), this trend may be related to the dynamics of osteon formation and the sequence of events which take place during the narrowing of the Haversian canal, namely: the reduction in the bone apposition

rate and a subsequent decrease in size of the osteoblasts and osteocytes as well as in thickness of osteocytic loose lamellae.

Furthermore, recent studies (van Oers *et al.* 2015; Vatsa *et al.* 2008) have hypothesized a relationship between osteocyte shape and bone loading pattern with more elongated lacunae in bones subjected to unidirectional loading (e.g. long bones), whereas bones which experience bidirectional loading (e.g. cranial bones) are characterized by more spherical lacunae.

When compared to other mammals, humans have different growth patterns, locomotion and mechanical strain, and this might be reflected not only in the size of osteocyte lacunae but also in their shape. Therefore, further studies on the inter-species variability of osteocyte lacunae should not be limited to investigating their dimensions but also their shape. In this regard, the use of other techniques such as micro and nano-CT would allow to overcome this limitation regarding 2D techniques and certainly improve the accuracy of the analysis as well as speed up data acquisition. Recent studies (Carter *et al.* 2013; Dong *et al.* 2014) in fact, obtained quantitative morphometric data on osteocyte lacunae from synchrotron radiation micro-CT images, which allow to analyze relatively large fields of view comprising more than ten thousand osteocyte lacunae.

Nonetheless, this study has demonstrated the potential for using osteocyte lacunae as another parameter for species discrimination although more research is needed. Sample size needs to be expanded, including different species and more individuals of different age in order to have a better understanding of the intra- and inter-species variability.

7.6 LIMITATIONS

The main limitation of this research regards the study sample, since most of the human individuals were adults. At present, there is still a lack of knowledge on infants and juveniles, especially in terms of the size of osteons and Haversian canals. It was however fundamental to concentrate once more on adults first since many variables examined in this study were still unknown and little investigated such as differences between types of bone and areas within the same bone.

Moreover, the study sample was limited to two species. However, unlike previous studies on bone histology, this research included more types of bone which allowed to have a wider overview of the intra- and inter-species variability of bone microarchitecture. The same approach should be used in future studies on other mammals commonly found in forensic context such as cattle (*Bos Taurus*), sheep (*Ovis aries*) and goat (*Capra hircus*).

In addition, although macroscopically there were no obvious signs of pathological conditions, no thorough information on the health conditions of the individuals used in this study was available. Nonetheless, this information could have helped to interpret the data since the possibility that part of the variability observed among individuals was due different health conditions can not be ruled out.

Finally, the histological approach is limited to two-dimensional analyses of bone microarchitecture and does not allow to acquire other data such as volumes, or three-dimensional images of the network of vascular canals, which would certainly represent valuable information in order to develop reliable techniques of species discrimination. In this regard, the use of other techniques such as micro and nano-CT would allow to overcome this limitation regarding 2D techniques and certainly improve the accuracy of the analysis as well as speed up data acquisition.

CHAPTER 8
CONCLUSIONS AND FURTHER RESEARCH

Several investigations have been carried out in the last decades on bone histology in the context of species discrimination. However, those researches focused exclusively on few specific skeletal elements, such as femur and rib. In forensic and archaeological contexts, it is often difficult, if not impossible, to identify the precise anatomical origin of tiny bone fragments. Accordingly, when trying to determine if the material is human or nonhuman, the analyst has to take into consideration the possibility that the fragment might belong to any location of the skeleton. An in-depth knowledge of human and nonhuman bone histology across the skeleton is therefore paramount in order to develop reliable histological methods for species discrimination.

In this regard, the results presented within this thesis have shed light on the intra-individual, intra-species and inter-species variability of bone microarchitecture in human and pig (*Sus scrofa*). Although the existence of this variability had already been hypothesized in the past, this represents the first attempt to systematically explore bone histology in entire skeletons and in different portions of the same bone.

The qualitative and quantitative differences observed within the same individual, within individuals of the same species, and even within different portions of the same bone can have implications not only when assessing the origin of an unknown bone fragment, but also when performing histological age-at-death estimation, since the current methods are based on analysis undertaken on precise locations on specific bones.

The observation of a different rate of remodeling in different bones and in different regions on each bone highlighted the influence of muscle attachments and mechanical

environment on bone microarchitecture, both in human and pig skeletons. This highlights the importance of a collaboration between experts in biomechanics and histology in order to have a better understanding of the mechanisms that regulate bone microarchitecture.

In addition, the proximal-to-distal increase in the rate of Haversian remodeling observed in all the pig specimens underlines the importance of further research on the more distal bones in other mammals since their microarchitecture may be similar to the human one. Overall, the comparison between long bone histomorphology in human and pig suggests that, even in case of fragmented remains, a discrimination between the two species could be usually performed by a qualitative assessment of the bone tissue provided the periosteal surface of the cortex is not compromised. Indeed, in pig long bones, the rest of the cortex showed a low-to-high rate of remodeling which resembles that of human bone. When the histomorphological analysis of bone tissue does not allow to rule out the human origin, such as in completely remodeled cortex (e.g. metatarsals), the size of osteons and Haversian canal can assist in the species discrimination. The histomorphometric analysis which involved the measurement of over 3000 secondary osteons and Haversian canals, revealed statistically significant difference between the two species ($p<0.01$) for all the parameters analyzed (maximum and minimum diameter, area, perimeter, and circularity). A discriminant function analysis revealed that the perimeter of the osteon and the minimum diameter of the Haversian canal were the most discriminant parameters. Thus, two equations based on these parameters have been provided in order to discriminate between human and pig. The models correctly classified 80,9% of cases in long bones and 73,3% of cases in flat bones, demonstrating high sensitivity and high specificity. Moreover, both human and pig exhibited peculiar types of secondary osteons which can aid species discrimination. Human bone showed numerous “drifting osteons”, a particular

type of osteon which “drifts” transversely during its formation. This morphotype was not observed in pig bone, except for a single drifting osteon at the anterior aspect of the ulna. The use of drifting osteons to discriminate between human and other mammals seems promising and deserves further research, especially in other mammals at different stages of skeletal maturity.

Similarly, pig bone exhibited numerous “anomalous” secondary osteons characterized by two or more longitudinal vascular canals. This anomaly was never found in any of the human samples and may represent another diagnostic characteristic which could assist in the histological discrimination between human and nonhuman bone. However, further research is necessary in order to verify their presence also in other species.

Finally, with regard to osteocyte lacunae, the results presented within this thesis have demonstrated the potential for their use as another parameter for species discrimination although more research is needed. Sample size needs to be expanded, including different species and more individuals of different age in order to have a better understanding of the intra- and inter-species variability. When compared to other mammals, humans have different growth patterns, locomotion and mechanical strain, and this might be reflected not only in the size of osteocyte lacunae but also in their shape. Therefore, further studies on the inter-species variability of osteocyte lacunae should not be limited to the investigation of their dimensions but also of their shape. For this purpose, the use of other techniques such as micro and nano-CT would certainly improve the accuracy of the analysis as well as speed up data acquisition.

Considering the results of this research, future work should investigate the intra-individual and intra-species variability in other mammals, without limiting the analyses on some specific bone. Furthermore, in order to develop reliable histological techniques

for species discrimination, there is also the need for an in-depth knowledge of the changes of human bone microarchitecture during ontogeny in different bones of the skeleton.

Moreover, although osteon density is not considered a reliable parameter to distinguish human and non-human bone, further research could verify whether there is a correlation between the density and the size of osteons since this may vary among species.

With regard to other histological techniques, future work could apply immunohistochemical techniques in decalcified bone tissues in order to evaluate the differences among types of collagen or among species-specific proteins.

Overall, although further research is needed, the histological analysis of bone tissue proved to be a powerful and informative technique to assist in species discrimination, both from a qualitative and quantitative perspective.

This thesis makes a significant contribution to knowledge of human and pig bone histology, providing new insight on the extent of intra-individual, intra-species and inter-species variability, and highlights new characteristics of bone tissue which can aid species discrimination by histological analysis.

References

Adams BJ, Crabtree PJ (2008) Comparative skeletal anatomy. A photographic atlas for medical examiners, coroners, forensic anthropologists, and archaeologists, Humana Press

Aerssens J, Boonen S, Lowet G, Dequeker J (1998) Interspecies differences in bone composition, density, and quality: potential implications for in vivo bone research, *Endocrinology* 139(2):663–670

Albert MJ (2012a) "La forense policial del 'caso Ruth y José' echa en falta un hueso de las pruebas", El País, 16 October 2012, https://elpais.com/ccaa/2012/10/16/andalucia/1350391997_752786.html (accessed August 2018)

Albert MJ (2012b) " Las explicationes de la forense del caso Ruth y José", El País, 19 September 2012, https://elpais.com/ccaa/2012/09/19/andalucia/1348052041_792553.html (accessed August 2018)

Albert MJ (2013) "José Bretón sentenced to 40 years for murder of his two young children", El País, 22 July 2013, https://elpais.com/elpais/2013/07/22/inenglish/1374497071_160243.html (accessed August 2018)

Albu I, Georgia R, Georoceneau M (1990) The canal system in the diaphyseal compacta of the femur in some mammals, *Anatomischer Anzeiger* 170(3-4):181–187

Alvira FC, Ramirez Rozzi F, Bilmes GM (2010) Laser-induced breakdown spectroscopy microanalysis of trace elements in Homo sapiens teeth, *Applied Spectroscopy* 64(3):313-319

Ardizzoni A (2001) Osteocyte lacunar size-lamellar thickness relationships in human secondary osteons, *Bone* 28(2):215–219

Ascenzi MG, Gill J, Lomovtsev A (2008) Orientation of collagen at the osteocyte lacunae in human secondary osteons, *Journal of Biomechanics* 41(16):3426–3435.

Baker BW, Shaffer BS (1999) Assumptions about Species: A Case Study of Tortoise Bones from SE Texas, *Journal of Field Archaeology* 26(1):69-74

Baltadjiev G (1995) Micromorphometric characteristics of osteons in compact bone of growing tibiae of human fetuses, *Acta Anatomica* 154:181–185

Barone R (1976) Anatomia comparata dei mammiferi domestici, vol. I, *Osteologia*, Edagricole, Bologna

Bass WM (2005) Human Osteology: A Laboratory and Field Manual. Columbia, MO: Missouri Archaeological Society

Bass WM, Driscoll PA (1983) Summary of Skeletal Identification in Tennessee: 1971–1981, *Journal of Forensic Sciences* 28(1):159–168

Beauthier JP, Lefèvre P, Meunier M, Orban R, Polet C,Werquin JP, Quatrehomme G (2010) Palatine sutures as an age indicator: a controlled study in elderly, *Journal of Forensic Sciences* 55(1):153–158

Beckett S, Rogers KD, Clement JG (2011) Inter-species variation in bone mineral behavior upon heating, *Journal of Forensic Sciences 56*(3):571–579

Benedix DC (2004) Differentiation of fragmented bone from Southeast Asia: the histological evidence. Phd thesis, The University of Tennessee, Knoxville

Biltz RM, Pellegrino ED (1969) The chemical anatomy of bone: a comparative study of bone composition in sixteen vertebrates, *Journal of Bone and Joint Surgery* 31A:456–466

Blanca MJ, Alarcón R, Arnau J, Bono R, Bendayan R (2017) Non-normal data: is ANOVA still a valid option?, *Psicothema* 29(4):552-557

Blau S, Briggs CA (2011) The role of forensic anthropology in Disaster Victim Identification (DVI), *Forensic Science International* 205:29-35

Bond JM (1996) Burnt Offerings: Animal Bone in Anglo-Saxon Cremations, *World Archaeology*, 28:76-88

Booth TJ, Madgwick R (2016) New evidence for diverse secondary burial practices in Iron Age Britain: a histological case study, *Journal of Archaeological Science* 67: 14–24

Bourrin S, Toromanoff A, Ammann P, Bonjour JP, Rizzoli R (2000) Dietary protein deficiency induces osteoporosis in aged male rats, *Journal of Bone and Mineral Research* 15(8):1555–1563

Bradley OC (1959) Topographical anatomy of the dog. Macmillan. New York

Bradtmiller B, Buikstra JE (1984) Effects of burning on human bone microstructure: a preliminary study, *Journal of Forensic Sciences* 29:535–540

Brandao-Burch A, Utting JC, Orriss IR, Arnett TR (2005) Acidosis inhibits bone formation by osteoblasts *in vitro* by preventing mineralization, *Calcified Tissue International* 77:167-174

Bratter P, Gawlik D, Lausch J, Rosick U (1977) On the distribution of trace elements in human skeleton, *Journal of Radioanalytical Chemistry* 37:393–403

Bridge CM, Powell J, Steele KL, Sigman ME (2007) Forensic comparative glass analysis by laser-induced breakdown spectroscopy, *Spectrochimica Acta Part B* 62:1419-1425

Brits D, Steyn M, L'Abbe EN (2014) A histomorphological analysis of human and non-human femora, *International Journal of Legal Medicine* 128(2):369– 377

Britz HM, Thomas CDL, Clement JG, Cooper DML (2009) The relation of femoral osteon geometry to age, sex, height and weight, *Bone* 45:77–83

Brogiolo GP, Mariotti V (2009) San Martino di Serravalle e San Bartolomeo De Castelàz. Due chiese di Valtellina: scavi e ricerche. Fondazione Gruppo Credito Valtellinese, Milano

Bromage TG, Goldman HM, McFarlin SC, Warshaw J, Boyde A, Riggs CM (2003) Circularly polarized light standards for investigations of collagen fiber orientation in bone, *The Anatomical Record* 274B(1):157–168

Brooks S, Suchey J (1990) Skeletal age determination base on the os pubis: a comparison of the Acsádi-Nemeskéri and Suchey– Brooks methods, *Journal of Human Evolution* 5:227–238

Brown KA, O'Donoghue K, Brown TA (1995) DNA in cremated bones from an early bronze age cemetery cairn, *International Journal of Osteoarchaeology* 5:181-187

Buckley M, Collins M, Thomas-Oates J, Wilson JC (2009) Species identification by analysis of bone collagen using matrix-assisted laser desorption/ionization time-of-flight mass spectrometry, *Mass Communications in Mass Spectrometry* 23:3843-3854

Buikstra JE, Ubelaker DH (1994) Standards for data collection from human skeletal remains: proceedings of a seminar at the field museum of natural history. Arkansas Archaeological Survey Press, Fayetteville

Bull G, Payne S (1982) Tooth eruption and epiphysial fusion in pigs and wild boar, in Wilson, Grigson, Payne:55-72

Burr DB (2002) Targeted and nontargeted remodeling, *Bone* 30(1):2–4

Burr DB, Martin RB, Schaffler MB, Radin EL (1985) Bone remodeling in response to in vivo fatigue microdamage, *Journal of Biomechanics* 18:189–200

Burr DB, Ruff CB, Thompson DD (1990) Patterns of skeletal histologic change through time: comparison of an Archaic Native American population with modern populations, *The Anatomical Record* 226:307–313

Burton P, Nyssen-Behets C, Dhem A (1989) Haversian bone remodeling in the human fetus, *Acta Anatomica* 135:171–175

Byard RW, James RA, Zucollo J (2001) Potential confusing arising from materials presenting as possible human remains, *The American Journal of Forensic Medicine and Pathology* 22(4):391-394

Byers SN (2017) Introduction to forensic anthropology, 5th edition. London: Routledge, Taylor & Francis Group

Byrd JE, Adams BJ (2003) Osteometric sorting of commingled human remains, *Journal of Forensic Sciences* 48(4):717–724

Caccia G, Magli F, Tagi VM, Porta DGA, Cummaudo M, Márquez-Grant N, Cattaneo C (2016) Histological determination of the human origin from dry bone: a cautionary note for subadults, *International Journal of Legal Medicine 130*(1):299–307

Carracedo A, Bär W, Lincoln P, Mayr W, Morling N, Olaisen B, Schneider P, Budowle B, Brinkmann B, Gill P, Holland M, Tully G, Wilson M (2000) DNA commission of the international society for forensic genetics: guidelines for mitochondrial DNA typing, *Forensic Science International* 110(2):79–85

Carter DR, Caler WE, Spengler DM, Frankel VH (1981) Uniaxial fatigue of human cortical bone. The influence of tissue physical characteristics, *Journal of Biomechanics* 14:461-470

Carter DR, Smith DJ, Spengler DM, Daly CH, Frankel VH (1980) Measurement and analysis of in vivo bone strains on the canine radius and ulna, *Journal of Biomechanics* 13:27-38

Carter Y, Thomas CDL, Clement JG, Peele AG, Hannah K, Cooper DML (2013) Variation in osteocyte lacunar morphology and density in the human femur - a synchrotron radiation micro-CT study, *Bone* 52(1):126–132

Cattaneo C (2007) Forensic anthropology: developments of a classical discipline in the new millennium, *Forensic Science International* 165:185-193

Cattaneo C, DiMartino S, Scali S, Craig OE, Grandi M, Sokol RJ (1999) Determining the human origin of fragments of burnt bone: A comparative study of histological, immunological and DNA techniques, *Forensic Science International 102*(2–3):181–191

Cattaneo C, Gelsthorpe K, Phillips P, Sokol RJ (1990) Blood in ancient human bone, *Nature* 347(6291):339

Cattaneo C, Gelsthorpe K, Phillips P, Sokol RJ (1992a) Reliable identification of human albumin in ancient bone using ELISA and monoclonal antibodies, *American Journal of Physical Anthropology* 87:366-372

Cattaneo C, Gelsthorpe K, Phillips P, Sokol RJ (1992b) Detection of blood proteins in ancient human bone using ELISA: a comparative study of the survival of IgG and albumin, *International Journal of Osteoarchaeology* 2:103-107

Cattaneo C, Gelsthorpe K, Phillips P, Sokol RJ (1994) Immunological detection of albumin in ancient human cremations using ELISA and monoclonal antibodies, *Journal of Archaeological Science* 21:565-571.

Cattaneo C, Mazzarelli D, Cappella A, Castoldi E, Mattia M, Poppa P, De Angelis D, Vitello A, Biehler-Gomez L (2018) A modern documented Italian identified skeletal collection of 2127 skeletons: the CAL Milano Cemetery Skeletal Collection, *Forensic Science International* 287:219.e1-219.e5

Cattaneo C, Porta D, Gibelli D, Gamba C (2009) Histological determination of the human origin of bone fragments, *Journal of Forensic Sciences* 54: 531-533

Cattaneo C, Grandi M (2004) Antropologia e Odontologia Forense. Guida allo studio dei resti umani, Monduzzi, Bologna

Cho H, Stout S, Madsen RW, Streeter MA (2002) Population-specific histological age-estimating method: a model for known African-American and European-American skeletal remains, *Journal of Forensic Sciences* 47(1):12–18

Christensen AM, Passalacqua N, Bartelink EJ (2014) Forensic anthropology: current methods and practice, first edition. Oxford, United Kingdom, Academic Press

Collins K, Vass A (2003) Elemental characterization of skeletal remains using laser-induced breakdown spectroscopy (LIBS). Student Abstracts: Biology at ORNL. Workforce Development for Teachers and Scientists (WDTS), US Department of Energy

Collins MJ, Nielsen-Marsh CM, Hiller J, Smith CI, Roberts JP (2002) The survival of organic matter in bone: a review, *Archaeometry* 44:383-394

Crescimanno A, Stout SD (2012) Differentiating fragmented human and nonhuman long bone using osteon circularity, *Journal of Forensic Sciences* 57(2):287–294

Crowder C (2005) Evaluating the use of quantitative bone histology to estimate adult age at death. Doctoral dissertation, University of Toronto, Ontario, Canada

Cuijpers SA (2006) Histological identification of bone fragments in archaeology. Telling humans apart from horses and cattle, *International Journal of Osteoarchaeology* 16:465–480

Cuijpers SA (2009) Distinguishing between the bone fragments of medium-sized mammals and children. A histological identification method for archaeology, *Anthropologischer Anzeiger* 67(2):181–203

Cummaudo M, Cappella A, Biraghi M, Raffone C, Màrquez-Grant N, Cattaneo C (2018) Histomorphological analysis of the variability of the human skeleton: forensic implications, *International Journal of Legal Medicine* 132(5):1493-1503

Currey JD (1959) Differences in the tensile strength of bone of different histological types, *Journal of Anatomy* 93:87-95

Currey JD (1960) Differences in the blood-supply of bone of different histological types, *Journal of Cell Science* s3-101:351-370

Currey JD (1964) Some effects of ageing in human Haversian systems, *Journal of Anatomy* 98(1):69-75

Currey JD (1981) What is bone for? Property–function relationships in bone. In: Cowin SC (ed.), Mechanical properties of bone. New York: American Society of Mechanical Engineers:13–26

Currey JD (2002) Bones. Structure and mechanics, 2nd edition. Princeton University Press. Princeton, New Jersey

Currey JD (2003) The many adaptations of bone, *Journal of Biomechanics* 36(10):1487-1495

Davoren J, Vanek D, Konjhodzic R, Crews J, Huffine E, Parson TJ (2007) Highly Effective DNA Extraction Method for Nuclear Short Tandem Repeat Testing of Skeletal Remains from Mass Graves. Croatian Medical Journal 48:478-485

Dawnay N, Oqden R, McEwing R, Carvalho GR, Thorpe RS (2007) Validation of the barcoding gene COI for use in forensic genetic species identification, *Forensic Science International* 173(1):1-6

de Margerie E, Cubo J, Castanet J (2002) Bone typology and growth rate: testing and quantifying 'Amprino's rule' in the mallard (Anas platyrhynchos), *Comptes Rendus Biologies* 325:221–230

de Margerie E, Robin J-P, Verrier D, Cubo J, Groscolas R, Castanet J (2004) Assessing a relationship between bone microstructure and growth rate: a fluorescent labelling study in the King Penguin chick (Aptenodytes patagonicus), *Journal of Experimental Biology* 207:869–879

de Ricqlès A (1977) Recherches paléohistologiques sur les os longs des tétrapodes VII (deuxième partie, fin), *Annales de paléontologie* 63:133–60

Diaz CMC, Rajtová V (1975) Comparative study of lamellar bone in some Carnivora, *Folia Morphologica* 23(3):221–229

Dittman K (2003) Histomorphometrische untersuchung der knochenmikrostructur von primaten and haustieren mit dem ziel der speziesdentifikaton unter berücksichtingung von domestikationseffekten, *Anthropologischer Anzeiger* 61(2):175–188

Dixon R, Dawson L, Taylor D (2008) The experimental degradation of archaeological human bone by anaerobic bacteria and the implications for recovery of ancient DNA. In: *The 9th International Conference on Ancient DNA and Associated Biomolecules*, Pompeii, Italy

Dominguez VM, Crowder CM (2012) The utility of osteon shape and circularity for differentiating human and non-human Haversian bone, *American Journal of Physical Anthropology* 149(1):84–91

Dong P, Haupert S, Hesse B, Langer M, Gouttenoire PJ, Bousson V, Peyrin F (2014) 3D osteocyte lacunar morphometric properties and distributions in human femoral cortical bone using synchrotron radiation micro-CT images, *Bone* 60:172–185

DPR 10.09.90 n° 285, art. 43
http://presidenza.governo.it/USRI/ufficio_studi/normativa/D.P.R.%2010%20settembre%201990,%20n.%20285.pdf (accessed August 2018)

Edwards HGM (2004) Forensic applications of Raman spectroscopy to the nondestructive analysis of biomaterials and their degradation. In: Pye K, Croft DJ, editors. *Forensic geoscience: Principles, techniques, and applications*. London: The Geological Society of London 232:159-170

English Heritage (2013) Science and the dead: A guideline for the destructive sampling of archaeological human remains for scientific analysis.

http://www.archaeologyuk.org/apabe/pdf/Science_and_the_Dead.pdf (accessed August 2018)

Enlow D (1966) An evaluation of the use of bone histology in forensic medicine and anthropology. In: Evans FG (ed.), *Studies one the anatomy and function of bone and joints*. Springer, Berlin, Heidelberg: 93-112

Enlow DH (1963) Principles of bone remodeling. Springfield, IL: CC Thomas

Enlow DH (1975) A Handbook of Facial Growth. W. B. Saunders, Philadelphia

Enlow DH, Brown SO (1956) A comparative histological study of fossil and recent bone tissue, part I, *Texas Journal of Science* 7(4):405–443

Enlow DH, Brown SO (1957) A comparative histological study of fossil and recent bone tissue, part II, *Texas Journal of Science* 9(2):186–214

Enlow DH, Brown SO (1958) A comparative histological study of fossil and recent bone tissue, part III, *Texas Journal of Science* 10(2):187–230

Eriksen MF (1991) Histologic estimation of age at death using the anterior cortex of the femur, *American Journal of Physical Anthropology* 84:171-179

Evans FG (1976) Mechanical properties and histology of cortical bone from younger and older men, *The Anatomical Record* 185:1–12

Everts V, Delaissé JM, Korper W, Jansen DC, Tigchelaar-Gutter W, Saftig P, Beertsen W (2002) The bone lining cell: Its role in cleaning Howship's lacunae and initiating bone formation, *Journal of Bone Mineral Research* 17(1):77–90

Falsetti ABA (1999) Thousand Tales of Dead Men: The Forensic Anthropology Cases of William R. Maples, Ph. D., *Journal of Forensic Sciences* 44(4):682–686

Fenton TW, Birkby WH, Cornelison J (2003) A fast and safe nonbleaching method for forensic skeletal preparation, *Journal of Forensic Sciences* 48:1–3

Ferretti M, Muglia MA, Remaggi F, Canè V, Palumbo C (1999) Histomorphometric study on the osteocyte lacuno-canalicular network in animals of different species. II. Parallel-fibered and lamellar bones, *Italian Journal of Anatomy and Embryology* 104(3):121–131

Foote JS (1916) A contribution to the comparative histology of the femur, *Smithsonian Contributions to Knowledge* 35(3):1–242

France DL (2009) Human and Nonhuman Bone Identification: A Colour Atlas, Boca Raton (FL): CRC Press

France DL (2011) Human and Non-Human Bone Identification. A Concise Field Guide, Boca Raton (FL): CRC Press

France DL (2017) Comparative Bone Identification. Human Subadult to Nonhuman, Boca Raton (FL): CRC Press

Francillon-Vieillot H, de Buffrénil V, Castanet J, Géraudie J, Meunier FJ, Sire J, Zylberberg L, de Ricqlès A (1990) Microstructure and mineralization of vertebrate skeletal tissues. In: Carter JG (ed.), *Skeletal biomineralization: patterns, processes and evolutionary trends*. Van Nostrand Reinhold, New York:471–530

Franklin D, Marks MK (2017) Species: Human versus Nonhuman. In: Houck MM (ed.), *Forensic Anthropology*. London, United Kingdom, Academic Press:129-136

Frasca P, Harper RA, Katz JL (1977) Collagen fibre orientations in human secondary osteons, *Acta Anatomica* (Basel) 98:1-13

Freemont AJ (1993) Basic bone cell biology: a review, *International Journal of Experimental Pathology* 74:411–416

Frost H (1973) Bone modeling and skeletal modeling errors. Orthopaedic Lectures Volume IV. Charles C. Thomas, Springfield, IL

Frost HM (1964) The Laws of Bone Structure. Springfield, Thomas.

Frost HM (1985) Bone microdamage: Factors that impair its repair. In: Uhthoff HK (ed.), *Current Concepts in Bone Fragility*. Berlin: Springer:123–148

Frost HM (1990) Skeletal structural adaptations to mechanical usage (SATMU), *The Anatomical Record* 226(4):403-439

Gasser T, Kneip A, Binding A, Prader A, Molinari L (1991) The dynamics of linear growth in distance, velocity and acceleration, *Annals of Human Biology* 18:187–205

Georgia R, Albu I (1988) The Haversian canal network in the femoral compact bone in some vertebrates, *Morphologie et Embryologie* (Bucur) 34(3):155–159

Gibson VA, Stover SM, Gibeling JC, Hazelwood SJ, Martin RB (2006) Osteonal effects on elastic modulus and fatigue life in equine bone, *Journal of Biomechanics* 39:217–225

Gilmore RM (1949) The Identification and Value of Mammal Bones from Archaeologic Excavations, *Journal of Mammalogy* 30(2):163-169

Glass GV, Peckham PD, Sanders JR (1972) Consequences of failure to meet assumptions underlying the fixed effects analyses of variance and covariance, *Review of Educational Research* 42:237-288

Goldman HM, McFarlin SC, Cooper DM, Thomas CD, Clement JG (2009) Ontogenetic patterning of cortical bone microstructure and geometry at the human mid-shaft femur, *The Anatomical Record* (Hoboken) 292:48-64

Gosman JH (2012) Growth and Development. Morphology, Mechanisms, and abnormalities. In: Crowder C, Stout SD (eds.), *Bone histology: an anthropological perspective*. CRC Press, Boca Raton: 23-44

Grisbaum GA, Ubelaker DH (2001) An Analysis of Forensic Anthropology Cases Submitted to the Smithsonian Institution by the Federal Bureau of Investigation from 1962 to 1994 (No. 45). Smithsonian Institution Press: Washington, D. C.

Haglund WD, Sorg MH (1997) Forensic taphonomy: the postmortem fate of human remains. Boca Raton: CRC Press

Hansen HB, Damgaard PB, Margaryan A, Stenderup J, Lynnerup N, Willerslev E, Allentoft ME (2017) Comparing ancient DNA preservation in petrous bone and tooth cementum, *PLoS ONE* 12(1):1-18

Harsányi L (1993) Differential diagnosis of human and animal bone. In: Grupe G, Garland AN (eds.), *Histology of ancient human bone: methods and diagnosis*. Proceedings of the Palaeohistopathology Workshop; Ocober 3–5, 1990, Göttingten, Germany. London: Springer-Verlag:79–94

Harwell MR, Rubinstein EN, Hayes WS, Olds CC (1992) Summarizing Monte Carlo results in methodological research: The one- and two-factor fixed effects ANOVA cases, *Journal of Educational and Behavioral Statistics* 17:315-339

Havers C (1691) Osteologia nova, or some new observations of the bones. Printed for Samuel Smith, London

Havill LM (2004) Osteon remodeling dynamics in Macaca mulatta: normal variation with regard to age, sex and skeletal maturity, *Calcified Tissue International* 74:95–102

Hedges REM, Millard AR, Pike AWG (1995) Measurements and relationships of diagenetic alteration of bone from three archaeological sites, *Journal of Archaeological Science* 22(2):201–209

Heller M, Bergmann G, Deuretzbacher G, Dürselen L, Pohl M, Claes L, Haas NP, Duda GN (2001) Musculo-skeletal loading conditions at the hip during walking and stair climbing, *Journal of Biomechanics* 34:883–893

Heřt J, Přibylová E, Lišková M (1972) Reaction of bone to mechanical stimuli, *Acta anatomica* 82:218-230

Heřt J, Lišková M, Landgrot B (1969) Influence of the long-term, continuous bending on the bone, *Folia Morphologica* (Prague) 17:389-399

Hidaka S, Matsumoto M, Ohsako S, Toyoshima Y, Nishinakagawa H (1998) A histometrical study on the long bones of raccoon dogs, Nyctereutes procyonoides and badgers, Meles meles, *Journal of Veterinary Medical Science*, 60(3):323–326

Hiller LP, Stover SM, Gibson VA, Gibeling JC, Prater CS, Hazelwood SJ, Yeh OC, Martin RB (2003) Osteon pullout in the equine third metacarpal bone: Effects of ex vivo fatigue, *Journal of Orthopaedic Research* 21(3):481–488

Hillier ML, Bell LS (2007) Differentiating human bone from animal bone: A review of histological methods, *Journal of Forensic Sciences 52*(2):249–263

Hillson S (2003) *Mammal Bones and Teeth. An Introductory Guide to Methods of Identification*, Institute of Archaeology, University College London

Hobdell MH, Howe CE (1971) Variation in bone matrix volume associated with osteocyte lacunae in mammalian and reptilian bone, *Israel Journal of Medical Sciences* 7:492-493.

Höss M, Pääbo S (1993) DNA extraction from Pleistocene bones by a silica-based purification method, *Nucleic Acids Research* 21:3913-3914

Iscan MY, Loth SR, Wright RK (1984) Age estimation from the rib by phase analysis: white males, *Journal of Forensic Sciences* 29(4):1094–1104

Jans MME, Nielsen-Marsh CM, Smith CI, Collins MJ, Kars H (2004) Characterisation of microbial attack on archaeological bone, *Journal of Archaeological Science* 31(1): 87–95

Johnson LC (1966) The kinetics of skeletal remodeling, *Birth Defects Original Article Series* 2:66–142

Johnson VO, Beckett S, Márquez-Grant N (2017) Differentiating human versus non-human bone by exploring the nutrient foramen: implications for forensic anthropology, *International Journal of Legal Medicine* 131(6):1757-1763

Jowsey J (1966) Studies of Haversian systems in man and some animals, *Journal of Anatomy* 100(4):857–864

Keenan KE, Mears CS, Skedros JG (2017) Utility of osteon circularity for determining species and interpreting load history in primates and nonprimates, *American Journal of Physical Anthropology* 162(4):657-681

Kerley ER (1965) The microscopic determination of age in human bone, *American Journal of Physical Anthropology* 23:149–164

Kerley ER, Ubelaker DH (1978) Revisions in the microscopic method of estimating age at death in human cortical bone, *American Journal of Physical Anthropology* 49(4):545-546

King C, Birch W (2015) Assessment of maceration techniques used to remove soft tissue from bone in cut mark analysis, *Journal of Forensic Sciences* 60(1):124–135

Klein RG, Cruz-Uribe KC (1984) Interpreting NISPs, MNIs, Age/Sex Profiles, and Descriptive Statistics in Faunal Analysis. In: Butzer KW and Freeman LG (eds.), *The Analysis of Animal Bones from Archaeological Sites*. Prehistoric Archaeology and Ecology Series, The University of Chicago Press, Chicago:63-100

Köchl S, Niederstätte H, Parson W (2005) DNA extraction and quantification of forensic samples using the phenol-chloroform method and real-time PCR, *Methods of Molecular Biology* 297:13-30

Komar DA, Buikstra JE (2008) Forensic anthropology. Contemporary theory and practice, Oxford University Press

Koo TK, Li MY (2016) A guideline of selecting and reporting intraclass correlation coefficients for reliability research, *Journal of chiropractic medicine* 15:155-163

Lander SL, Brits D, Hosie M (2014) The effects of freezing, boiling and degreasing on the microstructure of bone, *HOMO* 65:131-142

Lanyon LE, Goodship AE, Pye CJ, MacFie JH (1982) Mechanically adaptive bone remodeling, *Journal of Biomechanics* 15:141-154

Lanyon LE, Magee PT, Baggott DG (1979) The relationship of functional stress and strain to the processes of bone remodeling: an experimental study on the sheep radius, *Journal of Biomechanics* 12:593-600

Larkin P (2011) Infrared and Raman spectroscopy. Waltham, MA: Elsevier

Lipson SF, Katz JL (1984) The relationship between elastic properties and microstructure of bovine cortical bone, *Journal of Biomechanics* 17(4):231-240

Liu D, Wagner HD, Weiner S (2000) Bending and fracture of compact circumferential and osteonal lamellar bone of the baboon tibia, *Journal of Material Science*: *Materials in Medicine* 11:49–60

Lix LM, Keselman JC, Keselman HJ (1996) Consequences of assumption violations revisited: A quantitative review of alternatives to the one-way analysis of variance F test, *Review of Educational Research* 66:579-619

Locke M (2004) Structure of long bones in mammals, *Journal of Morphology* 262:546–565

Locke M, Dean RL (2003) Vascular spaces in compact bone: a technique to correct a common misinterpretation of structure, *The American Biology Teacher* 65:701–707

Loreille OM, Diegoli TM, Irwin JA, Coble MD, Parsons TJ (2007) High efficiency DNA extraction from bone by total demineralization, *Forensic Science International* 1:191-195

Lowe JS, Anderson PG (2015) Stevens & Lowe's Human Histology, fourth edition. Elsevier/Mosby, Philadelphia (PA)

Lowenstein JM (1980) Species-specific proteins in fossils, *Naturwissenschaften* 67:343–346

Lowenstein JM, Sarich VM, Richardson BJ (1981) Albumin systematics of the extinct mammoth and Tasmanian Wolf, *Nature* 291:409–411

MacKinnon G, Mundorff AZ (2006) World Trade Center—September 11, 2001. In: Thompson TJU, Black SM (eds.),, *Forensic Human Identification: An Introduction*. CRC Press, Boca Raton, FL:485–499

Maggiano IS, Maggiano CM, Tiesler V, Kierdorf H, Stout SD, Schultz M (2011) A distinct region of microarchitectural variation in femoral compact bone: Histomorphology of the endosteal lamellar pocket, *International Journal of Osteoarchaeology* 21:743-750

Mairs S, Swift B, Rutty GN (2004) Detergent: an alternative approach to traditional bone cleaning methods for forensic practice, *The American Journal of Forensic Medicine and Pathology* 25:276-284

Majeska RJ (2001) Cell biology of bone. In: Cowin SC (ed.), *Bone Mechanics Handbook*, 2_{nd} edition. CRC Press. Boca Raton, Florida:(2)1-24

Malluche HH, Faugere MC (1990) Bone biopsies: histology and histomorphometry of bone. In: Avioli LV, Krane SM (eds.), *Metabolic bone disease*. London: WB Saunders:283–328

Maresh MM (1970) Measurements from roentgenograms. In: McCammon RW (ed.), *Human growth and development*, Springfield IL: C.C. Thomas:157:200

Marks MK (1995) William M. Bass and the Development of Forensic Anthropology in Tennessee, *Journal of Forensic Sciences* 40 (5):741–750

Marks MK, Marden K, Mileusnic-Polchan D (2009) Forensic osteology of child abuse. In: Steadman DW (ed.), *Hard Evidence: Case Studies in Physical Anthropology*, 2nd edn. Upper Saddle River, NJ: Prentice Hall:205–220

Marotti G (1979) Osteocyte orientation in human lamellar bone and its relevance to the morphometry of periosteocytic lacunae, *Metabolic Bone Disease & Related Research* 333:325–333

Marshall PL, Stoljarova M, Schmedes SE, King JL, Budowle B (2014) A high volume extraction and purification method for recovering DNA from human bone, *Forensic Science International* 12:155-160

Martin MZ, Labbé N, André N, Harris R, Ebinger M, Wullschleger SD, Vass AA (2007) High resolution applications of laser-induced breakdown spectroscopy for environmental and forensic applications, *Spectrochimica Acta Part B: Atomic Spectroscopy* 62:1426–1432

Martin RB (1991) On the significance of remodeling space and activation rate changes in bone remodeling, *Bone* 12:391–400

Martin RB (2000) Toward a unifying theory of bone remodeling, *Bone* 26(1):1–6

Martin RB (2002) Is all cortical bone remodeling initiated by microdamage?, *Bone* 30:8–13

Martin RB (2003) Fatigue damage, remodeling, and the minimization of skeletal weight, *Journal of Theoretical Biology* 220(2):271–276

Martin RB, Burr DB (1982) A hypothetical mechanism for the stimulation of osteonal remodeling by fatigue damage, *Journal of Biomechanics* 15:137-139

Martin RB, Burr DB (1989) Structure, function, and adaptation of compact bone. New York: Raven Press:105–142

Martin RB, Burr DB, Sharkey NA, Fyhrie DP (2015) Skeletal Tissue Mechanics, second edition. Springer Science+Business Media, New York

Martin RB, Gibson VA, Stover SM, Gibeling JC, Griffin LV (1996) Osteonal structure in the equine third metacarpus, *Bone* 19(2):165–171

Martiniaková M, Grosskopf B, Omelka R, Vondráková M, Bauerová M (2006a) Differences among species in compact bone tissue microstructure of mammalian skeleton: use of a discriminant function analysis for species identification, *Journal of Forensic Sciences* 51(6):1235-1239

Martiniaková M, Grosskopf B, Omelka R, Vondráková M, Bauerová M (2007) Histological analysis of ovine compact bone tissue, *Journal of Veterinary Medical Science* 69(4):409-411

Martiniaková M, Grosskopf B, Vondráková M, Omelka R, Fabiš M (2006b) Differences in femoral compact bone tissue microscopic structure between adult cows (Bos taurus) and pigs (Sus scrofa domestica), *Journal of Veterinary Medicine Series C: Anatomia Histologia Embryologia* 35(3):167–170

Martiniaková M, Vondráková M, Fabiš M (2003) Investigation of the microscopic structure of rabbit compact bone tissue, *Scripta Medica* 76(4):215–220

McCullough French K, Mavroudas SR, Dominguez VM (2015) Prevalence of drifting osteons across mammalian species, *The 84$_{th}$ Annual Meeting of the American Association of Physical Anthropologists* (poster abstract)

McFarlin SC, Terranova CJ, Zihlman AL, Enlow DH, Bromage TG (2008) Regional variability in secondary remodeling within long bone cortices of catarrhine primates: the influence of bone growth dynamics, *Journal of Anatomy* 213:308–324

McLaughlin G, Lednev IK (2012) Spectroscopic discrimination of bone samples from various species, *American Journal of Analytical Chemistry* 3:161–167

Mittleman RE, Barnhart JS, Davis JH, Fernandez R, Hyman BA, Lengel RD, Lew EO, Rao VJ (2000) The Crash of ValuJet Flight 592: A Forensic Approach to Severe Body Fragmentation. Miami-Dade County Medical Examiner Department, Miami, FL

Mori R, Kodaka T, Sano T, Yamagishi N, Asari M, Naito Y (2003) Comparative histology of the laminar bone between young calves and foals, *Cells Tissues Organs* 175(1):43–50

Morris ZH (2007) Quantitative and spatial analysis of the microscopic bone structures of deer (Odocoileus virginianus), dog (Canis familiaris), and pig (Sus scrofa domesticus).

M.A. thesis. Louisiana State University and Agricultural and Mechanical College. Baton Rouge, LA

Moyle DD, Welborn III JW, Cooke FW (1978) Work to fracture of canine femoral bone, *Journal of Biomechanics* 11:435–40

Mulhern DM (2000) Rib remodeling in a skeletal population from Kulubnarti, Nubia, *American Journal of Physical Anthropology* 111:519–530

Mulhern DM, Ubelaker DH (2001) Differences in osteon banding between human and nonhuman bone, *Journal of Forensic Sciences 46*(2):220–222

Mulhern DM, Ubelaker DH (2003) Histological examination of bone development in juvenile chimpanzees, *American Journal of Physical Anthropology* 122(2):127–33

Mulhern DM, Ubelaker DH (2012) Differentiating human from nonhuman bone microstructure. In: Crowder C, Stout SD (eds.), *Bone histology: an anthropological perspective*. CRC Press, Boca Raton: 109-134

Mulhern DM, Van Gerven DP (1997) Patterns of femoral bone remodeling dynamics in a Medieval Nubian population, *American Journal of Physical Anthropology* 104:133–146

Müller K, Chadefaux C, Thomas N, Reiche I (2011) Microbial attack of archaeological bones versus high concentrations of heavy metals in the burial environment. A case study of animal bones from a mediaeval copper workshop in Paris, *Palaeogeography, Palaeoclimatology, Palaeoecology* 310(1–2):39–51

Mundorff AZ (2012) Integrating forensic anthropology into disaster victim identification, *Forensic Science, Medicine and Pathology* 8:131-139

Mundorff AZ (2014) Anthropologist-Directed Triage: Three Distinct Mass Fatality Events Involving Fragmentation and Commingling of Human Remains. In: Adams BJ, Byrd JE (eds.), *Recovery Analysis, and Identification of Commingled Human Remains*, Humana Press, New York:365-388

Nawrocki SP (2007) Cleaning bones. University of Indianapolis Archaeology and Forensics Laboratory, http://archlab.uindy.edu/documents/Clea- ningBones.pdf (accessed August 2018)

Nelson R (1992) A microscopic comparison of fresh and burned bone, *Journal of Forensic Sciences* 37:1055–1056

Netter FH (2014) Atlas of Human Anatomy, 6th edition. Saunders, Elsevier. Philadelphia, PA

Nijweide PJ, Burger EH, Klein-Nulend J (2002) The osteocyte. In: Bilezikian JP, Raisz LG, Rodan GA (eds.), *Principles of Bone Biology*, 2nd edition. San Diego: Academic Press:93–107

O'Brien F, Taylor D, Lee CT (2005) The effect of bone microstructure on the initiation and growth of microcracks, *Journal of Orthopaedic Research* 23(2):475–480

Outram AK, Knüsel CJ, Knight S, Harding AF (2005) Understanding Complex Fragmented Assemblages of Human and Animal Remains: A Fully Integrated Approach, *Journal of Archaeological Science* 32:1699–1710

Owsley DW, Mires AM, Keith MS (1985) Case involving differentiation of deer and human bone fragments, *Journal of Forensic Sciences* 30(2):572–578

Owsley DW, Roberts DE, Manning EM (1992) Field recovery and analysis of horse skeletal remains, *Journal of Forensic Sciences* 37(1):163–175

Pagan F, Lim C, Keglovic M, McNevin D (2012) Comparison of DNA extraction methods for identification of human remains, *Australian Journal of Forensic Sciences* 44(2):117-127

Parfitt A (1983) The physiologic and clinical significance of bone histomorphometric data. In: Recker RR (ed.), *Bone histomorphometry: techniques and interpretation*. Boca Raton: CRC Press:143-266

Parfitt AM (2002) Targeted and nontargeted bone remodeling: relationship to basic multicellular unit origination and progression, *Bone* 30(1):5-7

Parfitt AM (2005) Targeted and nontargeted remodeling: Relationship to basic multicellular unit organization and progression, *Bone* 30(1):5–7

Pereira F, Carneiro J, van Asch B (2010) A guide for mitochondrial DNA analysis in non-human forensic investigations, *The Open Forensic Science Journal* 3:33-44

Pfeiffer S (1996) Cortical bone histology in juveniles. Microscopic examinations of bioarchaeological remains: keeping a close eye on ancient tissues. In: Grupe G and Peters J (eds.), *Documenta Archaeobiologiae Band 4*, Veriag Marie Leidorf GmbH, Rahden/Westf

Pfeiffer S (1998) Variability in osteon size in recent human populations, *American Journal of Physical Anthropology* 106:219–222

Pfeiffer S, Crowder C, Harrington L, Brown M (2006) Secondary osteon and Haversian canal dimensions as behavioral indicators *American Journal of Physical Anthropology* 131:460–468

Pirok DJ, Ramser JR, Takahashi H, Villanueva AR, Frost HM (1966) Normal histological, tetracycline and dynamic parameters in human, mineralized bone sections, *Henry Ford Hospital Medical Bulletin* 14:195–218

Pokines JT (2015) Identification of nonhuman remains received in a medical examiner setting, *Journal of Forensic Identification* 65(3):223-246

Portney LG, Watkins MP (2000) Foundations of clinical research: applications to practice. New Jersey: Prentice Hall

Potter A, Reuther JD, Lowenstein JM, Scheuenstuhl G (2010) Assessing the reliability of pRIA for identifying ancient proteins from archaeological contexts, *Journal of Archaeological Science* 37:910-918

Przybeck TR (1985) Histomorphology of the rib: bone mass and cortical remodeling. In: Davis RT and Leathers CW (eds.), *Behavior and pathology of aging in rhesus monkeys*. Alan R. Liss, New York

Qiu S, Fyhrie DP, Palnitkar S, Rao DS (2003) Histomorphometric assessment of Haversian canal and osteocyte lacunae in different-sized osteons in human rib, *The Anatomical Record* 272A:520–525

Qiu S, Rao DS, Palnitkar S, Parfitt AM (2006) Differences in osteocyte and lacunar density between Black and White American women, *Bone* 38:130-135

Qiu S, Rao DS, Palnitkar S, Parfitt AM (2010) Dependence of Bone Yield (Volume of Bone Formed per Unit of Cement Surface Area) on Resorption Cavity Size During Osteonal Remodeling in Human Rib: Implications for Osteoblast Function and the Pathogenesis of Age-Related Bone Loss, *Journal of Bone Mineral Research*, 25(2):423-430

Quekett J (1849) On the intimate structure of bone as composing the skeleton in the four great classes of animals: mammals, birds, reptiles, and fishes, with some remarks on the great value of the knowledge of such structure in determining the affinities of minute fragments of organic remains, *Transactions of the Microscopical Society of London* 2:40–42

Rajtová V, Briancin J, Kokardova M (1995) Lamellar bone structure in small ruminants, *Folia Veterinaria* 39: 59–64

Reid R, Roberts F, MacDuff E (2011) Pathology Illustrated, seventh edition. Churchill Livingstone

Reilly DT, Burstein AH (1975) The elastic and ultimate properties of compact bone tissue, *Journal of Biomechanics* 8:393–405

Reilly GC, Currey JD (2000) The effects of damage and microcracking on the impact strength of bone, *Journal of Biomechanics* 33:337–343

Reinecke GW, Hochrein MJ (2008) Pieces of the Puzzle: FBI Evidence Response Team approaches to Scenes with Commingled Evidence. In: Adams BJ, Byrd JE (eds.), *Recovery, Analysis, and Identification of Commingled Human Remains*. Humana Press

Remaggi F, Canè V, Palumbo C, Ferretti M (1998) Histomorphometric study on the osteocyte lacuno-canalicular network in animals of different species. I. Woven-fibered and parallel-fibered bones, *Italian Journal of Anatomy and Embryology* 103(4):145-155

Rerolle C, Saint-Martin P, Dedouit F, Rousseau H, Telmon N (2013) Is the corticomedullary index valid to distinguish human from nonhuman bones: a multislice computed tomography study, *Forensic Science International* 231(1-3):406.e 1-5

Rho J, Kuhn-Spearing L, Zioupos P (1998) Mechanical Properties and the Hierarchical Structure of Bone, *Medical Engineering & Physics* 20(2):92-102

Riggs CM, Lanyon LE, Boyde A (1993) Functional associations between collagen fibre orientation and locomotor strain direction in cortical bone of the equine radius, *Anatomy and Embryology* 187:231-238

Robling AG, Castillo AB, Turner CH (2006) Biomechanical and molecular regulation of bone remodeling, *Annual Review of Biomededical Engeneering* 8(1):455–498

Robling AG, Stout SD (1999) Morphology of the drifting osteon, *Cells Tissues Organs* 164:192-204

Robling AG, Stout SD (2008) Histomorphometry of human cortical bone: applications to age estimation. In: Katzenberg MA and Saunders SR (eds.) *Biological Anthropology of the Human Skeleton*, 2nd edition. Wiley & Sons.

Romanus B (1974) Physical properties and chemical content of canine femoral cortical bone in nutritional osteopenia, *Acta Orthopaedica Scandinavica*, supplement 155

Rougé-Maillart C, Vielle B, Jousset N, Chappard D, Telmon N, Cunha E (2009) Development of a method to estimate skeletal age at death in adults using the acetabulum

and the auricular surface on a Portuguese population, *Forensic Science International* 188(1–3):91–95

Ruff C (2003) Growth in bone strength, body size, and muscle size in a juvenile longitudinal sample, *Bone* 33:317–329

Russo GA, Kirk EC (2013) Foramen magnum position in bipedal mammals, *Journal of Human Evolution 65*(5):656–670

Sajantila A, Ström M, Budowle B, Karhunen PJ, Peltonen L (1991) The polymerase chain reaction and post-mortem forensic identity testing: application of amplified D1S80 and HLA-DQa loci to the identification of fire victims, *Forensic Science International* 51:23–34

Sauer NJ, Lackey MWL (2000) Anthropology: skeletal analysis. In: Siegel JA, Saukko PJ, Knupfer GC (eds.), *Encyclopaedia of Forensic Sciences*:261–270

Saulsman B, Oxnard CE, Franklin D (2010) Long bone morphometrics for human from non-human discrimination, *Forensic Science International* 202(1-3):110.e1-5

Schaffler MB, Burr DB (1984) Primate cortical bone microstructure: relationship to locomotion, *American Journal of Physical Anthropology* 65:191–197

Schaffler MB, Choi K, Milgrom C (1995) Aging and matrix microdamage accumulation in human compact bone, *Bone* 17(6):521-525

Schaffler MB, Kennedy OD (2012) Osteocyte signaling in bone, *Current Osteoporosis Reports* 10(2):118-125

Shipman P, Foster G, Schoeninger M (1984) Burnt bones and teeth: an experimental study of color, morphology, crystal structure and shrinkage, *Journal of Archaeological Science* 2:307–325

Sigman ME (2010) Application of laser-induced breakdown spectroscopy to forensic science: analysis of paint and glass samples, *Final Technical Report*, US Department of Justice

Singh IJ, Tonna EA, Gandel CP (1974) A comparative histological study of mammalian bone, *Journal of Morphology* 144:421-438

Singh VK, Rai AK (2011) Prospects for laser-induced breakdown spectroscopy for biomedical applications: A review, *Lasers in Medical Science* 26:673-687

Siriboonpiputtana T, Rinthachai T, Shotivaranon J, Peonim V, Rerkamnuaychoke B (2018) Forensic genetic analysis of bone remain samples, *Forensic Science International* 284:167-175

Skedros JG (2012) Interpreting load history in limb-bone diaphyses. Important considerations and their biomechanical foundations. In: Crowder C, Stout SD (eds.), *Bone histology: an anthropological perspective*. CRC Press, Boca Raton:153-220

Skedros JG, Baucom SL (2007) Mathematical analysis of trabecular "trajectories" in apparent trajectorial structures: the unfortunate historical emphasis on the human proximal femur, *Journal of Theoretical Biology* 244(1):15–45

Skedros JG, Grunander TR, Hamrick MW (2005) Spatial distribution of osteocyte lacunae in equine radii and third metacarpals: considerations for cellular communication, microdamage detection and metabolism, *Cells Tissues Organs* 180:215-36

Skedros JG, Hunt KJ, Bloebaum RD (2004) Relationships of loading history and structural and material characteristics of bone: development of the mule deer calcaneus, *Journal of Morphology* 259(3):281-307

Skedros JG, Mason MW, Bloebaum RD (1994) Differences in osteonal micromorphology between tensile and compressive cortices of a bending skeletal system: indications of potential strain-specific differences in bone microstructure, *The Anatomical Record* 239:405–413

Skedros JG, Mendenhall SD, Kiser CJ, Winet H (2009) Interpreting cortical bone adaptation and load history by quantifying osteon morphotypes in circularly polarized light images, *Bone* 44(3):392–403

Skedros JG, Sybrowsky CL, Parry TR, Bloebaum RD (2003) Regional differences in cortical bone organization and microdamage prevalence in Rocky Mountain mule deer, *The Anatomical Record* 274A:837–850

Sledzik PS, Dirkmaat D, Mann RW, Holland TD, Mundorff AZ, Adams BJ, Crowder CM, DePaolo F (2009) Disaster victim recovery and identification. Forensic anthropology in the aftermath of September 11. In: Steadman DW (ed.), *Hard evidence. Case studies in forensic anthropology*, Upper Saddle River (NJ). Pearson Education:289-302

Smith SL, Buschang PH (2004) Variation in longitudinal diaphyseal long bone growth in children three to ten years of age, *Annals of Human Biology* 16:648–657

Stout SD (2009) Small bones of contention. In: Steadman DW (ed.), *Hard Evidence: Case Studies in Physical Anthropology*, 2nd edn, Upper Saddle River, NJ. Prentice Hall:239–247

Stout SD, Crowder C (2012) Bone remodeling, histomorphology, and histomorphometry. In: Crowder C, Stout SD (eds.), *Bone histology: an anthropological perspective*. CRC Press, Boca Raton:1– 21

Stout SD, Lueck R (1995) Bone remodeling rates and skeletal maturation in three archaeological skeletal populations, *American Journal of Physical Anthropology* 98:161–171

Stover SM, Pool RR, Martin RB, Morgan JP (1992) Histological features of the dorsal cortex of the third metacarpal bone mid-diaphysis during postnatal growth in thoroughbred horses, *Journal of Anatomy* 181:455–469

Tabachnick BG, Fidell LS (2012) Using multivariate statistics (6th ed). Boston, MA: Pearson

Taylor D, Kuiper JH (2001) The prediction of stress fractures using a stressed volume concept, *Journal of Orthopaedic Research* 19(5):919-926

Taylor D, O'Reilly P, Vallet L, Lee TC (2003) The fatigue strength of compact bone in torsion. *Journal of Biomechanics* 36(8):1103–1109

Tersigni MA (2007) Frozen human bone: a microscopic investigation, *Journal of Forensic Sciences* 52(1):16-20

Tersigni MTA (2008) Osteon area and circularity: A method for the assessment for human and non-human fragmentary remains. Abstract. *Proceedings of the American Academy of Forensic Sciences*. Annual Meeting, Washington DC, 14:375

Tersigni-Tarrant MA, Shirley NR (2013) Brief History of Forensic Anthropology. In: Tersigni-Tarrant MA, Shirley NR (eds.), *Forensic Anthropology. An Introduction*, Boca Raton, FL. CRC Press:1-16

Theobald FV (1899) A text-book of agricultural zoology, William Blackwood: Edinburgh & London

Thompson DD (1980) Age changes in bone mineralization, cortical thickness and Haversian canal area, *Calcified Tissue International* 31:5–11

Thompson T (2015) The archaeology of cremation: burned human remains in funerary studies. Oxbow Books, Philadelphia

Thorup VM, Tøgersen FA, Jørgensen B, Jensen BR (2007) Biomechanical gait analysis of pigs walking on solid concrete floor, *Animal* 1:708-715

Turner CH, Wang T, Burr DB (2001) Shear strength and fatigue properties of human cortical bone determined from pure shear tests, *Calcified Tissue International* 69:373–378

Ubelaker DH (1979) Human Skeletal Remains: Excavation, Analysis and Interpretation. Washington, DC: Smithsonian Institute Press

Ubelaker DH (2000) The Forensic Anthropology Legacy of T. Dale Stewart (1901–1997), *Journal of Forensic Sciences* 45(2):245–252

Ubelaker DH, Scammell H (1992) Bones: a forensic detective's casebook, 1st edition. New York, NY: Edward Burlingame Books

Uhre ML, Eriksen AM, Simonsen KP, Rasmussen AR, Hjort BB, Lynnerup N (2015) Enzymatic maceration of bone: a gentler technique than boiling, *Medicine, Science and the Law* 55(2):90-96

Urbanová P, Novotný V (2005) Distinguishing between human and non-human bones: histometric method for forensic anthropology, *Anthropologie* 43:77–85

van Oers RFM, Ruimerman R, Tanck E, Hilbers PA, Huiskes R (2008) A unified theory for osteonal and hemi-osteonal remodeling, *Bone* 42(2):250–259

van Oers RFM, Wang H, Bacabac RG (2015) Osteocyte shape and mechanical loading, *Current Osteoporosis Reports* 13:61-66

Vass AA, Martin M, Synstelien J, Collins K (2005) Elemental characterization of skeletal remains using laser-induced breakdown spectroscopy (LIBS), *Proceedings of the American Academy of Forensic Sciences* 11:307-308

Vatsa A, Breuls RG, Semeins CM, Salmon PL, Smit TH, Klein-Nulend J (2008) Osteocyte morphology in fibula and calvaria—is there a role for mechanosensing?, *Bone* 43:452–458

Virkler K, Lednev IK (2009a) Analysis of body fluids for forensic purposes: From laboratory testing to non-destructive rapid confirmatory identification at a crime scene, *Forensic Science International* 188:1-17

Virkler K, Lednev IK (2009b) Blood species identification for forensic purposes using Raman spectroscopy combined with advanced statistical analysis, *Analytical Chemistry* 81(18):7773-7777

Von Wachenfelt H, Nilsson CJ, Pinzke S (2010) Gait and force analysis of provoked pig gait on clean and fouled rubber mat surfaces, *Biosystems Engeneering* 106, 86–96

Walsh PS, Metzger DA, Higuchi R (1991) Chelex-100 as a medium for simple extraction of DNA for PCR-based typing from forensic material, *Biotechniques* 10(4):506-513

Waseda Y, Matsubara E, Shinoda K (2011) X-ray diffraction crystallography: Introduction, examples, and solved problems. Berlin: Springer

Weiner S, Traub W (1992) Bone structure: from angstroms to microns, *FASEB* 6:879–885

Weiner S, Traub W, Wagner HD (1999) Lamellar bone: structure-function relations, *Journal of Structural* Biology 126:241–55

White TD, Folkens PA (2005) The Human Bone Manual. Elsevier Academic Press, San Diego, CA

Whitman EJ (2004) Differentiating between human and non-human secondary osteons in human, canine and bovine rib tissue [thesis]. East Lansing, MI: Michigan State University

Yin L, Vekatesan S, Kalyanasundaram S, Qin Q (2010) Influence of enzymatic maceration on the microstructure and microhardness of compact bone, *Biomedical Materials* 5(1):15006

Young DR, Niklowitz WJ, Brown RJ, Jee WSS (1986) Immobilization-associated osteoporosis in primates, *Bone* 7:109-117

Zerwekh JE (1992) Bone metabolism, *Seminars in Nephrology* 12:79–90

Zimmermann HA, Schultz JJ, Sigman ME (2014) Preliminary validation of handheld X-ray fluorescence (HHXRF) spectrometry: distinguishing osseous and dental tissue from non-bone material of similar chemical composition, *Journal of Forensic Sciences* 60(2):382-390

Zoetis T, Tassinari MS, Bagi C, Walthall K, Hurtt ME (2003) Species Comparison of Postnatal Bone Growth and Development, *Birth Defects Research Part B - Developmental and Reproductive Toxicology* 68(2):86–110

APPENDIX A

WHOLE SLIDE IMAGES OF HUMAN ADULT (HA1) CROSS-SECTIONS

This appendix includes the whole slide images of human adult (HA1) cross-sections

Table A.1 provides a legend of the abbreviation used to indicate the different aspect of each bone and the type of tissue observed.

Abbreviation	**Directional term (aspect)**
A	anterior
P	posterior
M	medial
L	lateral
D	dorsal
P	palmar
S	superior
I	inferior
Abbreviation	**Type of tissue**
Irregular Haversian bone	
IH	Scattered secondary osteon in a lamellar matrix
IHcr	Scattered secondary osteons organized in circumferential rows
Dense Haversian bone	
DH	Tightly packed secondary osteons
DHcr	Tightly packed secondary osteons organized in circumferential rows
Lamellar tissue	
LT	Lamellar tissue
aLT	Avascular lamellar tissue
LTlo	Lamellar tissue with longitudinal vascular canals
LTra	Lamellar tissue with radial vascular canals
LTcr	Lamellar tissue with circumferential vascular canals
LTret	Lamellar tissue with reticular vascular canals
RC	Resorption cavities

Table A.1 – Legend of the abbreviations used in the whole slide images

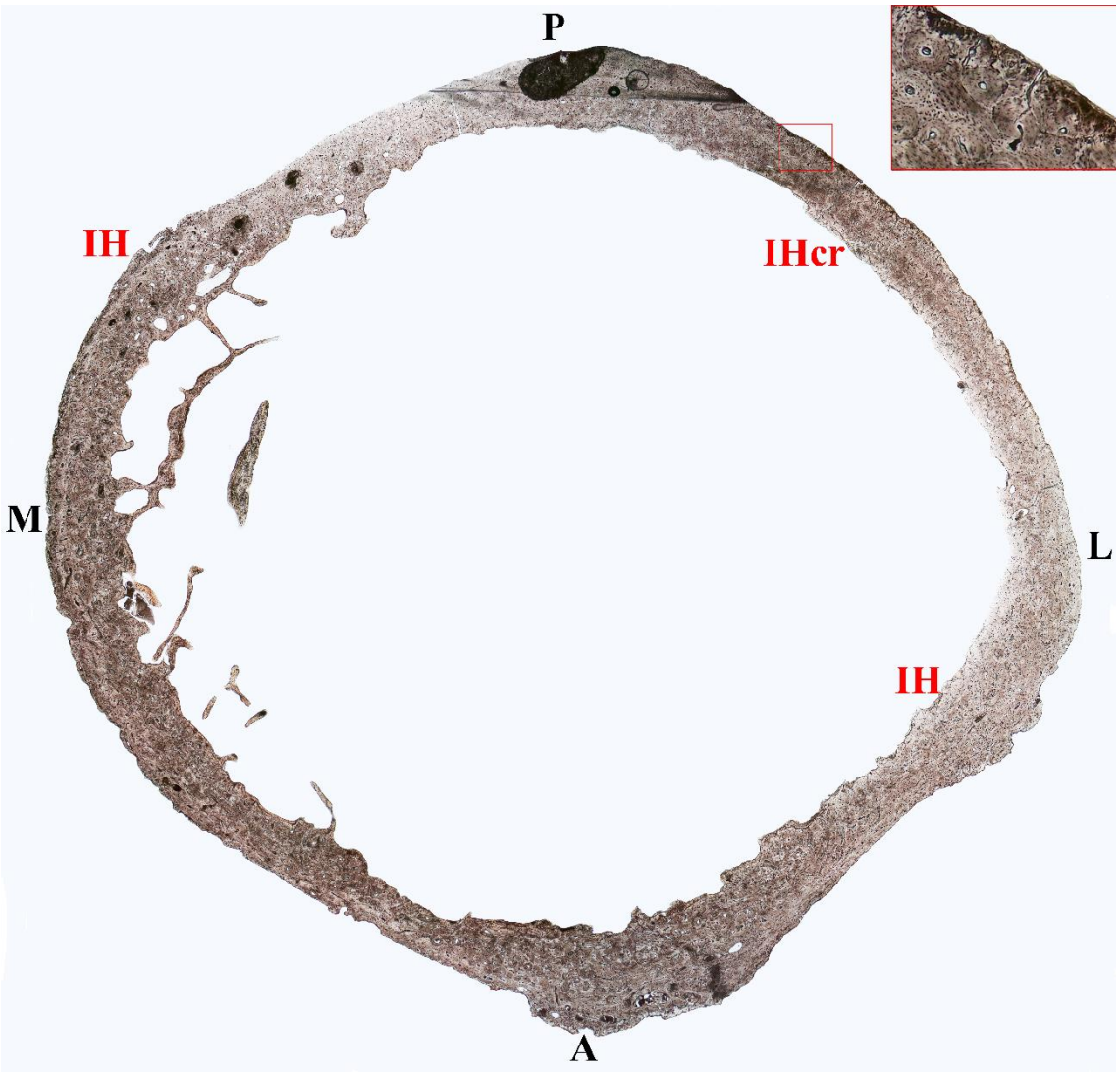

Figure A.1 – Human adult (HA1) – Humerus (proximal metaphysis)

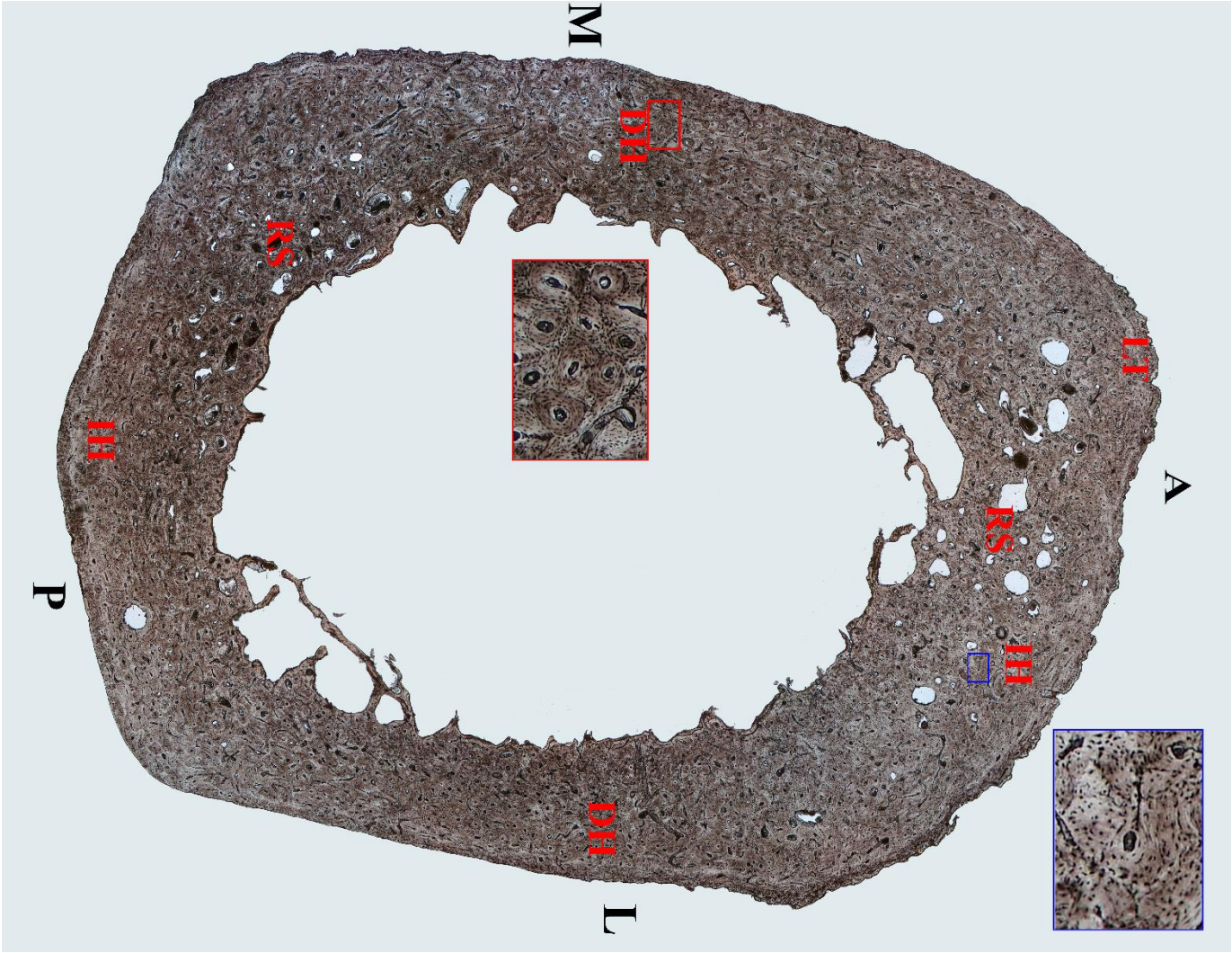

Figure A.2 – Human adult (HA1) – Humerus (diaphysis)

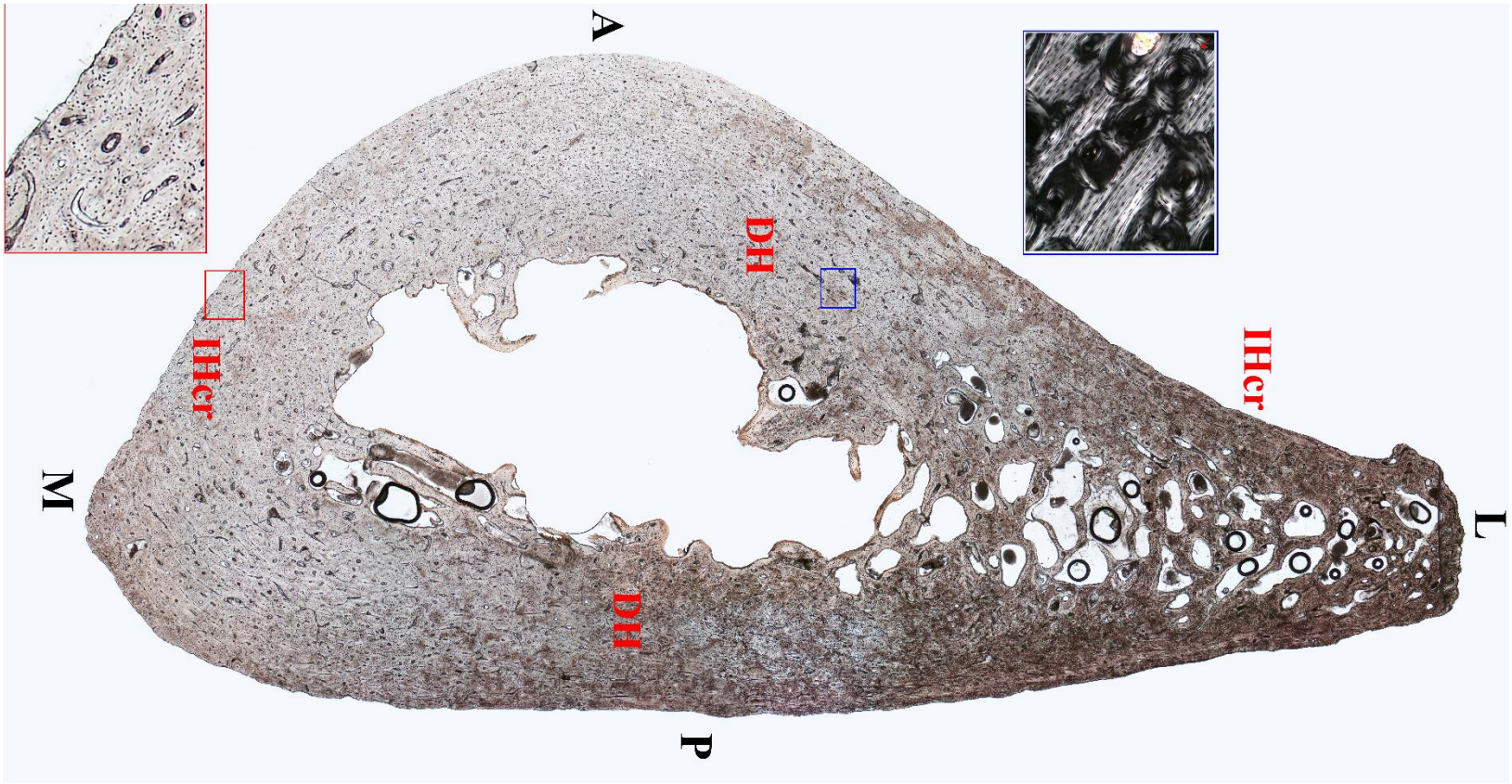

Figure A.3 – Human adult (HA1) – Humerus (distal metaphysis)

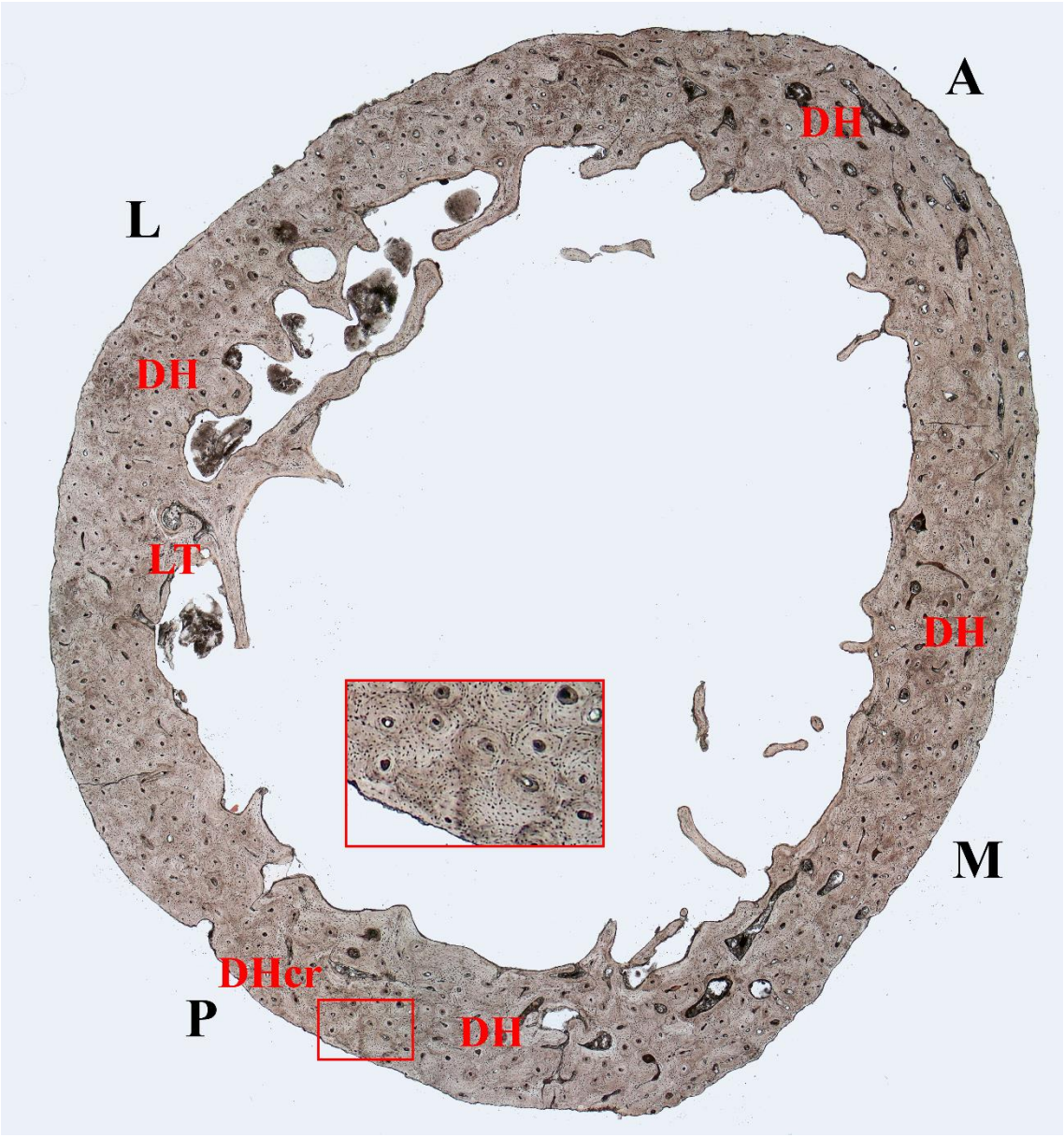

Figure A.4 – Human adult (HA1) – Radius (proximal metaphysis)

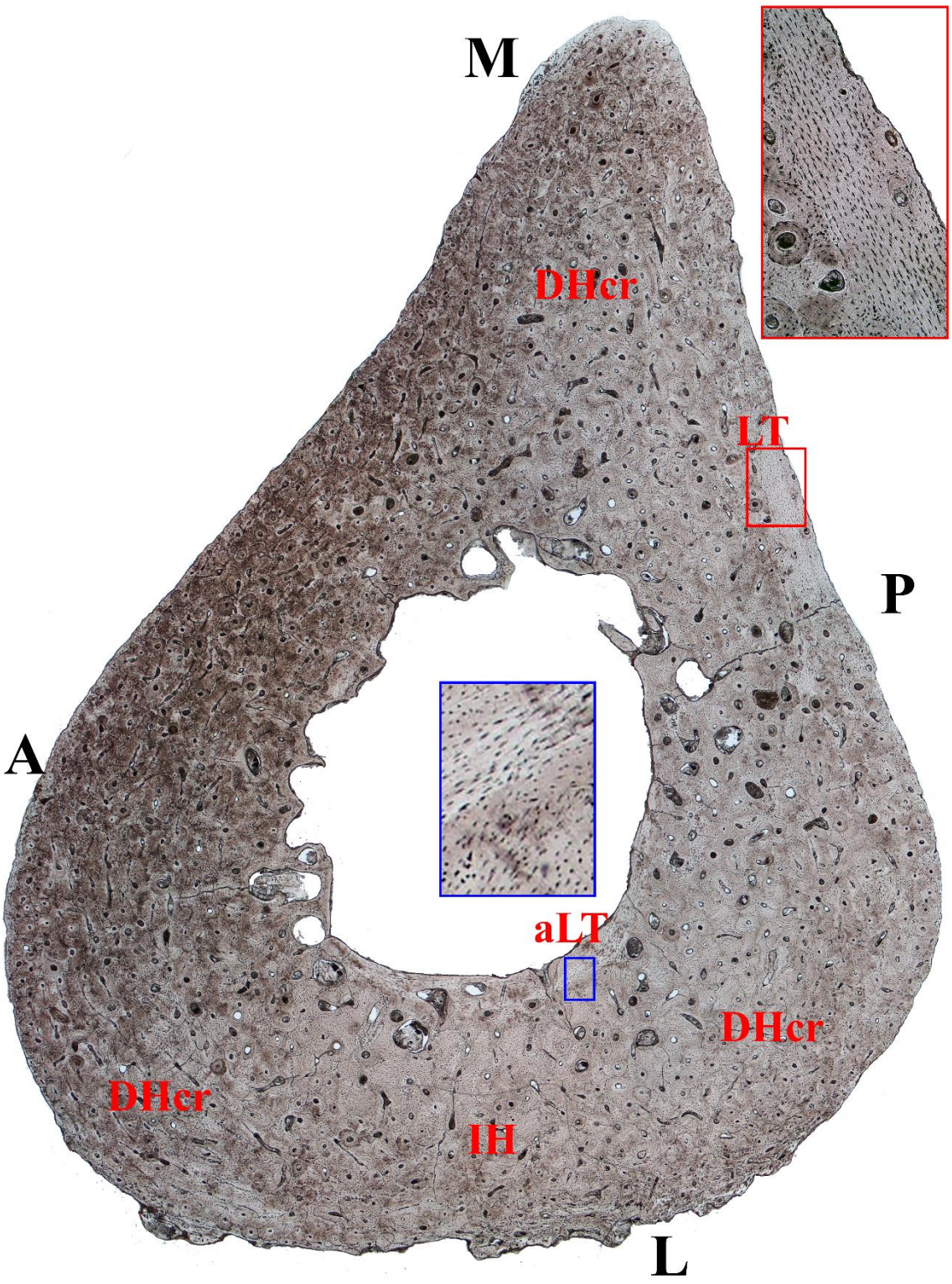

Figure A.5 – Human adult (HA1) – Radius (diaphysis)

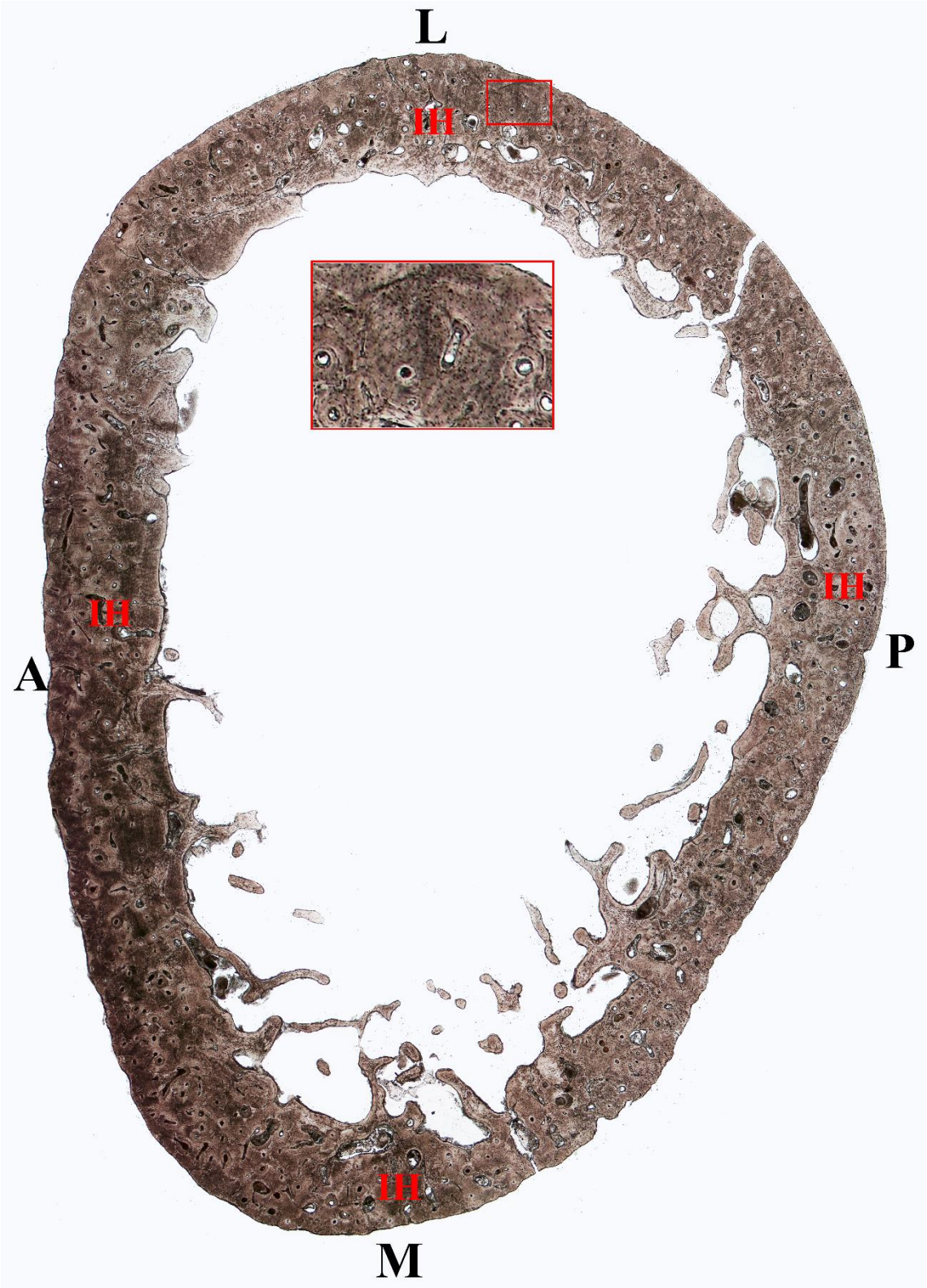
L
IH
IH
IH
IH
A
P
M

Figure A.6 – Human adult (HA1) – Radius (distal metaphysis)

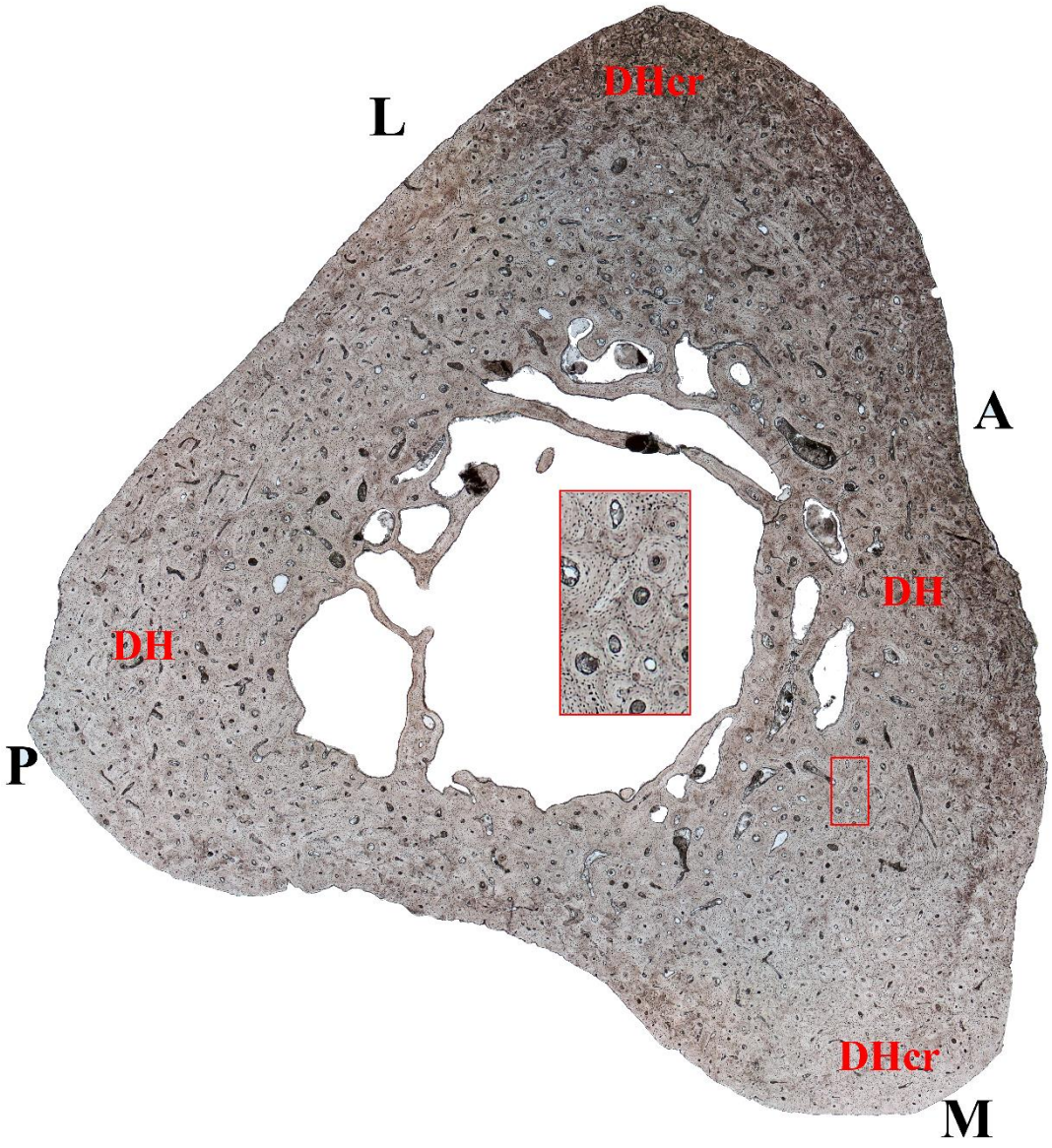

Figure A.7 – Human adult (HA1) – Ulna (proximal metaphysis)

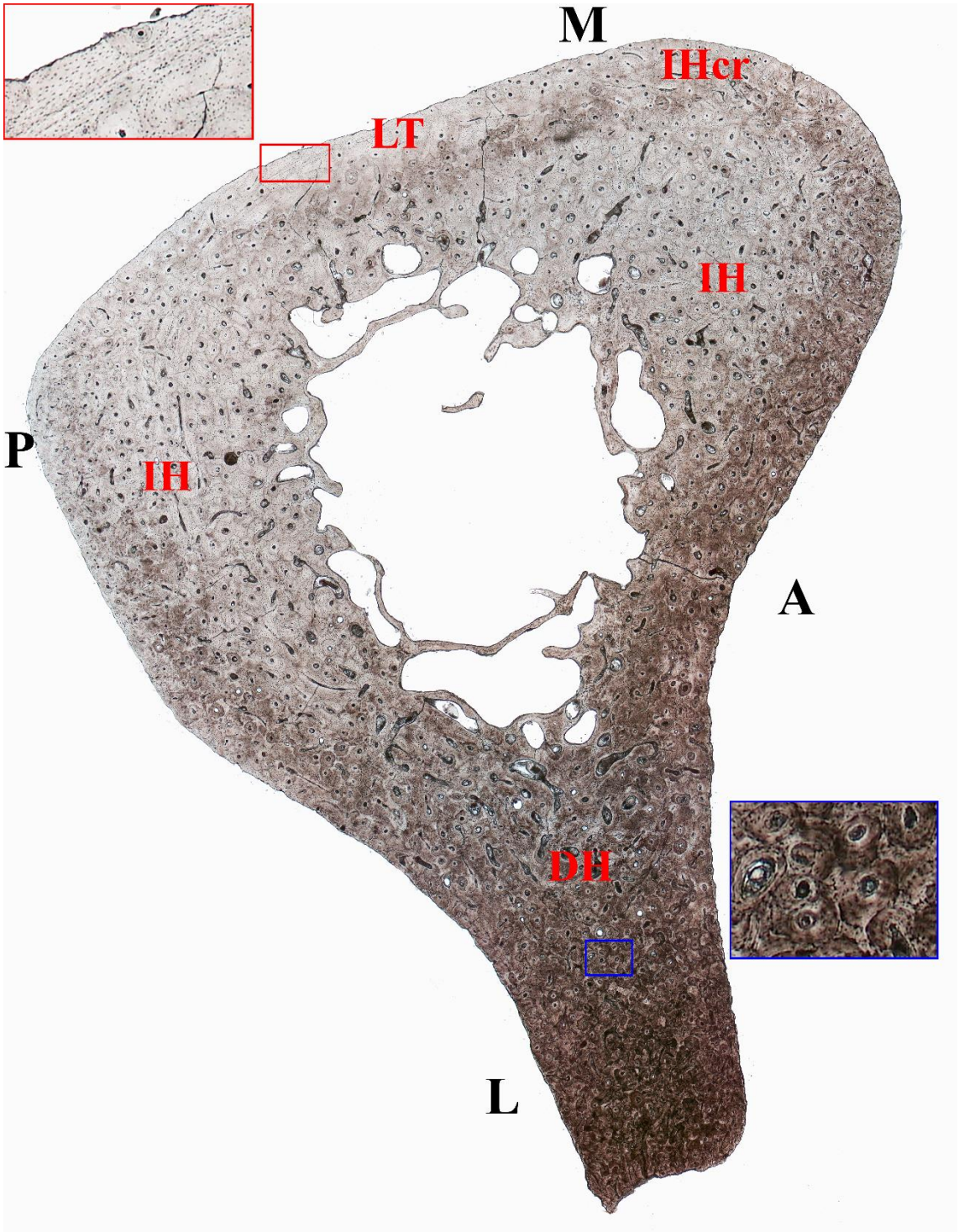

Figure A.8 – Human adult (HA1) – Ulna (diaphysis)

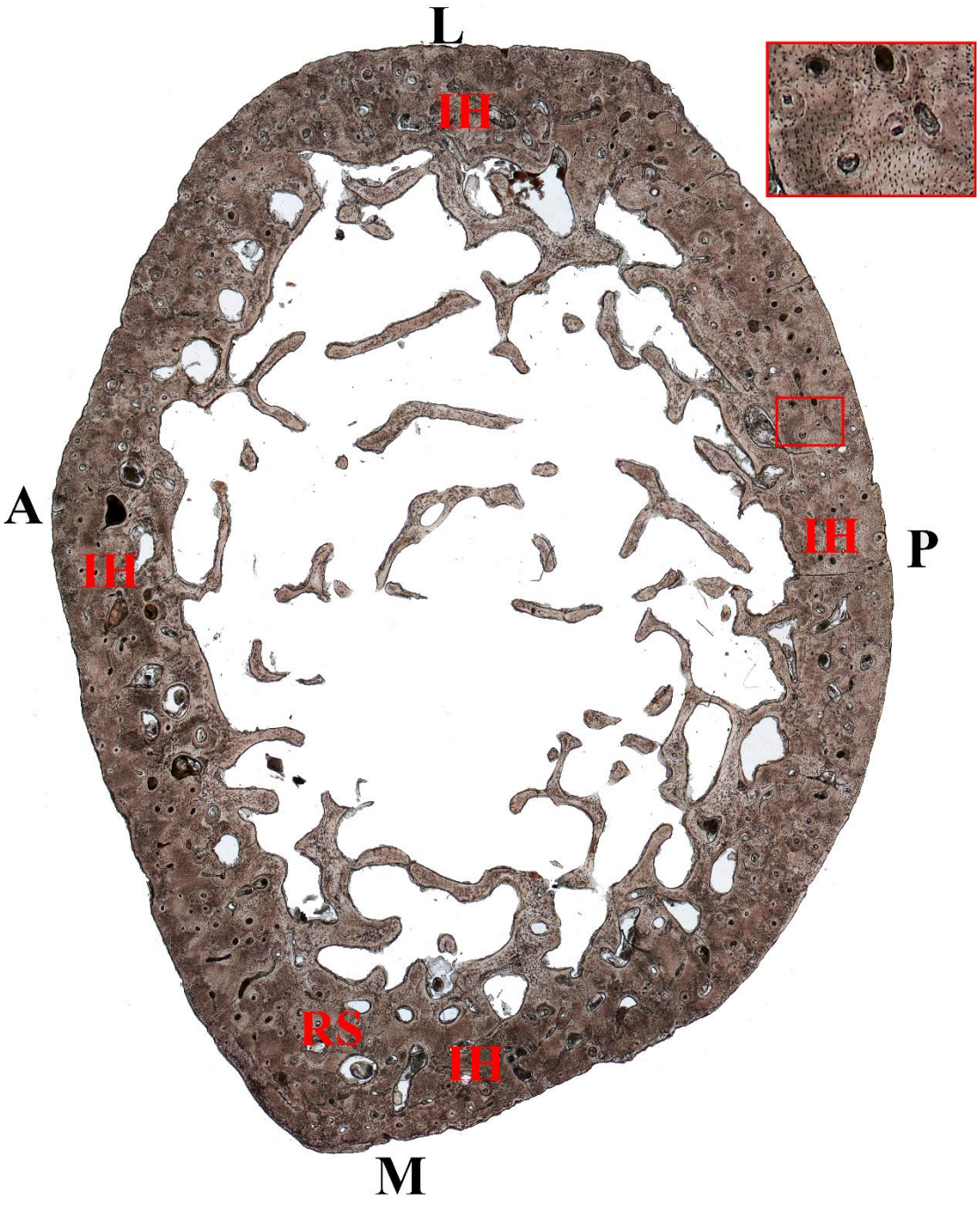

Figure A.9 – Human adult (HA1) – Ulna (distal metaphysis)

Figure A.10 – Human adult (HA1) – Femur (neck)

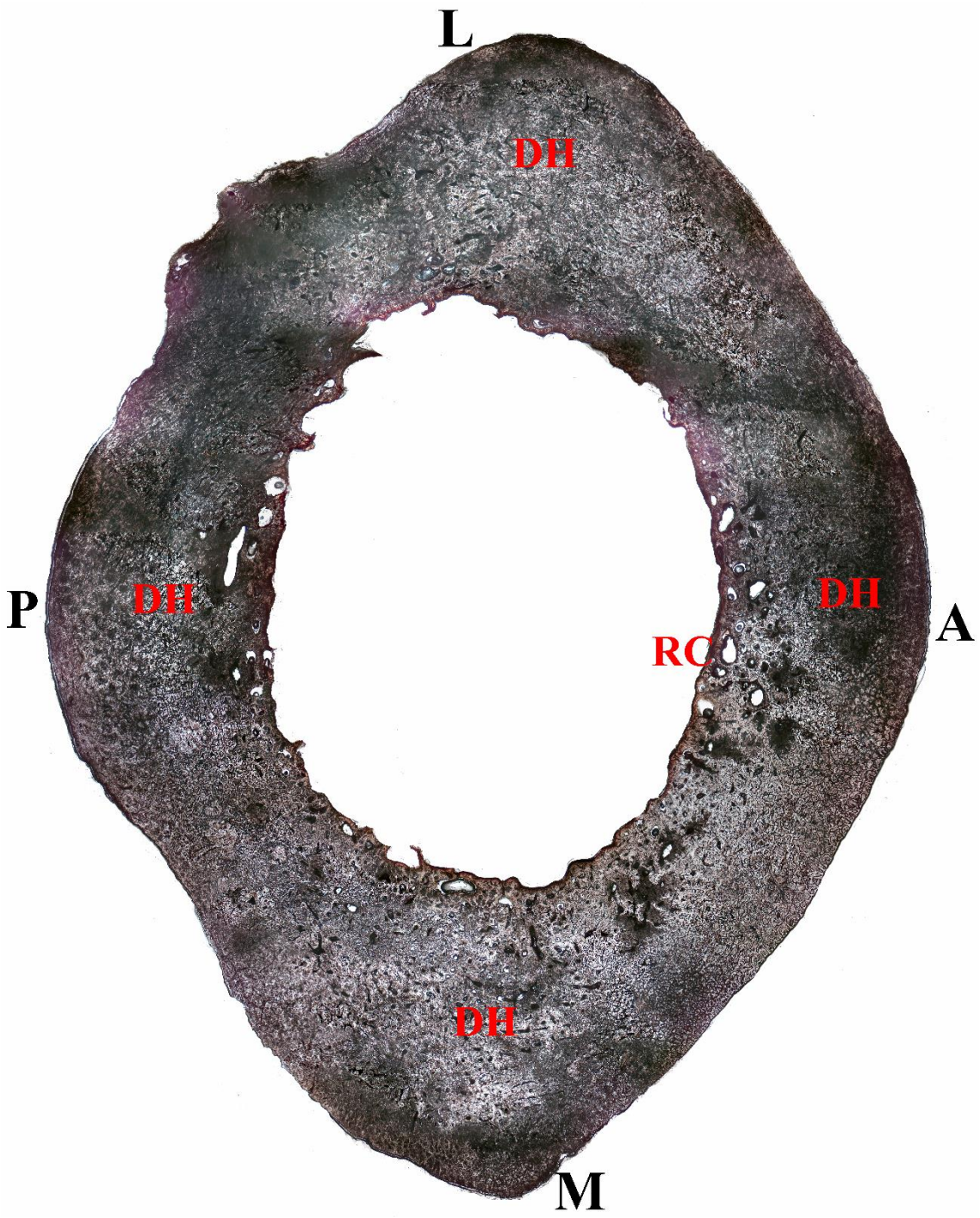

Figure A.11 – Human adult (HA1) – Femur (proximal metaphysis)

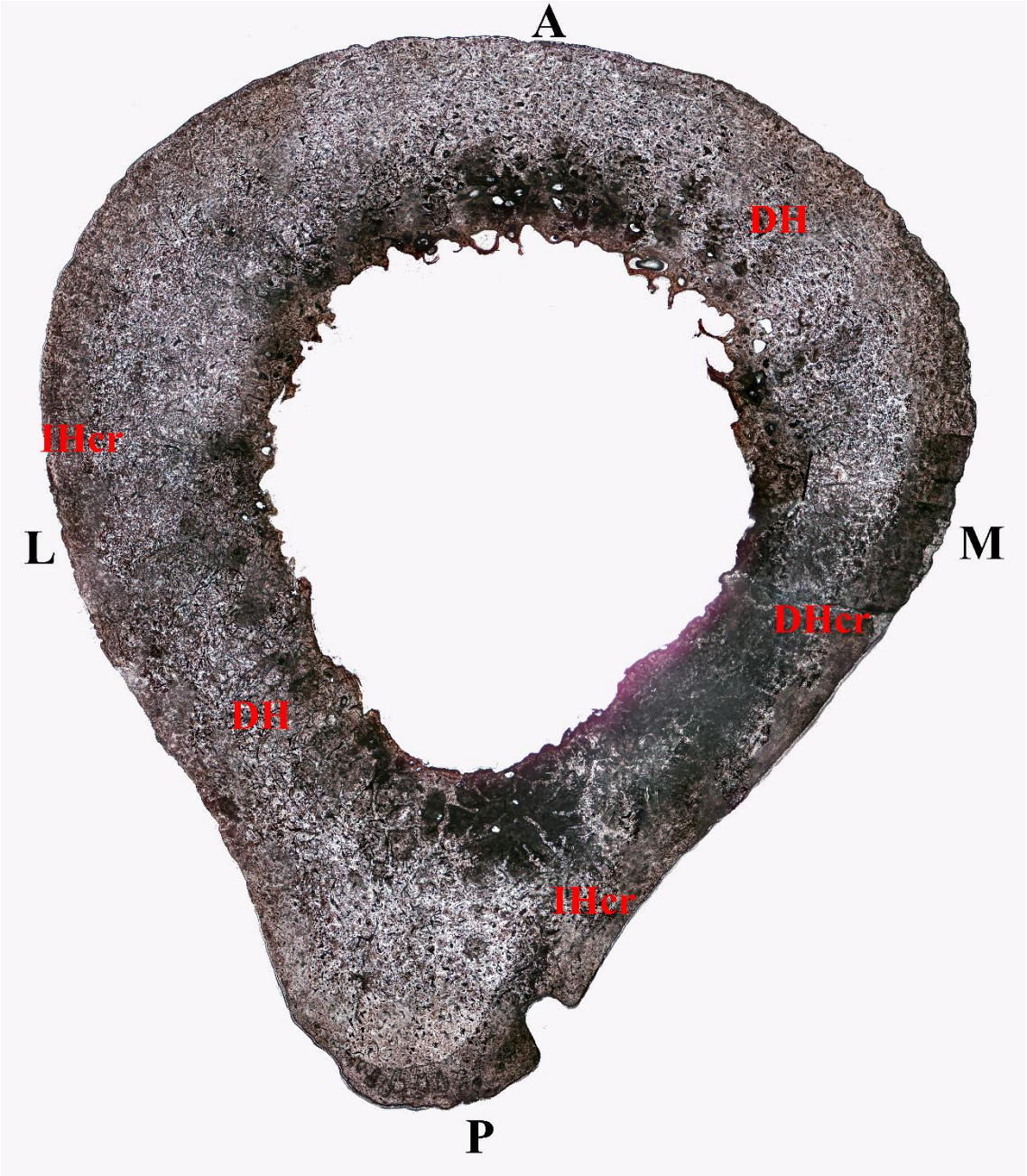

Figure A.12 – Human adult (HA1) – Femur (diaphysis)

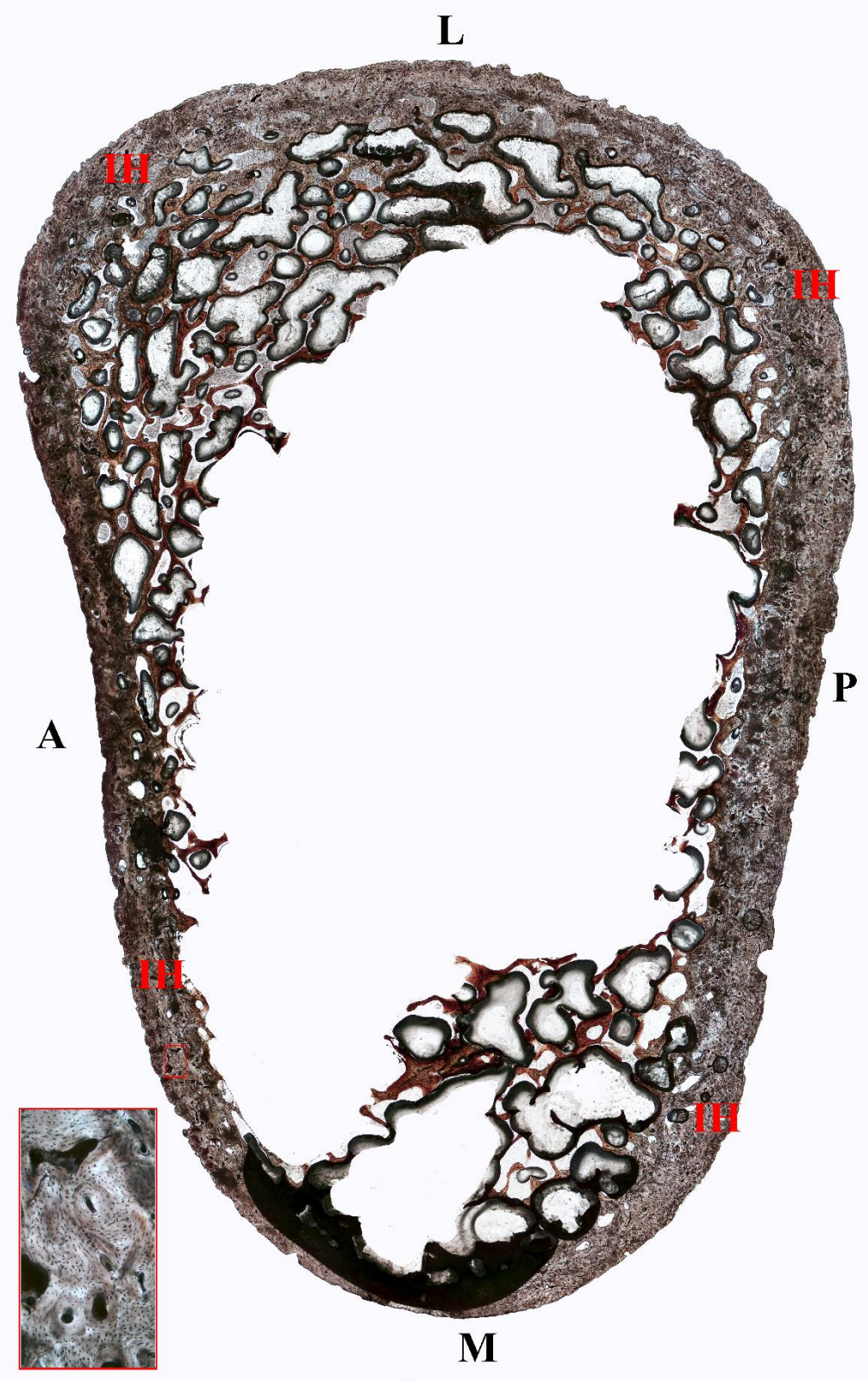

Figure A.13 – Human adult (HA1) – Femur (distal metaphysis)

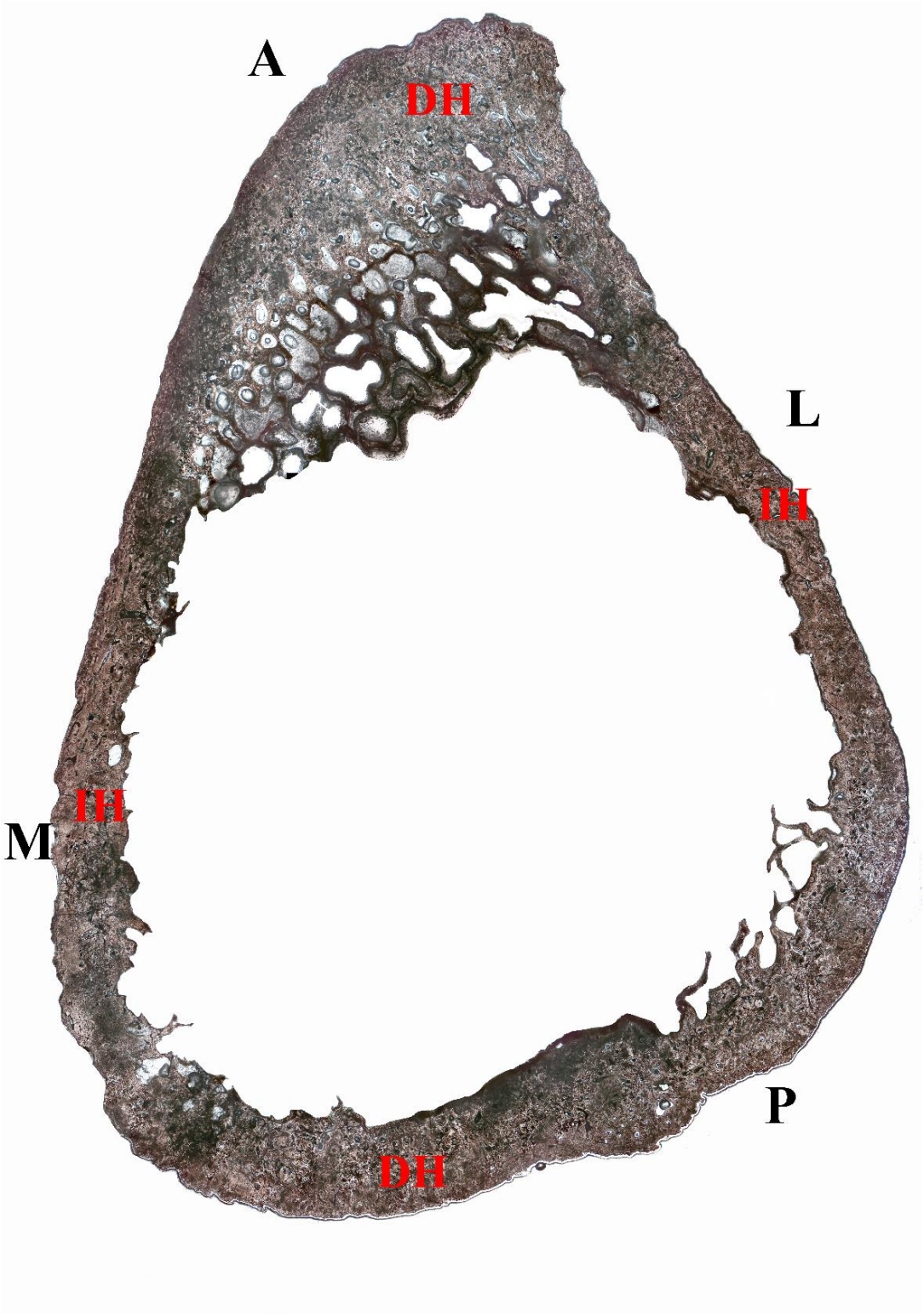

Figure A.14 – Human adult (HA1) – Tibia (proximal metaphysis)

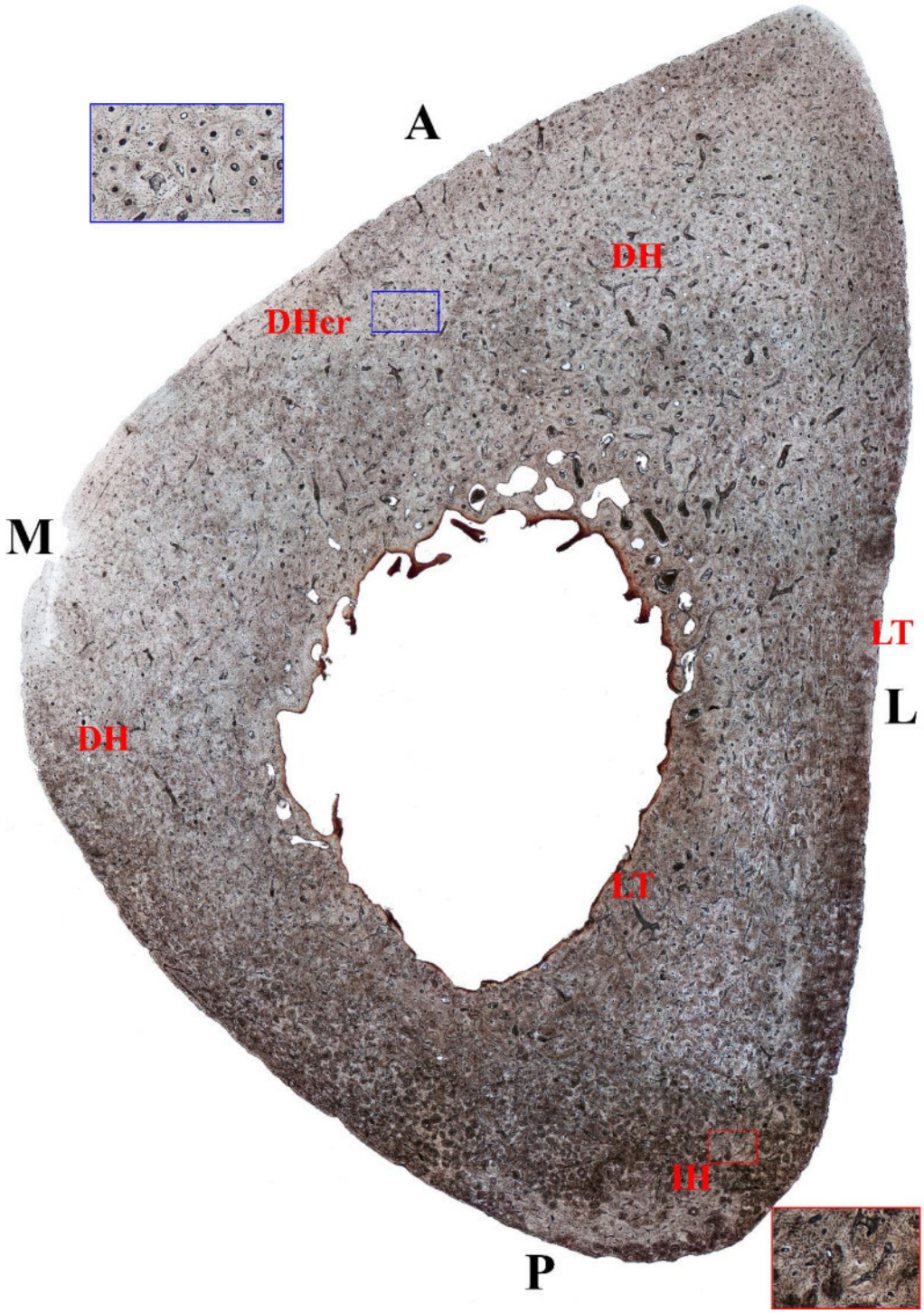

Figure A.15 – Human adult (HA1) – Tibia (diaphysis)

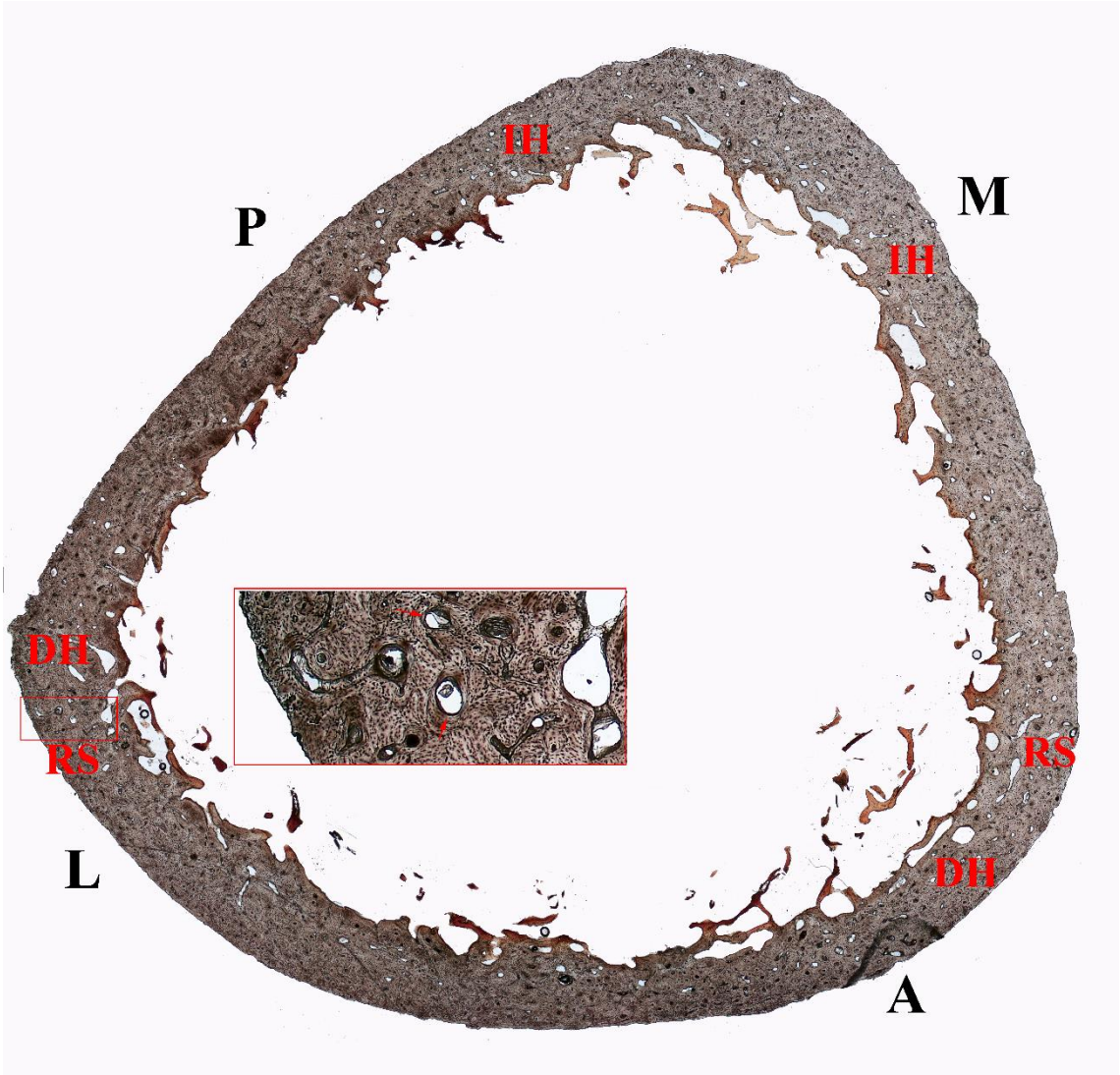

Figure A.16 – Human adult (HA1) – Tibia (distal metaphysis)

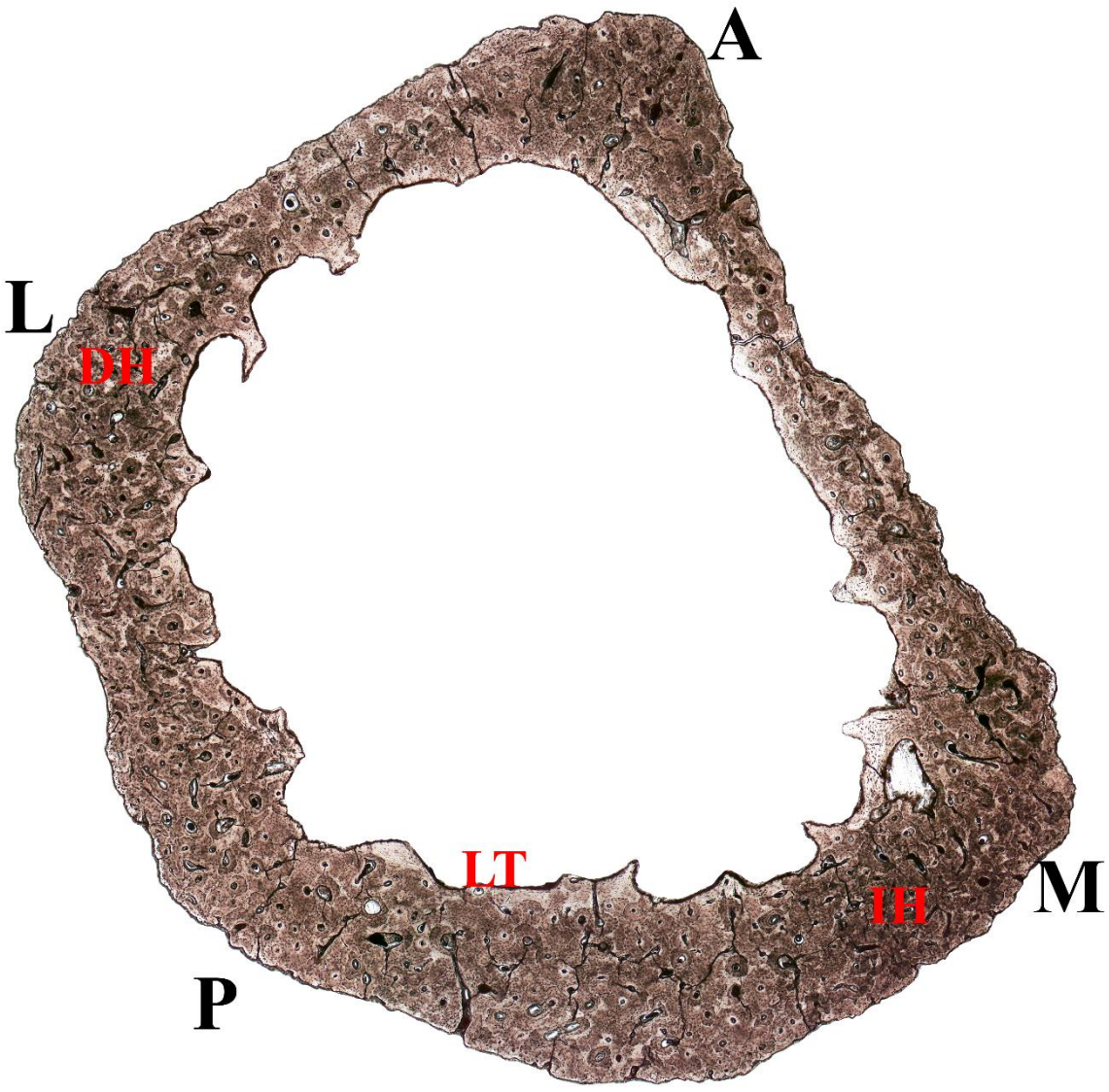

Figure A.17 – Human adult (HA1) – Fibula (proximal metaphysis)

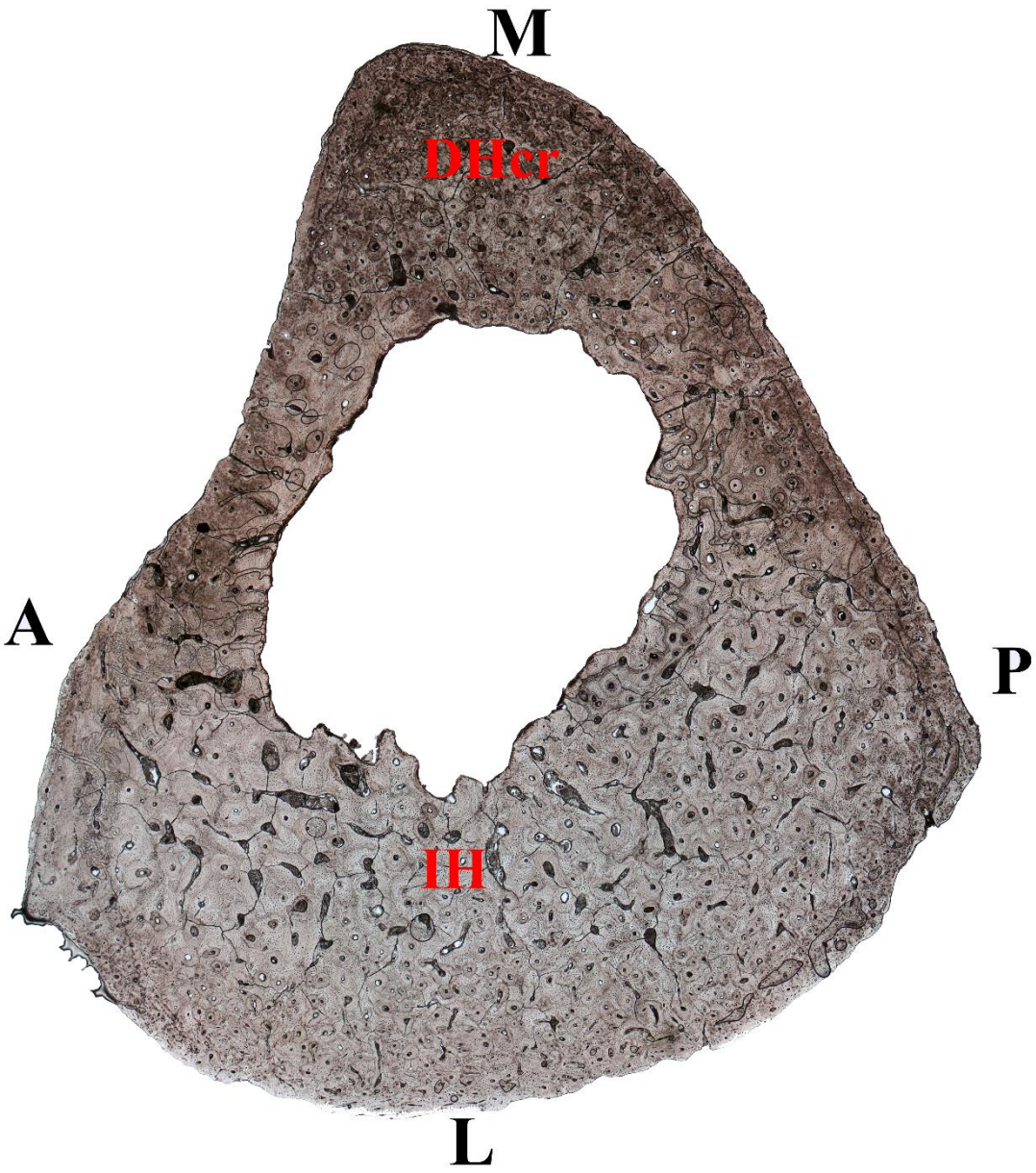

Figure A.18 – Human adult (HA1) – Fibula (diaphysis)

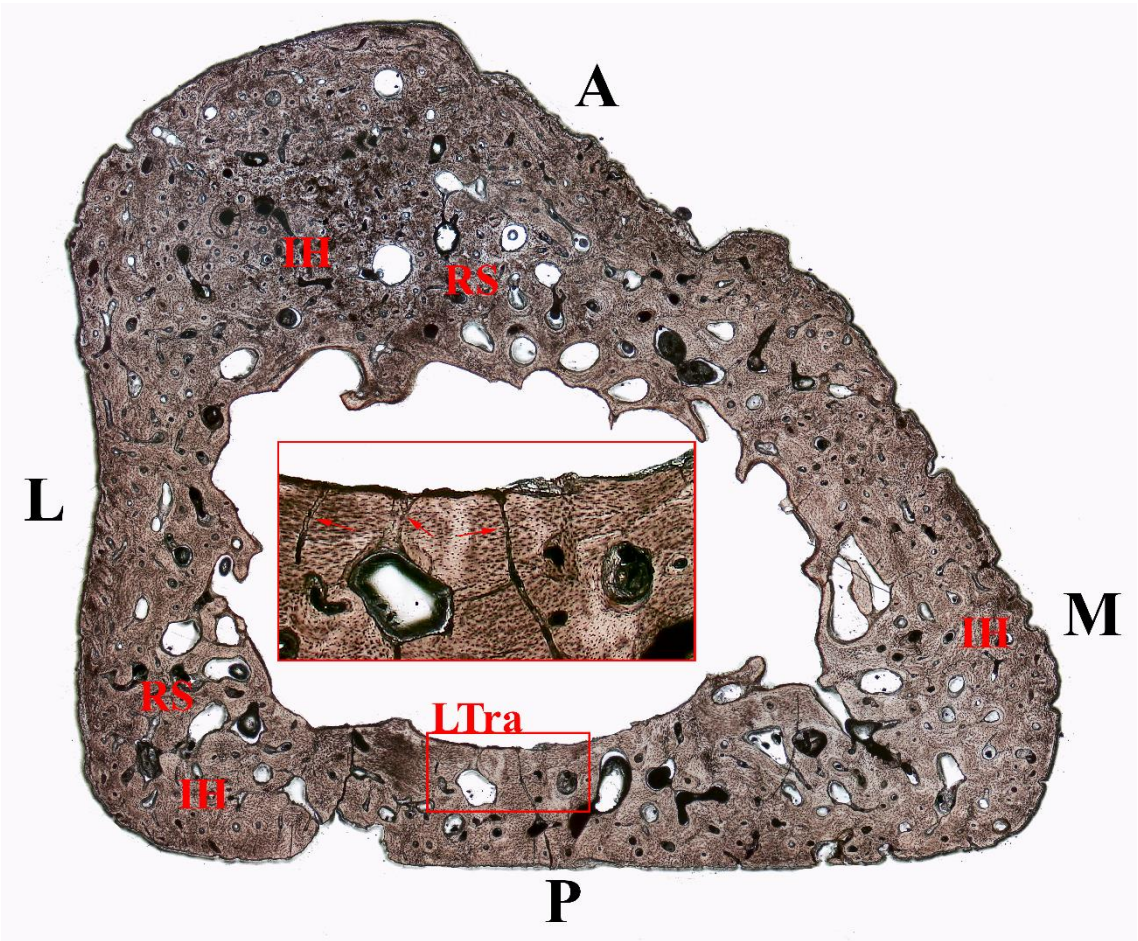

Figure A.19 – Human adult (HA1) – Fibula (distal metaphysis)

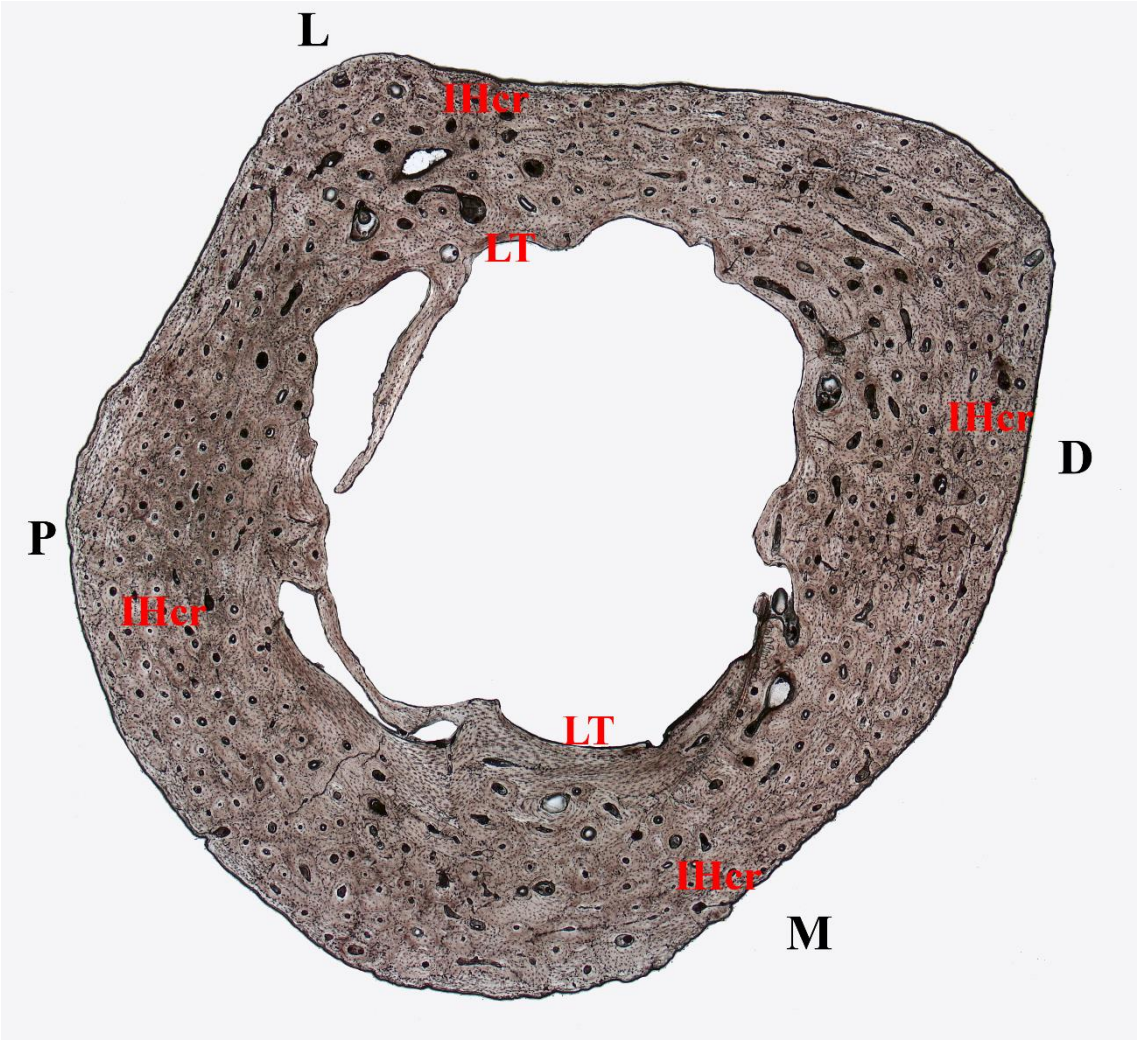

Figure A.20 – Human adult (HA1) – Metacarpal (head)

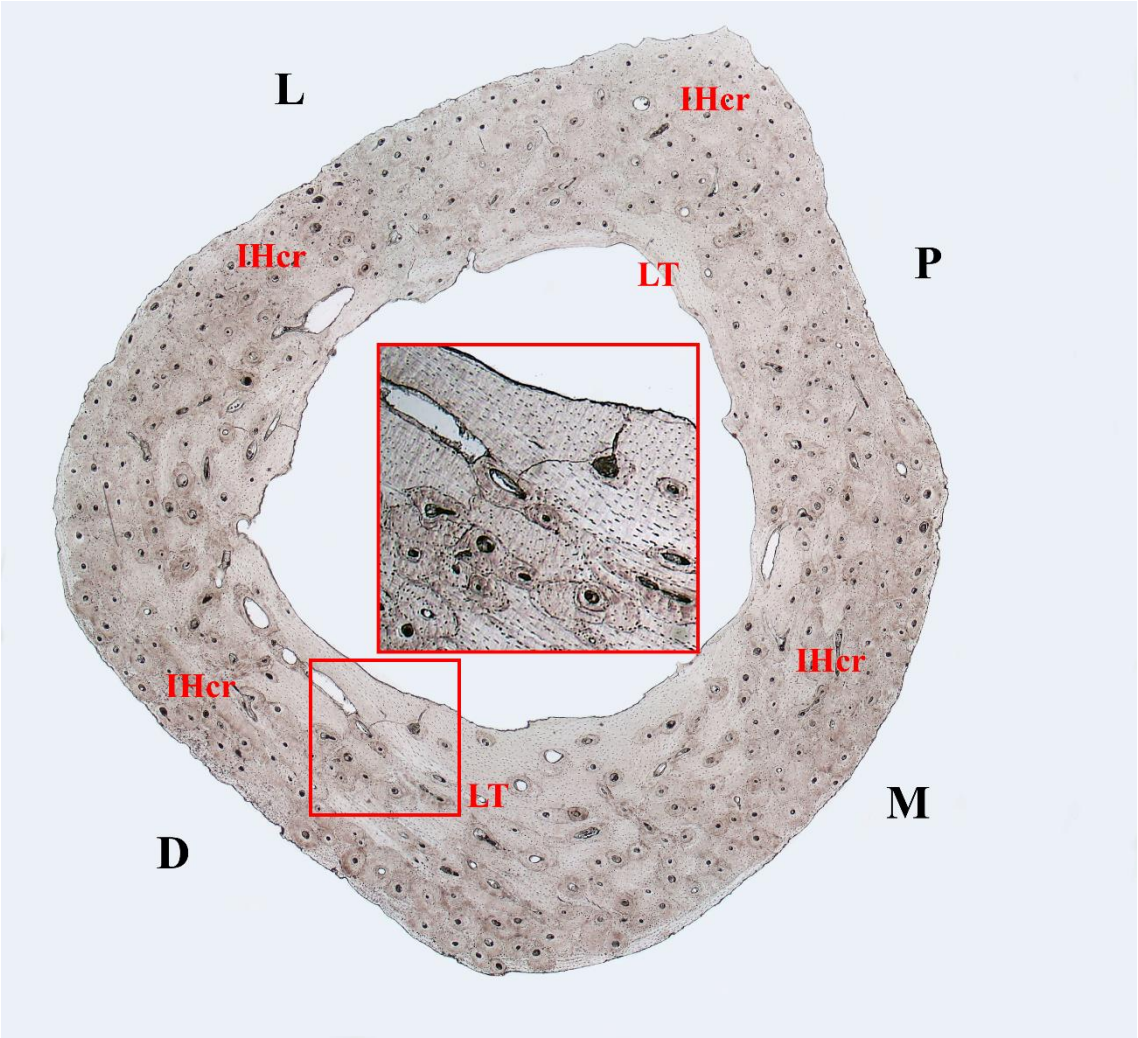

Figure A.21 – Human adult (HA1) – Metacarpal (body)

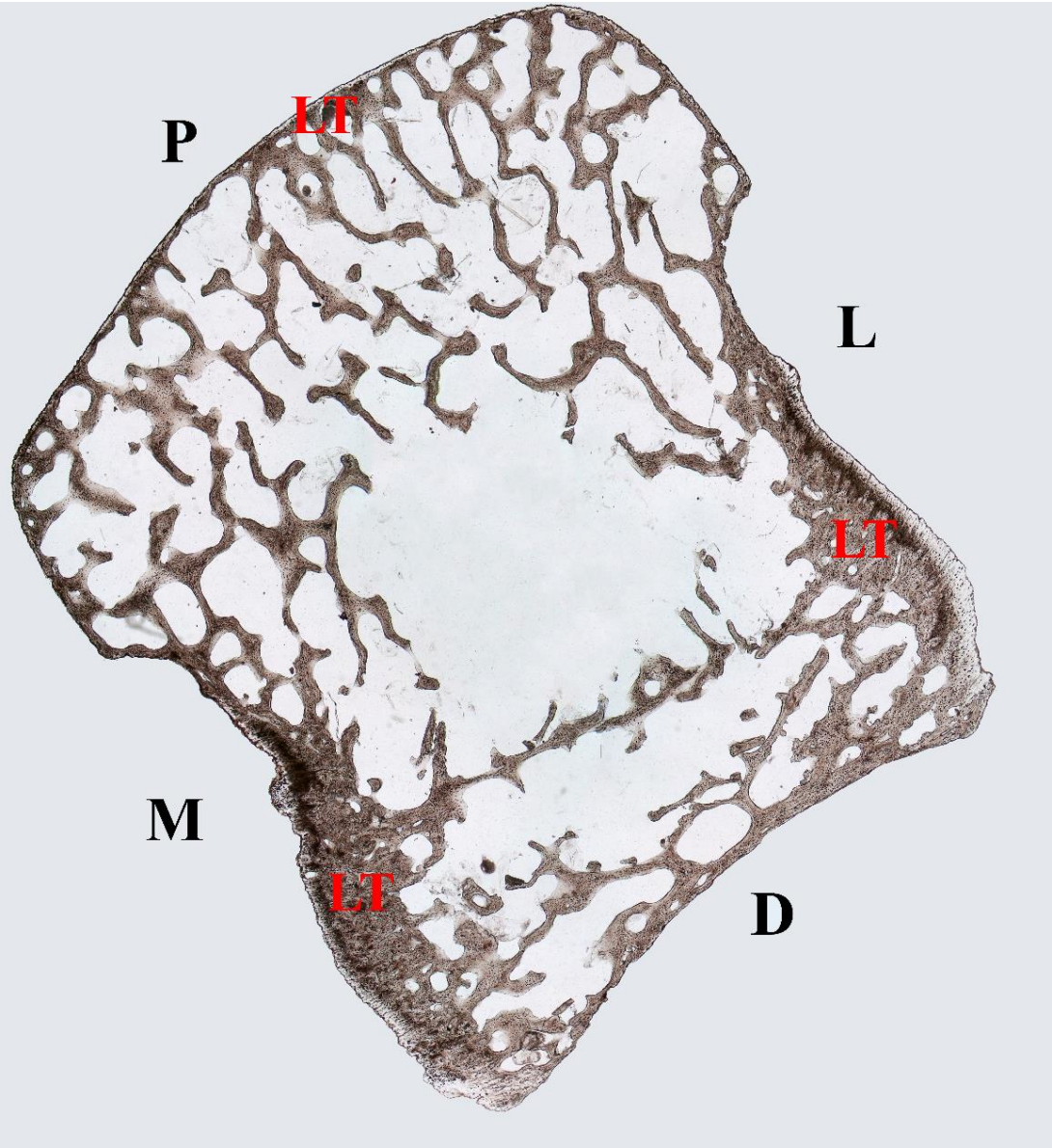

Figure A.22 – Human adult (HA1) – Metacarpal (base)

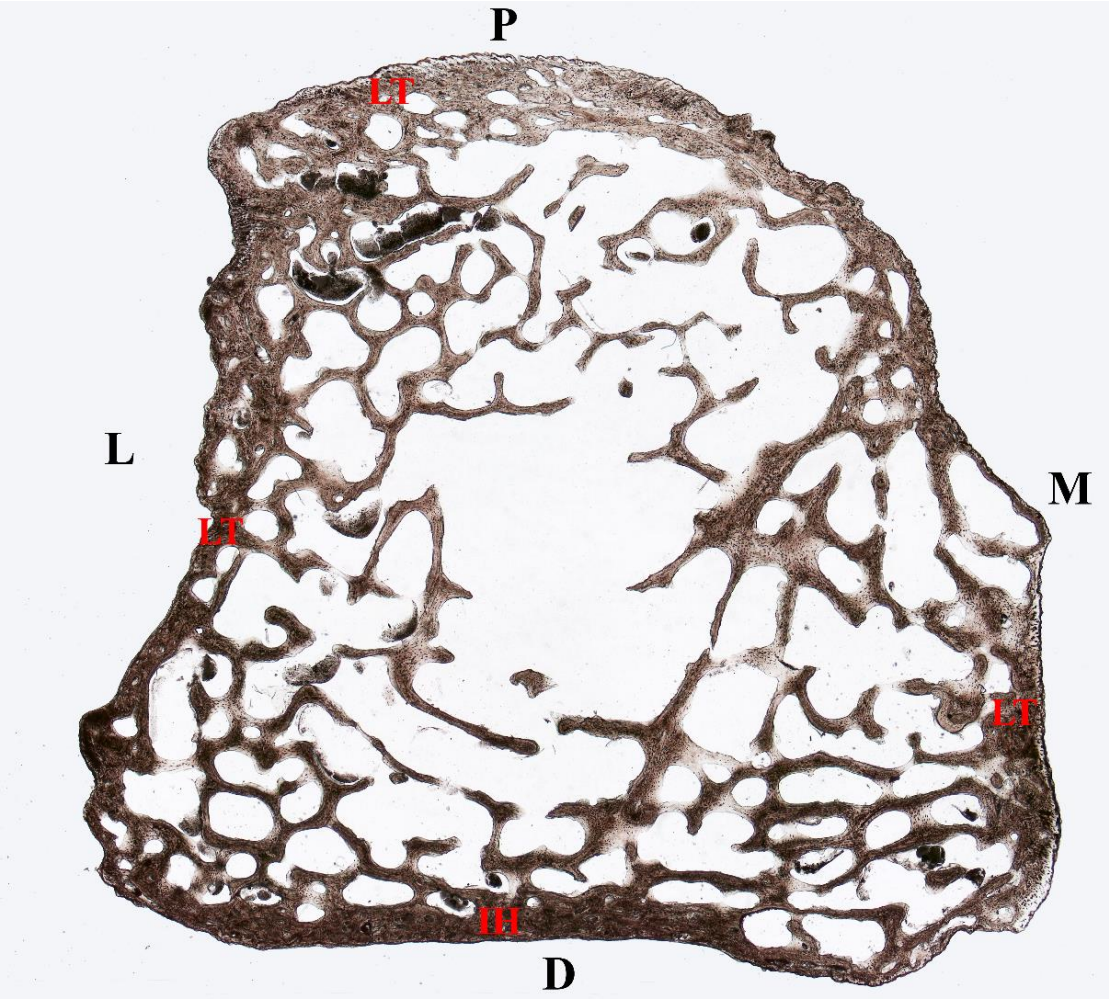

Figure A.23 – Human adult (HA1) – Metatarsal (head)

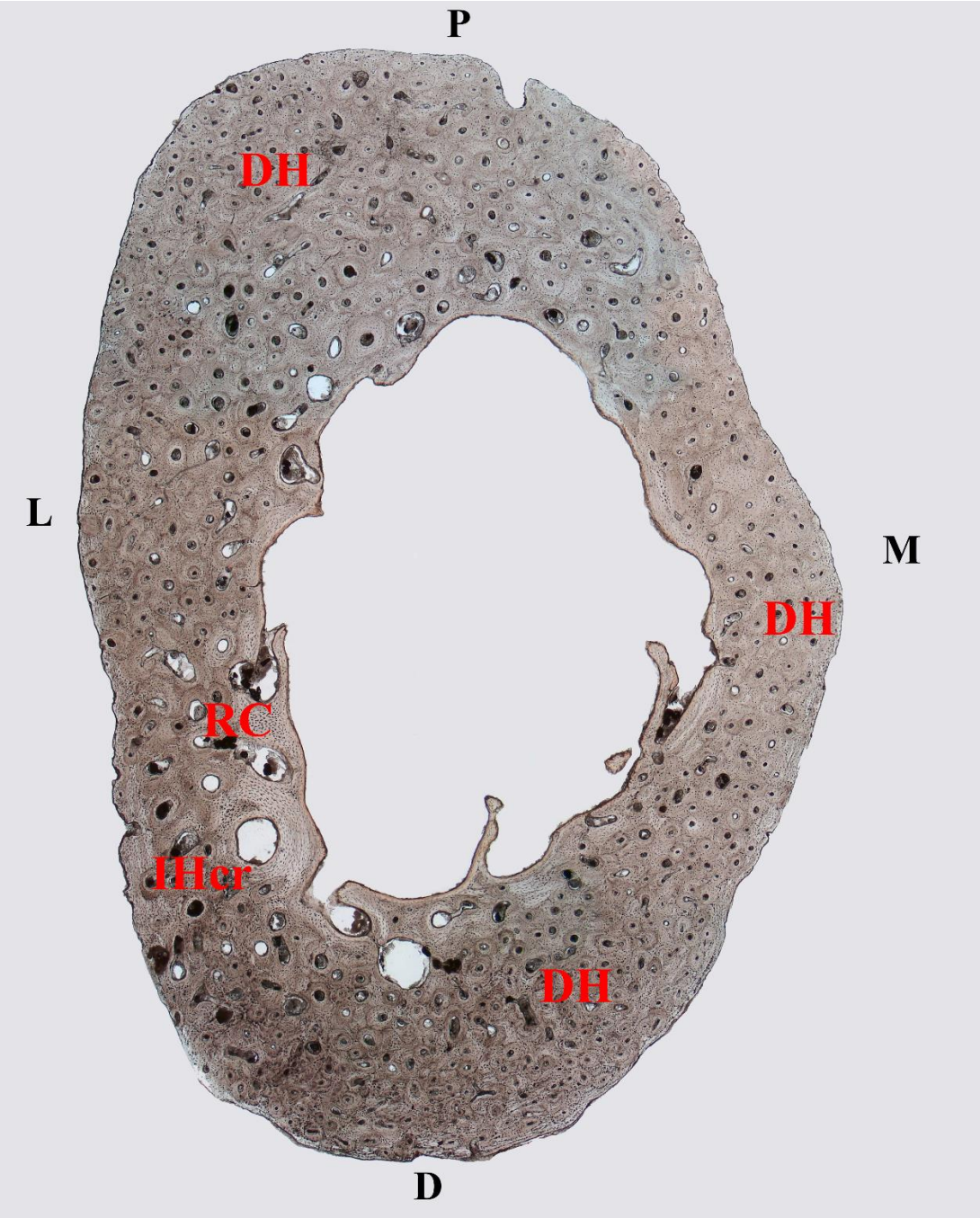

Figure A.24 – Human adult (HA1) – Metatarsal (body)

Figure A.25 – Human adult (HA1) – Metatarsal (base)

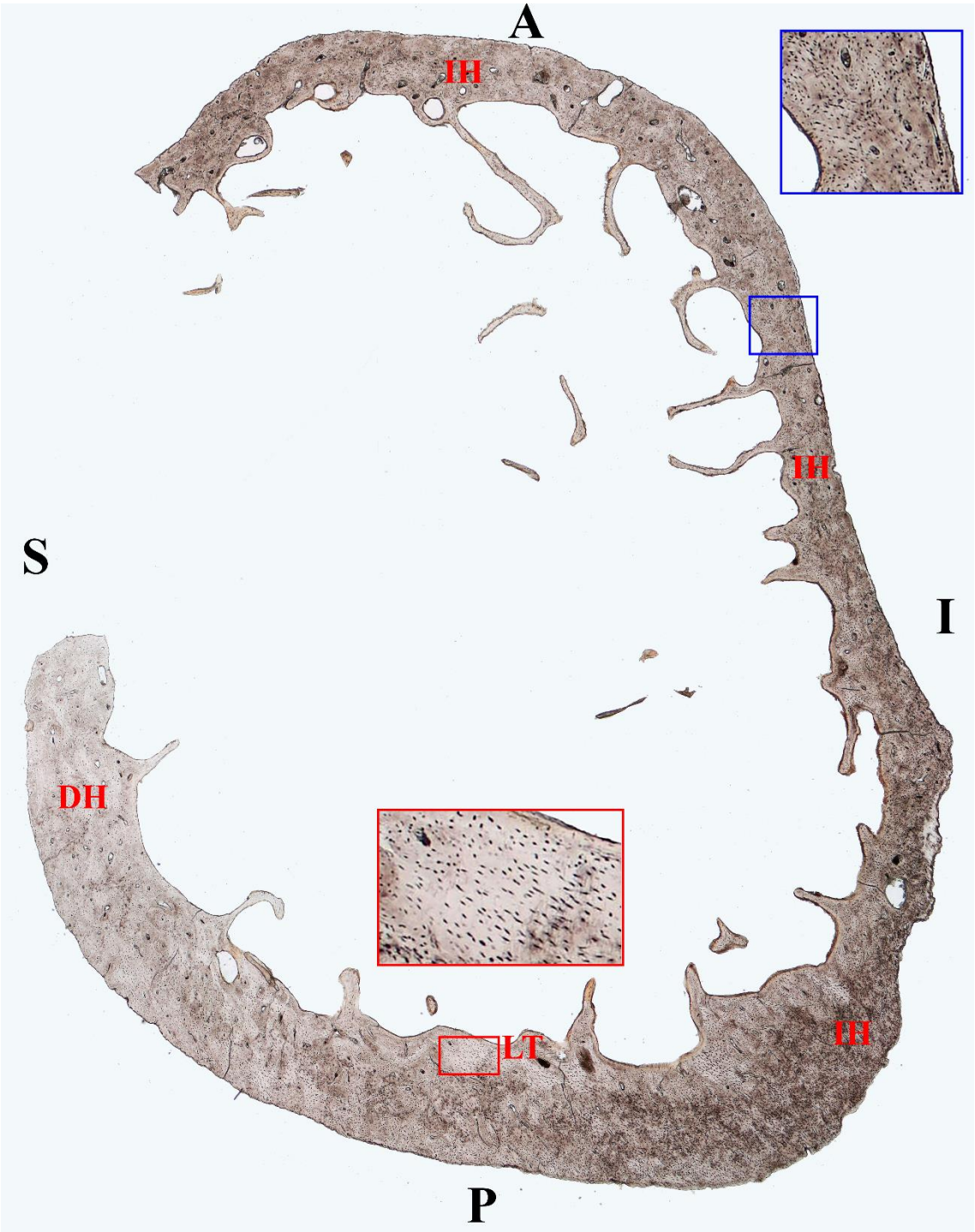

Figure A.26 – Human adult (HA1) – Clavicle (medial end)

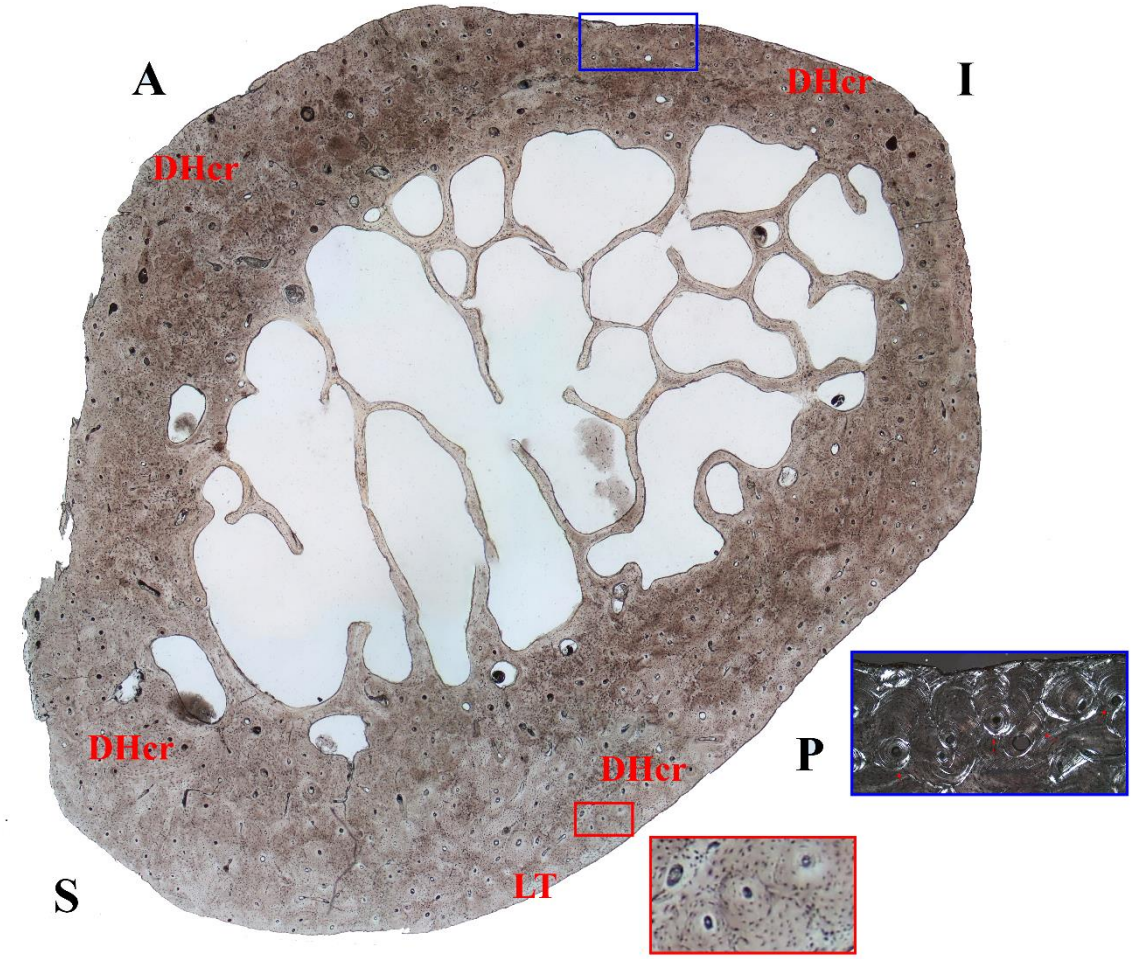

Figure A.27 – Human adult (HA1) – Clavicle (body)

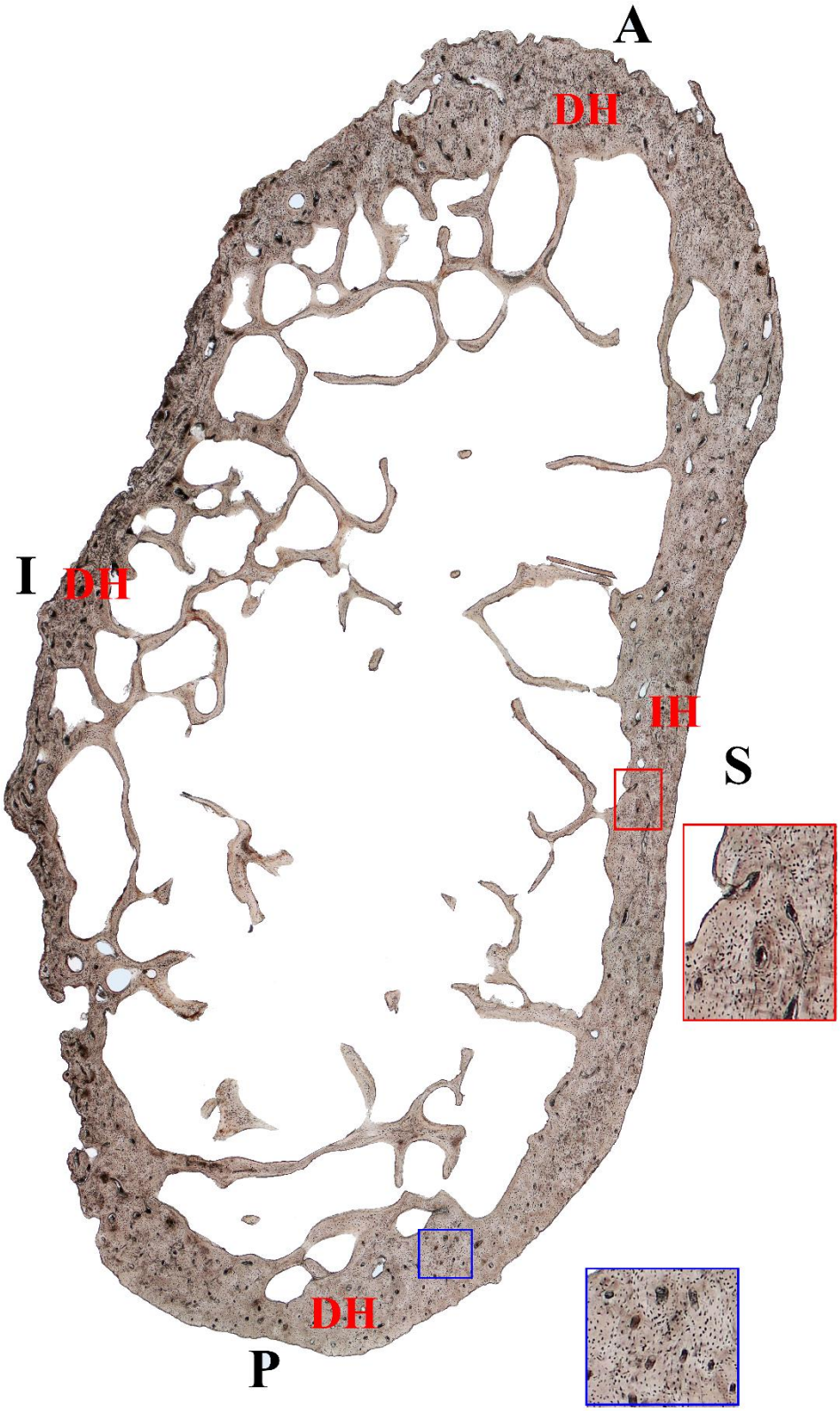

Figure A.28 – Human adult (HA1) – Clavicle (lateral end)

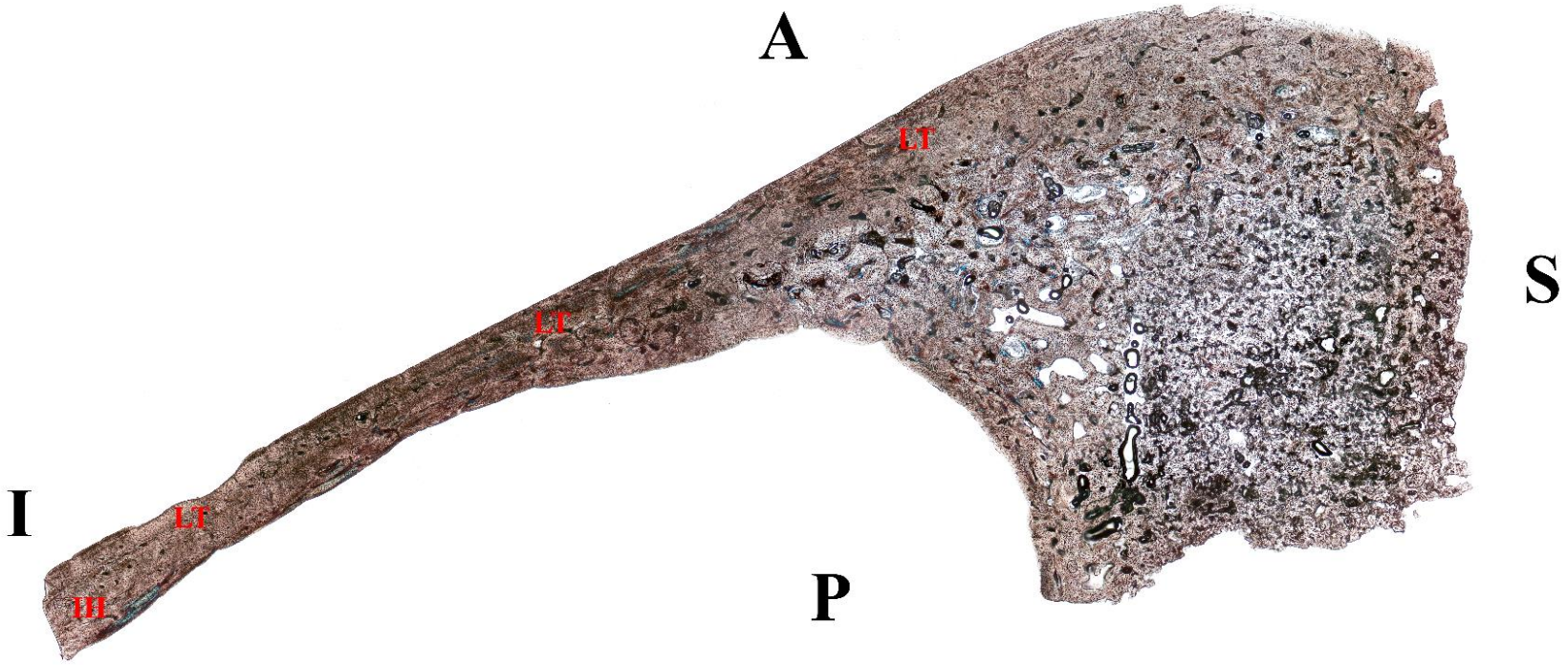

Figure A.29 – Human adult (HA1) – Frontal (glabella)

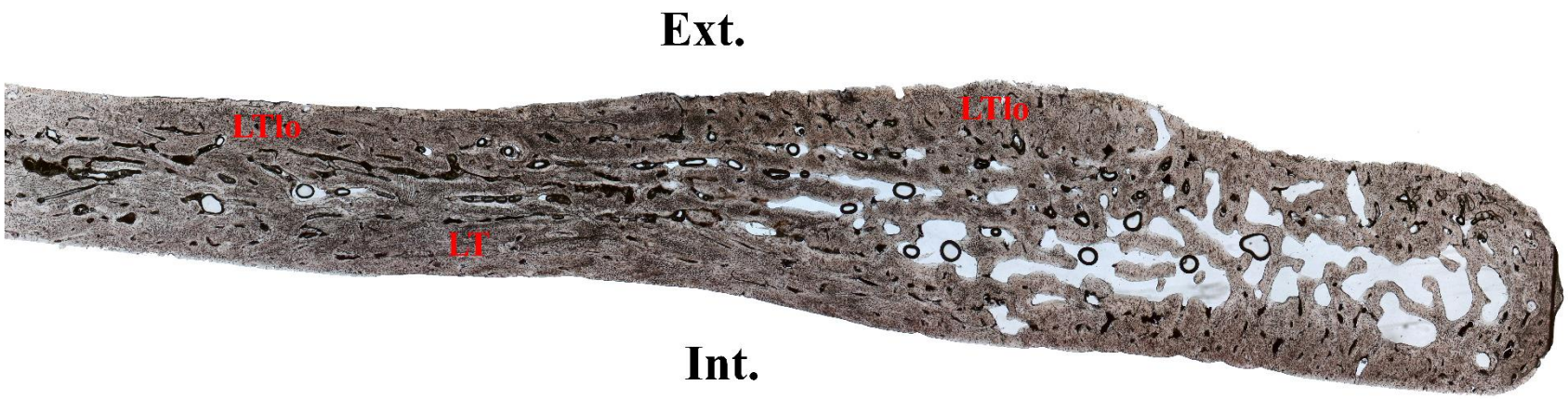

Figure A.30 – Human adult (HA1) – Zygomatic process of frontal bone

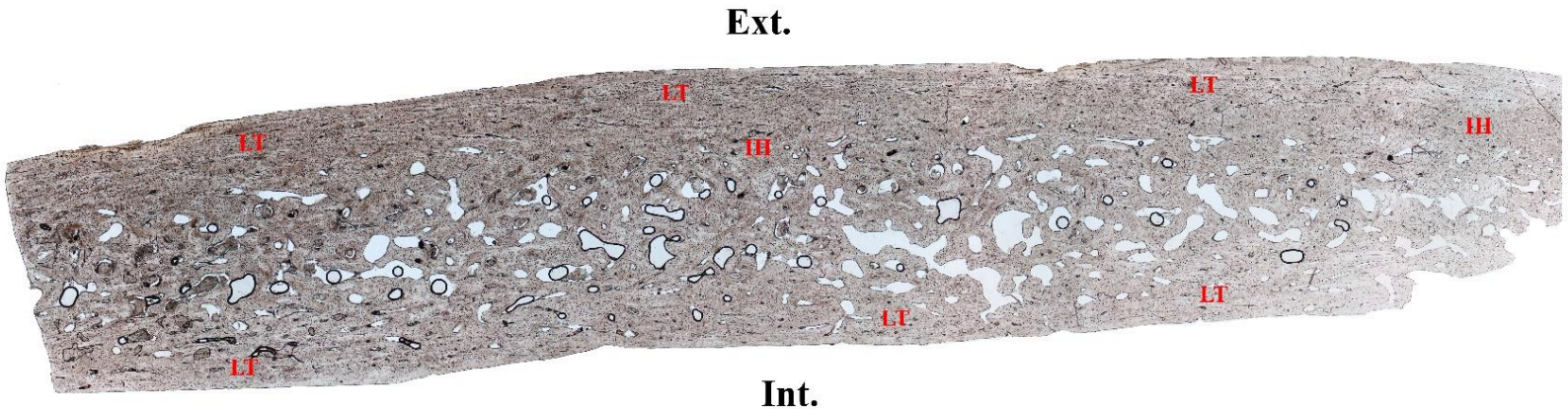

Figure A.31 – Human adult (HA1) – Parietal

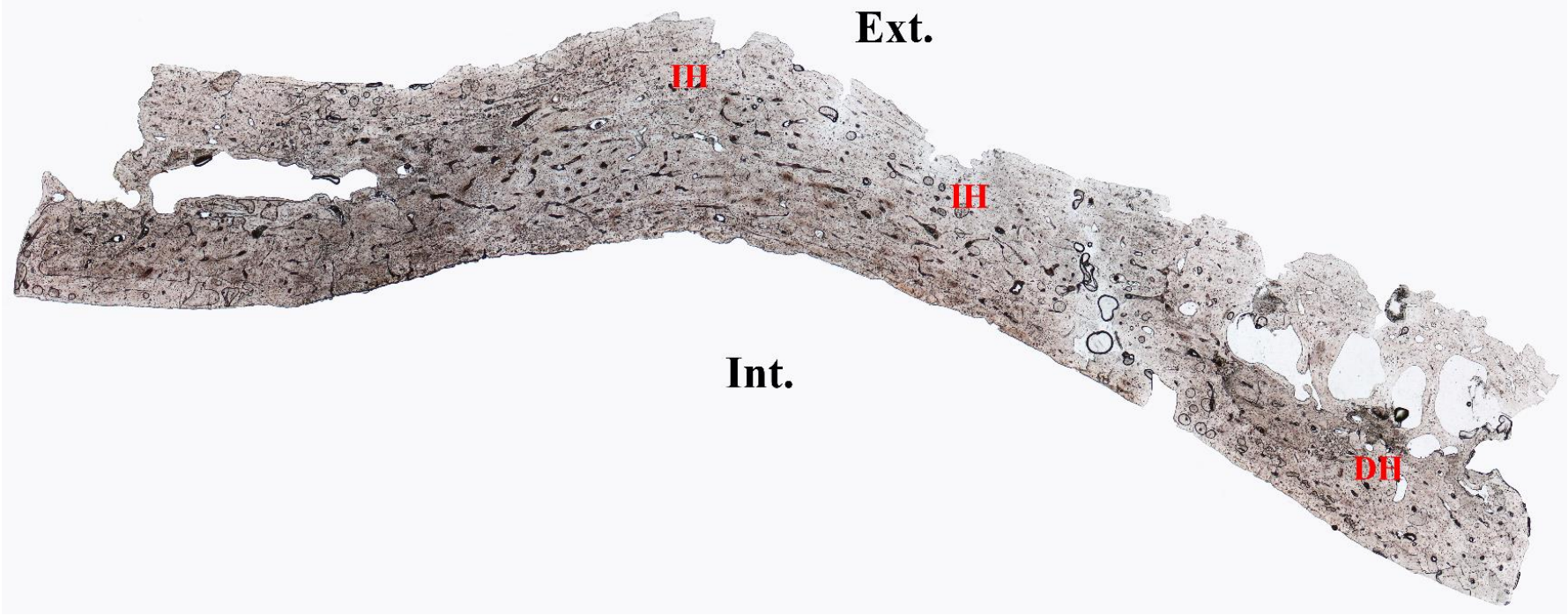

Figure A.32 – Human adult (HA1) – Occipital

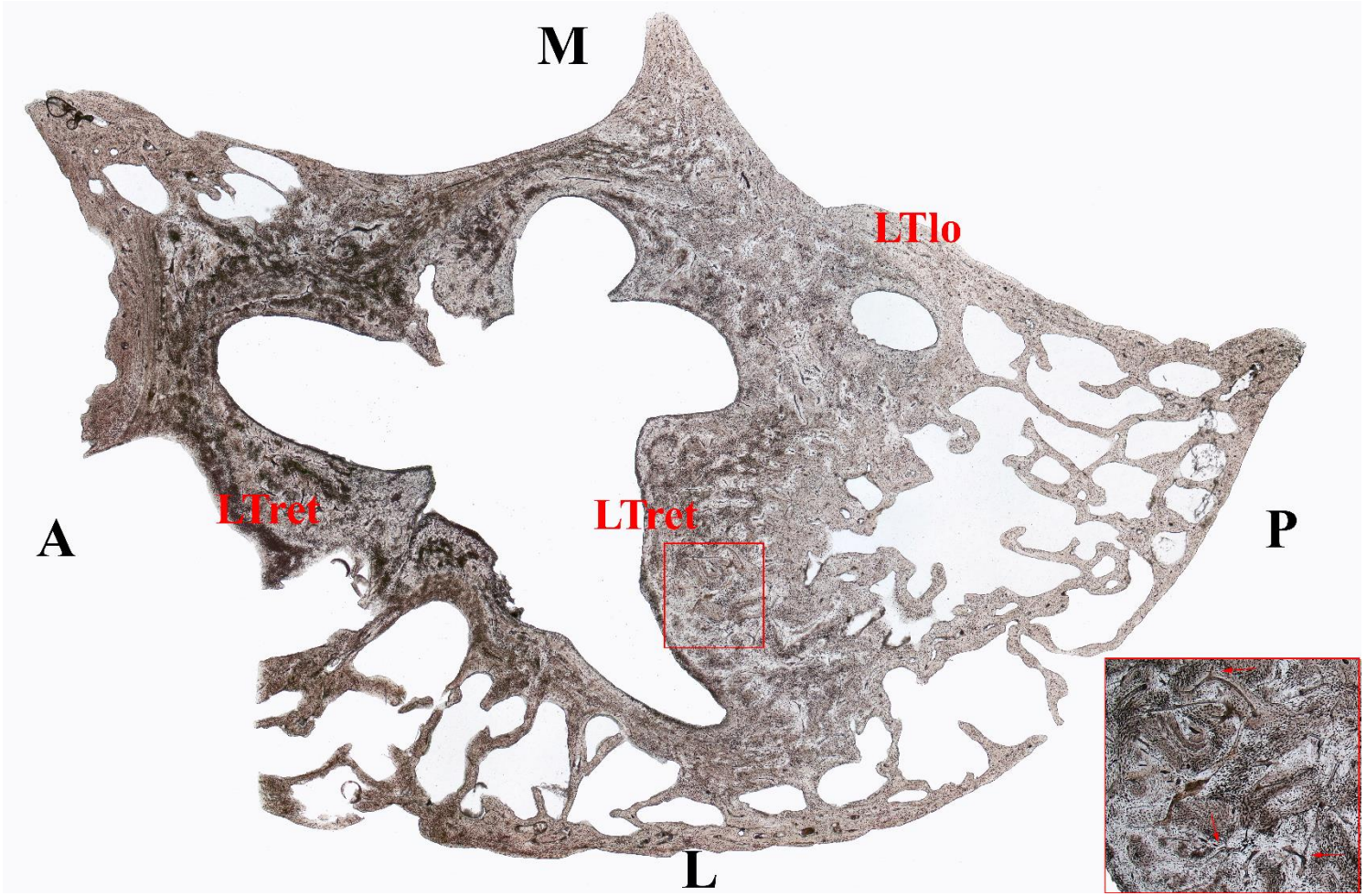

Figure A.33 – Human adult (HA1) – Petrous

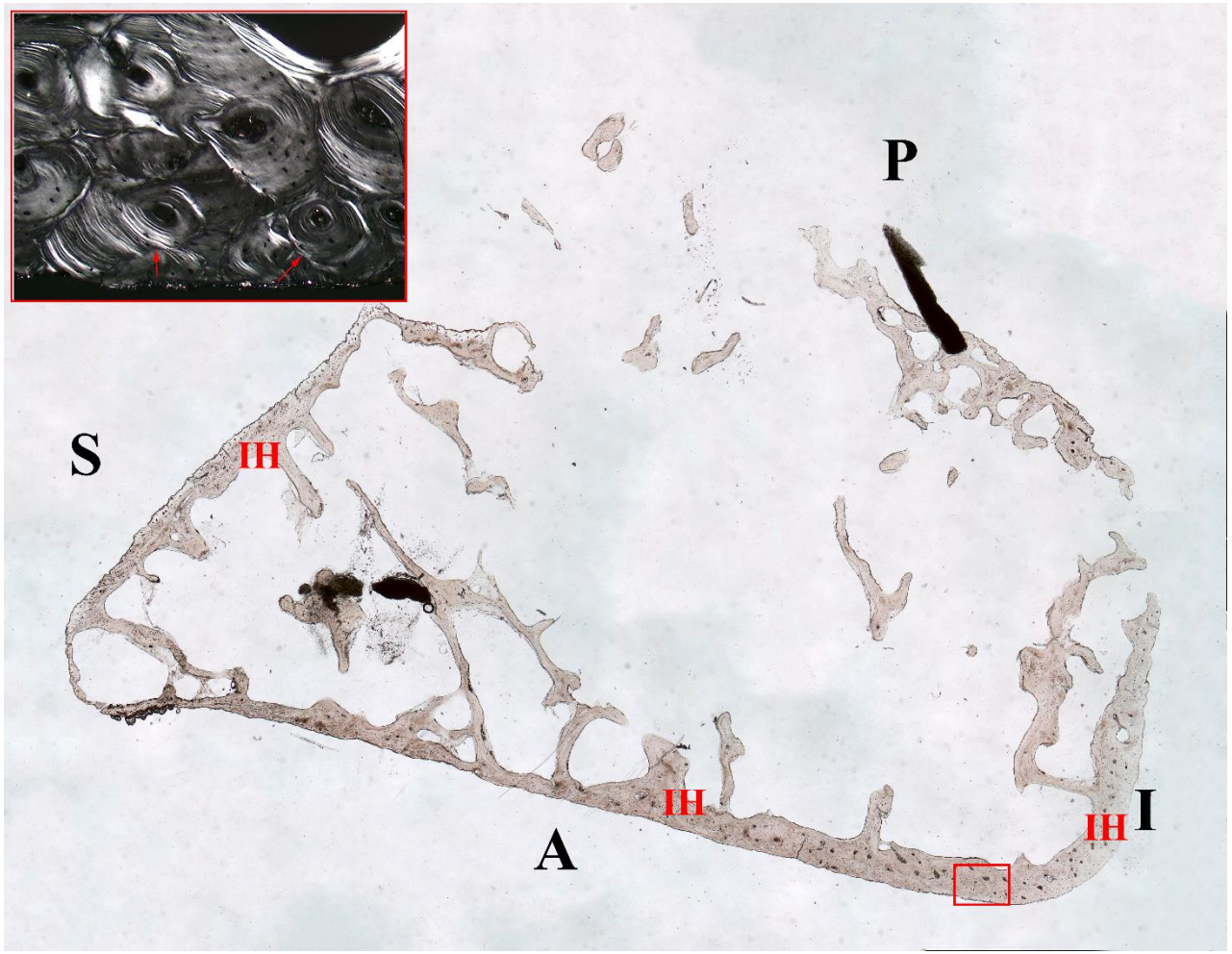

Figure A.34 – Human adult (HA1) – Rib (head)

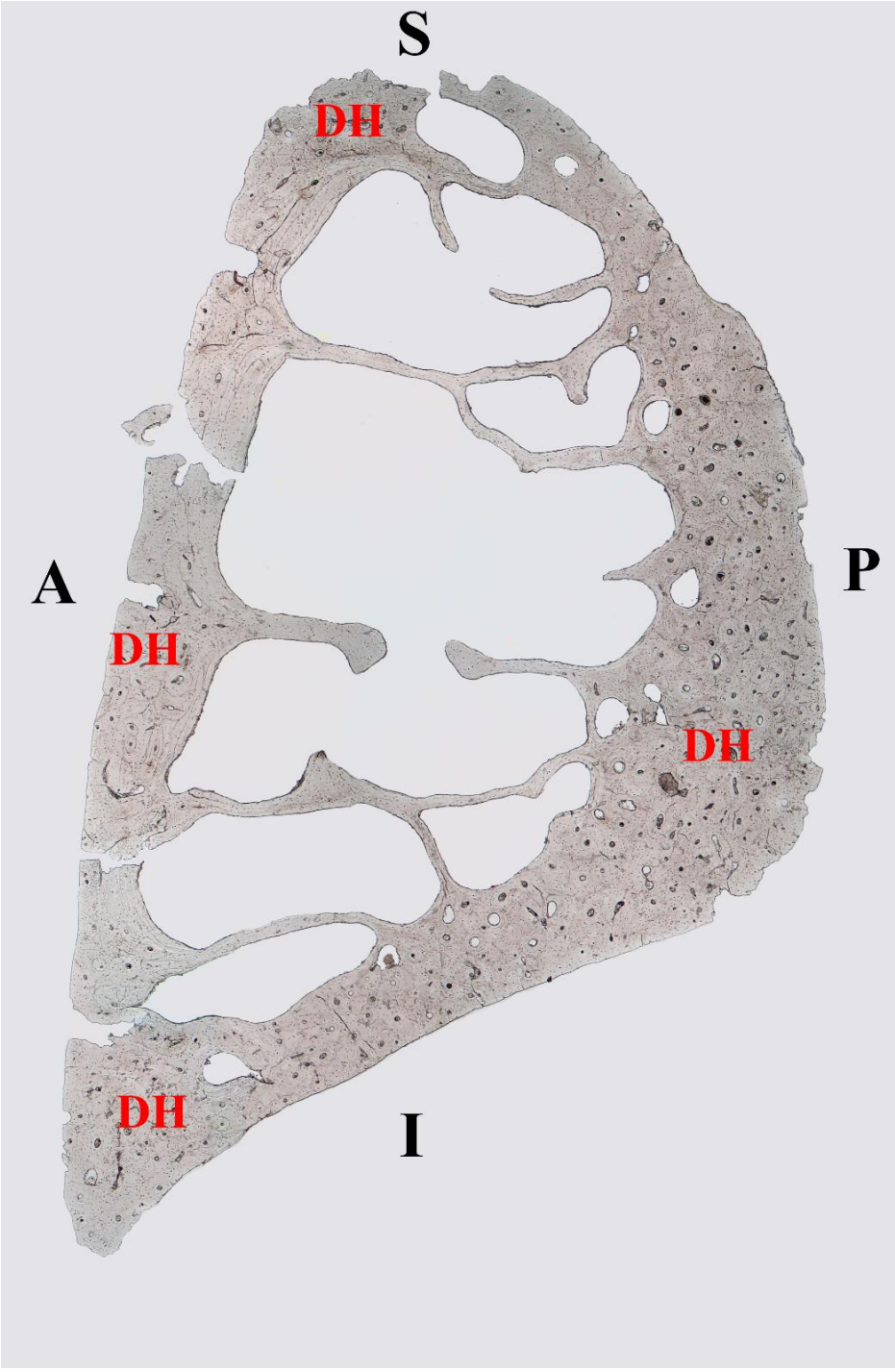

Figure A.35 – Human adult (HA1) – Rib (body)

Figure A.36 – Human adult (HA1) – Scapula (superior border)

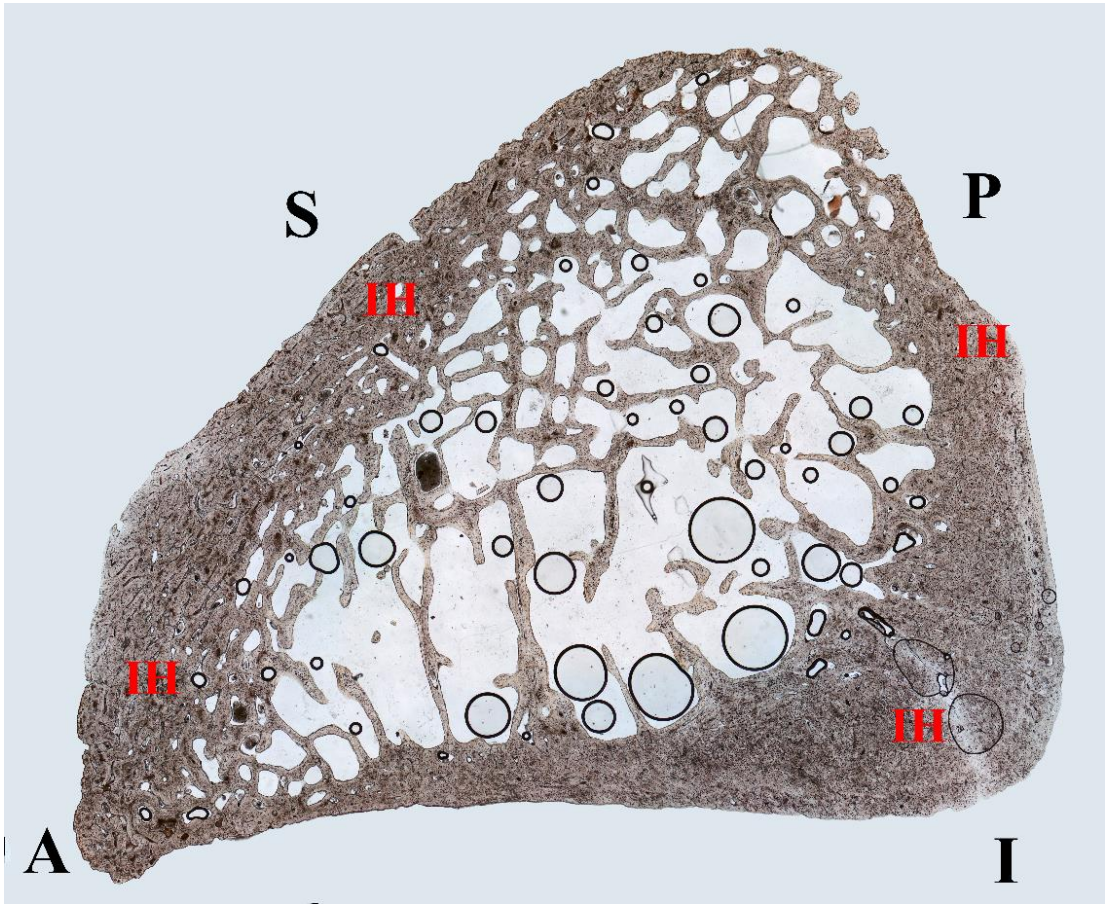

Figure A.37 – Human adult (HA1) – Scapula (acromion)

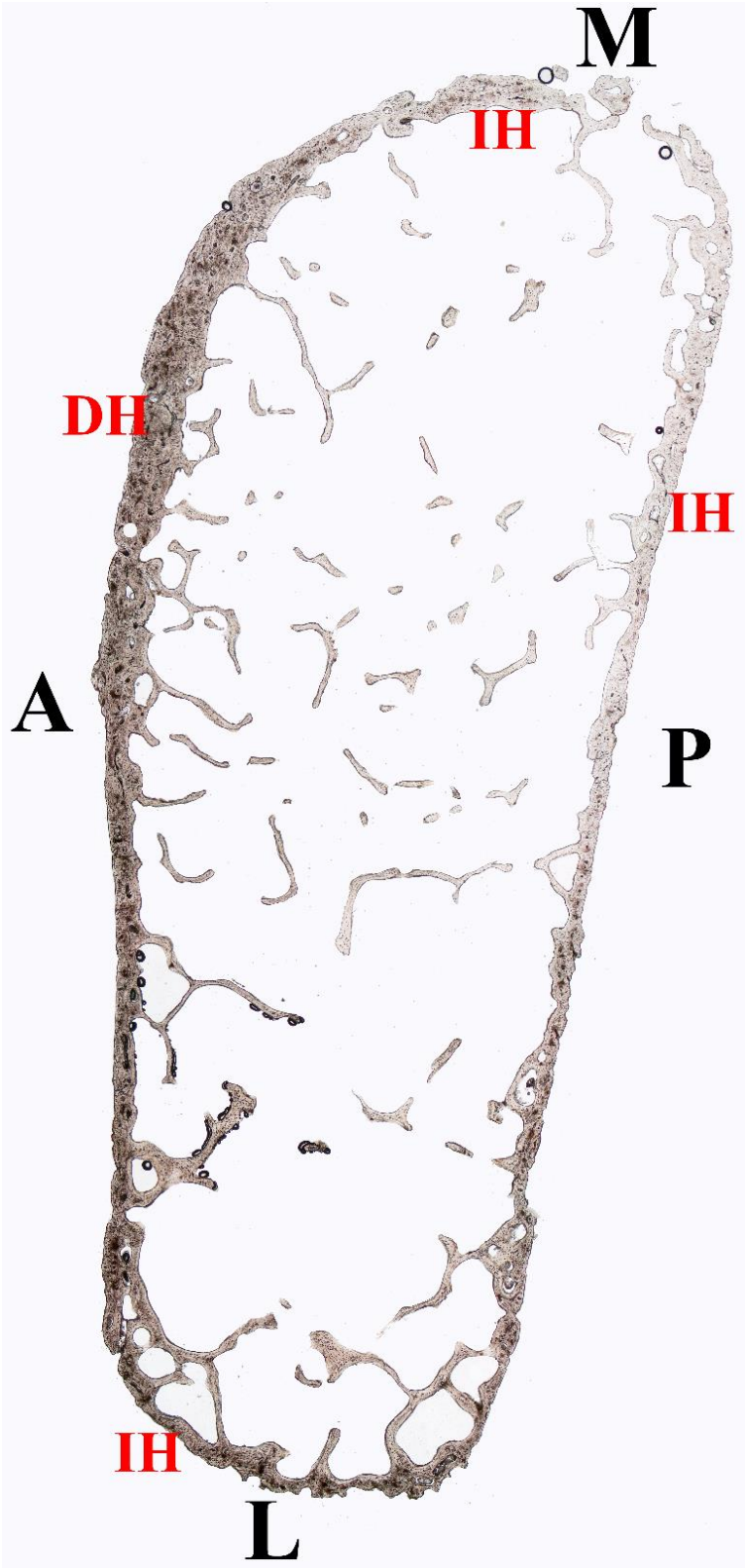

Figure A.38 – Human adult (HA1) – Sternum

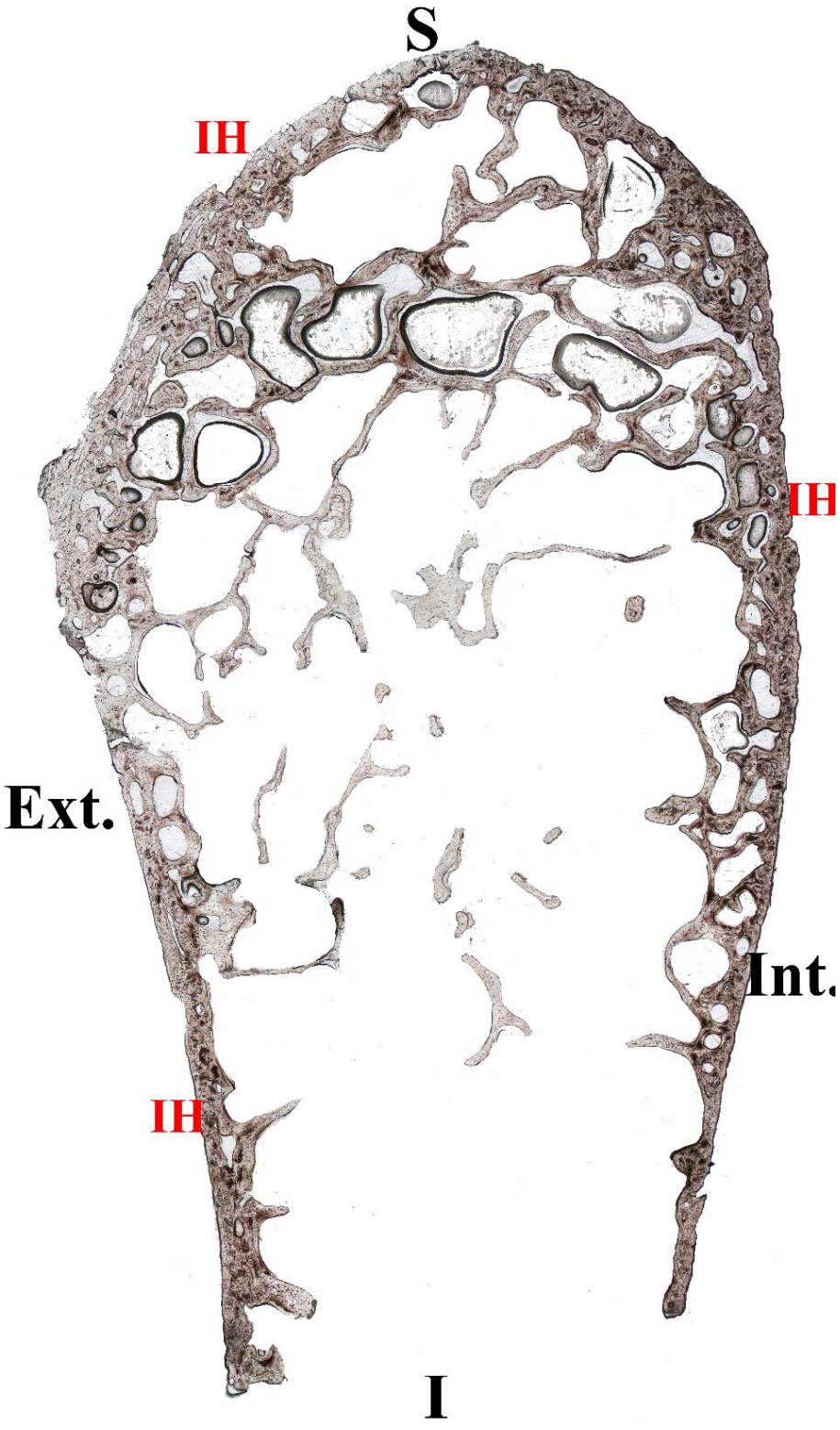

Figure A.39 – Human adult (HA1) – Iliac crest (longitudinal)

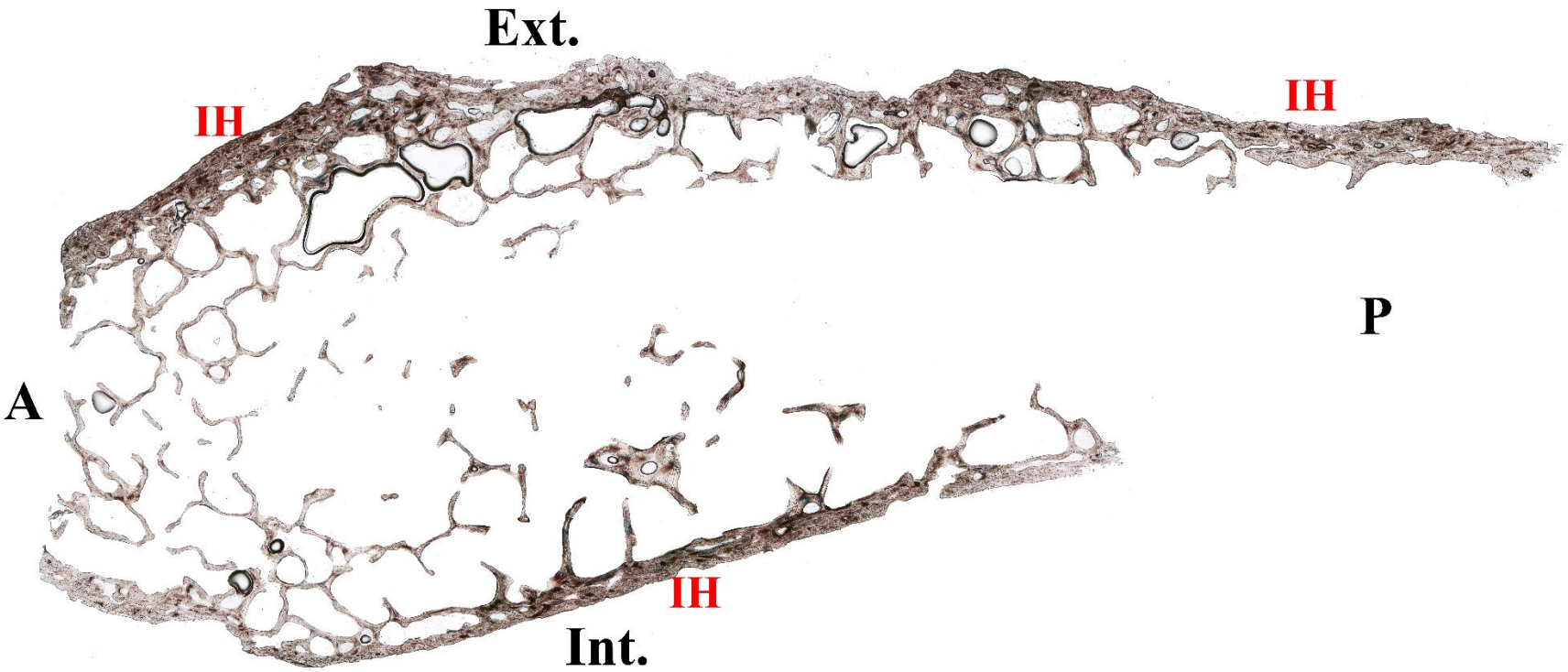

Figure A.40 – Human adult (HA1) – Iliac crest (transversal)

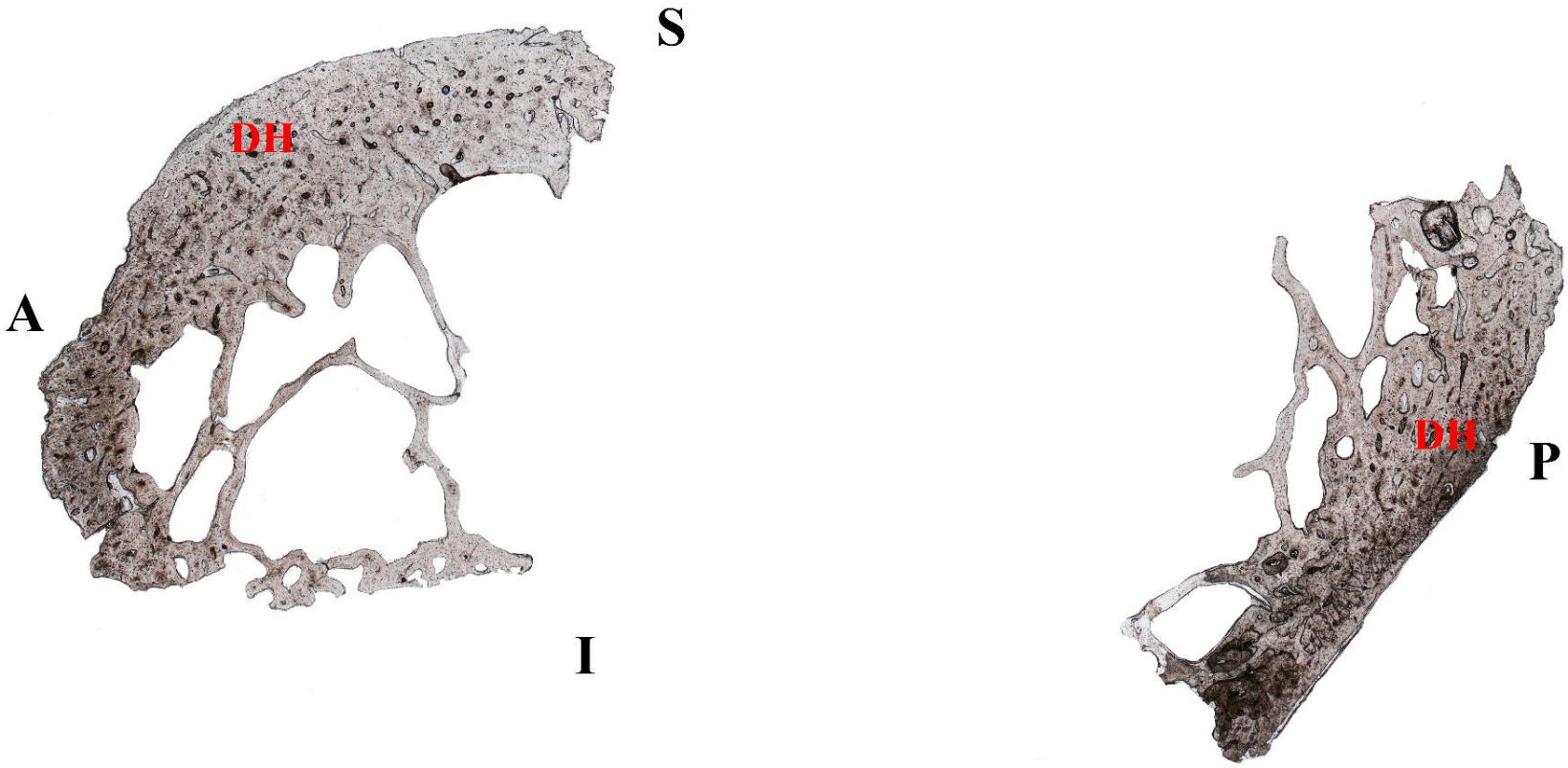

Figure A.41 – Human adult (HA1) – Iliopubic ramus

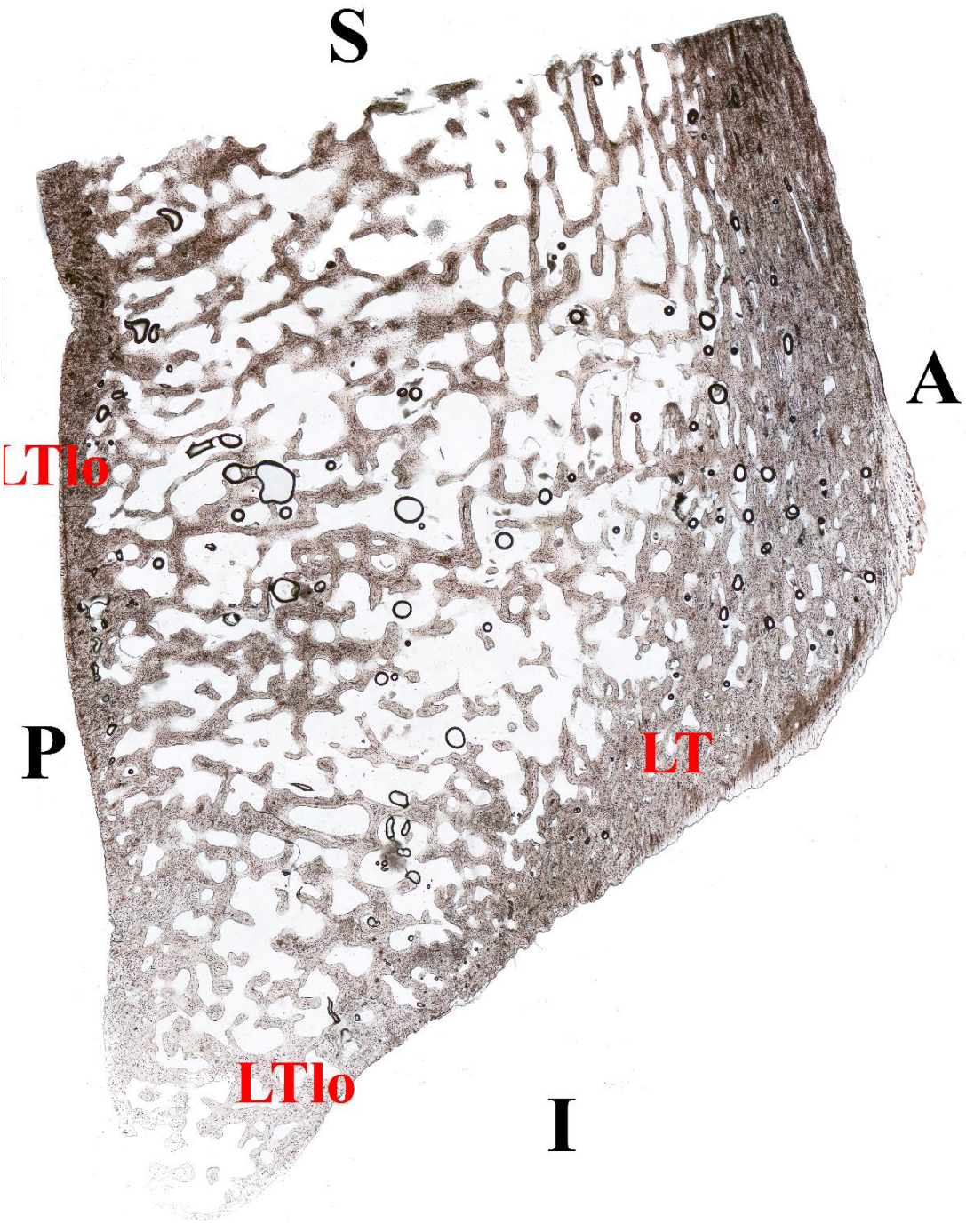

Figure A.42 – Human adult (HA1) – Patella

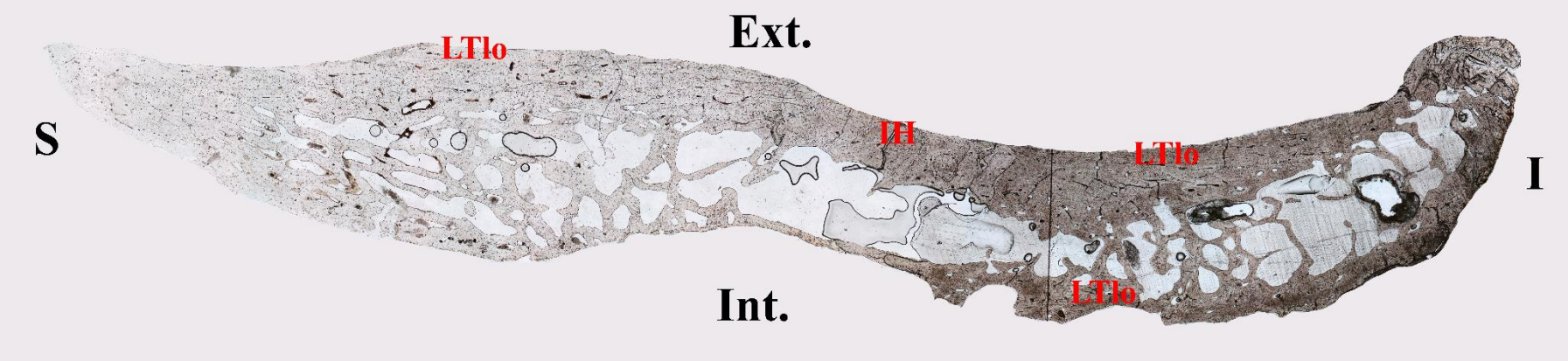

Figure A.43 – Human adult (HA1) – Mandible (gonion)

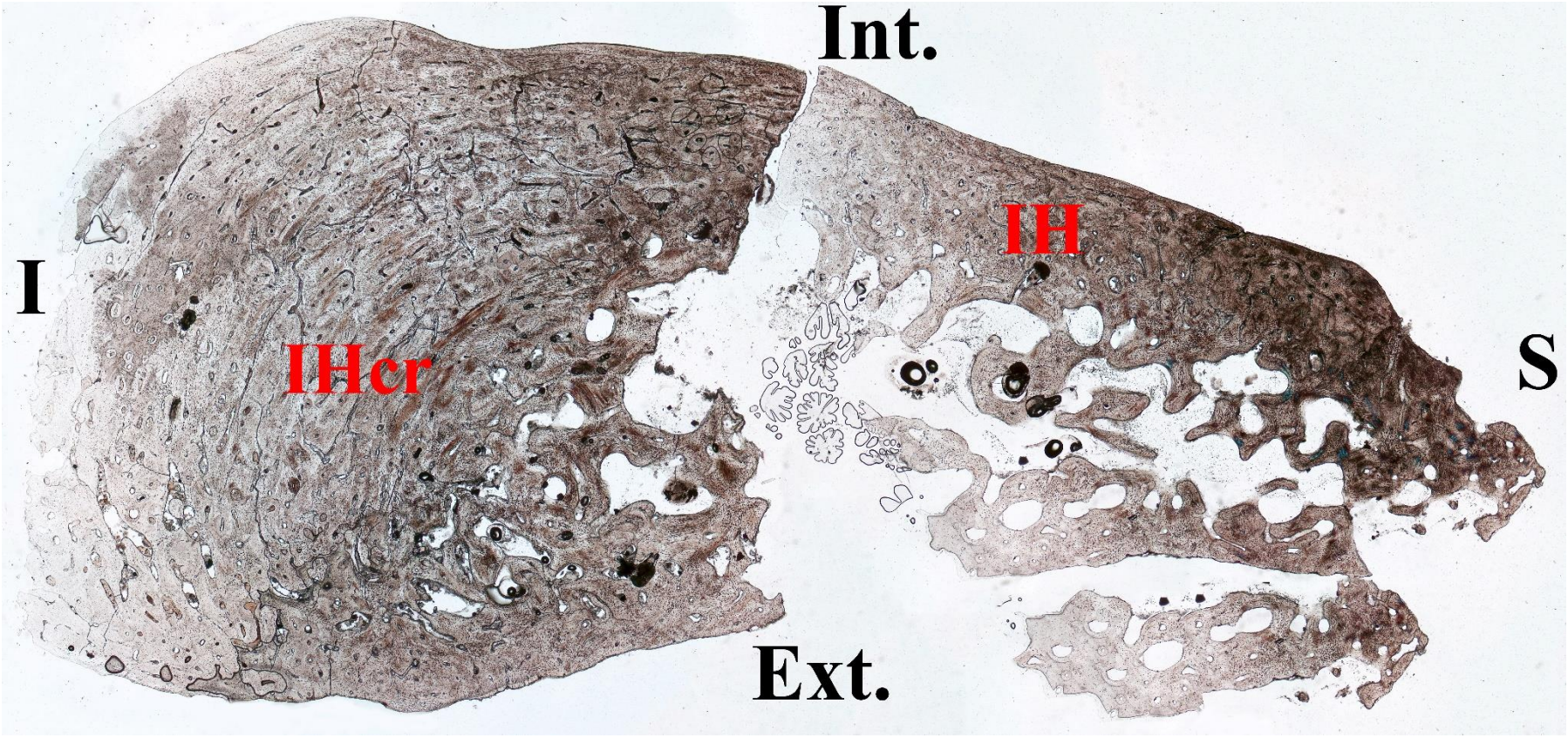

Figure A.44 – Human adult (HA1) – Mandible (mental protuberance)

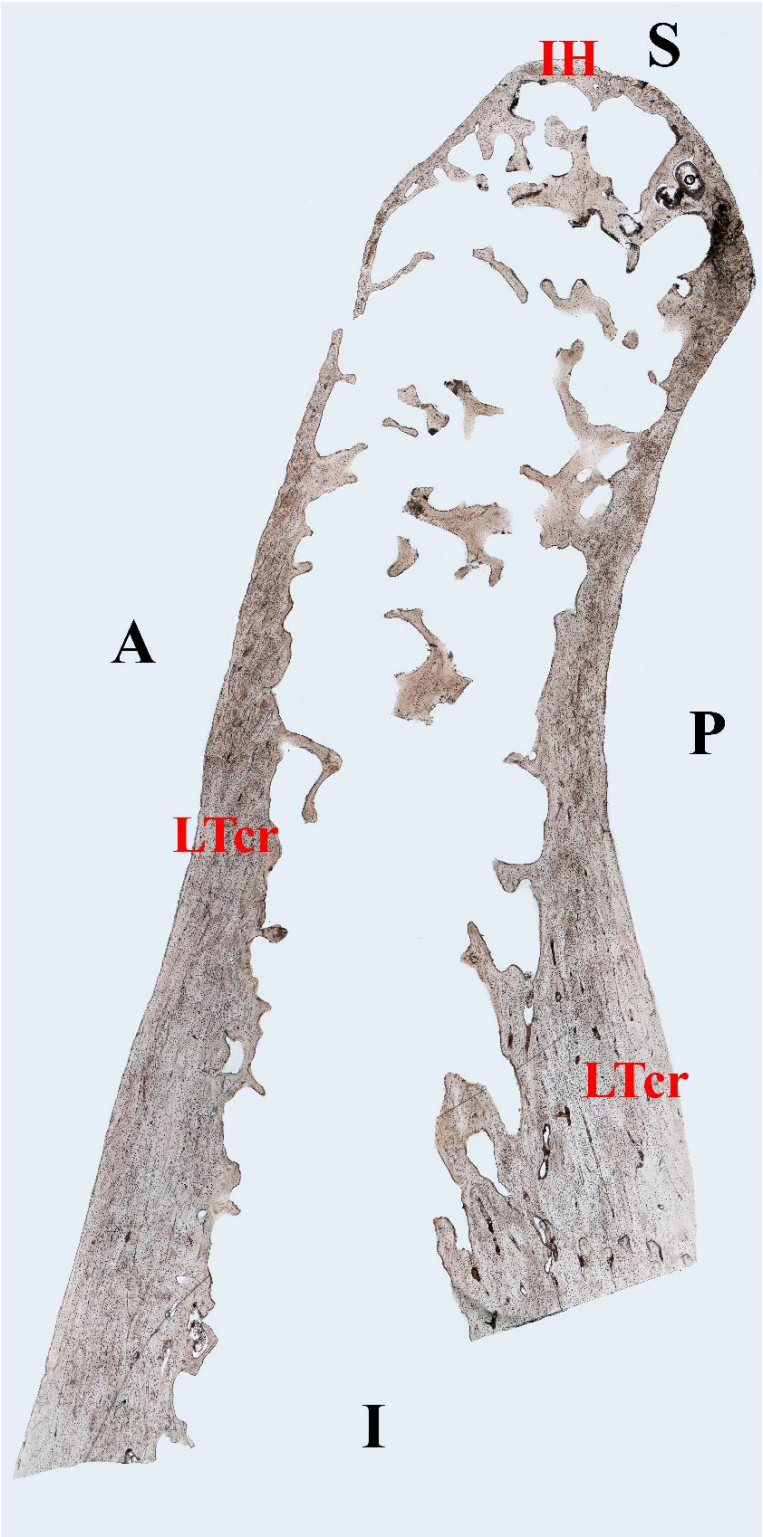

Figure A.45 – Human adult (HA1) – Mandible (mandibular condyle)

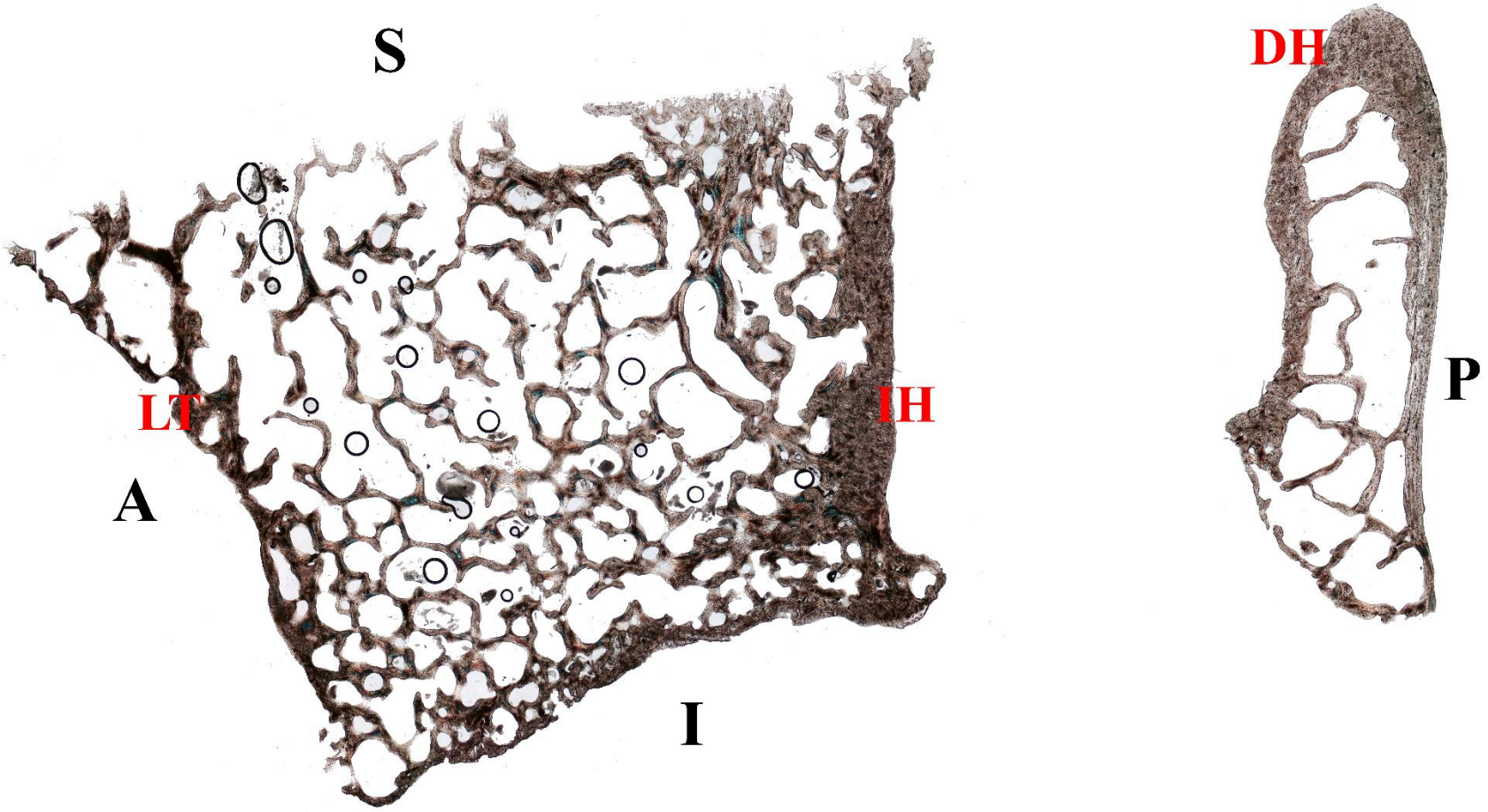

Figure A.46 – Human adult (HA1) – Cervical vertebra (longitudinal)

APPENDIX B

DESCRIPTIVE STATISTICS FOR OSTEON AND HAVERSIAN CANAL PARAMETERS IN HUMAN AND PIG (*SUS SCROFA*)

The following tables provide descriptive statistics of each cross-section analyzed during the histomorphometric analyses. In each table, the mean value, the standard deviation, the maximum and minimum value for osteon and Haversian canal parameters are reported.

HUMAN ADULT (HA1)										
Bone		**On.Dm$_{max}$ (µm)**	**On.Dm$_{min}$ (µm)**	**On.Ar (µm^2)**	**On.Pm (µm)**	**HC.Dm$_{max}$ (µm)**	**HC.Dm$_{min}$ (µm)**	**HC.Ar (µm^2)**	**HC.Pm (µm)**	**On.Cr**
Humerus (n=136)	Mean	239,58	173,69	33549,04	677,03	53,84	38,45	1728,36	152,7	0,89
	St.dev	54,81	34,11	12892,33	137,29	14,55	10,74	812,78	36,98	0,05
	Min	111,2	79,75	7122,36	310,65	20,94	16,98	290,24	66,2	0,71
	Max	383,91	260,5	68174,21	980,36	101,42	64,36	3474,24	245,09	0,97
Radius (n=130)	Mean	228,7	176,03	31738,13	650,18	48,64	36,05	1453,62	139,13	0,91
	St.dev	50,52	39,35	12242,89	132,59	12,64	10,05	725,42	34,22	0,04
	Min	132,16	87,2	8705,67	353,69	20,47	14,43	245,44	58,45	0,76
	Max	350,25	266,23	66297,41	960,5	78,21	63,38	3558,33	217,45	0,97
Ulna (n=126)	Mean	222,41	173,04	31480,39	641,19	51,05	.39,07	1690,49	147,99	0,91
	St.dev	57,75	44,55	15302,72	161,05	13,9	11,3	823	37,29	0,04
	Min	116,01	88,79	8462,18	340,74	23,04	16,01	388,61	76,02	0,73
	Max	413,23	321,01	84195,76	1137,03	96,86	63,01	3581,22	219,71	0,97
Femur (n=182)	Mean	208,18	158,81	26604,58	599,59	48,42	36,24	1485,85	140,57	0,90
	St.dev	47,24	33,46	10492,91	123,2	13,34	9,85	725,92	34,9	0,04
	Min	122,06	79,06	8427,61	349,13	19,98	15,15	305,33	66,96	0,71
	Max	367,6	244,27	61261,59	960,65	83,39	63,77	3566,13	224,67	0,98
Tibia (n=138)	Mean	222,84	174,35	31565,81	645,61	51,14	40,35	1729,55	150,98	0,91
	St.dev	51,54	40,85	13474,83	140,84	12,45	10,15	769,86	34,66	0,03
	Min	114,55	89,06	8879,52	357,6	21,19	15,74	298,52	64,02	0,83
	Max	348,94	302,79	75311,94	1009,65	78,53	61,86	3491,29	219,07	0,97
Fibula (n=107)	Mean	189,48	155,98	25335,45	566,25	46,31	38,1	1586,58	141,4	0,92
	St.dev	55,93	46,9	14313,32	162,34	14,18	11,5	851,11	40,96	0,03
	Min	100,77	83,33	7253,73	317,75	17,01	13,83	231,56	56,43	0,79
	Max	315,54	278,45	65870,96	925,91	84,99	60,96	3401,04	222,4	0,97

HUMAN ADULT (HA1)										
Bone		**On.Dm$_{max}$ (µm)**	**On.Dm$_{min}$ (µm)**	**On.Ar (µm^2)**	**On.Pm (µm)**	**HC.Dm$_{max}$ (µm)**	**HC.Dm$_{min}$ (µm)**	**HC.Ar (µm^2)**	**HC.Pm (µm)**	**On.Cr**
Metacarpal (n=87)	Mean	206,63	148,39	24505,17	579,77	50,91	40,71	1716,71	149,67	0,88
	St.dev	48,69	32,17	9628,85	120,58	13,49	11,23	815,62	36,56	0,04
	Min	125,65	85,4	9376,72	361,31	26,05	19,3	425,62	79,22	0,76
	Max	329,03	223,08	49300,97	878,08	79,49	71,72	3592,42	228,99	0,96
Metatarsal (n=52)	Mean	198,05	159,83	25744,36	580,03	49,93	39,78	1690,88	147,36	0,91
	St.dev	47,01	37,22	12976,49	135,98	13,49	10,89	840,82	37,1	0,04
	Min	109,04	73,98	7456,58	321,55	23,73	20,48	431,46	75,72	0,77
	Max	332,25	283,11	86173,82	1088,39	74	63,67	3586,09	218,93	0,97
Clavicle (n=70)	Mean	219,03	175,02	31046,18	635,27	52,23	39,85	1695,9	151,64	0,91
	St.dev	60,02	43,35	15363,21	155,28	12,18	8,92	678,89	31,38	0,04
	Min	110,21	90,64	7637,73	320,1	26,53	19,98	450,94	81,65	0,69
	Max	393,78	286,13	74180,58	1025,29	85,42	58,63	3421,49	220,94	0,97
Frontal (n=14)	Mean	215,07	156,66	26420,05	595,39	59,21	43,03	2041,26	166,98	0,91
	St.dev	47,55	24,42	9033,55	112,25	8,33	8,6	647,75	24,14	0,02
	Min	126,98	114,6	10981,8	379,25	50,11	27,55	1053,82	127,57	0,88
	Max	280,28	193,09	41031,63	758,7	81,75	61,61	3930,87	230,57	0,96
Parietal (n=25)	Mean	224,96	143,66	25155,1	594,06	55,54	35,98	1705,35	153,76	0,85
	St.dev	57,81	37,69	11385,37	138,31	15,41	10,27	775,74	37,14	0,05
	Min	120,82	89,64	8323,88	340,42	29,20	16,29	434,87	81,54	0,72
	Max	333,77	227,47	53714,43	859,01	87,11	54,74	2987,6	222,21	0,94
Occipital (n=31)	Mean	214,17	145,54	25539,27	588,13	57,18	37,05	1755,99	158,06	0,89
	St.dev	47,46	33,88	10663,17	123,63	14,47	9,27	764,17	34,89	0,04
	Min	146,23	90,39	10550,82	391,19	32,14	19,66	630,15	96,45	0,77
	Max	308,54	215,42	48281,24	822,77	86,99	55,52	3347,47	222,33	0,96

HUMAN ADULT (HA1)										
Bone		**On.Dm$_{max}$ (µm)**	**On.Dm$_{min}$ (µm)**	**On.Ar (µm^2)**	**On.Pm (µm)**	**HC.Dm$_{max}$ (µm)**	**HC.Dm$_{min}$ (µm)**	**HC.Ar (µm^2)**	**HC.Pm (µm)**	**On.Cr**
Petrous (n=4)	Mean	193,41	134,09	20154,11	525,75	47,7	27,83	1157,91	127,82	0,91
	St.dev	17,18	14,91	3582,49	44,9	15,68	9,77	677,35	41,44	0,01
	Min	172,13	120,03	16431,55	476,08	25,37	17,24	346,24	71,6	0,90
	Max	213,61	147,76	23727,91	567,28	60,37	40,78	1980,53	169,24	0,93
Rib (n=53)	Mean	177,07	135,68	19707,78	506,08	39,89	31,12	1061,26	117,42	0,90
	St.dev	50,28	40,96	10714,75	136,19	10,25	9,22	572,43	30,42	0,04
	Min	94,92	68,3	6661,35	298,84	17,5	14,39	219,14	55,08	0,77
	Max	328,22	248,99	48832,5	853,92	69,73	50,9	2922,83	199,99	0,97
Scapula (n=21)	Mean	192,02	138,38	21748,61	535,95	45,83	33,14	1242,41	130,67	0,89
	St.dev	56,87	39,04	12416,37	148,37	8,84	6,6	469,75	25,61	0,04
	Min	111,21	79,04	6813,77	311,58	31,61	19,75	544,44	88,94	0,80
	Max	351,42	232,35	60628,03	924,58	61,99	46,55	2345,28	181,7	0,96
Sternum (n=32)	Mean	161,88	123,29	15822,17	458,63	40,88	30,05	1029,39	117,08	0,90
	St.dev	38,18	27,33	6387,68	99,59	13,56	7,64	545,08	32,45	0,04
	Min	84,54	66,2	4654,52	249,95	18,89	15,45	235,7	57,45	0,82
	Max	242,08	163,03	29449,39	646,71	73,12	45,88	2218,66	187,09	0,97
Iliac crest (n=19)	Mean	158,27	119,43	14860,02	450,93	47,22	34,13	1338,9	134,57	0,89
	St.dev	40,71	26,62	6267,96	107,06	15,17	8,95	650,6	35,31	0,05
	Min	99,94	72,85	6150,99	286,37	22,72	21,22	418,8	75,06	0,76
	Max	229,55	162,4	25602,28	617,16	79,79	52,69	2683,24	200,92	0,96
Iliopubic ramus (n=45)	Mean	203,33	152,45	25161,87	573,82	53,19	37,26	1685,55	151,02	0,90
	St.dev	53,12	43,41	12205,78	147,63	16,47	9,91	854,13	41,25	0,03
	Min	85,33	71,96	4472,39	252,11	26,85	17,87	396,4	75,78	0,80
	Max	311,9	235,92	53745,11	858,41	91,3	59,73	3693,71	228,35	0,96

HUMAN ADULT (HA1)										
Bone		**On.Dm$_{max}$ (µm)**	**On.Dm$_{min}$ (µm)**	**On.Ar (µm^2)**	**On.Pm (µm)**	**HC.Dm$_{max}$ (µm)**	**HC.Dm$_{min}$ (µm)**	**HC.Ar (µm^2)**	**HC.Pm (µm)**	**On.Cr**
Ischiopubic ramus (n=10)	Mean	206,64	142,78	24047,66	568,66	50,27	32,89	1347,56	137,06	0,89
	St.dev	63,53	33,75	11189,93	150,11	14,99	7,59	551,44	32,71	0,03
	Min	101,82	64,26	5839,82	286,45	24,67	17,76	444,12	78,67	0,83
	Max	304,43	185,44	43896,02	802,58	81,21	43,83	2108,12	193,35	0,93
Mandible (n=35)	Mean	240,5	165,62	33020,97	669,6	54,77	40,55	1888,53	159,34	0,87
	St.dev	70,79	42,73	16192,2	180,04	15,36	10,04	946,08	40,77	0,05
	Min	124,09	80,58	9017,82	361,57	31,21	22,5	572,68	90,52	0,78
	Max	384,96	260,74	68078,28	1004,43	86,37	60,16	3890,45	236,55	0,94

Table B.1 – Descriptive statistics of osteon and Haversian canal parameters for the human adult individual HA1

HUMAN JUVENILE (HJ) – LONG BONES										
Bone		**On.Dm$_{max}$ (µm)**	**On.Dm$_{min}$ (µm)**	**On.Ar (µm^2)**	**On.Pm (µm)**	**HC.Dm$_{max}$ (µm)**	**HC.Dm$_{min}$ (µm)**	**HC.Ar (µm^2)**	**HC.Pm (µm)**	**On.Cr**
Humerus (n=30)	Mean	241,58	177,64	33903,69	681,77	52,05	34,4	1485,11	143,44	0,89
	St.dev	43,4	34,78	10305,64	103,93	15,84	7,78	675,95	34,31	0,04
	Min	159,57	112,64	15916,81	482,5	30,01	20,81	501,59	84,5	0,78
	Max	320,38	237,97	54920,67	868,37	92,39	52,15	3442,43	227,91	0,95
Radius (n=23)	Mean	260,2	190,24	38732,13	733,9	50,54	37,65	1550,04	142,58	0,88
	St.dev	54,83	41,79	13686,08	141,84	12,66	9,8	717,21	31,16	0,05
	Min	170,62	108,41	15549,63	457,84	32,65	21,81	712,45	97,39	0,77
	Max	411,94	282,47	68536,04	1040,82	80,04	61,73	3436,1	214,86	0,96
Ulna (n=18)	Mean	241,54	196,46	37266,44	706,78	45,47	36,47	1445,05	137,48	0,91
	St.dev	56,16	33,5	14281,17	134,42	14,69	9,15	701,72	35,65	0,04
	Min	147,14	133,88	15614,4	452,16	23,26	19,18	411,01	79,35	0,84
	Max	393,98	276,58	79907,9	1072,89	83,89	51,01	2929,16	211,74	0,97
Femur (n=30)	Mean	231,36	174,35	32142,19	658,41	33,32	22,47	627,57	93,21	0,91
	St.dev	38,14	30,61	9698,32	98,04	7,49	4,57	235,76	17,58	0,03
	Min	160,22	107,39	16812,85	489,76	22,89	13,96	336,99	70,81	0,81
	Max	305,34	243,47	59796,77	911,43	51,34	32,08	1267,6	136,66	0,98
Tibia (n=36)	Mean	271,25	209,1	45787,44	786,57	51,68	38,41	1626,68	147,45	0,91
	St.dev	46,95	43,07	13867,49	134,44	10,47	8,88	546,31	25,87	0,04
	Min	152,01	101,35	12130,57	429	28,69	20,99	532,75	83,82	0,81
	Max	345,43	286,47	65524,58	998,03	71,51	53,68	2557,6	189,07	0,97
Fibula (n=12)	Mean	250,52	185,95	38446,51	720,65	56,92	40,73	1958,94	159,91	0,90
	St.dev	60,55	40,38	15443,86	154,11	19,65	9,6	984,53	43,02	0,03
	Min	125,2	119,11	12186,58	400,9	33,43	27,99	704,17	97,86	0,84
	Max	341,63	276,46	74400,2	1025,34	94,14	57,01	3692,74	230,85	0,95

HUMAN JUVENILE (HJ) – FLAT BONES										
Bone		**On.Dm$_{max}$ (µm)**	**On.Dm$_{min}$ (µm)**	**On.Ar (µm^2)**	**On.Pm (µm)**	**HC.Dm$_{max}$ (µm)**	**HC.Dm$_{min}$ (µm)**	**HC.Ar (µm^2)**	**HC.Pm (µm)**	**On.Cr**
Rib (n=8)	Mean	211,88	163,16	28863,31	609,39	47,62	31,94	1277,64	131,02	0,91
	St.dev	54,14	57,17	14889,19	155,56	16,66	12,07	882,93	41,25	0,04
	Min	123,64	95,91	12482,66	418,58	30,71	21,64	599,95	90,64	0,83
	Max	281,3	239,72	49871,7	822,15	79,06	59,09	3317,28	216,6	0,97
Occipital (n=5)	Mean	239,04	151,08	28701,39	620,53	54,47	25,84	1223,67	140,37	0,87
	St.dev	100,33	44,21	18640,69	215,09	17,63	3,06	539,92	40,79	0,06
	Min	109,81	97,74	8796,25	342,14	35,94	22,07	617	94,73	0,79
	Max	391,31	211,53	59016,14	943,79	78,83	29,38	2002,45	197,88	0,94

Table B.2 – Descriptive statistics of osteon and Haversian canal parameters for the human juvenile individual HJ

PIG JUVENILE (PJ)										
Bone		**On.Dm$_{max}$ (µm)**	**On.Dm$_{min}$ (µm)**	**On.Ar (µm^2)**	**On.Pm (µm)**	**HC.Dm$_{max}$ (µm)**	**HC.Dm$_{min}$ (µm)**	**HC.Ar (µm^2)**	**HC.Pm (µm)**	**On.Cr**
Humerus (n=7)	Mean	203,99	176,92	28670,72	609,2	41,92	32,76	1147,94	119,43	0,96
	St.dev	24,6	14,73	5405,28	62,74	13,06	11,23	769,37	37,68	0,02
	Min	167,52	158,24	20947,28	518,84	27,37	20,13	443,64	78,81	0,91
	Max	239,24	200,17	33408,99	672,82	63,51	53,99	2678,37	186,74	0,98
Radius (n=67)	Mean	212,9	171,56	29558,96	623,97	37,6	26,18	858,71	108,91	0,92
	St.dev	41,21	37,93	11163,43	116,88	9,99	7,3	449,15	25,48	0,03
	Min	121,5	101,82	10689,61	383,14	21,68	13,55	302,41	69,02	0,84
	Max	319,27	269,96	61705,71	924,65	64,39	56,02	2871,21	196,04	0,96
Ulna (n=54)	Mean	197,91	159,77	25912,03	583,09	38,47	27	895,28	110,01	0,91
	St.dev	43,67	39,83	10924,73	125,24	11,78	7,09	493,62	29,47	0,03
	Min	111,11	73,36	6777,25	306,9	17,89	14,04	224,01	56,93	0,80
	Max	288,94	252,18	47942,3	811,5	78,92	43,25	2658,89	201,56	0,98
Femur (n=18)	Mean	170,65	140,27	20108,51	496,76	32,04	22,69	644,32	90,33	0,92
	St.dev	48,99	50,57	13160,24	155,68	11,23	11,13	735,71	34,76	0,05
	Min	107,49	72,72	5143,44	271,17	20,71	13,97	234,72	59,83	0,77
	Max	266,48	228,69	46015,83	769,89	70,53	58,29	3425,88	211,41	0,98
Tibia (n=51)	Mean	202,05	160,62	26868,5	589,19	40,88	27,01	978,74	117,37	0,92
	St.dev	51,35	40,1	12847,07	140,88	9,63	6,15	391,3	23,9	0,03
	Min	117,56	87,71	8046,79	330,41	20,09	14,23	292,67	171,03	0,85
	Max	311,98	269,29	67185,16	934,65	62,51	44,68	2117,86	62,81	0,98
Fibula (n=16)	Mean	175	135,94	18829,93	508,24	27,47	18,67	436,48	78,64	0,88
	St.dev	38,7	33,02	7722,6	109,5	6,33	4,6	155,91	13,08	0,05
	Min	123,11	91,61	8539,13	356,03	20,94	9,36	242,03	64,48	0,81
	Max	244,88	187,02	31422,13	690,93	37,4	26,66	725,11	100	0,95

PIG JUVENILE (PJ)										
Bone		**On.Dm$_{max}$ (µm)**	**On.Dm$_{min}$ (µm)**	**On.Ar (µm^2)**	**On.Pm (µm)**	**HC.Dm$_{max}$ (µm)**	**HC.Dm$_{min}$ (µm)**	**HC.Ar (µm^2)**	**HC.Pm (µm)**	**On.Cr**
Metacarpal (n=47)	Mean	176,89	138,27	19637,04	511,43	35,79	24,38	726,73	100,41	0,91
	St.dev	37,51	29,32	7844,86	101,29	10,68	6,79	396,55	24,73	0,03
	Min	103,26	82,68	6549,83	300,25	18,89	13,22	220,11	56,2	0,80
	Max	291,83	225,72	48617,74	812,09	77,38	45,44	2664,73	196	0,97
Metatarsal (n=29)	Mean	198,59	149,3	24251,83	575,5	45,23	23,9	975,57	122,36	0,89
	St.dev	43,94	32,75	10099,34	118,71	8,87	5,72	373,65	21,35	0,05
	Min	133,43	93,93	9438,57	362,31	32,57	15,6	528,86	96	0,77
	Max	321,39	218,28	50397,15	818,98	63,78	35,84	1916,74	173,53	0,95
Rib (n=12)	Mean	165,73	130,39	18015,31	474,45	33,92	25,31	748,04	100,48	0,93
	St.dev	54,31	38,62	9832,43	145,84	11,62	5,57	396,87	26,78	0,02
	Min	79,74	69,51	4362,82	242,54	21,85	17,46	378,87	72,66	0,89
	Max	238,89	188,88	32320,6	662,6	54,19	34,74	1508,16	148,75	0,95

Table B.3 – Descriptive statistics of osteon and Haversian canal parameters for the pig juvenile PJ

HUMAN – HUMERUS – INTRA-SPECIES										
Individual		**On.Dm$_{max}$ (µm)**	**On.Dm$_{min}$ (µm)**	**On.Ar (µm^2)**	**On.Pm (µm)**	**HC.Dm$_{max}$ (µm)**	**Hc.Dm$_{min}$ (µm)**	**HC.Ar (µm^2)**	**HC.Pm (µm)**	**On.Cr**
HA1 (n=36)	Mean	224,56	167,31	31538,02	655,78	55,49	42,67	2063,91	162,99	0,88
	St.dev	61,94	35,3	13887,72	164,18	15,95	12,21	958,44	42,33	0,05
	Min	11,20	79,75	7122,36	310,65	23,13	17,54	388,63	75,37	0,71
	Max	357,15	233,87	57431,27	948,73	83,89	64,36	3474,24	222,33	0,97
HA2 (n=18)	Mean	254,46	216,11	44131,93	753,13	53,65	46,43	1939,9	156,73	0,96
	St.dev	34,39	29	12126,76	102,09	10,02	9,93	750,08	30,3	0,01
	Min	191,80	153,96	22386,78	552,30	36,93	28,26	805,95	104,12	0,92
	Max	324,21	288,25	75282,60	991,40	71,62	64,90	3444,87	210,74	0,98
HA3 (n=20)	Mean	243,93	190,89	37133,47	695,39	53,46	41,73	1732,88	149,67	0,95
	St.dev	37,72	23,75	9755,6	97,01	10,54	8,66	623,13	28,68	0,02
	Min	158,35	133,58	16928,75	469,18	33,73	27,86	656,44	93,59	0,90
	Max	329,23	239,08	56304,66	874,67	70,41	55,04	2757,75	191,92	0,98
HA6 (n=35)	Mean	230,68	190,26	34625,04	665,71	43,87	34,18	1197,6	123,25	0,96
	St.dev	36,19	32,38	10863,81	107,89	10,89	8,33	545,53	29,37	0,01
	Min	164,22	134,94	16457,36	465,36	19,54	18,62	306,79	63,08	0,92
	Max	299,01	236,57	54888,05	843,13	66,79	52,38	2532,76	182,02	0,98
HA7 (n=15)	Mean	216,95	178,79	30481,16	628,18	51,61	42,73	1783,47	151,68	0,96
	St.dev	27,41	23,9	7552,74	80,27	9,1	9,16	619,56	27,98	0,02
	Min	166,99	140,49	19630,49	503,4	32,13	23,77	583,40	89,85	0,91
	Max	265,30	213,48	42251,02	753,69	66,58	57,12	2751,41	189,27	0,98
HA13 (n=34)	Mean	217,62	180,24	31171,12	632,67	46,47	36,89	1322,04	130,71	0,95
	St.dev	36,34	34,96	10745,72	104,78	9,65	7,45	473,88	25,78	0,02
	Min	156,32	125,19	18709,13	500,61	22,03	19,05	329,20	66,68	0,90
	Max	305,06	290,41	66886,16	935,37	59,92	52,15	2283,43	173,11	0,98
Total (n=158)	Mean	229,56	184,81	34183,07	666,49	50,14	39,86	1629,71	143,77	0,94
	St.dev	43,97	34,26	11946,45	122,72	12,45	10,21	760,64	35,21	0,04
	Min	111,20	79,75	7122,36	310,65	19,54	17,54	306,79	63,08	0,71
	Max	357,15	290,41	75282,6	991,40	83,89	64,90	3474,24	222,33	0,98

Table B.4 – Humerus - descriptive statistics of osteon and Haversian canal parameters in different human individuals

HUMAN – RADIUS – INTRA-SPECIES										
Individual		**On.Dm$_{max}$ (µm)**	**On.Dm$_{min}$ (µm)**	**On.Ar (µm^2)**	**On.Pm (µm)**	**HC.Dm$_{max}$ (µm)**	**Hc.Dm$_{min}$ (µm)**	**HC.Ar (µm^2)**	**HC.Pm (µm)**	**On.Cr**
HA1 (n=50)	Mean	244,56	188,69	36387,9	699,85	43,68	30,58	1088,72	122,27	0,90
	St.dev	49,8	44,39	13310,31	137,2	10,82	6,6	436,73	25,94	0,04
	Min	132,16	87,20	8705,67	353,69	20,47	14,43	245,44	58,45	0,76
	Max	350,25	266,23	66297,41	960,5	70,72	44,53	2246,42	179,64	0,96
HA3 (n=19)	Mean	248,86	200,98	39887,87	713,37	54,22	44,92	1902	155,66	0,96
	St.dev	46,08	36,24	13601,09	125,76	11,33	9,02	687,72	29,33	0,01
	Min	177,17	141,77	19910,02	514,40	36,02	27,95	805,95	104,18	0,90
	Max	314,91	282,75	65816,27	926,27	73,83	59,58	3030,94	200,9	0,97
HA4 (n=19)	Mean	265,17	204,97	42814,09	746,74	57,54	46,76	2092,2	162,95	0,94
	St.dev	46,05	41,68	14861,54	131,2	11,81	10,28	873,11	33,65	0,02
	Min	188,79	138,41	21709,39	530,38	35,43	29,44	851,23	106,19	0,89
	Max	340,59	289,78	70415,27	980,64	81,49	65,11	3936,23	226,92	0,97
HA6 (n=29)	Mean	218,73	184,5	32425,41	642,99	47,08	40,08	1483,41	136,89	0,96
	St.dev	38,42	30,21	10710,95	105,83	11,48	8,14	638,26	29,29	0,02
	Min	164,73	139,30	17771,51	483	28,05	25,82	565,87	86,42	0,91
	Max	313,24	261,77	59199,25	873,08	72,16	59,67	3112,26	201,20	0,98
HA7 (n=25)	Mean	216,74	182,61	31382,8	633,13	43,76	36,88	1268,94	126,39	0,96
	St.dev	35,77	28,39	10060,89	98,07	11,32	7,52	648,60	29,30	0,01
	Min	147,38	118,71	13361,65	416,86	21,90	21,30	374,48	69,71	0,93
	Max	311,09	271,80	66598,36	927,66	82,29	60,13	3760,92	223,09	0,98
HA13 (n=32)	Mean	233,48	186,69	36005,05	670,53	52,41	41,68	1738,85	147,33	0,95
	St.dev	64,60	47,35	18972,69	174,3	14,04	11,03	896,56	37,83	0,02
	Min	153,13	122,22	16460,76	466,32	27,46	25,97	542	85,19	0,87
	Max	394,08	305,11	88247,85	1085,03	87,87	65,90	4398,85	242,57	0,98
Total (n=174)	Mean	236,94	189,87	36021,84	681,99	48,53	38,44	1571,91	138	0,94
	St.dev	50,45	39,88	14196,65	136,54	12,69	10,25	1226,58	33,5	0,04
	Min	132,16	87,20	8705,67	353,69	20,47	14,43	245,44	58,45	0,76
	Max	394,08	305,11	88247,85	1085,03	87,87	65,90	4398,85	242,57	0,98

Table B.5 – Radius - descriptive statistics of osteon and Haversian canal parameters in different human individuals

HUMAN – ULNA – INTRA-SPECIES										
Individual		**On.Dm$_{max}$ (µm)**	**On.Dm$_{min}$ (µm)**	**On.Ar (µm^2)**	**On.Pm (µm)**	**HC.Dm$_{max}$ (µm)**	**Hc.Dm$_{min}$ (µm)**	**HC.Ar (µm^2)**	**HC.Pm (µm)**	**On.Cr**
HA1 (n=36)	Mean	231,17	180,08	33840,61	670,21	55,09	42,06	1924,47	156,92	0,88
	St.dev	70,24	51,74	18841,75	192,5	16,55	11,82	910,77	41,24	0,05
	Min	119,93	96,86	9117,10	358,75	24,79	17,87	424,67	76,02	0,73
	Max	413,23	321,01	84195,76	1137,03	96,86	58,57	3465,96	219,71	0,95
HA3 (n=29)	Mean	221,84	183,46	33245,79	645,94	48,97	41,68	1640,97	143,7	0,96
	St.dev	54,34	41,8	14950,83	146,01	11,26	9,64	705,67	32,72	0,01
	Min	128,52	102,68	10441,25	372,61	27,95	24,01	540,54	83,78	0,92
	Max	358,63	291,87	74667,55	992,42	67,64	60,60	3086,45	200,12	0,98
HA4 (n=24)	Mean	236,18	201,02	37664,65	692,26	56,49	49,52	2135,8	165,14	0,96
	St.dev	40,86	37,3	13115,37	114,65	9,23	9,15	693,7	27,63	0,02
	Min	178,54	141,79	21662,64	551,29	36,39	29,22	906,75	109,08	0,87
	Max	350,28	267,29	73823,63	984,71	74,59	67,35	3482,85	213,11	0,98
HA5 (n=34)	Mean	213,68	180,8	30942,09	627,05	45,92	39,37	1422,18	134,26	0,96
	St.dev	36,28	25,32	10244,45	99,61	9,38	8,24	557,54	26,88	0,01
	Min	168,2	137,76	19339,79	499,42	25,12	24,46	500,12	82,14	0,93
	Max	312,74	255,91	66031,52	923,64	66,13	55,20	2735,83	189,68	0,99
HA6 (n=38)	Mean	216,27	182,2	31415,84	630,97	49,8	40,28	1554,3	141	0,96
	St.dev	36,66	30,55	10578,13	104,60	10,96	8,42	601,68	28,59	0,01
	Min	151,99	134,45	16065,83	455,49	27,18	24,42	531,78	84,23	0,94
	Max	324,67	242,24	62994,25	914,97	73,29	53,59	2958,38	199,23	0,99
HA13 (n=38)	Mean	235,72	199,6	37877,86	694,55	53,18	45,2	1931,67	155,19	0,96
	St.dev	43,17	32,62	12652,66	116,81	12,23	11,18	868,43	36,07	0,01
	Min	181,45	141,69	20289,86	513,74	26,81	20,75	462,63	78,84	0,92
	Max	317,04	258,97	62798,97	903,79	82,11	65,78	3926	227,91	0,98
Total (n=199)	Mean	225,45	187,35	34027,8	659,11	51,42	42,7	1748,99	148,74	0,95
	St.dev	48,83	37,92	13789,54	134,5	12,41	10,28	775,61	34,07	0,04
	Min	119,93	96,86	9117,10	358,75	24,79	17,87	424,67	76,02	0,73
	Max	413,23	321,01	84195,76	1137,03	96,86	67,35	3926	227,91	0,99

Table B.6 – Ulna - descriptive statistics of osteon and Haversian canal parameters in different human individuals

HUMAN – FEMUR – INTRA-SPECIES										
Individual		**On.Dm$_{max}$ (µm)**	**On.Dm$_{min}$ (µm)**	**On.Ar (µm^2)**	**On.Pm (µm)**	**HC.Dm$_{max}$ (µm)**	**Hc.Dm$_{min}$ (µm)**	**HC.Ar (µm^2)**	**HC.Pm (µm)**	**On.Cr**
HA1 (n=43)	Mean	200,66	151,49	25521,31	583,4	48,12	38,39	1640	147,43	0,90
	St.dev	46,93	37,83	10883,85	125,74	13,08	10,05	749,58	34,93	0,03
	Min	131	79,06	9934,30	382,99	21,55	21,65	429,52	76,02	0,82
	Max	336,27	229,83	57658,22	893,6	77,23	57,24	3139,21	207,74	0,97
HA14 (n=29)	Mean	284,81	230,09	52493,21	821,77	59,88	49,6	2280,93	171,14	0,95
	St.dev	51,76	42,86	16778,71	141	12,95	9,33	908,62	34,31	0,02
	Min	175,73	150,99	21345,13	524,33	37,45	32,88	939,86	111,03	0,87
	Max	374,98	291,25	82275,09	1039,19	91,14	70,47	4636,01	250,4	0,98
HA15 (n=32)	Mean	276,06	231,07	50560,99	808,44	56,02	43,64	1870,09	154,88	0,95
	St.dev	42,62	39,57	14945,71	120,65	13,29	9,79	791,02	35,5	0,02
	Min	193,94	175,41	26380,47	581,31	24,78	22,72	413,93	74,78	0,88
	Max	340,45	298,79	78515,63	1007,89	74,65	62,35	3494,05	212,28	0,98
HA16 (n=40)	Mean	223,12	186,56	32771,58	645,45	47,41	38,93	1471,75	135,21	0,95
	St.dev	42,17	36,13	12237,28	120,11	13,38	10,67	859,27	36,52	0,02
	Min	140,75	105,28	12680,86	406,15	30,01	19,54	405,65	75,47	0,90
	Max	301,28	266,69	60122,55	883,78	88,25	66,58	4377,43	240,76	0,98
HA17 (n=31)	Mean	228,51	190,12	34776,48	670,35	51,91	41,08	1659,2	146,28	0,96
	St.dev	31,02	21,69	8745,46	84	10,73	6,99	625,1	26,96	0,01
	Min	178,13	155,64	22946,31	547,4	38,84	30,7	893,6	109,91	0,93
	Max	295,89	247,77	56698,62	860,46	78,65	60,01	3390,33	211,91	0,97
HA18 (n=35)	Mean	240,95	200,66	38691,89	702,9	47,32	39,82	1463,03	136,92	0,96
	St.dev	43,97	35,74	12789,83	118,6	8,59	7,85	568	25,45	0,01
	Min	152,62	135,23	16286,43	468,48	33,7	29,07	690,53	95,77	0,93
	Max	317,07	274,23	66046,62	923,94	73,06	67,51	3578,3	216,12	0,98
Total (n=210)	Mean	238,87	195,05	38003,91	695,18	51,24	41,48	1704,86	147,59	0,94
	St.dev	52,20	45,46	15886,51	146,04	12,89	9,9	796,41	34,38	0,03
	Min	131	79,06	9934,30	382,99	21,55	19,54	405,65	74,78	0,82
	Max	374,98	298,79	82275,09	1039,19	91,14	70,47	4636,01	250,4	0,98

Table B.7 – Femur - descriptive statistics of osteon and Haversian canal parameters in different human individuals

HUMAN – TIBIA – INTRA-SPECIES										
Individual		**On.Dm$_{max}$ (µm)**	**On.Dm$_{min}$ (µm)**	**On.Ar (µm^2)**	**On.Pm (µm)**	**HC.Dm$_{max}$ (µm)**	**Hc.Dm$_{min}$ (µm)**	**HC.Ar (µm^2)**	**HC.Pm (µm)**	**On.Cr**
HA1 (n=43)	Mean	206,3	166,36	29574,32	617,95	49,62	39,55	1731,87	150,89	0,92
	St.dev	53,48	44,59	15616,75	157,91	13,16	9,66	824,89	36,91	0,02
	Min	126,17	101,75	11128,4	389,39	27,91	21,65	545,94	87,12	0,84
	Max	327,75	302,79	75311,94	1009,65	78,16	61,86	3491,29	219,07	0,97
HA2 (n=36)	Mean	258,72	220,04	45422,64	763,1	52,18	43,38	1754,07	148,78	0,96
	St.dev	41,12	36,33	14180,92	117,21	12,59	9,85	775,3	33,41	0,02
	Min	185,22	144,64	22467,13	542,08	30,91	28,69	653,52	92,94	0,91
	Max	362,93	314,34	86110,52	1068,9	76,98	69,53	3563,69	217	0,99
HA3 (n=35)	Mean	246,28	207,95	41929,08	727,83	54,33	46,3	1977,93	158,68	0,96
	St.dev	48,3	39,28	16141,88	133,96	10,74	8,63	724,37	30,52	0,01
	Min	175,15	135,69	18488,53	496,22	22,43	20,54	344,78	67,94	0,92
	Max	400,31	335,66	98668,16	1137,36	76,08	66,39	3831,04	225,73	0,98
HA6 (n=46)	Mean	219,24	185,81	32856,75	649,01	48,78	41,68	1594,85	141,77	0,96
	St.dev	35,83	25,47	9491,03	95,69	10,13	9,69	676,98	30,47	0,01
	Min	150,03	125,61	14584,45	438,03	23,04	21,50	337,47	67,64	0,91
	Max	304,22	247,38	56981,55	857,41	71,33	67,17	3689,33	220,7	0,98
HA7 (n=37)	Mean	228,59	193,85	35893,65	677,74	45,86	39,09	1442,63	133,9	0,96
	St.dev	33,41	29,16	10157,26	96,47	11,69	10,52	805,15	34,26	0,01
	Min	157,79	140,65	17344,14	473,31	26,13	23,98	474,31	80,8	0,93
	Max	308,62	256,22	65341,96	926,99	77,22	67,12	3780,4	222,01	0,98
HA16 (n=34)	Mean	247,8	205,09	40867,3	720,01	55,62	46,02	2040,14	159,84	0,96
	St.dev	48,55	37,78	15313,35	134,38	12,84	11,36	1011,22	37,81	0,01
	Min	172,23	137,53	18586,9	492,37	32,37	25,4	718,78	98,38	0,93
	Max	366,82	286,55	80391,95	1026,52	87,08	73,12	4865,38	252,24	0,98
Total (n=231)	Mean	232,78	195	37244,12	688	50,85	42,47	1744,37	148,52	0,95
	St.dev	47,18	39,57	14558,98	132,85	12,19	10,24	819,47	34,73	0,02
	Min	126,17	101,75	11128,4	389,39	22,43	20,54	337,47	67,64	0,84
	Max	400,31	335,66	98668,16	1137,36	87,08	73,12	4865,38	252,24	0,99

Table B.8 – Tibia - descriptive statistics of osteon and Haversian canal parameters in different human individuals

HUMAN – METATARSAL – INTRA-SPECIES										
Individual		**On.Dm$_{max}$ (µm)**	**On.Dm$_{min}$ (µm)**	**On.Ar (µm^2)**	**On.Pm (µm)**	**HC.Dm$_{max}$ (µm)**	**Hc.Dm$_{min}$ (µm)**	**HC.Ar (µm^2)**	**HC.Pm (µm)**	**On.Cr**
HA1 (n=39)	Mean	199,14	164,91	27165,6	590,39	50,39	41,78	1816,21	151,63	0,93
	St.dev	50,05	37,96	14272	147,12	14,3	11,49	894,24	39,24	0,03
	Min	117,26	106,46	10565,92	372,93	23,73	20,48	431,46	75,72	0,85
	Max	332,25	283,11	86173,82	1088,39	74	63,67	3586,09	218,93	0,97
HA2 (n=14)	Mean	189,53	160,94	23998,21	553,34	47,81	40,95	1502,14	139,05	0,95
	St.dev	35,68	27,57	8374,37	98,36	6,14	4,48	379,29	17,76	0,02
	Min	133,57	120,6	12509,93	402,03	35,76	31,68	903,34	109,76	0,93
	Max	256,57	211,98	37440,67	709,25	54,06	45,91	2127,6	166,89	0,99
HA5 (n=28)	Mean	191,93	159,1	24501,89	562,84	50,18	41,31	1635,44	144,12	0,96
	St.dev	24,38	19,37	5833,53	65,1	9,89	9,21	638,78	28,37	0,02
	Min	154,08	125,64	16826,97	465,52	29,97	24,75	632,09	93,96	0,90
	Max	251,27	193,6	38677,59	718,47	70,98	58,29	3063,57	198,76	0,98
HA6 (n=27)	Mean	193,86	163,13	25588,66	568,53	48,87	39,8	1533,74	138,77	0,95
	St.dev	45,54	33,15	11261,33	120,01	13,14	9,23	746,18	34,23	0,02
	Min	125,9	109,67	10927,74	376,51	26,38	22,34	448,99	77,22	0,91
	Max	364,06	265,93	68683,59	972,61	77,21	58,05	3342,6	212,05	0,98
HA7 (n=21)	Mean	186,77	152,27	23234,55	543,99	42,14	36,42	1228,43	123,86	0,95
	St.dev	37,09	34,92	9596,15	115,15	9,8	8,97	599,03	29,6	0,02
	Min	123,33	97,3	9775,07	355,72	28,61	23,1	536,16	85,48	0,89
	Max	276,56	220,26	48026,07	825,62	63,67	51,85	2511,82	181,69	0,99
HA13 (n=22)	Mean	237,49	190,54	38126,5	682,43	50,56	42,48	1797,34	150,4	0,95
	St.dev	67,99	56,74	21884,48	198,03	13,01	10,35	868,16	36,29	0,02
	Min	148,47	116,18	13678,18	427,53	34,26	30,08	790,85	102,13	0,91
	Max	364,14	288	86002,89	1073,13	79,96	64,51	3606,06	220,29	0,98
Total (n=151)	Mean	199,83	165,12	27146,28	584,89	48,72	40,62	1618,57	142,73	0,95
	St.dev	47,98	37,81	13696,98	136,78	12,12	9,72	759,69	33,91	0,02
	Min	117,26	97,3	9775,07	355,72	23,73	20,48	431,46	75,72	0,85
	Max	364,14	288	86173,82	1088,39	79,96	64,51	3606,06	220,29	0,99

Table B.9 – Metatarsal - descriptive statistics of osteon and Haversian canal parameters in different human individuals

HUMAN – RIB – INTRA-SPECIES										
Individual		**On.Dm$_{max}$ (µm)**	**On.Dm$_{min}$ (µm)**	**On.Ar (µm^2)**	**On.Pm (µm)**	**HC.Dm$_{max}$ (µm)**	**Hc.Dm$_{min}$ (µm)**	**HC.Ar (µm^2)**	**HC.Pm (µm)**	**On.Cr**
HA1 (n=48)	Mean	177,36	139,02	20279,75	511,05	39,49	31,43	1063,24	116,98	0,91
	St.dev	51,85	41,28	11030,5	140,45	10,27	9,31	583,51	30,85	0,03
	Min	94,92	68,30	6661,35	298,84	17,50	14,39	219,14	55,08	0,80
	Max	328,22	248,99	48832,5	853,92	69,73	50,9	2922,83	199,99	0,97
HA8 (n=14)	Mean	226,13	180,14	33366,27	649,28	47,43	37,8	1511,61	135,59	0,94
	St.dev	56,44	46,68	17808,65	161,32	15,83	13,6	1092,55	44,31	0,03
	Min	145,21	130,37	16108,1	455,02	21,68	17,45	344,78	69,33	0,86
	Max	337,66	301,12	80254,14	1017,2	83,93	74,93	4854,18	250,84	0,98
HA9 (n=10)	Mean	195,86	148,76	22945,29	546,14	41,17	35,62	1157,25	120,85	0,93
	St.dev	36,56	37,75	10078,18	115,1	9,51	8,27	530,64	26,96	0,02
	Min	154,59	118,11	13805,28	431,76	27,25	25,86	558,07	85,81	0,89
	Max	250,53	236,82	43968,58	761,86	60,08	48,97	2212,82	169,66	0,96
HA10 (n=9)	Mean	207,92	176,43	28473,1	607,14	36,56	35,07	970,54	111,78	0,96
	St.dev	36,64	26,78	7650,06	84,48	5,26	10,14	372,6	21,37	0,02
	Min	145,42	144,4	15817,47	453,84	25,13	23,03	451,43	77,27	0,93
	Max	277,12	220,64	42948,37	753,87	41,55	51,94	1629,91	146,35	0,98
HA11 (n=20)	Mean	211,2	163,89	28743,2	604,01	42,57	34,33	1214,32	121,95	0,94
	St.dev	53,85	42,45	14013,99	150,63	14,75	8,81	779,14	37,23	0,02
	Min	117,94	110,48	11100,62	377,22	23,85	19,7	318	65,05	0,89
	Max	315,52	258,82	57542,07	883,99	82,26	58,49	3678,13	220,57	0,99
HA12 (n=21)	Mean	190,59	151,98	23800,79	546,61	42,55	34,57	1196,59	121,94	0,95
	St.dev	52,66	41,53	12763,26	140,99	12,55	9,33	672,67	33,94	0,02
	Min	111,31	98,91	8229,41	326,5	25,62	23,77	403,22	72,7	0,89
	Max	329,36	285,53	65579,12	943,95	67,98	54,6	2773,82	190,29	0,98
Total (n=122)	Mean	194,55	153,6	24597,93	558,24	41,35	33,79	1163,28	120,72	0,93
	St.dev	52,75	42,92	13080,86	145,48	12,02	9,83	694,36	33,33	0,03
	Min	94,92	68,3	6661,35	298,84	17,5	14,39	219,14	55,08	0,80
	Max	337	301,12	80254,14	1017,2	83,93	74,93	4854,18	250,84	0,99

Table B.10 – Rib - descriptive statistics of osteon and Haversian canal parameters in different human individuals

PIG – HUMERUS – INTRA-SPECIES										
Individual		**On.Dm$_{max}$ (µm)**	**On.Dm$_{min}$ (µm)**	**On.Ar (µm^2)**	**On.Pm (µm)**	**HC.Dm$_{max}$ (µm)**	**Hc.Dm$_{min}$ (µm)**	**HC.Ar (µm^2)**	**HC.Pm (µm)**	**On.Cr**
PJ1 (n=7)	Mean	203,99	176,92	28670,72	609,2	41,92	32,76	1147,94	119,44	0,96
	St.dev	24,6	14,73	5405,28	62,74	13,06	11,23	769,37	37,68	0,02
	Min	167,52	158,24	20947,28	518,84	27,37	20,13	443,64	78,81	0,91
	Max	239,24	200,17	33408,99	672,82	63,51	53,99	2678,37	186,74	0,98
PJ2 (n=11)	Mean	183,81	147,32	21224,32	524,77	33,75	25,69	714,84	95,46	0,95
	St.dev	29,72	22,39	5685,44	73,12	8,17	7,83	461,24	26,37	0,02
	Min	134,26	116,67	12150,05	399	26,16	19,74	384,22	71,12	0,92
	Max	229,72	181,97	29472,77	628,19	52,8	45,79	1943,52	158,42	0,98
PJ3 (n=15)	Mean	166,16	132,49	17480,69	475,73	32,12	24,89	566,75	91,21	0,95
	St.dev	27,88	25,19	5949,92	80,33	9,69	6,32	298,83	23,67	0,02
	Min	123,26	90,24	9061,65	346,33	22,82	16,86	146,21	64,82	0,90
	Max	219,13	175,42	30358,09	633,59	53,05	38,99	1364,02	140,48	0,98
PJ4 (n=16)	Mean	175,89	151,87	21669,61	521,99	32,31	26,94	793,19	97,2	0,97
	St.dev	41,1	26,69	9266,1	105,49	12,88	9,63	576,33	35,94	0,01
	Min	117,64	108,15	10762,17	375,54	18,42	15,91	250,31	58,99	0,93
	Max	302,55	202,43	49176,3	816,51	53,68	45,04	1815,45	154,92	0,98
PJ5 (n=32)	Mean	185,21	151,41	22999,57	539,11	31,65	26,28	666,33	92,81	0,96
	St.dev	41,76	32,78	10518,39	111,33	6,77	5,24	262,5	18,51	0,02
	Min	138,88	106,07	12934,41	416,5	18,78	17,45	235,21	56,11	0,91
	Max	317,75	272,7	59147,14	870,38	44,07	35,09	1245,2	129,37	0,98
PJ6 (n=16)	Mean	163,12	137,29	17851,75	477,74	29,98	23,09	570,83	85,31	0,96
	St.dev	26,33	23,32	5862,92	78,18	8,78	5,49	309,65	23,49	0,01
	Min	122,52	98,61	10921,41	377,82	16,07	15,42	183,1	49,88	0,93
	Max	208,32	184,06	28281,62	608,19	44,76	31	1099,1	123,96	0,98
Total (n=97)	Mean	178,28	147,61	21285,58	519,79	32,54	26,05	696,36	94,27	0,96
	St.dev	36,17	28,73	8606,82	98,74	9,59	7,3	428,18	26,55	0,02
	Min	117,64	90,24	9061,65	346,33	16,07	15,42	146,21	49,88	0,90
	Max	317,75	272,7	59147,14	870,38	63,51	53,99	2678,37	186,74	0,98

Table B.11 – Humerus - descriptive statistics of osteon and Haversian canal parameters in different pigs

PIG – RADIUS – INTRA-SPECIES										
Individual		**On.Dm$_{max}$ (µm)**	**On.Dm$_{min}$ (µm)**	**On.Ar (µm^2)**	**On.Pm (µm)**	**HC.Dm$_{max}$ (µm)**	**Hc.Dm$_{min}$ (µm)**	**HC.Ar (µm^2)**	**HC.Pm (µm)**	**On.Cr**
PJ1 (n=29)	Mean	228,68	183,89	33667,22	664,62	40,51	29,37	1042,97	119,11	0,93
	St.dev	44,45	41,88	12834,88	128,87	11,64	8,9	580,05	30,84	0,02
	Min	142,53	115,26	13202,89	417,58	26,05	14,56	408,57	75,84	0,86
	Max	319,27	269,96	61705,71	924,65	64,39	56,02	2871,21	196,04	0,96
PJ2 (n=32)	Mean	200,45	167,96	27774,68	595,44	40,52	31,63	1090,37	115,36	0,96
	St.dev	34,53	31,59	9060,58	100,39	13,85	11,71	756,2	38,55	0,01
	Min	142,40	109,25	12220,66	403,33	22,34	18,14	314,59	65,36	0,93
	Max	261,94	221,42	42722,89	748,37	69,10	59,62	3047,5	199,57	0,98
PJ3 (n=44)	Mean	205,53	172,58	28337,18	603,35	38,89	32,17	1048,68	112,9	0,96
	St.dev	31,04	28,14	8215,08	89,73	12,78	10,2	688,59	35,98	0,02
	Min	118,8	87,97	8532,31	336,23	21,91	17,57	321,89	67,91	0,91
	Max	278,89	230,85	48749,23	794,67	69,87	53,01	2867,31	196,43	0,98
PJ4 (n=11)	Mean	177,91	153,58	21415,04	525,25	34,39	26,98	705,19	97,11	0,96
	St.dev	27,47	21,41	6274,16	75,82	5,37	4,56	242,52	16,16	0,01
	Min	146,46	120,15	12742,22	411,4	26,33	18,7	401,27	73,38	0,95
	Max	239,73	193,56	35800,53	689,23	45,4	32,3	1227,18	130,53	0,97
PJ5 (n=15)	Mean	184,3	151,25	22416,32	538,43	32,82	25,44	659,75	92,46	0,95
	St.dev	24,44	23,84	6044,63	74,14	8,85	6,16	341,09	24,14	0,02
	Min	136,93	114,45	11498,48	385,25	21,64	14,67	224,5	57,84	0,91
	Max	230,74	194,33	33577,48	658,3	51,71	35,92	1433,17	143,63	0,97
PJ6 (n=9)	Mean	216,78	182,6	31311,15	636,35	60,93	46,41	2244,31	172,29	0,95
	St.dev	26,52	31,24	8498,01	86,26	11,91	7	747,81	31,05	0,02
	Min	164,57	119,92	16121,34	467,01	42,61	36,24	1241,3	127,93	0,93
	Max	250,42	236,2	47485,04	781,9	76,75	57,01	3288,55	207,55	0,98
Total (n=140)	Mean	205,44	170,73	28325,61	603,26	40,01	31,25	1065,23	115,14	0,95
	St.dev	36,77	32,85	9858,29	106,23	13,25	10,39	713,07	36,8	0,02
	Min	118,8	87,97	8532,31	336,23	21,64	14,56	224,5	57,84	0,86
	Max	319,27	269,96	61705,71	924,65	76,75	59,62	3288,55	207,55	0,98

Table B.12 – Radius - descriptive statistics of osteon and Haversian canal parameters in different pigs

PIG – ULNA – INTRA-SPECIES										
Individual		**On.Dm$_{max}$ (µm)**	**On.Dm$_{min}$ (µm)**	**On.Ar (µm^2)**	**On.Pm (µm)**	**HC.Dm$_{max}$ (µm)**	**Hc.Dm$_{min}$ (µm)**	**HC.Ar (µm^2)**	**HC.Pm (µm)**	**On.Cr**
PJ1 (n=26)	Mean	182,94	144,81	21595,44	538,18	34,78	24,91	774,24	101,01	0,91
	St.dev	32,34	30,9	7110,81	95,56	9,04	6,1	443,28	25,62	0,03
	Min	111,11	73,36	6777,25	306,9	17,89	15,06	224,01	56,93	0,83
	Max	245,85	215,14	34293,83	713,33	63,52	39,09	2260,06	175,41	0,98
PJ2 (n=35)	Mean	203,86	173,19	27743,24	596,28	38,57	31,29	998,58	110,36	0,96
	St.dev	34,36	27,15	8103,03	88,43	12,43	10,94	669,03	35,65	0,01
	Min	149,02	125,49	16068,75	455,91	20,75	16,19	249,82	58	0,93
	Max	296,08	237,59	47096,43	797,56	64,96	57,91	2508,41	182,05	0,99
PJ3 (n=19)	Mean	170,65	145,45	19854,68	501,68	32,33	26,37	830,4	93,67	0,96
	St.dev	28,96	25,73	6933,88	84,44	15,84	14,91	960,09	48,63	0,01
	Min	127,16	108,22	10619	371,93	14,11	12,58	131,97	42,51	0,92
	Max	236,01	202,37	38284,6	706,12	74,37	62,24	3561,74	215,46	0,99
PJ4 (n=16)	Mean	184,03	155,22	23577,01	544,88	48,2	40,28	1782,18	138,99	0,95
	St.dev	40,14	35,3	10380,84	120,22	23,24	19,85	1513,04	66,93	0,02
	Min	117,37	109,6	10649,19	374,39	17,49	14,72	224,5	55,06	0,93
	Max	255,97	216,98	44793,52	768,55	81,98	77,33	4943,29	251,87	0,98
PJ5 (n=33)	Mean	163	138,3	18160,85	479,36	34,57	30,22	871,33	103,01	0,96
	St.dev	30,64	25,7	6933	85,35	9,98	9,38	516,78	30,68	0,01
	Min	111,68	98,12	8531,33	333,59	18,16	18,14	223,52	55,38	0,92
	Max	255,05	212,55	42511,06	745,65	57,22	49,67	2137,82	167,35	0,99
PJ6 (n=16)	Mean	173,98	149,11	21337,43	516,94	37,19	31,2	1015,81	107,71	0,96
	St.dev	39,09	30,56	9349,93	110,1	15,37	13,55	931,73	44,55	0,01
	Min	113,78	106,36	9454,15	347,58	20,43	17,57	289,26	61,61	0,94
	Max	270,27	210,79	46235,94	779,45	70,09	61,04	3230,3	205,68	0,98
Total (n=145)	Mean	180,97	151,89	22259,81	532,43	37,07	30,24	995,72	107,69	0,95
	St.dev	36,38	31,07	8578,63	102,57	14,3	12,68	853,25	41,73	0,03
	Min	111,11	73,36	6777,25	306,9	14,11	12,58	131,97	42,51	0,83
	Max	296,08	237,59	47096,43	797,56	81,98	77,33	4943,29	251,87	0,99

Table B.13 – Ulna - descriptive statistics of osteon and Haversian canal parameters in different pigs

PIG – FEMUR – INTRA-SPECIES										
Individual		**On.Dm$_{max}$ (µm)**	**On.Dm$_{min}$ (µm)**	**On.Ar (µm^2)**	**On.Pm (µm)**	**HC.Dm$_{max}$ (µm)**	**Hc.Dm$_{min}$ (µm)**	**HC.Ar (µm^2)**	**HC.Pm (µm)**	**On.Cr**
PJ1 (n=5)	Mean	219,09	199,83	34840,8	664,72	42,1	33,52	1290,19	121,53	0,97
	St.dev	36,99	26,14	10336,5	100,99	17,55	16,62	1254,65	55,51	0,003
	Min	180,59	173,27	24350,26	559,86	25,55	20,47	377,89	72,55	0,97
	Max	260,81	228,69	46015,83	769,89	70,53	58,29	3425,88	211,41	0,98
PJ2 (n=16)	Mean	188,23	153,54	23667,92	549,74	30,92	23,53	629,3	86,9	0,95
	St.dev	43,46	29,42	8692,66	108,08	11,34	8,69	526,71	32,44	0,02
	Min	116,54	107,50	10143,22	361,92	17,79	14,8	154,37	46,12	0,91
	Max	264,9	200,05	38275,34	714,29	61,2	47,93	2248,37	172,19	0,99
PJ3 (n=12)	Mean	156,5	119,75	15181,56	447,73	23,75	18,79	342,14	66,84	0,94
	St.dev	25,26	21,31	3983,45	58,59	5,77	4,34	170,78	16,31	0,02
	Min	118,31	99,34	9985,44	362,75	14,71	13,04	136,84	43,45	0,89
	Max	199,93	162,66	23062,7	554,53	35,38	26,71	760,17	101,32	0,97
PJ4 (n=8)	Mean	167,28	131,7	17232,26	475,07	26,04	19,78	427,69	74,42	0,94
	St.dev	23,4	22,64	4686,64	64,85	5,67	5,59	209,51	17,99	0,02
	Min	130,55	101,45	10731	374,41	17,89	11,03	174,82	50,13	0,91
	Max	206,68	161,26	23361,21	560,54	34,44	26,38	722,67	98,2	0,98
PJ5 (n=13)	Mean	165	132,93	17316,49	474,05	34,14	25,27	806,88	96,13	0,95
	St.dev	30,97	20,58	5414,02	72,53	16,66	12,37	765,39	45,26	0,02
	Min	130,79	104,31	11534,03	389,77	14,03	12,56	148,04	45,49	0,91
	Max	239,29	168,46	30351,76	638,85	64,53	48,77	2193,34	174,18	0,98
PJ6 (n=13)	Mean	159,57	133,66	17010,49	468,68	30,59	23,92	640,9	88,02	0,96
	St.dev	18,9	24,29	4480,37	60,08	12,69	8,4	550,61	34,1	0,01
	Min	134,05	108,46	12014,19	397,62	16,88	13,42	176,77	49,81	0,94
	Max	197,56	195,71	26597,17	595,47	59,81	41,81	1890,44	162,49	0,98
Total (n=67)	Mean	172,28	140,48	19689,23	500,72	30,45	23,39	639,82	86,41	0,95
	St.dev	35,13	31,12	8110,47	97,25	12,66	9,75	623,49	35,89	0,02
	Min	116,54	99,34	9985,44	361,92	14,03	11,03	136,84	43,45	0,89
	Max	264,9	228,69	46015,83	769,89	70,53	58,29	3425,88	211,41	0,99

Table B.14 – Femur - descriptive statistics of osteon and Haversian canal parameters in different pigs

PIG – TIBIA – INTRA-SPECIES										
Individual		**On.Dm$_{max}$ (µm)**	**On.Dm$_{min}$ (µm)**	**On.Ar (µm^2)**	**On.Pm (µm)**	**HC.Dm$_{max}$ (µm)**	**Hc.Dm$_{min}$ (µm)**	**HC.Ar (µm^2)**	**HC.Pm (µm)**	**On.Cr**
PJ1 (n=32)	Mean	218,18	173,21	30469,25	634,01	43,03	28,74	1077,52	123,6	0,93
	St.dev	46,69	34,11	11066,06	120,63	9,84	5,73	390,86	22,59	0,03
	Min	141,24	118,02	13521,38	422,23	29,61	19,36	554,67	85,64	0,85
	Max	310,99	269,29	57883,43	891,29	62,51	44,68	2117,86	171,03	0,98
PJ2 (n=19)	Mean	156,13	129,99	16049,14	454,74	31,72	25,29	653,37	91,06	0,95
	St.dev	23,8	20,13	5024,88	66,42	8,37	6,95	338,05	23,54	0,02
	Min	119,49	101,47	10194,36	365,18	17,50	15,37	191,38	50,87	0,92
	Max	214,64	171,99	27292,09	599,75	49,09	40,89	1285,13	130,94	0,98
PJ3 (n=14)	Mean	151,82	130,64	16001,51	453,6	27,82	21,22	437,2	74,44	0,96
	St.dev	21,55	20,8	4395,42	61,21	11,46	6,29	238,33	20,01	0,01
	Min	118,36	102,11	10307,82	364,83	15,37	13,28	146,09	44,59	0,93
	Max	194,78	164,24	25028,62	570,88	60,64	31,90	938,89	113,11	0,98
PJ4 (n=26)	Mean	178,75	149,97	21241,95	521,37	34,31	27,77	774,7	98,86	0,96
	St.dev	30,2	22,22	6009,45	77,17	8,82	7,13	431,65	26,04	0,01
	Min	122,19	95,69	9730,76	358,78	21,3	18,79	318,97	66,48	0,91
	Max	245,62	199,08	31945,63	648,47	51,81	42,64	1813,01	155,05	0,98
PJ5 (n=41)	Mean	161,22	133,26	17297,1	471,67	32,09	26,34	708,75	93,97	0,96
	St.dev	25,57	18,98	4818,8	65,25	8,75	7,56	416,91	26,21	0,02
	Min	107,5	102,06	9162,45	344,17	16,81	14,03	183,10	50,2	0,90
	Max	205,73	184,64	28819,73	612,71	52,01	44,68	1787,69	153,09	0,98
PJ6 (n=11)	Mean	161,11	145,91	19189,2	493,3	26,53	22,57	489,59	79,6	0,97
	St.dev	18,45	23,52	4720,22	64,23	5,86	5,77	216,4	17,06	0,01
	Min	123,46	100,84	9823,28	357,87	19,06	12,64	221,09	56,29	0,96
	Max	182,85	175,57	25225,85	567,09	38,7	32,04	863,9	107,89	0,99
Total (n=143)	Mean	175,56	145,52	20814,85	514,68	34,05	26,2	752,46	98,09	0,95
	St.dev	39,39	29,09	8735,55	106,08	10,39	7,06	423,11	28,14	0,02
	Min	107,5	95,69	9162,45	344,17	15,37	12,64	146,09	44,59	0,85
	Max	310,99	269,29	57883,43	891,29	62,51	44,68	2117,86	171,03	0,99

Table B.15 – Tibia - descriptive statistics of osteon and Haversian canal parameters in different pigs

PIG – METATARSAL – INTRA-SPECIES										
Individual		**On.Dm$_{max}$ (µm)**	**On.Dm$_{min}$ (µm)**	**On.Ar (µm^2)**	**On.Pm (µm)**	**HC.Dm$_{max}$ (µm)**	**Hc.Dm$_{min}$ (µm)**	**HC.Ar (µm^2)**	**HC.Pm (µm)**	**On.Cr**
PJ1 (n=29)	Mean	198,59	149,3	24251,83	575,5	45,23	23,9	975,56	122,36	0,89
	St.dev	43,94	32,75	10099,34	118,71	8,87	5,72	373,65	21,34	0,05
	Min	133,43	93,93	9438,57	362,31	32,57	15,6	528,86	96	0,77
	Max	321,39	218,28	50397,15	818,98	63,78	35,84	1916,74	173,53	0,95
PJ2 (n=22)	Mean	175,71	146,05	20313,5	515,83	27,11	23,12	476,57	80,15	0,95
	St.dev	13,86	16,93	3545,01	44,6	5,23	4,48	173,71	14,62	0,01
	Min	145,67	121,18	14502,63	436,69	19,75	15,46	219,14	56,13	0,92
	Max	206,6	177,02	28262,14	609,09	35,75	31,6	735,82	100,44	0,98
PJ3 (n=28)	Mean	148,56	125,22	14950,48	434,61	30,3	25,42	613	88,04	0,96
	St.dev	31,28	24,56	5633,12	82,23	8,89	6,08	340,73	23,5	0,02
	Min	103,52	82,49	7191,66	311,96	17,79	15,45	200,63	53,3	0,92
	Max	222,48	169,32	25508,29	587,86	53,52	39,08	1636,24	149,73	0,98
PJ4 (n=21)	Mean	152,63	131	15656,98	449,66	31,25	26,14	676,62	91,46	0,96
	St.dev	21,22	18,31	3971,76	56,89	9,24	8,27	425,77	27,62	0,01
	Min	120,31	101,12	9852,01	358,88	18,14	12,58	175,8	51,52	0,93
	Max	188,35	174,71	23360,24	551,64	49,19	44,32	1727,79	149,67	0,98
PJ5 (n=19)	Mean	167,91	133,85	17805,3	483,74	30,52	25,73	618,43	88,41	0,95
	St.dev	25,28	14,21	3653,69	52,09	7,43	6,28	319,36	23,03	0,02
	Min	123,68	114,11	11976,2	393,09	19,2	18,2	224,5	55,03	0,89
	Max	232,43	165,52	26347,84	610,28	46,84	38,87	1345,03	133,57	0,98
PJ6 (n=22)	Mean	146,32	126,74	14910,41	436,35	30,15	24,96	632,18	87,66	0,96
	St.dev	20,05	19,38	3965,84	58,52	9,32	8,92	421,1	28,45	0,02
	Min	113,23	92,11	9261,8	350,44	16,35	14,72	197,71	51,33	0,94
	Max	191,02	158,33	21156,19	523,25	48,6	48,59	1794,51	153	0,98
Total (n=141)	Mean	165,95	135,68	18183,87	485,39	33,02	24,83	679,48	94,37	0,94
	St.dev	34,56	24,44	6915,57	93,05	10,39	6,67	383,17	27,27	0,04
	Min	103,52	82,49	7191,66	311,96	16,35	12,58	175,8	51,33	0,77
	Max	321,39	218,28	50397,15	818,98	63,78	48,59	1916,74	173,53	0,98

Table B.16 – Metatarsal - descriptive statistics of osteon and Haversian canal parameters in different pigs

PIG – RIB – INTRA-SPECIES										
Individual		**On.Dm$_{max}$ (µm)**	**On.Dm$_{min}$ (µm)**	**On.Ar (µm^2)**	**On.Pm (µm)**	**HC.Dm$_{max}$ (µm)**	**Hc.Dm$_{min}$ (µm)**	**HC.Ar (µm^2)**	**HC.Pm (µm)**	**On.Cr**
PJ1 (n=12)	Mean	165,73	130,39	18015,31	474,45	33,92	25,31	748,04	100,48	0,93
	St.dev	54,31	38,62	9832,43	145,84	11,62	5,57	396,87	26,78	0,02
	Min	79,74	69,51	4362,82	242,54	21,85	17,46	378,87	72,66	0,89
	Max	238,89	188,88	32320,6	662,6	54,19	34,74	1508,16	148,75	0,95
PJ2 (n=18)	Mean	157,72	128,89	16333,66	455,24	28,93	23,61	580,72	84,74	0,96
	St.dev	24,84	23,74	5378,67	73,31	10,32	8	362,53	27,65	0,02
	Min	107,92	89,1	7910,93	320,18	11,88	9,79	105,67	38,41	0,91
	Max	202,65	182,41	28455,96	605,23	47,17	38,18	1276,85	130,75	0,98
PJ3 (n=19)	Mean	189,57	154	23886,15	549,49	30,41	23,94	611,21	86,42	0,95
	St.dev	44,23	35,84	11244,21	123,79	9,83	8,29	466,3	28,52	0,02
	Min	125,35	108,47	11658,21	389,96	15,74	13,04	135,87	42,54	0,88
	Max	293,77	237,32	57282,99	876,98	58,19	48,11	2267,85	172,21	0,98
PJ4 (n=14)	Mean	174,31	132,99	18085,56	487,38	35,43	26,92	772,03	99,76	0,93
	St.dev	29,8	24,3	5438,9	76,31	10,24	6,84	436,54	25,7	0,02
	Min	113,62	100,67	9099,15	345,78	21,78	18,16	275,63	61,89	0,87
	Max	218,89	179,21	26195,42	589,48	63,75	44,05	2067,7	168,35	0,97
PJ5 (n=7)	Mean	158,07	132,88	16335,96	456,61	27,28	22,81	502,07	80,79	0,96
	St.dev	20,16	27,37	5743,74	70,95	7,22	5,45	215,72	17,23	0,01
	Min	141,95	109,15	12337,54	402,7	18,98	17,57	281,96	62,2	0,95
	Max	201,04	188,91	28750,58	606,66	37,3	31,62	833,22	105,26	0,98
PJ6 (n=16)	Mean	137,51	113,91	12644,67	401,16	32,11	27,11	729,79	93,84	0,96
	St.dev	24,11	22,54	4381,93	70,41	10,94	9,54	472,05	31,31	0,02
	Min	100,67	76,84	6356,5	291,61	18,14	15,37	186,51	51,52	0,89
	Max	171,13	157,72	20794,37	516,26	49,94	46,08	1579,26	143,17	0,98
Total (n=86)	Mean	164,84	132,85	17835,94	474,03	31,47	25,04	663,28	91,12	0,95
	St.dev	38,64	31,34	8321,39	107,68	10,33	7,69	415,28	27,59	0,02
	Min	79,74	69,51	4362,82	242,54	11,88	9,79	105,67	38,41	0,87
	Max	293,77	237,32	57282,99	876,98	63,75	48,11	2267,85	172,21	0,98

Table B.17 – Rib - descriptive statistics of osteon and Haversian canal parameters in different pigs